EPFL

Thèse n° 9402

The role of the Nimrod proteins in the *Drosophila* immune system

Présentée le 14 janvier 2022

Faculté des sciences de la vie
Unité du Prof. Lemaitre
Programme doctoral en approches moléculaires du vivant

pour l'obtention du grade de Docteur ès Sciences

par

Bianca Marie PETRIGNANI

Acceptée sur proposition du jury

Prof. V. Simanis, président du jury
Prof. B. Lemaitre, directeur de thèse
Prof. F. Peri, rapporteuse
Prof. I. Evans, rapporteur
Prof. B. McCabe, rapporteur

École polytechnique fédérale de Lausanne

2022

Acknowledgments

First and foremost, I would like to thank Prof. Bruno Lemaitre for giving me twice the chance to work in his laboratory and accomplish my Ph.D. thesis. Thank you, Bruno, for your guidance and your continuous support. Thank you so much for having enriched my Ph.D. with support and friendship. I would also like to show gratitude to the members of my Ph.D. jury, Prof. Viesturs Simanis, Prof. Francesca Peri, Prof. Brian McCabe, and Prof. Ivan Evans, for valuating this work and for their helpful contributions. Finally, I would like to acknowledge Estee Kurant and her laboratory for their help and contribution in this work.

I would like to thank all my present and former colleagues of the Lemaitre laboratory. I had the chance to meet really incredible people from all over the world. Thank you for having been inspiring colleagues and beautiful friends. I am profoundly grateful to Samuel and Florent for their supervision and precious scientific advices. Without your assistance and dedicated involvement in my research, the NimB4 paper would have never been accomplished. You have been incredible colleagues, friends, and inspiring people in my career. I would like to thank Alice. This thesis would have been impossible without your support. Thank you for being such a special friend and colleague since the beginning of this adventure. I would like to thank Elodie for introducing me to the Nimrod superfamily and helping me a lot at the beginning of my Ph.D. Thank you, Hannah for your enthusiasm in the laboratory and your excellent proofreading and English corrections throughout my thesis. Thank you, Alexia, Faustine, Chloe and Julie for your great personalities and precious company at work. Thank you Asya for this incredible year working together. It has been a pleasure introducing you to the hemocyte world. Thank you, Li, Mark, and Yan, who provided stimulating discussion and happy distraction during coffee breaks! Thank you, Jean Philippe, Christophe, and Fanny, for all the precious and kind help you both constantly gave me during my work. Thank you, Veronique Mercedes and Tatiana, for your support and organizing unique events for the lab.

In addition, I would like to thank my cousin Heloise and my friends Claudia, Claire, Fatma, and Alexis who always supported me and with whom I shared a lot.

Most importantly, none of this could have happened without my family. I would like to express my gratitude to my parents, Solange and Paolo, my grandparents, Jean et Elisabeth, my sister

and brother Camilla and Gianluca. Without your tremendous encouragement and love in the past few years, it would be impossible for me to complete my Ph.D. Finally, I could not have achieved this life adventure without Radiana. Il destino ci ha fatto incontrare durante questa avventura. Sei stato il regalo più grande della mia vita.

Lausanne, 27th June 2020

Abstract

The use of tractable model organisms such as *Drosophila melanogaster* and the powerful genetic tools they offer has contributed significantly to recent advances in comprehension of innate immunity, notably phagocytosis. To date, several phagocytic transmembrane receptors, opsonins, and ligands have been discovered in *Drosophila melanogaster*. Many of them belong to the Nimrod family, which includes both secreted and transmembrane proteins containing several *NIM* repeats. Genetic and biochemical studies have revealed the roles of transmembrane Nimrod receptors such as Draper, Simu and Eater in phagocytosis. However, the function of the five secreted Nimrod members, the Nimrod B proteins, remains unstudied. The goals of my thesis were to characterize the function of the secreted Nimrod B proteins using newly generated CRISPR-Cas9 null mutations, focusing on *NimB5*, *NimB4*, and *NimB1* genes. In this work, we first found that the secreted protein, NimB5, is produced in the fat body upon nutrient scarcity downstream of metabolic sensors and ecdysone signaling. We provide evidence that NimB5 binds to hemocytes to down-regulate their proliferation and adhesion. Blocking this signaling loop results in conditional lethality when larvae are raised on a poor diet due to excessive hemocyte numbers and insufficient energy storage. This pointed to a role of NimB5 in the allocation of resources to blood cells, tailoring the investment in the immune system to metabolic resource availability.

In the second part of this thesis, we analyzed the function of NimB4 to reveal its crucial role in clearance of apoptotic cells. NimB4 is expressed by macrophages and glial cells, the two main types of phagocytes in *Drosophila*. Our study points to a role of NimB4 in phagosome maturation, more specifically in the fusion between the phagosome and lysosomes. We propose that similar to bridging molecules, NimB4 binds to apoptotic corpses to engage a phagosome maturation program dedicated to efferocytosis.

Finally, in the last part of the thesis, we present preliminary results on the role of *NimB1* in the *Drosophila* immune system. *NimB1* is expressed mainly in hemocytes and regulates hemocyte number. Additionally, NimB1 shares several characteristics with NimB4, notably the ability to bind to apoptotic cells. As such, we hypothesize that it could play a similar function in the phagocytosis of apoptotic cells. However, the exact role of NimB1 in phagocytosis is still

unclear, and additional work is necessary to understand if NimB1 plays a role in the uptake of apoptotic cells or phagosome maturation.

Collectively, this thesis has revealed that the NimB proteins play specific roles in efferocytosis or in blood cell number regulation. Thus, this work extended our knowledge on the *Drosophila* cellular immune response by providing new insight on the conserved Nimrod family of proteins.

Keywords

Drosophila, innate immunity, hemocytes/macrophages, Nimrod, phagocytosis, apoptotic cells, adhesion, proliferation, adhesion

Résumé

L'utilisation d'organismes modèles tels que *Drosophila melanogaster* ainsi que de ses outils génétiques ont contribué de manière notable à l'approfondissement de nos connaissances sur l'immunité innée, et notamment la phagocytose. À ce jour, plusieurs récepteurs phagocytaires, opsonines, et ligands ont été découverts chez la drosophile. Un grand nombre d'entre eux appartiennent à la famille Nimrod, qui comprend à la fois des protéines sécrétées et des protéines transmembranaires contenant plusieurs répétitions *NIM*. Des études génétiques et biochimiques ont révélé le rôle des récepteurs transmembranaires Nimrod tels que Draper, Simu et Eater dans la phagocytose. Cependant, au sein de la famille Nimrod, cinq autres protéines secrétées, nommées Nimrod B, n'ont pas encore été étudiées.

L'objectif de cette thèse est de caractériser la fonction des protéines Nimrod B. Pour cela, nous avons généré des mutations nulles CRISPR-Cas9 dans chacun des gènes d'intérêt, et en particulier *NimB5*, *NimB4* et *NimB1*. En utilisant ces mutants, nous avons démontré que lors d'un jeûne, l'activation de senseurs métaboliques ainsi que l'hormone de croissance Ecydsone induisent la sécrétion de la protéine NimB5 depuis le corps gras. Par la suite, NimB5 se lie aux hémocytes afin d'inhiber leur prolifération et leur adhésion. De plus, nous avons remarqué que lorsque les larves de drosophile grandissent dans un milieu pauvre en nutriments, le blocage de la signalisation initiée par NimB5 entraîne la formation excessive d'hémocytes et l'appauvrissement des ressources métaboliques. Cette observation met en évidence le fait que NimB5 est responsable de la distribution des ressources métaboliques envers les macrophages, ainsi que du maintien d'un état d'équilibre entre l'énergie investie dans le système immunitaire et la conservation des ressources métaboliques.

Dans la deuxième partie de cette thèse, nous avons analysé la fonction de NimB4 et mis en évidence son rôle dans l'élimination des cellules apoptotiques. NimB4 est exprimé par les macrophages et les cellules gliales, deux types de cellules phagocytaires ayant un rôle majoritaire chez la drosophile. De plus, notre étude met en évidence le rôle de NimB4 dans la maturation des phagosomes, et plus précisément dans la fusion entre les phagosomes et les lysosomes. En effet, NimB4 se lie aux corps apoptotiques de la même manière que les « bridging molecules » afin d'initier un programme spécifique de maturation propre à l'efferocytose.

Finalement, dans la dernière partie de la thèse, nous présentons des données préliminaires sur le rôle de NimB1 dans le système immunitaire de la drosophile. NimB1 est exprimé principalement dans les hémocytes et a pour mission d'ajuster leur nombre. Nous avons remarqué que les protéines NimB1 et NimB4 partagent des caractéristiques communes, notamment la capacité à se lier aux cellules apoptotiques. Suite à nos observations, nous avons émis l'hypothèse que NimB1 joue un rôle semblable à NimB4 dans l'efferocytose. Il est donc désormais nécessaire d'élucider le rôle exact de NimB1 dans la phagocytose et, en particulier, de comprendre si NimB1 joue un rôle dans le prélèvement des cellules apoptotiques ou dans la maturation du phagosome.

En résumé, cette thèse met en évidence le fait que les protéines NimB jouent des rôles spécifiques dans l'efferocytose ainsi que dans la régulation du nombre de macrophages. Ce travail de recherche élargit nos connaissances sur la réponse cellulaire immunitaire chez la drosophile ainsi que nos connaissances sur les protéines appartenant à la famille Nimrod.

Mots-clés

Drosophila melanogaster, immunité innée, hémocytes/macrophages, Nimrod, phagocytose, cellules apoptotiques, adhésion, prolifération, adhésion

Contents

Chapter 1

Chapter 2

Chapter 3

Chapter 4

Chapter 5

List of Figures

List of Supplementary Figures

Chapter 1
Introduction

Phagocytosis is an elegant and complex process for the ingestion and elimination of pathogens and apoptotic cells. As such, phagocytosis plays a key role in host defense and tissue homeostasis. This introduction summarizes current knowledge on the molecular mechanisms of phagocytosis in mammalian cells, and describes the phagocytosis of apoptotic cells in *Drosophila melanogaster (Drosophila)*.

Phagocytosis is a receptor-mediated mechanism that consists of the recognition and internalization of particles by the cell. Particles (larger than 0,5 μm in diameter) are internalized into plasma membrane-derived vesicles called phagosomes. Phagocytic targets have various origins, including altered self-entities such as apoptotic cells, and foreign agents such as bacteria. Regardless of the nature of the engulfed particle, phagocytosis relies on three fundamental steps: phagosome formation, maturation, and resolution.

Phagocytosis was first described at the end of the nineteenth century by the Russian zoologist Élie Metchnikoff while studying marine invertebrate organisms. He observed the uptake of particles by a specific subset of cells in starfish larvae. Based on this finding, he hypothesized that these so-called phagocytes could play a key role in host defense by ingesting particles. Metchnikoff's brilliant observation laid the foundation for understanding the key role of phagocytosis in cellular immunity.

The evolutionary conservation of phagocytic processes in unicellular and metazoan organisms underscores its importance for survival. In unicellular organisms and metazoans, phagocytosis is an essential mode of nutrient uptake (Mills, 2020). In higher metazoans phagocytosis plays an immune role during infection by eliminating pathogens, and a remodeling role during development by eliminating apoptotic cells. In higher organisms, phagocytosis is a mechanism exclusive to specific cells: either non-professional phagocytes such as glial cells or professional phagocytes such as macrophages or hemocytes. Non-professional phagocytes are crucial in clearing apoptotic cells in organs that macrophages cannot access, such as the brain. They prevent the accumulation of apoptotic particles which may lead to inflammation or damage to neighboring tissue (Tremblay *et al*, 2019).

1.1 Molecular mechanisms of phagocytosis in mammals

1.1.1 Phagocytic receptors direct target recognition

In mammals, both professional and non-professional phagocytes can recognize phagocytic targets. A first challenge for phagocytic cells is to distinguish "self" from "non-self" such as healthy living cells from infectious pathogens or apoptotic cells. To do so, phagocytes have membrane receptors that recognize and bind specific ligands displayed on various phagocytic targets. Because particles can display different ligands, it is not surprising that numerous receptor types can mediate this process. In recent years, many surface receptors of mammalian phagocytes have been identified and characterized (Flannagan *et al*, 2012; Cockram *et al*, 2021). However, the mammalian system is highly complex and relies on many redundant phagocytic components. Thus, addressing specific roles of phagocytic receptors remains a complex and active research area. We will discuss receptors involved in phagocytosis of foreign bodies and those mediating uptakes of apoptotic cells separately, as these two processes differ in several ways.

Receptors	Ligands
Pattern-recognition receptors	
Mannose receptor (CD206)	Mannan
Dectin-1 (CLEC7A)	β1,3-glucan
CD14	Lipopolysaccharide-binding protein
Scavenger receptor A (CD204)	Lipopolysaccharide, lipoteichoic acid
CD36	*Plasmodium falciparum*–infected erythrocytes
MARCO	Bacteria
Opsonic receptors	
FcγRI (CD64)	IgG1 = IgG3 > IgG4
FcγRIIa (CD32a)	IgG3 ≥ IgG1 = IgG2
FcγRIIc (CD32c)	IgG
FcγRIIIa (CD16a)	IgG
FcαRI (CD89)	IgA1, IgA2
FcεRI	IgE
CR1 (CD45)	Mannan-binding lectin, C1q, C4b, C3b
CR3 ($\alpha_M\beta_2$, CD11b/CD18, Mac-1)	iC3b
CR4 ($\alpha_V\beta_2$, CD11c/CD18, gp150/95)	iC3b
$\alpha_5\beta_1$	Fibronectin, vitronectin
Apoptotic corpse receptors	
TIM-1	Phosphatidylserine
TIM-4	Phosphatidylserine
BAI1	Phosphatidylserine
Stabilin-2	Phosphatidylserine
Mer	Gas6, protein S
$\alpha_V\beta_3$	MFG-E8
$\alpha_V\beta_5$	Apoptotic cells
CD36	Oxidized lipids

Figure 1.1 Human receptors mediating phagocytosis

List of human pattern-recognition receptors, opsonic receptors, apoptotic corpse receptors and their respective ligands. BAI (brain-specific angiogenesis inhibitor), CR (complement receptor), Ig (immunoglobuin), MFG (Milk fat globule), TIM (T cell immunoglobulin mucin) (Adapted from (Flannagan *et al*, 2012)).

1.1.1.2 Receptors of foreign particles

The first step towards internalization and degradation of phagocytic particles is their detection. This involves two types of receptors when it comes to foreign bodies (i.e., pathogens): receptors that detect microbial molecules directly (pattern-recognition receptors) and those that interact with foreign bodies indirectly via opsonins (opsonic receptor) (**Figure 1.1**). Pattern-recognition receptors have evolved to recognize target motifs of invading organisms called pathogen-associated molecular patterns (PAMPs). PAMPs commonly correspond to cell wall components of pathogens, including polysaccharides of yeasts, β-1,3 glucans of fungi, or peptidoglycans and lipopolysaccharide (LPS) of bacteria. Non-opsonic receptors are typified by the class A scavenger receptor family, which are able to bind LPS or lipoteichoic acid of gram-negative bacteria (**Figure 1.1**) (Peiser *et al*, 2000).

Conversely, opsonic receptors recognize opsonins produced by the host (e.g., antibodies, complement, mannose-binding lectin) that coat the phagocytic target. Opsonins create a link between the phagocyte and the foreign particle, increasing binding sensitivity between the two entities. To date, the best-characterized opsonic phagocytic receptors are the Fc receptors (FcR) and the complement receptors (CR) (**Figure 1.2**). For instance, FcRs bind the constant portion of immunoglobulin G or A. Complement receptors, such as CR3, bind to protein fragment iC3b deposited on the non-self particle following activation of the complement cascade (**Figure 1.1 and Figure 1.2**) (Ross *et al*, 1992; Mosser & Zhang, 2011; Walbaum *et al*, 2021; Fu & Harrison, 2021).

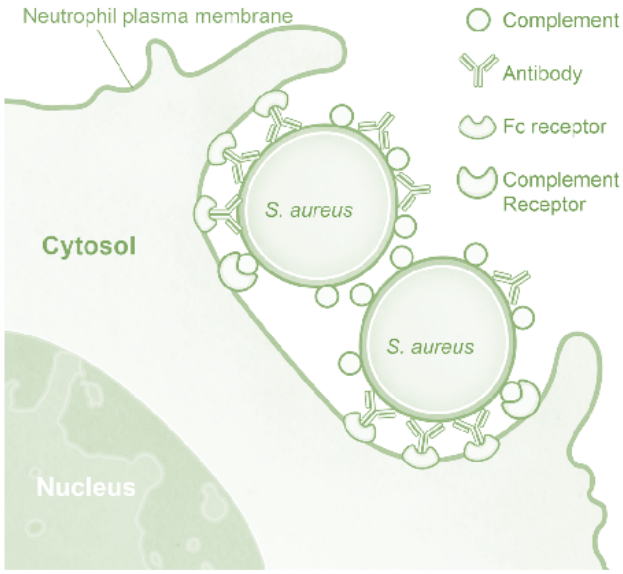

Figure 1.2 Phagocytosis of *Staphylococcus aureus* opsonized by complement proteins
The opsonized bacteria are efficiently bound by complement receptor and Fc receptors on the surface of neutrophils. Ligation of both receptors drives phagocytosis (Adapted from (McGuinness *et al*, 2016).

1.1.1.3 Receptors of apoptotic cells

The phagocytosis of apoptotic cells, or efferocytosis, is a crucial process for tissue homeostasis. In a healthy human, apoptotic corpse receptors must clear more than 10 billion apoptotic cells every day (Susan Elmore, 2007). This process involves hugely complex ligand and receptor interactions, where phagocytic receptors recognize "eat-me" signals exposed on the plasma membrane of apoptotic cells (Elliott & Ravichandran, 2016; Boada-Romero *et al*, 2020; Cockram *et al*, 2021). One of the best characterized "eat-me" signals is phosphatidylserine (PS), a negatively charged phospholipid that is localized in the inner leaflet of the lipid bilayer in healthy cells. Under normal conditions, PS is constantly transported from the outer leaflet to the inner leaflet of the lipid bilayer by the flippase ATP11C to maintain membrane asymmetry. During apoptosis, inactivation of this flippase induces translocation of PS to the outer leaflet of the lipid bilayer and marks the beginning of the apoptotic process (Fadok *et al*, 1998; Segawa & Nagata, 2015; Segawa *et al*, 2014). Binding of the phagocytic receptors to PS on the apoptotic cell triggers formation of the phagocytic cup. Therefore, inhibition of PS translocation to the outer plasma membrane can prevent phagocytosis of apoptotic cells (Callahan *et al*, 2000). Phagocytic receptors for apoptotic cells can bind PS directly or indirectly. Those that directly

bind PS include Tim4 (T-cell immunoglobulin and mucin-domain-containing molecule), BAI1 (brain-specific angiogenesis inhibitor 1), and Stabilin-2. Indirect PS receptors include the TAM receptors (TYRO3, AXL and MER) and the integrin αvβ3 receptor. These receptors bind to 'eat me' signals such as PS through bridging molecules (Figure 1.1 and Figure 1.3).

Bridging molecules are secreted molecules that recognize phosphatidylserine and function as a bridge between apoptotic cells and cell surface receptors of phagocytes. The main function of bridging molecules is to enhance the interaction between apoptotic cells and the phagocyte. An example of a bridging molecule is the glycoprotein milk fat globule-EGF factor 8 (MFG-E8), which is secreted by phagocytic cells and connects the receptor integrin αvβ3 to PS (Hanayama *et al*, 2002; Fuller & Van Eldik, 2008; Akakura *et al*, 2004). Mice lacking the MFG-E8 gene spontaneously develop a lupus-like disease caused by impaired clearance of apoptotic cells (Yamaguchi *et al*, 2010).

Despite the diversity of phagocytic receptors for apoptotic cell, all share a key common property: a low affinity for the ligand. To compensate this low affinity, the binding of apoptotic cells includes several receptors which create multiple direct or indirect binding events between the phagocyte and the apoptotic cell. This multi binding results in the formation of a "phagocytic synapse," which increases the overall affinity through a synergistic response (Figure 1.3) (Barth *et al*, 2017).

Phagocytic receptors are not always involved in binding of the phagocytic target, but may instead affect phagocytosis indirectly or be involved in its downstream steps. For instance, the receptor Tim4 alone does not support efferocytosis but enhances TAM-dependent efferocytosis (Miyanishi *et al*, 2007; Yanagihashi *et al*, 2017). Another example is the transmembrane receptor Integrin β1 which is involved in the phagocytosis of certain bacteria and critically regulates phagosome maturation (Wang *et al*, 2008).

In sum, phagocytic receptors are diverse in terms of the nature of the phagocytic targets that they recognize, how they bind those targets, and the phagocytic processes that they mediate. In the next section, we will describe how activation of the phagocytic receptor leads to phagosome formation.

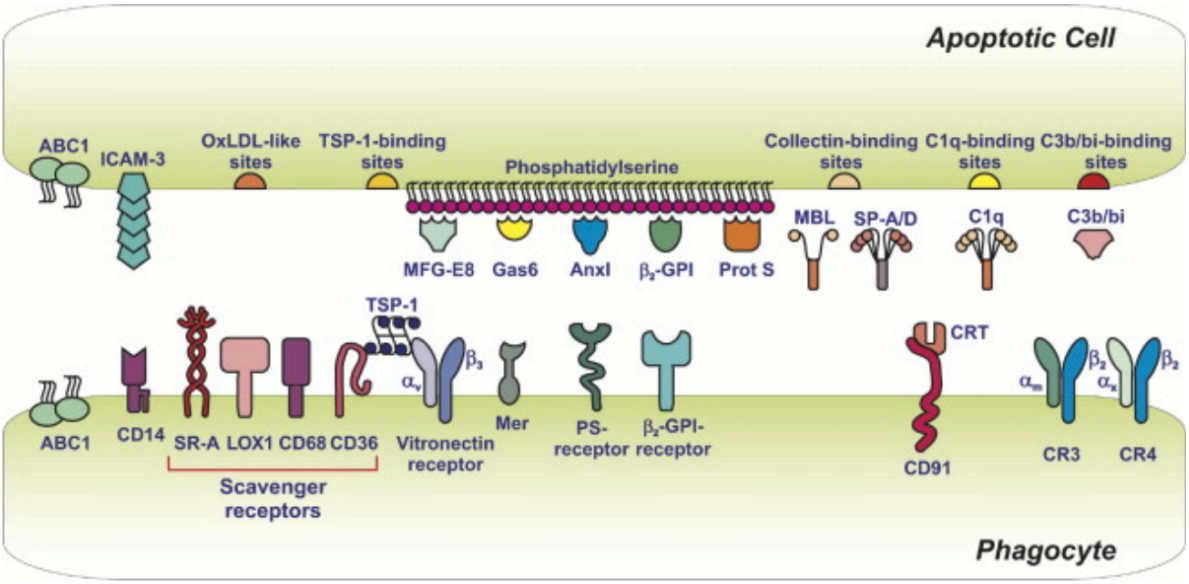

Figure 1.3 The efferocytosis engulfment synapse

The apoptotic cell displays various 'eat-me' signals that are recognized directly or indirectly via different phagocytic receptors and bridging molecules. ABC1 (ATP binding-cassette-transporter 1); AnxI (Annexin I); β2-GPI (β2-glycoprotein-I); C1q (complement protein C1q); C3b/bi (complement protein C3b/bi); CD14 (lipopolysaccharide receptor CD14); CD91 (calreticulin/heat shock protein receptor); CR3 (complement receptor 3); CR4 (complement receptor 4); CRT (calreticulin); Gas6 (growth arrest-specific 6) ICAM-3 (intercellular adhesion molecule 3); LOX1 (lectin-like oxidized low-density lipoprotein particle receptor 1); MBL (mannose binding lectin); Mer (receptor-tyrosine-kinase); MFG-E8 (milk-fat-globule-EGF-factor 8); OxLDL (oxidized low-density lipoprotein particle); Prot S (protein S); PS-receptor (phosphatidylserine receptor); SP-A/D, (lung surfactant protein A or D); SR-A (class A macrophage scavenger receptor); TSP-1 (thrombospondin-1) (Adapted form (Lauber *et al*, 2004)).

1.1.2 The mechanism of phagocytosis

After recognizing the target particle, phagocytic receptors initiate intracellular signaling that induces formation of pseudopods. This occurs through remodeling of the cytoskeleton and changes in the membrane lipids. From receptor activation to the end of the process, phagocytosis is conceptually divided into two phases: phagosome formation and phagosome maturation. Phagosome formation and maturation are known in great detail for the Fc receptors in mammals. This chapter explains the molecular mechanisms involved in formation, maturation, and resolution of the phagosome triggered by Fc receptor activation.

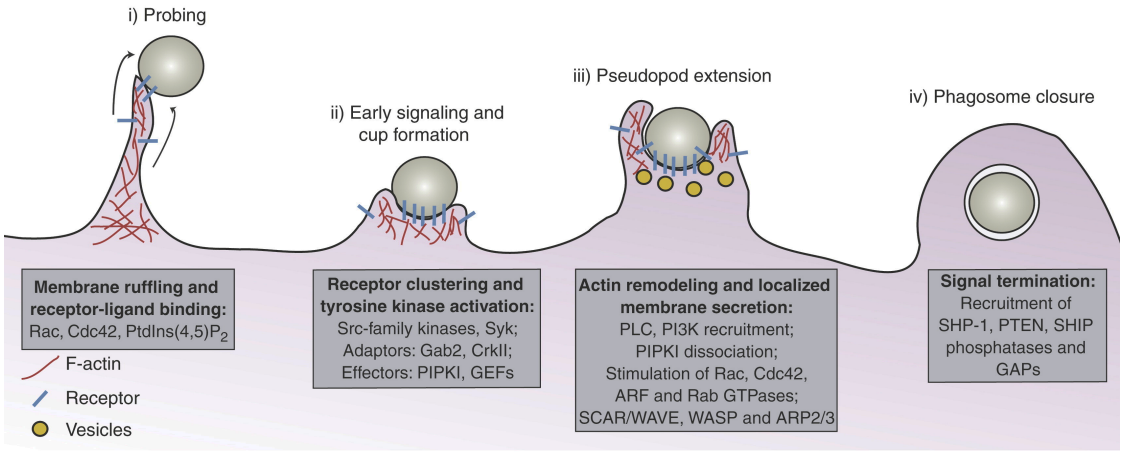

Figure 1.4 Four major stages during phagosome maturation
(i) During the first step of "probing", membrane extensions enriched in phagocytic receptors (blue) and actin filaments (red) bind the target particle. (ii) During cup formation, receptors cluster underneath the target particle. Receptors initiate intracellular signaling that results in remodeling of the actin filaments and drives the growth of membrane pseudopods to encircle the attached prey. (iii) During pseudopod extension, coordinated activation of lipid-modifying enzymes and an assortment of GTPases leads to a concerted assembly of highly dynamic actin filaments that drive the growth of membrane pseudopods to encircle the prey. (iv) Lastly, during "phagosome closure" the tips of the pseudopods meet and fuse, detaching the phagosome from the surface membrane (Adapted from (Botelho & Grinstein, 2011)).

1.1.2.1 Step 1: Phagosome formation

Phagosome formation requires the formation of pseudopods, which are primarily produced by polymerization of actin filaments (Rougerie *et al*, 2013) (**Figure 1.4**). Additionally, phagosome formation is accompanied by changes in the lipid membrane that initiate signaling events and regulate progression of phagocytosis. Finally, the developing phagosome recruits intracellular protein such as Rho GTPase and Rab proteins which have roles in phagosome formation and maturation. The Rho GTPase proteins (Rac1, Rac2, and Cdc42) play an essential regulatory role in actin cytoskeleton organization (Hall, 1998) (**Figure 1.5**), while Rab proteins (Rab5 and Rab7) have a central regulatory role in the dynamic interactions between the phagosome and intracellular compartments (Flannagan *et al*, 2012) (**Figure 1.5**).

Lipids are key directors of phagocytosis. Indeed, changes in membrane lipid composition mark the beginning of phagosome formation. Upon activation of the phagocytic receptor, an increase in PI(4,5)P2 density in the lipid membrane results in formation of the phagocytic cup (Botelho *et al*, 2000; Scott *et al*, 2005; Minakami *et al*, 2010; Maxson & Grinstein, 2020). This altered abundance of PI(4,5)P2 facilitates activation of the Rho GTPases, Rac1, Rac2, and

Cdc42 proteins (Hoppe & Swanson, 2004a). The activated Rho GTPase proteins localize to different areas of the phagocytic cup. Cdc42 is activated at the leading margin of pseudopodia (Hoppe & Swanson, 2004b), Rac1 is activated throughout the entire nascent phagosome (Ikeda *et al*, 2017), and Rac2 is activated mainly at the base of the phagocytic cup (Park & Cox, 2009; Koh *et al*, 2005; Hoppe & Swanson, 2004a). Altogether, Cdc42, Rac1, and Rac2 participate in regulating pseudopod extension by activating the actin nucleation-promoting factor Wiskott–Aldrich Syndrome protein (WASp). In turn, WASp activates Arp2/3, a multi-subunit effector that catalyzes the nucleation of branched actin filaments necessary for pseudopod extension (Zalevsky *et al*, 2001; May *et al*, 2000; Higgs & Pollard, 2000; Rohatgi *et al*, 2000). As a result, pseudopods extend to engulf the phagocytic particle and form the phagosome (Figure 1.4).

The final step of phagosome formation is sealing of the vacuole by fusion of the pseudopods. Dynamin-2 GTPase protein plays a critical role in effective scission of the phagosome from the plasma membrane. Dynamin-2 assembles at the phagosome closure site into a ring-shaped polymer with contractile properties. It plays a central role as inhibition of dynamin activity reduces internalization (Marie-Anaïs *et al*, 2016; Mularski *et al*, 2021). In addition to Dynamin-2, myosin motor proteins such as Myosin X or Myosin IC help in this process by generating a contractile force on the phagocytic cup (Swanson *et al*, 1999; Cox *et al*, 2002; Barger *et al*, 2020).

1.1.2.2 Step 2: the early phagosome

Phagosomes need to go through a maturation process in order to eliminate microbes and apoptotic cells successfully. During maturation, phagosomes undergo biochemical modifications through a series of membrane fusion and fission events with early endosomes, late endosomes, and lysosomes. It is not yet clear whether phagosome membrane trafficking events involve a complete fusion with endosomal membranes or whether they represent transient and reversible fusion that define the “kiss-and-run” model (Desjardins, 1995; Duclos *et al*, 2000). Regardless of the exact mechanism, it is known that the phagosome becomes acidic, highly oxidative, and enriched with hydrolytic enzymes that facilitate cargo processing and destruction (Figure 1.5). Interestingly, phagosome maturation varies from one phagocytic cell to another depending on the nature of their cargo. For instance, dendritic cells have developed a mechanism to preserve antigens from the ingested particle in order to later

initiate adaptive immune responses (Blander & Medzhitov, 2006; Savina & Amigorena, 2007). Conversely, antigens derived from apoptotic corpses are quickly degraded and immunologically silenced to prevent inflammation or autoimmune disease (Ravichandran 2010).

The formation of early phagosomes is marked by the presence of proteins of the Rab family, which play a key role in the maturation process. The Rab proteins can direct vesicular traffic leaving and arriving from the phagosome (Kinchen & Ravichandran, 2008; Yeo *et al*, 2016; Gutierrez, 2013). For instance, Rab5 is generally considered a regulator of the initial fusion event which tethers early phagosomes to early endosomes (Stenmark, 2009; Vieira *et al*, 2003; Yuan & Song, 2020). Once Rab5 has reached the membrane, it associates with early endosome antigen 1 (EEA1) (Figure 1.5)(Christoforidis *et al*, 1999; McBride *et al*, 1999). Upon binding to Rab5, EEA1 assembles into macromolecular complexes on the phagosome membrane and binds to Syntaxin 13 (soluble NSF-attachment protein receptor, SNARE protein) (Collins *et al*, 2002; Dingjan *et al*, 2018). On the phagosome membrane, EEA1 functions as a bridge by tethering the early phagosome to incoming endocytic vesicles, whereas SNARE induces the formation of hairpin-like complexes between the phagosome and endocytic vesicles, reducing the free-energy barrier and promoting fusion of the two structures.

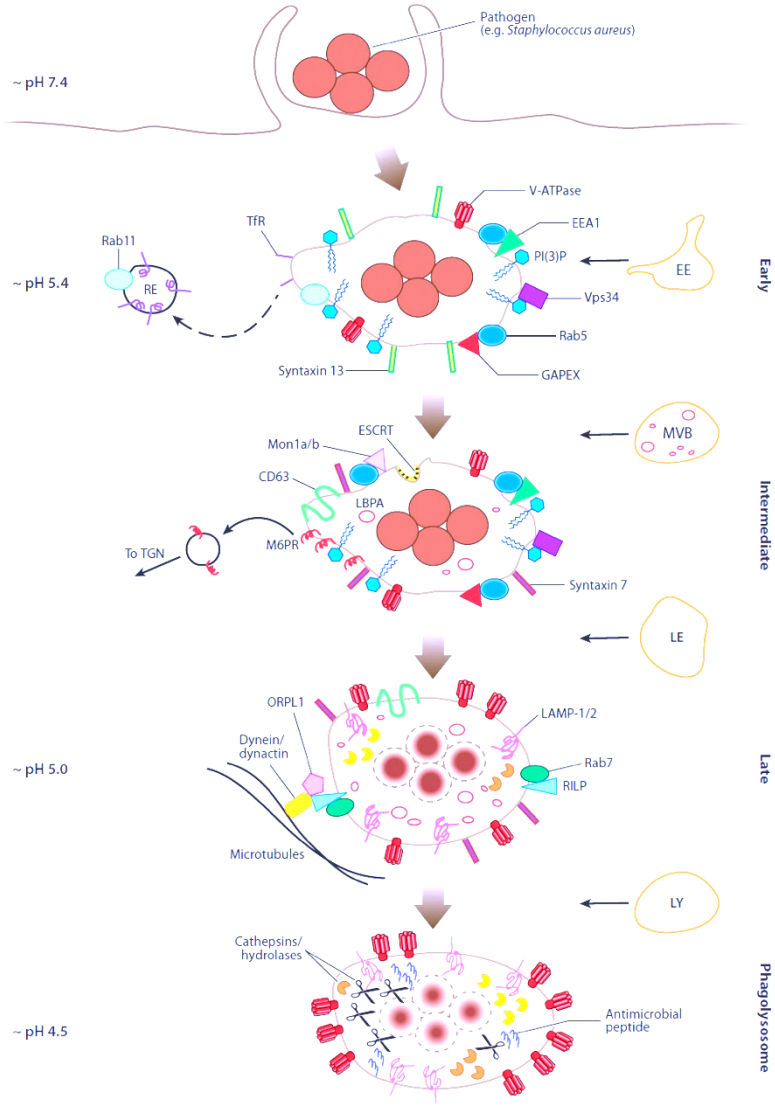

Figure 1.5 The phagocytic process in mammalian cells

Recognition of the target particle by the surface receptor leads to formation of the early phagosome. This initial plasma membrane derived vacuole does not have the ability to digest the internalized materiel. Newly formed phagosomes undergo a series of subsequent fission and fusion events with cellular organelles including the early endosome (EE), late endosome (LE) and lysosome (LY). Rab5 is a key regulator in the initial fusion events. Another GTPase, Rab7, is needed for late phagosome-lysosome fusion. Phagosome maturation culminates in the formation of a highly acidic phagolysosome. During this last step, the phagolysosome acquires important components for the final particle destruction step (lipases, proteases, nucleases). Endoplasmic Reticulum (RE). (Adapted from (Flannagan *et al*, 2012).

Additionally, Rab5 coordinates the membrane localization and activation of class III PI-3K vacuolar protein-sorting 34 (Vps34); which helps EEA1 attach to the cytosolic face of the phagosome (Marat & Haucke, 2016) (**Figure 1.5**).

We would expect that the repeated cycles of phagosome fusion with endocytic compartments would increase the phagosome size; however, the surface area of the phagosome remains

constant, and receptors present on the maturing phagosome are returned to the plasma membrane. The phagosome maintains homeostasis by a recycling pathway characterized by three mechanisms.

The first recycling pathway comprises the Rab4 and Rab11 proteins, which can associate with the early phagosome (Cox *et al*, 2000; Damiani *et al*, 2004; Leiva *et al*, 2006; Grant & Donaldson, 2009). Rab4 plays a role in fast recycling, where proteins from early endosomes are transported directly back to the plasma membrane. In contrast, Rab11 recycles components more slowly through the trans-Golgi network (TGN) (Lindsay *et al*, 2002) (Figure 1.5). The second recycling pathway involves the Vps26-Vps29-Vps35 complex and participates in recycling by retrieving phagosome components from the TGN (Baños-Mateos *et al*, 2019; Seaman, 2012). Finally, the third recycling mechanism is mediated by invagination of the phagosome membrane, leading to the formation of intraluminal vesicles (ILVs) (Lee *et al*, 2005). ILVs are formed through the action of a series of protein complexes, known as the endosomal sorting complex required for transport (ESCRT) (Raiborg & Stenmark, 2009).

1.1.2.3 Step 3: the late phagosome

The membrane and luminal composition of the maturing phagosome continue to change as it progresses to the late phagosome stage. As maturation proceeds, Rab5 disappears from the membrane and is replaced by Rab7. Rab5- Rab7 phagosome transitions are mediated by the guanine nucleotide exchange factor (GEF) Mon1-Ccz1. Mon1 binds to Ccz1 and the resulting Rab5–Mon1–Ccz1 complex recruits Rab7. Thus, by recruiting Rab7, the Mon1–Ccz1 complex plays an essential role in converting early phagosomes to late phagosomes (Poteryaev *et al*, 2010; Rink *et al*, 2005; Kinchen & Ravichandran, 2010). The exchange of Rab7 is also mediated by the HOPS (homotypic fusion and protein sorting) protein complex. Evidence suggests that Mon1 interacts directly with the core proteins of the HOPS complex. Thus, Rab5–Mon1–Ccz1 and the HOPS complex together fully complete the transition from early to late phagosomes (Pols *et al*, 2013; Langemeyer *et al*, 2020) (Figure 1.5 and Figure 1.6).

The Rab7 protein is essential for the maturation of the phagocytic vacuole; expression of dominant-negative Rab7 inhibits phagolysosome formation and acidification (Vieira *et al*, 2003). Rab7 assures the phagosome maturation together with two proteins, ORPL1 (oxysterol-binding protein-related protein1) and RILP (interacting lysosomal protein) (Johansson *et al*,

2007; Ma *et al*, 2018). Once ORPL1 and RILP associate with Rab7 on the late phagosome, they bind to the dynein-dynactin complex. The binding between Rab7 and dynein-dynactin complex brings the phagosome into contact with microtubules, which direct the convergence of the phagosomes and lysosomes (Harrison *et al*, 2003) (**Figure 1.5**). Once the phagosome and the lysosome are in close contact, VAMP7 (vesicle-associated membrane protein 7) and VAMP8, two SNARE proteins, complete the membrane fusion (Pryor *et al*, 2004).

Finally, lysosome-associated membrane protein 1 and 2 (LAMP-1 and LAMP2) also play a role in phagosome-lysosome fusion (Huynh *et al*, 2007). LAMPs are a family of glycosylated proteins that are present on the lysosomal membrane. LAMP proteins are incorporated through fusion of late endosomes with the phagosome membrane and play a fundamental role in regulating membrane fusion between the lysosome and phagosome (Huynh *et al*, 2007; Nguyen & Yates, 2021) (**Figure 1.5**).

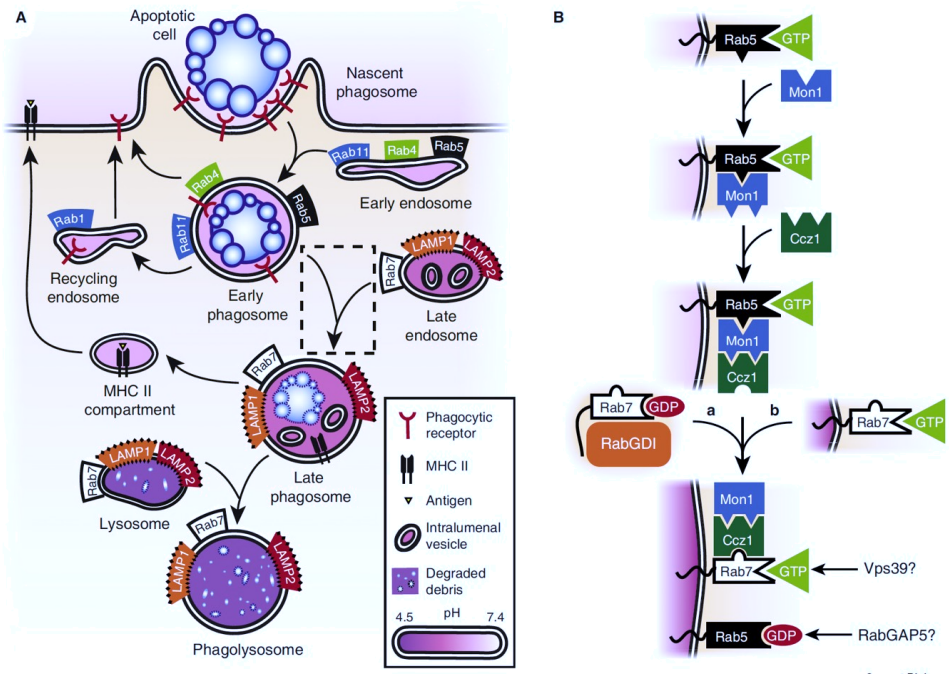

Figure 1.6 An overview of phagosome maturation

The phagosome transitions from an early phagosome to a late phagosome and ultimately to a phagolysosome as it fuses with organelles of the endocytic pathway, becoming progressively more acidic. Rab5 marks the early phagosome, from which Rab4 mediates fast recycling and Rab11 mediates slow recycling. Rab7 marks the late phagosome. Lysosomal-associated membrane glycoprotein 1 and 2 (LAMP1 and LAMP2) associate with late endosomes, late phagosomes, lysosomes and also phagolysosomes. Rab5- Rab7 phagosome transitions are mediated by the guanine nucleotide exchange factor (GEF) Mon1-Ccz1. Mon1 binds to Ccz1 and that the resulting complex Rab5–Mon1–Ccz1 is able to recruit Rab7. By recruiting Rab7, the Mon1–Ccz1 complex plays an important role in converting early phagosomes to late phagosomes. (Adapted from (Bohdanowicz & Grinstein, 2010)).

1.1.2.4 Step 4: the phagolysosome

The ultimate stage of the phagosome maturation process involves the fusion of late phagosomes with lysosomes to create the phagolysosome. The primary change happening at this stage of maturation is increased phagosome acidity (Geisow *et al*, 1981). Phagolysosome acidification occurs through accumulation of proton-pumping vacuolar ATPases (V-ATPases) on the membrane, which reduce the internal pH (Lukacs *et al*, 1991; Marshansky & Futai, 2008; Kissing *et al*, 2015). V-ATPase is a multimeric protein complex that translocates protons (H+) into the lumen of the phagosome using cytosolic ATP as an energy source. The V-ATP protein complex is composed of two functional subcomplexes, V1 and V0. The V1 subcomplex comprises eight subunits and mediates ATP hydrolysis**.** The V0 subcomplex constitutes the membrane pore through which protons are pumped using ATP (Colacurcio & Nixon, 2016; Wang *et al*, 2020). The resulting acidification of the late phagosome produces an essential digestive effect.

Additionally, the decreasing pH indirectly enhances the degradative capacity of the phagosome by activating proteolytic enzymes essential for protein degradation such as cathepsin D and L (Turk *et al*, 2012) (**Figure 1.5**). The proteolytic ability of the phagolysosome is enhanced by the presence of lysozymes and lipases, and of NADPH oxidase on the membrane. The activity of NADPH generates superoxide (O_2^-), which transforms into H_2O_2 and reacts with O_2 to generate reactive oxygen species (ROS). The presence of reactive oxygen species enhances the proteolytic ability of the phagolysosome (Winterbourn, 2008; DeCoursey, 2010). Phagosome maturation and acidification are thus crucial for an effective immune system. Pathogens have evolved strategies to circumvent phagosome maturation and persist in host cells. For instance, *Mycobacterium tuberculosis* arrests phagosome maturation at the early stage (Vergne et al.,2005), while *Salmonella* inhibits phagosome fusion with the lysosome (Buchmeier & Heffron, 1991).

1.2 Phagocytosis of apoptotic cells in *Drosophila*

The rapid and efficient phagocytic clearance of apoptotic cells, termed efferocytosis, is critical in maintaining tissue homeostasis (Fuch and Steller, 2011; Galluzzi et al., 2012). The

importance of efferocytosis in homeostasis is highlighted by many human diseases characterized by defective apoptotic cell clearance including atherosclerosis, chronic obstructive pulmonary disease, and systemic lupus erythematosus (Schrijvers *et al*, 2005; Shao & Cohen, 2011).

Highly complex and redundant phagocytic components characterize the mammalian phagocytic system. Due in part to this, the specific role of each protein remains unresolved. Therefore, in the last decades, researchers have expanded the study of phagocytosis to genetically tractable model organisms, such as the fruit fly *Drosophila. Drosophila* phagocytic cells such as macrophages and glial cells share functional features with mammalian phagocytic cells (Shklover *et al*, 2015). As such, *Drosophila* is a suitable model to dissect the process of efferocytosis. This chapter summarizes apoptotic clearance pathways in *Drosophila* and discusses the physiological outcomes and consequences of this process.

1.2.1 Professional and non-professional phagocytes in *Drosophila*

In *Drosophila*, the clearance of apoptotic cells is mediated by two types of phagocytes: professional (globally called macrophages) and non-professional (tissue-resident neighboring cells) (Shklover *et al*, 2015).

Blood cells named plasmatocytes or macrophages function as professional phagocytes. Furthermore, recent studies show that embryonic and larval macrophages can be classified in subpopulations that have varying phagocytic ability (Shin *et al*, 2020; cattenoz 2020 phagocytosis - Cerca con Google; Zizzo *et al*, 2012).

Drosophila macrophages develop during two spatially and temporally distinct hematopoietic waves, named embryonic and lymph gland hematopoiesis (Banerjee et al., 2019). The first hematopoietic wave originates from the embryonic procephalic mesoderm during embryogenesis (Holz *et al*, 2003). During the subsequent larval stage, these embryonic macrophages multiply in specific local environments, the hematopoietic pockets (Makhijani *et al*, 2017; Petraki *et al*, 2015; Markus *et al*, 2009; Leitão & Sucena, 2015). At the end of the larval stage, the second wave of hematopoiesis occurs in the lymph gland, a specialized hematopoietic organ. The lymph gland acts as a reservoir of macrophages and ruptures at the onset of pupariation, releasing differentiated macrophages into circulation (Rugendorff *et al*,

1994; Lan *et al*, 2020; Yu *et al*, 2018). Macrophages in the adult stage consist of a mixed population derived from the embryonic and the larval stages (Holz *et al*, 2003).

Macrophages play a crucial role in efferocytosis throughout *Drosophila* development, including during embryogenesis, metamorphosis, and adult emergence. However, starting from the end of embryogenesis tissues rely on their resident non-professional phagocytes, such as glial cells, epidermal cells, and ovarian follicle epithelial cells, to perform phagocytosis (Shklover *et al*, 2015; Serizier & McCall, 2017) .

Glial cells represent the second major phagocytic population in *Drosophila.* Glial cells are responsible for clearing apoptotic cells in the nervous system during development (Kurant, 2011) and are characterized mainly by their morphology and proximity to neurons in the central nervous system (CNS). In the CNS, different types of glial cells have specific spatial organization. The first layer of glial cells, associated with the surface of the CNS, is composed of a subset of cells termed perineurial glia (Figure 1.7). Perineural glia cells and macrophages secrete a dense carbohydrate-rich substrate, covering the CNS and acting as a chemical and physical barrier (Leiserson *et al*, 2000). Under the perineurial glia, the subperineural glial cells cover the entire CNS and build the blood-brain barrier (Schwabe *et al*, 2005). Deeper in the CNS, three specialized glial subtypes are associated with neurons: the cortex, the ensheathing glia, and the astrocytes. Among these cell types, astrocytes have a crucial role in phagocytosis during metamorphosis (Hakim *et al*, 2014; Tasdemir-Yilmaz & Freeman, 2014; Freeman, 2015). Non-professional phagocytes differ from macrophages in many aspects, including in cell morphology and the phagocytic receptors they present. Nevertheless, particle uptake and signaling machinery are similar across these two cell types.

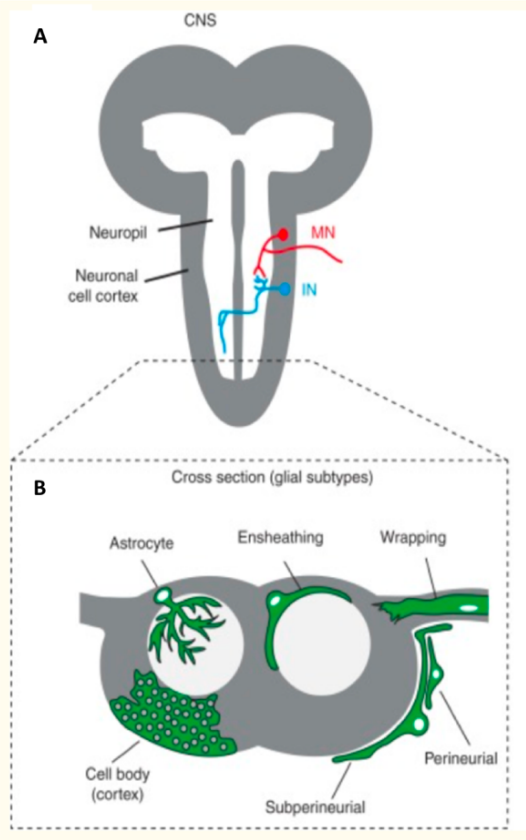

Figure 1.7 Subtypes, positions and morphology of *Drosophila* glia
(A) Overview of the *Drosophila* larval central nervous system (CNS). The neuronal cell cortex (in dark gray) is composed of neuronal and glial cell bodies. CNS synaptic contacts between neurons are found within the neuropil (in light gray). Interneurons (IN) in blue maintain all projections within the neuropil. Motoneurons (MN) in red extend axon terminals outside the CNS. (B) Cross-sectional view of glial subtypes (green) (adapted from (Freeman, 2015)).

1.2.2 Apoptosis in *Drosophila*

Professional and non-professional phagocytes are able to recognize and uptake apoptotic cells. In *Drosophila* apoptotic cells derive from a genetically regulated process called programmed cell death (PCD). Apoptosis is the canonical form of PCD (Kerr *et al*, 1972) characterized by cell shrinkage, chromatin fragmentation, and membrane blebbing (Denton *et al*, 2013). However, what defines apoptosis is the activation of cysteine proteases named caspases, which are divided into initiator caspases and effector caspases (Fuchs & Steller, 2011; Feinstein-Rotkopf & Arama, 2009).Initiator caspases initiate the apoptotic signal while effector caspases carry

out proteolysis that results in apoptosis. In *Drosophila*, the first apoptotic cells appear at the embryonic stage 11 in the procephalic region. However, apoptosis quickly spreads to the other segments and reaches a peak level at stages 12 and 13 when nearly all segments contain apoptotic cells (Lin *et al*, 2009). Apoptotic events continue during the larval stage and are critical for development of the nervous system (Pinto-Teixeira *et al*, 2016). Finally, a third massive wave of apoptosis controlled by the steroid hormone ecdysone occurs during the larval-pupal transition (Nicolson *et al*, 2015).

Like in mammals, the regulation of apoptosis in *Drosophila* is highly plastic and involves a wide variety of intracellular regulatory proteins that transduce signals from both inside and outside the cell (Denton *et al*, 2013; Galluzzi *et al*, 2012; Kroemer *et al*, 2009). Regulation of cellular apoptosis relies on inhibitor proteins called IAPs (inhibitor of apoptosis protein), which maintain cell survival (Figure 1.8) (Huh *et al*, 2007). Among *Drosophila* IAPs, the protein Diap1 plays a critical role in regulating apoptosis. In normal conditions, Diap1 promotes degradation of the initiator caspase Dronc (Meier *et al*, 2000; Denton *et al*, 2013). When apoptosis is genetically programmed, "IAP antagonists" such as Reaper (Rpr), Head involution defective (Hid) and Grim promote the degradation of Diap1. As such, embryos homozygous for the H99 deficiency (which deletes the Rpr, Hid, and Grim genes) fail to undergo apoptosis and consequently die (Miura, 2012).

In brief, apoptosis starts with the activation of Rpr, Hid, and Grim, which inactivate Diap1. This allows the initiator caspase Dronc to activate the effector caspases Drice and Dcp-1. Finally, activated Drice and Dcp-1 cleave many cellular substrates causing the ordered dismantling of the cell (Figure 1.8).

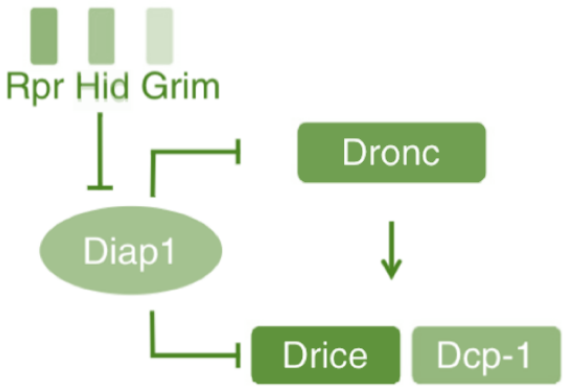

Figure 1.8 The core components of cell death machinery in *Drosophila*
Activation of the initiator caspase Dronc acts to transduce the death signal by cleavage and activation of effector caspases, Drice and Dcp-1. Activated effector caspases then cleave many cellular substrates causing ordered dismantling of the cell. Diap1 is essential for cell survival by binding to and inhibiting Dronc and Drice. During apoptosis Rpr, Grim and Hid bind Diap1, promoting its ubiquitination and degradation, thereby alleviating the block on caspase activation (adapted from (Denton *et al*, 2013).

1.2.3 Phagocytic Receptors in *Drosophila*

Professional and non-professional phagocytes recognize apoptotic cells through dedicated receptors present on the membrane of phagocytic cells. While some may be direct phagocytic receptors, others may indirectly affect phagocytosis or be involved in the downstream steps of phagocytosis. In *Drosophila*, studies have identified four phagocytic receptors that recognize and bind apoptotic cells: Croquemort, Integrin, Draper, and Simu. The following paragraph will provide a critical summary of these phagocytic receptors in *Drosophila* (Figure 1.9 and Figure 1.10).

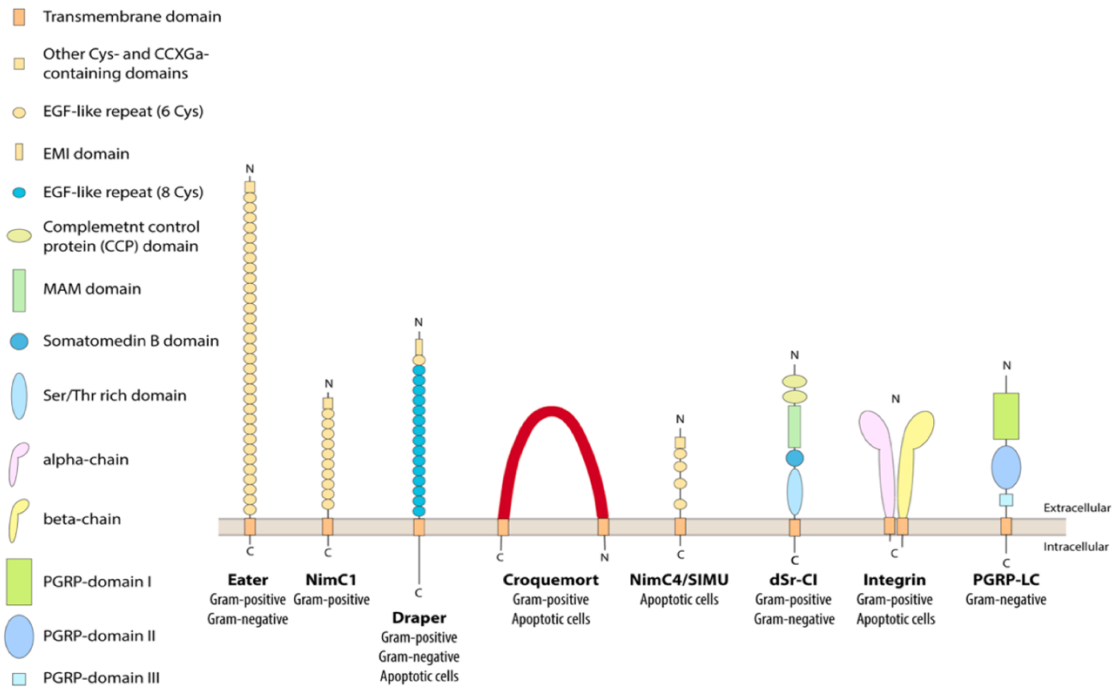

Figure 1.9 Plasma-membrane phagocytic receptors in *Drosophila*
Graphical illustration of *Drosophila* phagocytic receptors involved in microbe and apoptotic cell engulfment. Intergin, Croquemort, NimC4 (SIMU) and Draper are the three main receptors involved in the phagocytosis of apoptotic cell (adapted from (Melcarne *et al*, 2019a)).

1.2.3.1 Croquemort

The Croquemort receptor shares 23% identity with the mammalian receptor CD36, which has been characterized as a receptor for apoptotic cells (Savill *et al*, 1992) (Figure 1.9). Croquemort was first identified on *Drosophila* embryonic hemocytes as a phagocytic receptor of apoptotic cells by Nathalie Franc in 1996. Subsequent studies produced conflicting results on the affinity of Croquemort to apoptotic cells and its underlying molecular mechanisms. Croquemort is also expressed on epithelial cells, where it contributes to clearance of degenerating neurites (Han et al., 2014). However, in this phagocytic context, Croquemort only plays a role in phagosome maturation; it does not participate in the uptake of degenerating neurites (Guillou *et al*, 2016; Han *et al*, 2014; Meehan *et al*, 2016). Finally, a study showing that silencing *croquemort* in plasmatocytes blocks lipid uptake suggested that Croquemort is also involved in acquiring lipids (Woodcock *et al*, 2015; Yeung *et al*, 2006). Considering that lipids play a crucial role in phagocytosis, we can hypothesize that the involvement of Croquemort lipid scavenging may influence the phagocytic process.

1.2.3.3 Integrins

Integrins are conserved receptors involved in many cellular processes, such as cell motility and cell spreading (Moreira *et al*, 2013; Ribeiro *et al*, 2014) (Figure 1.9). All integrins are heterodimers of non-covalently associated α and β subunits (Campbell & Humphries, 2011). For example, *Drosophila* expresses five α subunits (PS1-5) and two β subunits (βPS and $\beta\nu$) (Brown, 2000). In addition to its role in cell adhesion, the $\beta\nu$ integrin was shown to mediate phagocytosis of apoptotic cells during embryogenesis (Nagaosa *et al*, 2011). RNAi studies suggested that the heterodimer $\beta\nu/\alpha$PS3 is required for effective phagocytosis of apoptotic cells in *Drosophila* embryos (Nonaka *et al*, 2013). αPS3/βPS are also expressed in epithelial follicle cells of the *Drosophila* ovary and engulf germline debris. As such, integrins fulfil a variety of roles depending on tissue, ranging from cell spreading to phagocytosis of apoptotic cells (Meehan *et al*, 2016).

1.2.3.4 Draper and Simu

Draper is an evolutionarily conserved receptor with homologs in *C.elegans (*CED-1), humans (MEGF10), and mice (JED1) (Mangahas & Zhou, 2005; Hamon *et al*, 2006). In *Drosophila*, Draper plays a central role in all forms of apoptotic cell clearance, either by professional or nonprofessional phagocytes (Freeman *et al*, 2003; Manaka *et al*, 2004; Fullard *et al*, 2009) (Figure 1.9). The *draper* gene encodes three isoforms, Draper I, II, and III, which vary in the number of extracellular EGF-like repeats and the sequences within the intracellular portion of the protein. In the Draper I isoform, the immunoreceptor tyrosine-based activation motif (ITAM) sequence plays a central role in the receptor signalization (Logan *et al*, 2012). When Draper is activated, the kinase Src42A (belonging to the Src family of protein tyrosine kinases) phosphorylates the intracellular ITAM motif (Ziegenfuss *et al*, 2008). Phosphorylation of ITAM allows the tyrosine kinase Shark to bind the intracellular domain. The Draper-Shark complex then plays two distinct roles in phagocytosis. First, it leads to the activation of Rac-1 which results in rearrangement of the actin cytoskeleton and allow internalization of apoptotic cells (Ziegenfuss *et al*, 2012). Second, the Draper-Shark complex induces the activation of the Stat92E transcription factor, which up-regulates *draper* expression. As such, the Draper-Shark complex regulates *draper* expression (Doherty *et al*, 2014).

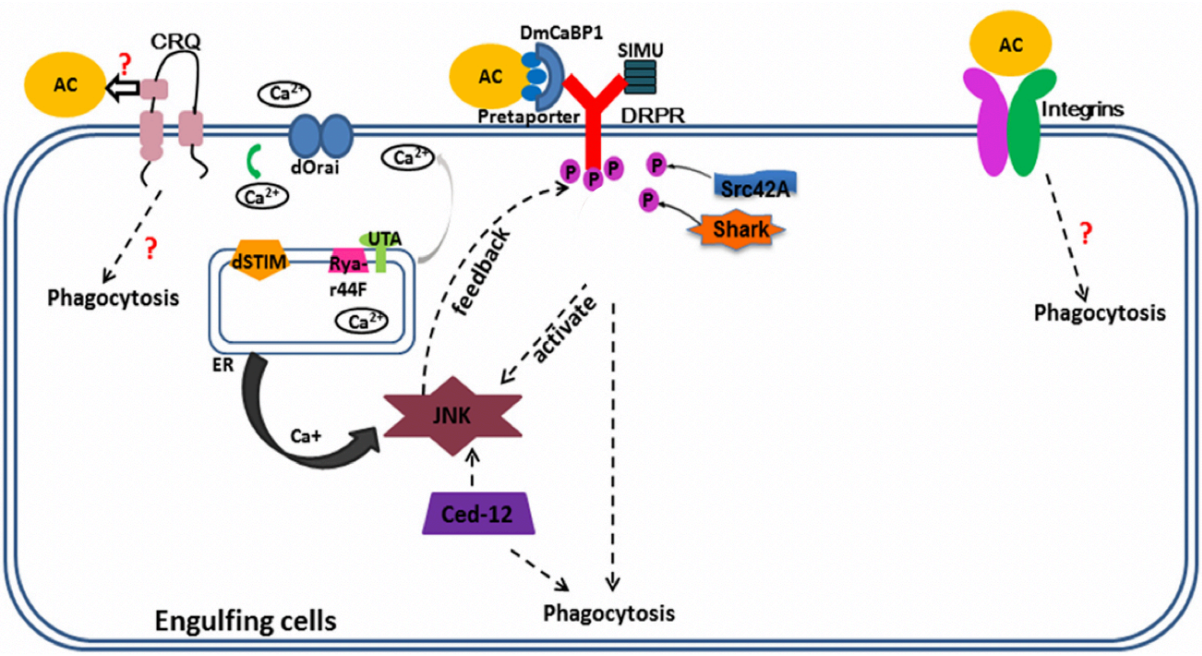

Figure 1.10 Overview of phagocytic receptors and key components playing a role in corpse recognition, internalization and processing

CRQ (Croquemort), DRPR (Draper) and Integrins are three receptors located at the plasma membrane. CRQ is expressed mainly in macrophages; its ligand and downstream signaling have not been clearly studied. DRPR (Draper), is expressed mainly in macrophage and in glial cells. Integrin functions in epithelial cells, follicle cells and hemocytes to engulf cell corpses. The Draper ligands represented here are DmCaBP1 and Pretaporter. Phosphorylated Draper interacts with Ced-6 thus elevates Jun N-terminal kinase (JNK) signaling and maintain Ca^{2+} homeostasis. JNK promotes Drpr enrichment both in glia and follicular epithelia (under Ced-12 activation), (adapted from (Zheng *et al*, 2017)).

The second isoform Draper II is required to terminate the phagocytic response. Instead of the ITAM sequence, Draper II has an immunoreceptor tyrosine-based inhibition motif (ITIM) sequence. At the end of the phagocytic event, the ITIM sequence recruits the protein tyrosine phosphatase Corkscrew which dephosphorylates the ITAM motif of Draper I. As such, Corkscrew prevents Shark from associating with Draper I and restores the basal expression level of *draper* (Logan *et al*, 2012; Underhill & Goodridge, 2007). In summary, Draper I is essential for phagocytosis, whereas Draper II is necessary for terminating the response. The function of the Draper III isoform remains unknown.

Draper is thought to work as a recognition receptor by binding different “eat me" signals situated on the surface of dying cells. The best characterized “eat me” signals are PS, the calcium-binding protein 1 (DmCaBP1), and the protein Pretaporter (Kuraishi *et al*, 2007; Okada *et al*, 2012a; Tung *et al*, 2013) (Figure 1.10). Both DmCaBP1 and Pretaporter proteins reside in the endoplasmic reticulum (ER) of healthy cells and are translocated to the membrane of cells after the induction of apoptosis (Okada *et al*, 2012b; Kuraishi *et al*, 2009). That Draper binds to multiple apoptotic ligands suggests that synergy may be necessary for recognition. Alternatively, different dying cells may express different patterns of “eat me” signals, and as such induce a context-specific phagocytic response (Birge & Ucker, 2008). Therefore, Draper may work in synergy with other receptors and activate different downstream signaling cascades depending on the “eat me” signal.

In addition to its role in apoptotic cell recognition, the Draper receptor has a role in corpse processing: phagocytic cells lacking *draper* cannot properly eliminate phagocytic cargo. For instance, in *draper* mutant embryos, glial cells cannot eliminate dead neurons that have been phagocytosed (Kurant *et al*, 2008b). Furthermore, macrophages of third instar larvae lacking Draper are deficient in phagosome maturation, where the phagosome cannot fuse to the

lysosome (Petrignani *et al*, 2021). However, Draper is not universally required for phagosome maturation. Indeed, in the *Drosophila* adult brain, Draper is mainly involved in the uptake of severed axons rather than in phagosome maturation (MacDonald *et al*, 2006).

SIMU (NimC4) is considered a tethering receptor that binds to apoptotic cells through PS recognition (Kurant *et al*, 2008b; Shklover *et al*, 2015), (**Figure 1.9 and Figure 1.10**). SIMU is expressed on macrophages and glial cells during embryogenesis and during the first days of adult life. In combination with Draper, this receptor plays a central role in phagocytosis of apoptotic cells. As SIMU lacks an intracellular region, it interacts with Draper to initiate phagocytosis. To date, the direct interaction between Draper and SIMU has not been demonstrated (Kurant *et al*, 2008a).

1.2.4 Efferocytosis during *Drosophila* development

The clearance of apoptotic cells by phagocytes is a critical event during the development of all multicellular organisms. In *Drosophila*, non-professional phagocytes including glial cells, epithelial cells, and follicle cells play a crucial role in removing apoptotic cells throughout animal development (**Figure 1.11**). Each phagocytic event presents some variables, including the nature of the phagocytic receptor, the recognition of the apoptotic cells, and the phagosome maturation process. This paragraph will describe three examples of phagocytic events occurring during *Drosophila* development, illustrating differences and similarities between phagocytic cell types.

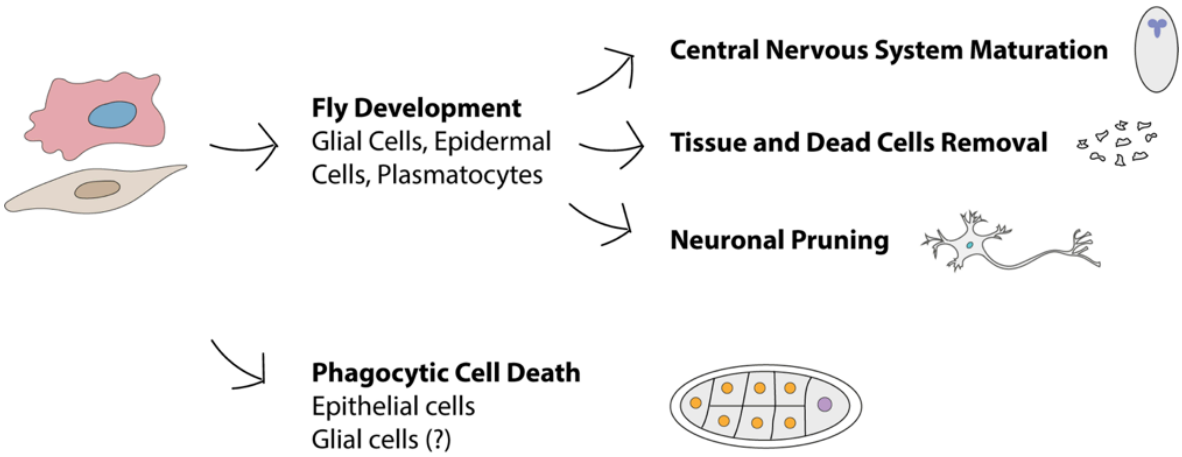

Figure 1.11 Physiological roles of phagocytosis in *Drosophila*
Macrophage-like plasmatocytes (red cell) and non-professional phagocytes (brown cell) phagocytose apoptotic cells during development. During development, phagocytosis represents a key determinant for remodeling and shaping organs. Starting at embryogenesis, glial cells play a fundamental role in central nervous system maturation by removing apoptotic neurons and pruned neuronal branches. During the larval stage, epidermal cells play an important role in neuronal pruning. Finally, in the *Drosophila* ovary, evidence supports the existence of phagocytic cell death, where epithelial follicle cells surrounding the nurse cells induce their death (adapted from (Melcarne *et al*, 2019a).

1.2.4.1 Glial phagocytosis during *Drosophila* nervous system maturation

During the development of the nervous system, the generation of unwanted surplus cells is controlled by apoptosis and subsequent phagocytic clearance. In parallel to the adjustment of neuron number, pruning and removal of excessive neuronal branches shapes the central nervous system in both vertebrates and invertebrates (Koester & O'Leary, 1994; Tissot & Stocker, 2000). In *Drosophila*, phagocytic glial cells eliminate surplus neurons and neuronal branches present in the nervous system during embryogenesis, metamorphosis, and in the emerging adult (Rogulja-Ortmann *et al*, 2007; Tissot & Stocker, 2000).

During embryogenesis, glial cells remove up to 30% of the total number of neurons, which undergo apoptosis (Rogulja-Ortmann *et al*, 2007; Kurant *et al*, 2008a). Glial phagocytosis relies on *simu* and *draper,* whose expression is controlled by the transcription factors Glial Cells Missing (Gcm) and Reversed Polarity (Repo) (Shklyar *et al*, 2014). SIMU recognizes the PS on apoptotic neurons and initiates engulfment, whereas Draper participates in degradation of the phagocytic cargo. However, no clear signaling pathway acting downstream activation of both receptors SIMU and Draper is yet characterized (Freeman *et al*, 2003; Kurant *et al*, 2008a; Shklyar *et al*, 2014).

During metamorphosis, neuronal changes are characterized by neuronal pruning, which consists of the removal of excessive neuronal branches and dying neurons, and synapse clearance. Interestingly, Draper is necessary for efficient neuronal phagocytosis (Awasaki *et al*, 2006; Kurant *et al*, 2008a; Logan *et al*, 2012; Manaka *et al*, 2004; Ziegenfuss *et al*, 2008). Draper activates the JNK pathway in the astrocytes and ensheathing glia, which triggers the removal of apoptotic neurons (Hilu-Dadia *et al*, 2018). On the contrary, SIMU, although highly expressed at this stage of development, is not present in glia but instead on macrophages

outside the CNS. The third stage of neuronal elimination occurs in emerging flies. In this context, neurons themselves seem to play a role in the regulation of phagocytosis. Indeed, it has been suggested that dying neurons can induce proliferation of the surrounding glia, which then participate in their engulfment (Kato *et al*, 2009). This process is essential for homeostasis of the brain tissue. In the absence of *draper* animal lifespan is reduced, and the CNS accumulates apoptotic bodies (Etchegaray et al.,2016) . Phagocytosis of dead cells, specifically neurons, is generally thought to be a beneficial mechanism. However, recent advances have shed light on specific mechanisms where glial phagocytosis of live neurons, or "phagoptosis", induces death of living cells (Brown & Neher, 2012).

In summary, glial phagocytosis is essential during *Drosophila* development. However, it must be tightly regulated for proper brain function. Defects in glial phagocytosis can lead to accumulation of dead neurons in the brain, which can cause secondary necrosis. Conversely, excessive glial phagocytosis can lead to excessive removal of healthy neurons.

1.2.4.2 Peripheral dendrite clearance by epidermal cells

During larval development, the formation of a functional neuronal system relies on the pruning of dendrites and axons. In this context, neurites often degenerate on-site and must be promptly removed to facilitate neurite regrowth and avoid inflammatory responses (Han *et al*, 2014) (Figure 1.12). Degenerating dendrites are efficiently removed by epidermal cells through the activity of the phagocytic receptor Draper. Once engulfed by phagocytes, neuronal debris undergoes degradation through phagosome maturation.

Interestingly, in this phagocytic step, a member of the CD36 family of receptors, Croquemort, is required for phagosome maturation. Croquemort loss-of-function leads to homotypic phagosome fusion (fusion between phagosomes), leading to many large vesicles that fail to degrade. As homotypic fusion rarely occurs during phagocytosis, these observations implicate Croquemort in prevention of this abnormal event. As such, Croquemort may participate in different steps of phagocytosis, including phagosome maturation (Han *et al*, 2014).

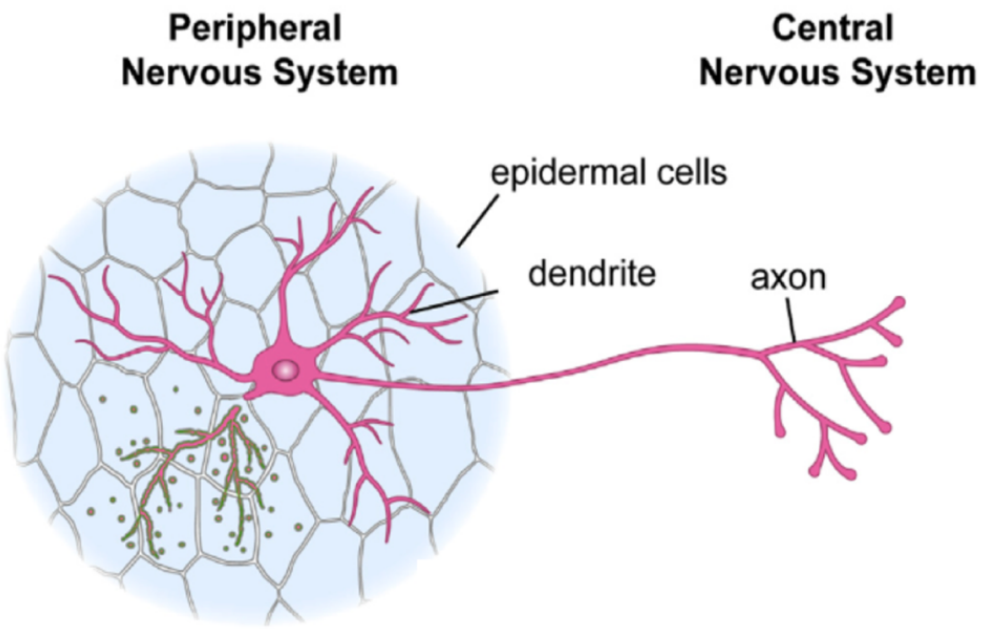

Figure 1.12 Phagocytic clearance of degenerating dendrites or axons

Drosophila dendritic arborization neurons extend dendritic arbors underneath the larval epidermis. During dendrite remodeling, epidermal cells function as the primary phagocytes that break down and engulf dendrites. Phosphatidylserine (in green) is dynamically exposed on degenerating dendrites during developmental pruning (adapted from Han et al.,2014).

1.2.4.3 Nurse cell clearance by follicular cells in *Drosophila* ovary

The *Drosophila* ovary is an excellent model for studying diverse types of programmed cell death and engulfment by non-professional phagocytes such as epithelial cells. The general structure of the ovary comprises 15-20 strings of units. These strings are called ovarioles, and the units are a series of progressively developing egg chambers (Figure 1.13) (Lebo & McCall, 2021). Once the egg chamber develops, it moves to the posterior end of the ovariole. At this stage, the egg chamber comprises three types of cells: the nurse cells, the oocyte, and the follicle cells. In the egg chamber, the cells are organized such that the oocyte is situated in the most posterior region. As a result, the oocyte is adjacent to 15 nurse cells, and a single layer of follicle cells encapsulates the entire germline (Etchegaray *et al*, 2012; Timmons *et al*, 2016; Serizier & McCall, 2017).

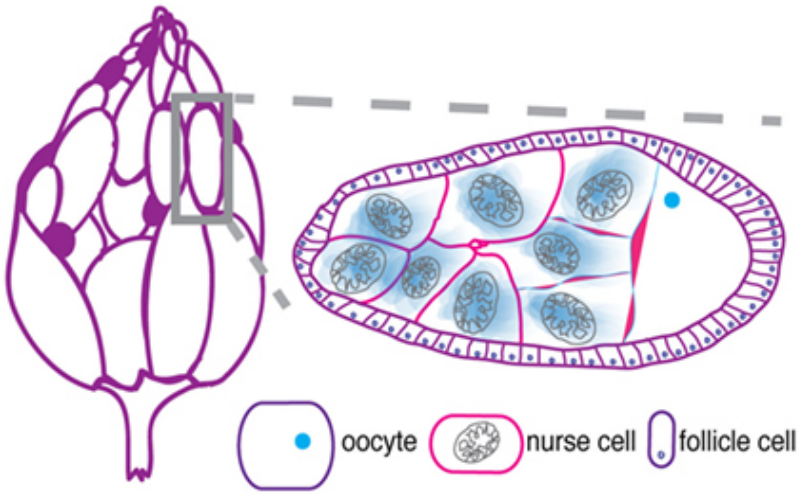

Figure 1.13 The *Drosophila* ovary. The ovary comprises strands of developing eggs called the egg chambers
Developed egg chambers (grey box), are composed of three main cell types: nurse cells, the oocyte and follicle cells. The single layer of follicle cells that encapsulate the entire germline are able to phagocytose the nurse cells once they are going through cell death (adapted from (Serizier & McCall, 2017)).

At the end of oogenesis, a significant cell death event occurs in the egg chamber when the 15 nurse cells die to produce a fully developed oocyte. In the ovary, caspase-mediated apoptosis plays only a minor role in the death of the nurse cells, as the absence of caspases does not significantly block cell death during late oogenesis (Timmons *et al*, 2016). Instead, an alternative death pathway orchestrated by the surrounding phagocyte follicle cells eliminates the nurse cell through non-autonomous cell death (Timmons *et al*, 2016; Serizier & McCall, 2017; Lebo & McCall, 2021). To induce the cell death, follicle cells invade the space between the nurse cells. This cytoplasmic invasion triggers the acidification and degradation of the nurse cells. Indeed, the acidification of the nurse cell originates from contact regions between nurse cells and the follicle cells. To date, the Draper receptors and the MAP kinase Basket (a component of the JNK pathway) are known to be necessary for nurse cell acidification. Once nurse cells initiate cell death through nuclear permeabilization, they are promptly removed by the follicle cells.

Draper plays a role in the phagocytic events following cell death. Draper on follicle cells acts as a critical engulfment receptor that recognizes the nurse cell “eat me” signals (Serizier & McCall, 2017). Once the Draper receptor is activated, it induces an intracellular signal that triggers Rac1 and activates the JNK signaling pathway to regulate phagocytosis. Thus, while the follicle cells

start to engulf the cell corpse, the JNK signaling pathway can modulate the expression of *draper* to increase the efficiency of the phagocytic process (Timmons *et al*, 2016).

As the clearance process continues, Draper remains associated with the phagosome membrane that surrounds the cell corpse. Draper becomes enclosed in the Rab-5 positive phagosome and stays on the phagosome until fusion with the lysosome. Thus, Draper interacts with the corpse processing machinery within the follicle cells, leading to phagosome acidification. In the absence of Draper, engulfment is greatly reduced, vesicles containing corpses accumulate, and acidification fails to occur (Timmons *et al*, 2016).

This alternative model to study phagocytosis highlights surprising complexity and variability in the phagocytic process. More specifically, we observed that a phagocytic receptor such as Draper can play three different roles in efferocytosis, participating in cell death, engulfment, and in phagosome maturation. This highlights the additional roles of receptors in phagocytosis.

1.3 Objectives of the present PhD thesis

Draper and SIMU are part of a large family of genes called the Nimrod family. Several members of the Nimrod superfamily were claimed to function as phagocytic receptors for apoptotic cells or bacteria, which indicates an essential role of this gene superfamily in the innate immune response of *Drosophila*. Also, some Nimrod genes are up-regulated upon sterile inflammation or immune challenge in vivo, suggesting a co-regulation in the innate immune response (Irving *et al*, 2005; Petrignani *et al*, 2021; Melcarne *et al*, 2019b).

The Nimrod superfamily is an evolutionarily conserved gene cluster that also occurs in the genomes of insects including *Anopheles gambiae* and *Apis mellifera.* In *Drosophila*, most of the Nimrod genes are located on the 2nd chromosome, except for *draper* and *eater* which are located on the third chromosome. All the genes of the Nimrod superfamily encode a protein containing various numbers of NIM repeats. The NIM domain is a particular type of epidermal growth factor (EGF) repeat, which often functions in coagulation, adhesion, and receptor-target interaction (Somogyi *et al*, 2010, 2008).

All the Nimrod members have a signal peptide followed by an N-terminal motif of different type and a short conserved CCxGY motif immediately preceding the first NIM domain. Furthermore, we can divide the Nimrod superfamily into two groups: (i) Draper-type proteins

(NimA, Draper*)* that have only one copy of the NIM motif, and (ii) proteins containing many NIM repeats (‘‘poly-NIM’’ proteins). Interestingly, the Draper-type protein gene group has a wide taxonomic distribution, whereas the poly-NIM proteins have been identified only in insects (Figure 1.9 and Figure 1.14) (Somogyi *et al*, 2010, 2008). Based on additional features, the poly-NIM group can be divided into two subgroups: Nimrod C- and Nimrod B-types. The products of *Nimrod C-type* genes (e.g., *Nimrod C1-4* and *eater*) are transmembrane proteins. In contrast, Nimrod B-type genes (e.g., nimrod B1-5) lack a transmembrane domain (Figure 1.14).

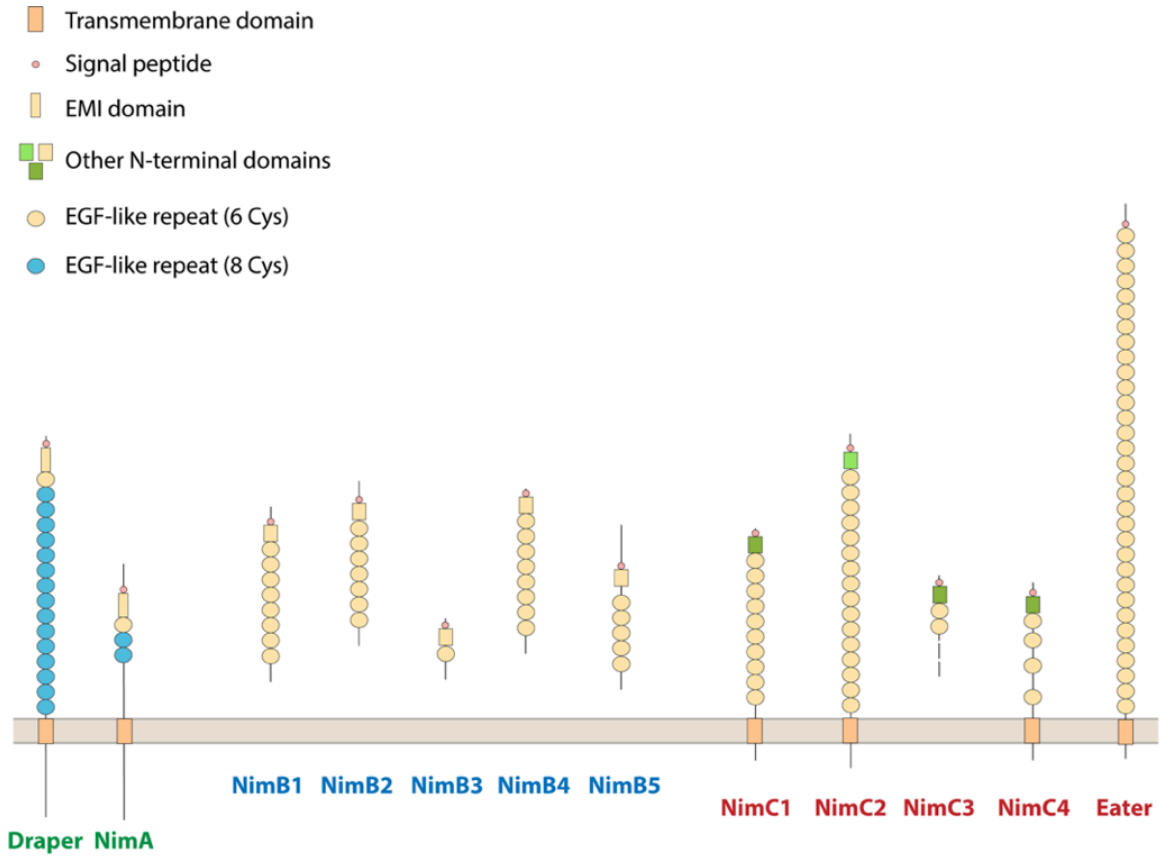

Figure 1.14 The *Drosophila* Nimrod family

The Nimrod family is composed of receptors characterized by the repetition in their protein sequence of a specific EGF-like repeat called NIM. Based on these standard structural features, we can classify the Nimrod superfamily into three groups: the NimA (in green), the NimB (in blue) and the NimC group (in red). All the members of the Nimrod family are localized on the second chromosome, except *draper* and *eater,* which are localized on the third chromosome (adapted from Melcarne et al.,2019).

The role of Nimrod B-type proteins (NimB1-NimB5) in immunity has never been investigated. In this context, this thesis aims to characterize the role of NimB5, NimB4, and NimB1 in *Drosophila* hematopoiesis and phagocytosis.

The first part of this thesis (Chapter 2) focuses on the role of NimB5 in hematopoiesis and cellular adhesion. In this work, we address the potential signaling function of NimB5 in *Drosophila* hemocyte hematopoiesis. Our work showed that NimB5 is produced by the fat body and regulates plasmatocyte adhesion and proliferation rate. Furthermore, NimB5 is induced upon starvation and adjusts plasmatocyte number to the metabolic state of the host. Thus, Nimrod B5 is part of a regulatory mechanism tailoring investment in the immune system to nutrient availability. Our work on NimB5 was published in The FEBS Journal (Ramond *et al*, 2020).

The second part of the thesis (Chapter 3) focuses on the role of NimB4 in the phagocytosis of apoptotic cells. Here, we reveal its crucial role in the clearance of apoptotic cells. We show that *NimB4* is expressed by macrophages and glial cells, the two main types of phagocytes in *Drosophila*. Our study points to the role of NimB4 in phagosome maturation, more specifically in the fusion between the phagosome and lysosomes. We propose that similar to bridging molecules, NimB4 binds to apoptotic corpses to engage a phagosome maturation program dedicated to efferocytosis. The results of this work were published in EMBO Reports (Petrignani *et al*, 2021).

The third objective of this thesis (Chapter 4) is to characterize the role of NimB1 in the *Drosophila* cellular immune response. Our work showed that *NimB1* is expressed mainly in hemocytes and regulates hemocyte number. Additionally, NimB1 shares several characteristics with NimB4, including binding to apoptotic cells. As such, we hypothesize that it has a similar function in phagocytosis of apoptotic cells. However, the exact role of NimB1 in phagocytosis is still unclear, and additional work is necessary to understand if NimB1 plays a role in the uptake of apoptotic cells or phagosome maturation. Therefore, the results of this fourth chapter of the thesis are presented as a draft.

Chapter 2

The adipokine NimrodB5 regulates peripheral hematopoiesis in *Drosophila*

Note: This chapter is based on the published article: "The adipokine NimrodB5 regulates peripheral hematopoiesis in *Drosophila*. 2020, FEBS"

Authors: Elodie Ramond, Bianca Petrignani, Jan Paul Dudzic, Jean-Philippe Boquete, Mickaël Poidevin, Shu Kondo, and Bruno Lemaitre

Contributions of Bianca Petrignani: Conducted the revision of the paper, performed FACS, qPCR, hemocyte imaging assays.

2.1 Abstract

In animals, growth is regulated by the complex interplay between paracrine and endocrine signals. When food is scarce, tissues compete for nutrients, leading to critical resource allocation and prioritization. Little is known about how the immune system maturation is coordinated with the growth of other tissues. Here, we describe a signaling mechanism that regulates the number of hemocytes (blood cells) according to the nutritional state of the *Drosophila* larva. Specifically, we found that a secreted protein, NimB5, is produced in the fat body upon nutrient scarcity downstream of metabolic sensors and ecdysone signaling. NimB5 is then secreted and binds to hemocytes to down-regulate their proliferation and adhesion. Blocking this signaling loop results in conditional lethality when larvae are raised on a poor diet, due to excessive hemocyte numbers and insufficient energy storage. Similar regulatory mechanisms shaping the immune system in response to nutrient availability are likely to be widespread in animals.

2.2 Introduction

In multicellular organisms, growth is regulated by the complex interplay between paracrine and endocrine signals. Tissues and organs respond to specific genetic programs to ensure optimal animal development with harmonious proportions [1]. Environmental cues, notably nutrient availability, further modify the output of these programs. Under food scarcity, critical resource allocation and prioritization between the various tissues of the organism are required to sustain life. This condition can favor brain development at the expense of other organs or an optimal size, with long-term consequences on animal fitness [2].

The immune system forms a network of tissues and circulating cells whose primary function is to prevent and limit microbial infections. The development and maintenance of an immune system are metabolically costly [3]. Theoretical considerations suggest that resource allocation towards the immune system is determined by the diversity of pathogens and the recurrence of infections, as well as by trade-offs with other physiological or reproductive functions [4-6]. Examples of trade-off have been shown in poultries where selection for increased body mass

resulted in a decrease in immune function [7] or conversely in *Drosophila* where selection for increased resistance to parasitoid wasps resulted in reduced larval competitive ability on a poor diet [8]. Another illustration is the allocation of resources an animal will invest in the production of immune cells. In humans, extremely high numbers of circulating leukocytes are continuously generated to anticipate potential infections by pathogens. While low lymphocyte or neutrophil numbers have been associated with increased risk of infection, the excessively high blood cell counts in certain lymphomas cause exhaustion of host resources and sometimes death [9]. As opposed to many vital physiological functions, the immune system provides minimal benefits under basal condition, revealing its importance mainly in case of an infection. When nutrients are scarce, it is expected that resources are re-allocated to critical developmental functions at the expense of the immune system [10,11]. This re-allocation would explain why starved children are more vulnerable to infections [12,13]. It also suggests the existence of flexible mechanisms, which allocate resources to the establishment of an immune system depending on nutritional inputs. However, our knowledge about how immune system development is coordinated with that of other organs in case of nutrient scarcity is limited. In this article, we describe a mechanism that regulates the number of hemocytes (i.e. insect blood cells) according to the nutritional state of the developing *Drosophila* larva.

The *Drosophila* cellular immune response involves three types of hemocytes, two of them, plasmatocytes and crystal cells, are found in the absence of infection. Plasmatocytes represent the most abundant population (i.e. 90-95%) and share functional similarities with mammalian macrophages. Crystal cells are non-phagocytic cells, which synthesize enzymes and substrates responsible for producing melanin at an injury site or for fighting an infection [14,15]. When faced with infestation by parasitoid wasps, *Drosophila* larvae produce a third type of blood cells: the lamellocytes. These cell types differentiate from plasmatocytes [16] or hemocyte progenitors [17] and form a capsule around wasp eggs or intruders, which are too large to be phagocytosed.

Like in vertebrates, *Drosophila* hematopoiesis occurs in several waves. The first wave of hematopoiesis occurs during embryogenesis and gives rise to approximately 700 plasmatocytes and 30 crystal cells [18]. The embryonic hemocyte population expands until the third larval stage to stop at metamorphosis. Outside the hematopoietic organ, larval hemocytes are found both in circulation and in sessile patches (referred to as peripheral hemocytes) [19-25]. Sessile hemocytes are attached to the internal surface of the larval

integument, forming patches, some of which are closely associated with secretory cells called oenocytes, as well as with the endings of peripheral neurons [21,26]. Larval hemocytes continuously swap between sessile patches and the hemolymph compartment [27,28]. Interestingly, it was demonstrated that peripheral hemocytes expand by self-renewal of mature cells that express the Hemolectin (Hml) hemocyte marker [21]. The second wave of hematopoiesis takes place in a dedicated organ called the lymph gland [19,20]. In contrast to peripheral hemocytes, the lymph gland functions as a reservoir of hemocyte progenitors that sustain a proliferative activity, concomitantly with a pool of mature hemocytes that does not expand. The lymph gland releases hemocytes at the onset of metamorphosis or upon parasitic infestation. The hemocyte population in pupae and adults consists of a pool of both embryonic and lymph gland-derived plasmatocytes with rare crystal cells [29].

In this study, we investigate whether peripheral hematopoiesis is influenced by nutrient scarcity. We first demonstrate that excessive hemocyte numbers can be detrimental under conditions of nutrient deprivation since they prevent the deposition of lipids in the fat body, which is the primary energy storage organ. We then show that peripheral hematopoiesis is down-regulated under poor dietary conditions, suggesting the existence of a regulatory pathway that adjusts hemocyte number to the metabolic state of the host. Finally, we identified an adipokine, NimB5, which is secreted by the fat body upon nutrient deprivation and ecdysone signaling, and which promotes hemocyte sessility and reduces their proliferation. Blocking this regulatory loop prevents the adjustment of hemocyte numbers to the nutrient state of the host, resulting in lethality under restrictive diets.

2.3 Results

2.3.1 High hemocyte numbers are detrimental to larvae upon nutrient scarcity

Production and maintenance of hemocytes are likely to have a significant metabolic cost. Therefore, we hypothesized that excessive hemocyte numbers might negatively impact *Drosophila* development. To test this hypothesis, we compared the viability of larvae with

normal, higher or lower hemocyte numbers when raised on a standard or a poor diet consisting of only 20% of each component. Larvae with increased hemocyte numbers were obtained by over-expressing *Pvf2* (*UAS-Pvf2*) [30] or *Ras85D* (*UAS-Ras85D^{V12}*) with the *Hml$^{\Delta}$-Gal4,UAS-GFP*, a *Gal4* driver specifically expressed in plasmatocytes, and differentiating crystal cells. We also used *eater^{1}* larvae, deficient for the Eater transmembrane receptor that were reported to have higher hemocyte counts [31-33]. Flow cytometry measurements on third instar (L3) wandering larvae showed that hemocyte numbers increased by 8.4- and 20.8-fold when over-expressing *Pvf2* or *Ras85D,* respectively, compared to wild-type when raised at 29°C (**Figure 2.1A**). Homozygous *eater^{1}* larvae, but not heterozygous animals, exhibited about 3-fold higher hemocyte numbers than wild type larvae when raised at 25°C (**Figure 2.1B**). Larvae with reduced hemocyte counts were obtained by silencing *Ras85D* in plasmatocytes, resulting in 3.6-fold lower hemocyte counts (**Figure 2.1A**). Of note, higher hemocyte numbers were accompanied with a significant differentiation of lamellocytes only in the *Hml$^{\Delta}$ > Pvf2* line (**Figure 2.1C**). Strikingly, all larvae with higher hemocyte numbers died when raised on a poor diet and switched at 29°C (> *Pvf2* and > *Ras85D^{V12}* at L1/L2 stages) (**Figure 2.1D**). We also noticed earlier lethality for *eater^{1}* mutant at the pupal stage when raised on poor diet at 25°C compared to normal diet (**Figure 2.1E**). In contrast, wild-type or *Ras85D RNAi* larvae with average or lower hemocyte numbers normally developed when raised on a poor diet.

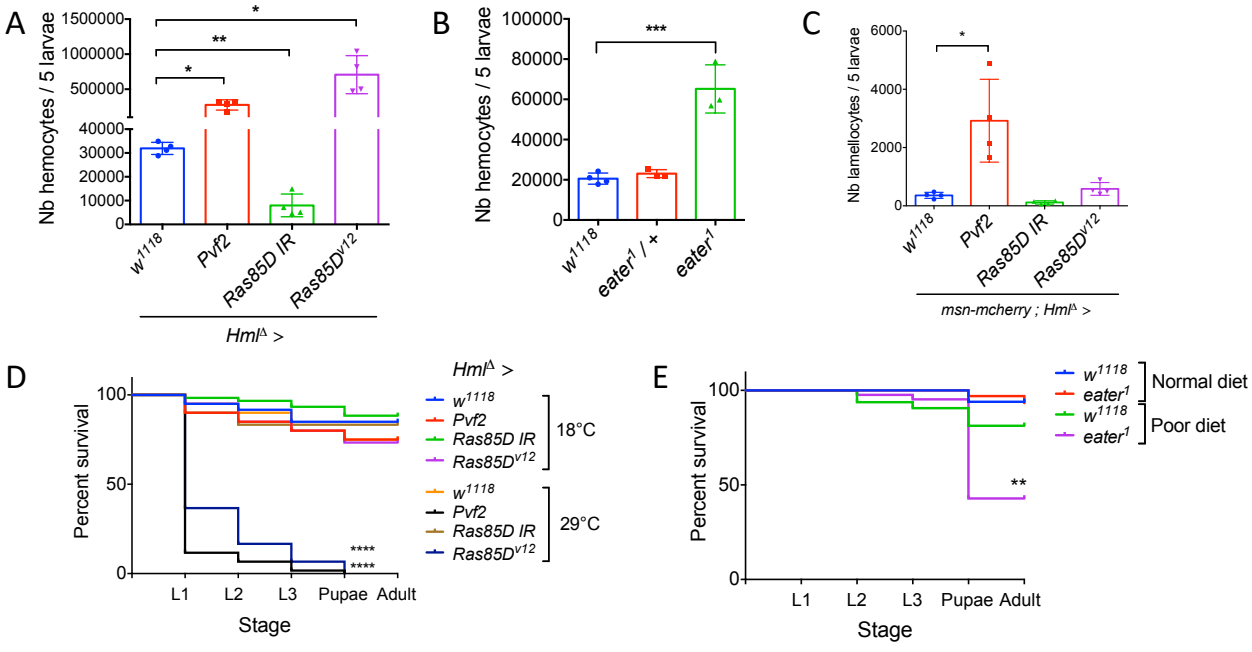

Figure 2.1 Blood cell hyperproliferation at early stage is deleterious for animal survival

(A-B) Total counts of peripheral hemocytes (A) from $Hml^{\Delta} > w^{1118}$, Hml^{Δ}> *Pvf2,* $Hml^{\Delta} >$ *Ras85D* IR and $Hml^{\Delta} >$ $Ras85D^{v12}$ (*Hml^{Δ}-Gal4,UAS-GFP*) and (B) w^{1118} (*Hml^{Δ}-Gal4,UAS-GFP*) and heterozygous and homozygous $eater^{1}$ mutant (*Hml^{Δ}-Gal4,UAS-GFP ;*$eater^{1}$) larvae. (C) Total counts of lamellocytes from same genetic backgrounds indicated in (A). (D) Survival curves of $Hml^{\Delta} > w^{1118}$, Hml^{Δ}> *Pvf2,* $Hml^{\Delta} >$ *Ras85D* IR and $Hml^{\Delta} >$ $Ras85D^{v12}$raised on poor diet at 18°C and 29°C. (E) Survival curves of w^{1118} (*Hml^{Δ}-Gal4,UAS-GFP*) and *Hml^{Δ}-Gal4,UAS-GFP ;*$eater^{1}$ raised on normal or poor diet at 25°C. For (A-C) Data are represented as mean ± SD from four independent experiments with 5 animals each. $*P < 0.05$, $**P < 0.01$, $***P < 0.001$ by Anova test. For (D-E), results correspond to the sum of at least 60 animals from 3 independent experiments and are analyzed by Kaplan-Meier test $**P <$ 0.01, $****P < 0.0001$.

A way to explain our results is that larvae with higher hemocyte counts are in an "inflammatory-like" state that is deleterious to the host. Indeed, chronic activation of the immune system has been associated with precocious lethality in *Drosophila* [34,35]. Therefore, we monitored in these larvae the level of activation of the Imd and Toll immune pathways using appropriate read-out genes *(Diptericin* and *Drosomycin,* respectively). We did not observe any chronic activation of these pathways nor defect in immune inducibility in larvae with higher hemocyte count (Figure 2.2A,B see ref [36] for $eater^{1}$ larvae). We then analyzed the level of activation of the JAK-STAT pathway by monitoring the expression of the target genes *Suppressor of cytokine signaling at 36E* (*Socs36*)*, Turandot A* (*TotA*) and *Turandot M* (*TotM*). We did not observe any significant difference although the level of JAK-STAT activation tended to be higher in *>Pvf2* larvae (Figure 2.2C). We also tested the level of JNK stress pathway activation in hemocytes by monitoring the expression of the JNK target gene *puckered (puc)* gene. We did not find any difference in *puc* transcription in hemocytes from these lines compared to the wild type (Figure 2.2D). Moreover, hemocytes from larvae over-expressing *Pvf2* or *Ras85D* retain the ability to phagocyte Gram-negative and Gram-positive bacteria, even more efficiently than the wild-type. In contrast, as expected [37], *eater* deficient larvae did not phagocytose well the Gram-positive bacterium *Staphylococcus aureus* (Figure 2.2E, F). These data indicate that hemocytes from larvae with higher blood cell count are fully functional and the lethality observed on a poor diet cannot be explained by the chronic activation or impairment of the immune system.

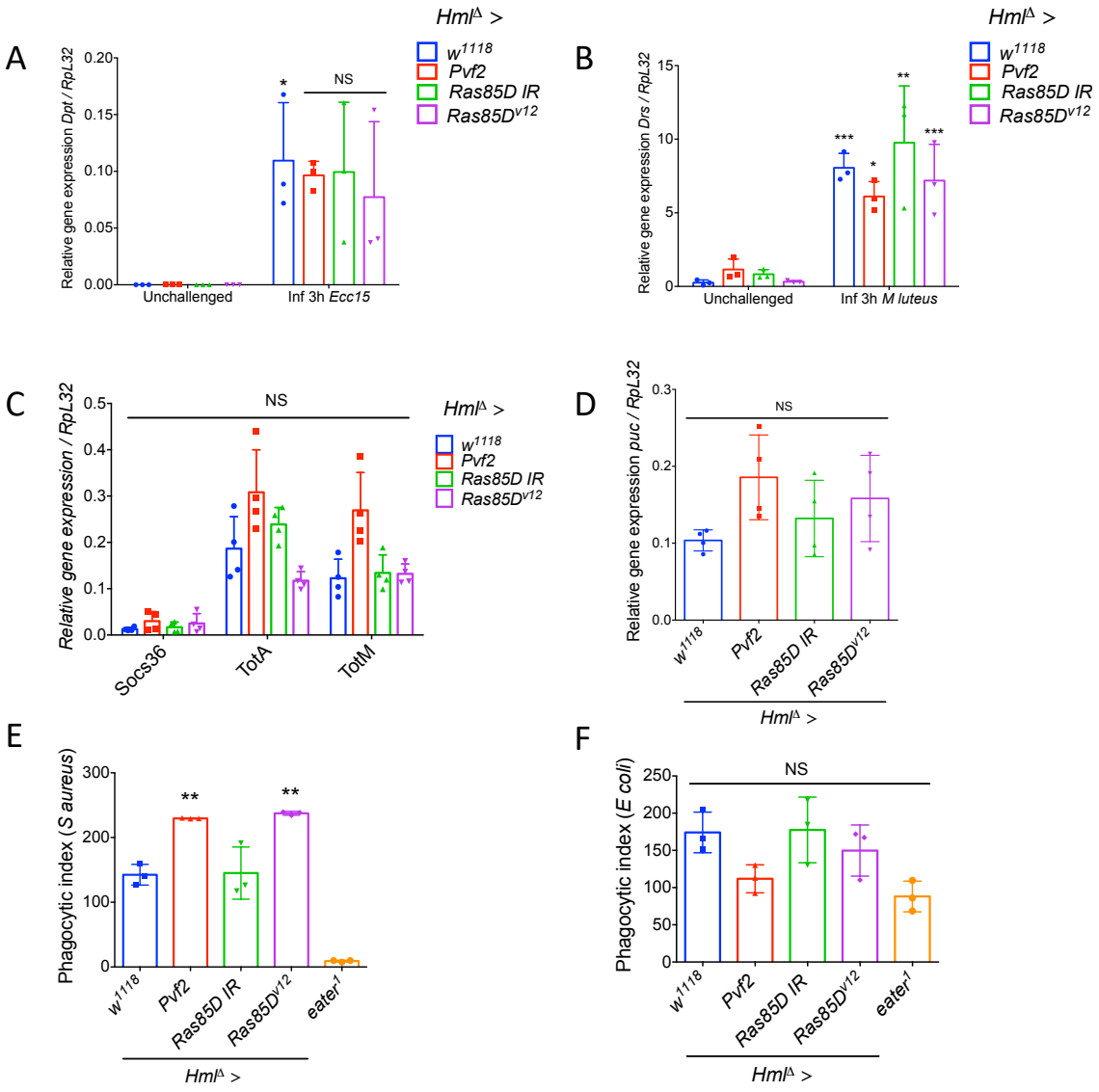

Figure 2.2 Over-proliferating hemocytes show limited stress activation

(A, B) RT-qPCR quantification of *Diptericin* (A) and *Drosomycin* (B) genes in fat body extracted from *Hml$^{\Delta}$ > w^{1118}*, *Hml$^{\Delta}$> Pvf2*, *Hml$^{\Delta}$ > Ras85D IR* and *Hml$^{\Delta}$ > Ras85D^{v12}* (*Hml$^{\Delta}$-Gal4,UAS-GFP*) animals, in unchallenged conditions and 3 hours post-infection with *Ecc15* (A) or *M. luteus* (B). Statistics compare an infected sample and its own unchallenged sample. (C, D) RT-qPCR measuring (C) the level of expression of JAK-STAT target genes *Socs36*, *TotA* and *TotM* in hemocytes and (D) the level of expression of the JNK pathway target gene *puckered* (*puc*) in hemocytes from *Hml$^{\Delta}$ > w^{1118}*, *Hml$^{\Delta}$> Pvf2*, *Hml$^{\Delta}$ > Ras85D IR* and *Hml$^{\Delta}$ > Ras85D^{v12}* (*Hml$^{\Delta}$-Gal4,UAS-GFP*) animals. All RT-qPCR results were normalized upon *RpL32* gene expression. (E, F) Phagocytic index of hemocytes extracted from *Hml$^{\Delta}$ > w^{1118}*, *Hml$^{\Delta}$> Pvf2*, *Hml$^{\Delta}$ > Ras85D IR*, *Hml$^{\Delta}$ > Ras85D^{v12}* (*Hml$^{\Delta}$-Gal4,UAS-GFP*) and *Hml$^{\Delta}$-Gal4,UAS-GFP ;eater^{1}*, using red pHrodo particles coupled with *S. aureus* (E) and *E. coli* (F). *eater^{1}* mutant is defective for Gram-positive bacteria internalization [32] and is used as a negative control. Statistics were performed against *Hml$^{\Delta}$>w^{1118}* line. Stars indicate P-values of *Anova* test. Data are represented as mean ± SD from three (A, B, E and F) or four (C, D) independent experiments with 5 animals each. *$P < 0.05$, **$P < 0.01$, ***$P < 0.001$ by Anova test.

Previous studies have shown that over-proliferating tissues can lead to energy-wasting in adipose tissue [38,39]. An alternative explanation is that the production of hemocytes consumes significant metabolic resources, and when too high, restricts the normal growth of the larva or pupa. To test this hypothesis, we measured triglyceride levels and visualized lipid droplets in the fat body. Interestingly, triglyceride contents decreased by 54%, 61% and 30% in fat bodies dissected from *Pvf2, Ras85D*-expressing and $eater^{1}$ larvae, respectively (Figure 2.3A, B). In contrast, *Ras85D* depleted larvae with reduced hemocyte counts showed a 46% increase in triglyceride content compared to wild-type. For all genotypes, triglyceride levels were inversely proportional to hemocyte counts. Fat body staining with Nile red and Bodipy confirmed triglyceride quantification (Figure 2.3C). Larvae with a higher number of hemocytes showed smaller lipid droplets of reduced intensity. In contrast, *Ras85D RNAi* larvae with a lower number of hemocytes exhibit larger lipid droplets and larger fat body cells. The fly CD36 homolog croquemort (crq) has been shown to contribute to lipid-specific uptake in hemocytes [40]. If hemocytes and fat body compete for lipids, we expected that crq^{Δ} deficient larvae, that have wild-type number of hemocytes (Figure 2.3D), have increased fat storage compare to wild-type. Indeed, Bodipy staining reveals larger lipid droplets of higher intensity in the fat body of *crq* deficient mutant compared to the wild-type (Figure 2.3E).

Collectively, these observations indicate that hemocyte production has a metabolic cost and that excessive hemocyte numbers affect larval viability upon nutrient deprivation, likely by depleting fat body energy storage.

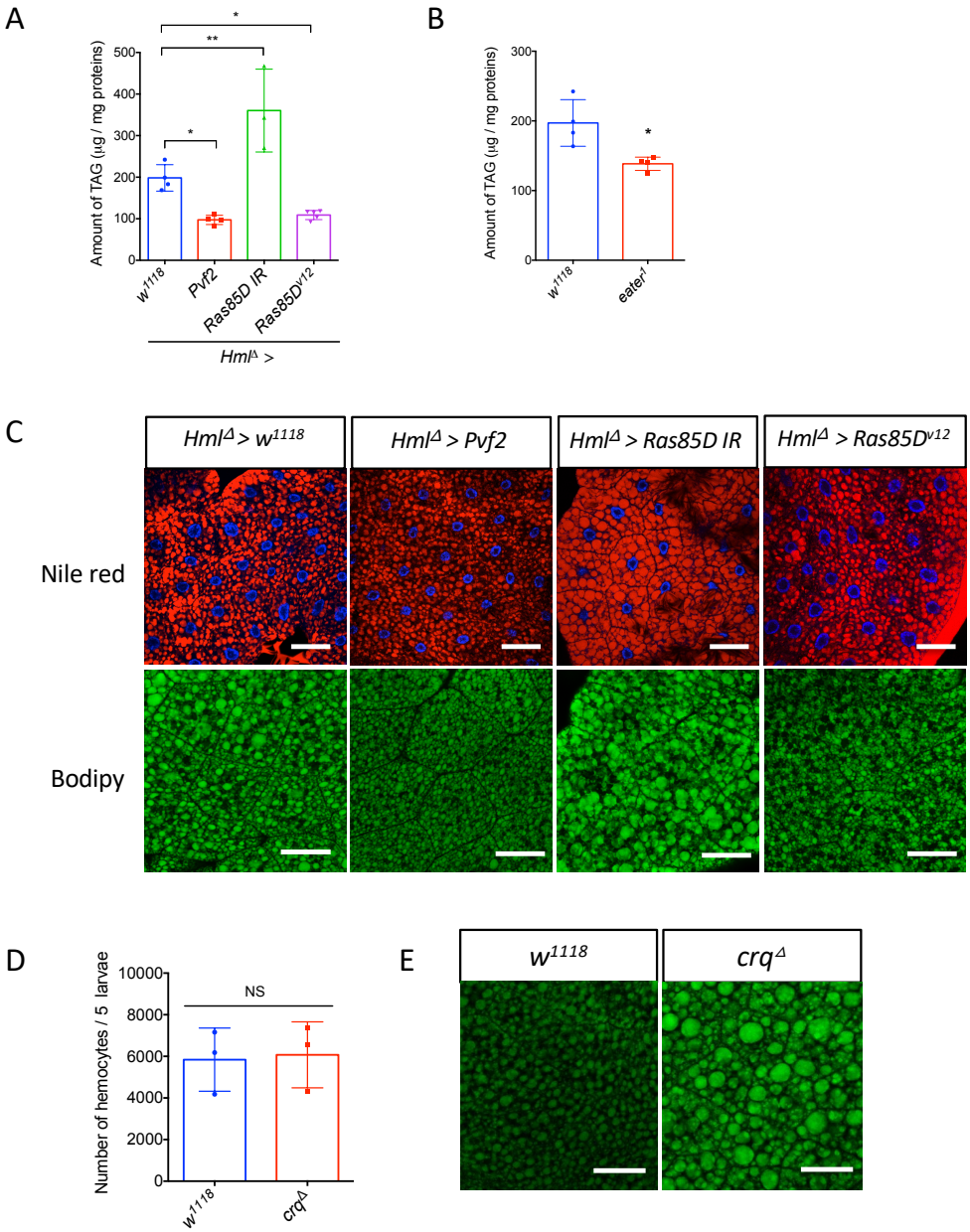

Figure 2.3 Fat body metabolism is linked to peripheral hematopoiesis

(A, B) Triacylglycerol (TAG) quantification of dissected fat bodies from *Hml$^{\Delta}$ > w^{1118}*, *Hml$^{\Delta}$> Pvf2, Hml$^{\Delta}$ > Ras85D IR* and *Hml$^{\Delta}$ > Ras85D^{v12}* (*Hml$^{\Delta}$-Gal4,UAS-GFP*) (A) and *eater^{1}* (*Hml$^{\Delta}$-Gal4,UAS-GFP;eater^{1}*) (B). TAG levels are normalized to protein quantity. (C) Representative confocal images of Nile red and Bodipy staining in fat bodies, corresponding to the genotypes in (A). Scale bars correspond to 60 µm for Nile red images and 33 µm for Bodipy images. n = 8 animals for each condition. (D) Total counts of peripheral hemocytes from *w^{1118}* and *crq$^{\Delta}$* mutant at L3 wandering larval stage. Animals are raised on normal diet. (E) Representative images of fat body from *w^{1118}* and *crq$^{\Delta}$* larvae. Tissue was Bodipy stained. Scale bars = 58 µm, n = 10 animals for each condition. Data are represented as mean ± SD from three (D) or four (A, B) independent experiments with 5 animals each. **P* < 0.05, ***P* < 0.01 by Anova test for (A) and **P* < 0.05 by Student's *t*-test for (B). NS = Not Significant.

2.3.2 Nutrient availability influences peripheral hemocyte homeostasis

We next investigated whether the growth rate of the hemocyte compartment in larvae is fixed or whether it can be adjusted by nutritional cues. Considering the metabolic cost of hemocyte production and maintenance, it might be beneficial to reduce their proliferation in conditions of nutrient shortage to prioritize the development of organs that are critical for survival. In contrast, a rich diet might lead to an even higher number of hemocytes and ergo, a better immune defense. To test this hypothesis, we measured hemocyte numbers of third instar larvae raised on a poor diet compared to standard food or a high-fat diet obtained by supplementing regular food with lard (6%) as described in [40]. Strikingly, larvae raised on a poor diet had a 2.1-fold decrease in hemocyte counts compared to larvae raised on a normal diet (**Figure 2.4A**). They also had fewer sessile hemocytes, no dorsal hemocyte patch and thinner lateral patches (**Figure 2.4B**). In contrast, larvae raised on a high-fat diet had a 1.5-fold increase in peripheral hemocyte numbers and showed more extended hemocyte patches on the dorsal side (**Figure 2.4B, C**). A higher number of hemocytes was also observed in larvae fed on a high glucose diet (10%) or fat diet (lard 6%), indicating that it was not correlated to nutrient type (**Figure 2.4D**). To confirm hemocytes variation according to food intake, we compared by RT-qPCR the size of the hemocyte compartment over the whole larva tissues by monitoring the expression of a hemocyte-specific gene, *Hml*, and a ubiquitous gene (*RpL32)*. A decrease of the *Hml / RpL32* ratio was observed when larvae were raised on a poor diet, consistent with a reduction of hemocyte number (**Figure 2.4E**). Of note, the *Hml / RpL32* ratio was also lower under high-fat condition, suggesting that hemocyte compartment expands less compared to the whole larval body under rich food intake. These data point to the existence of a regulatory mechanism that couples blood cell proliferation to nutritive input.

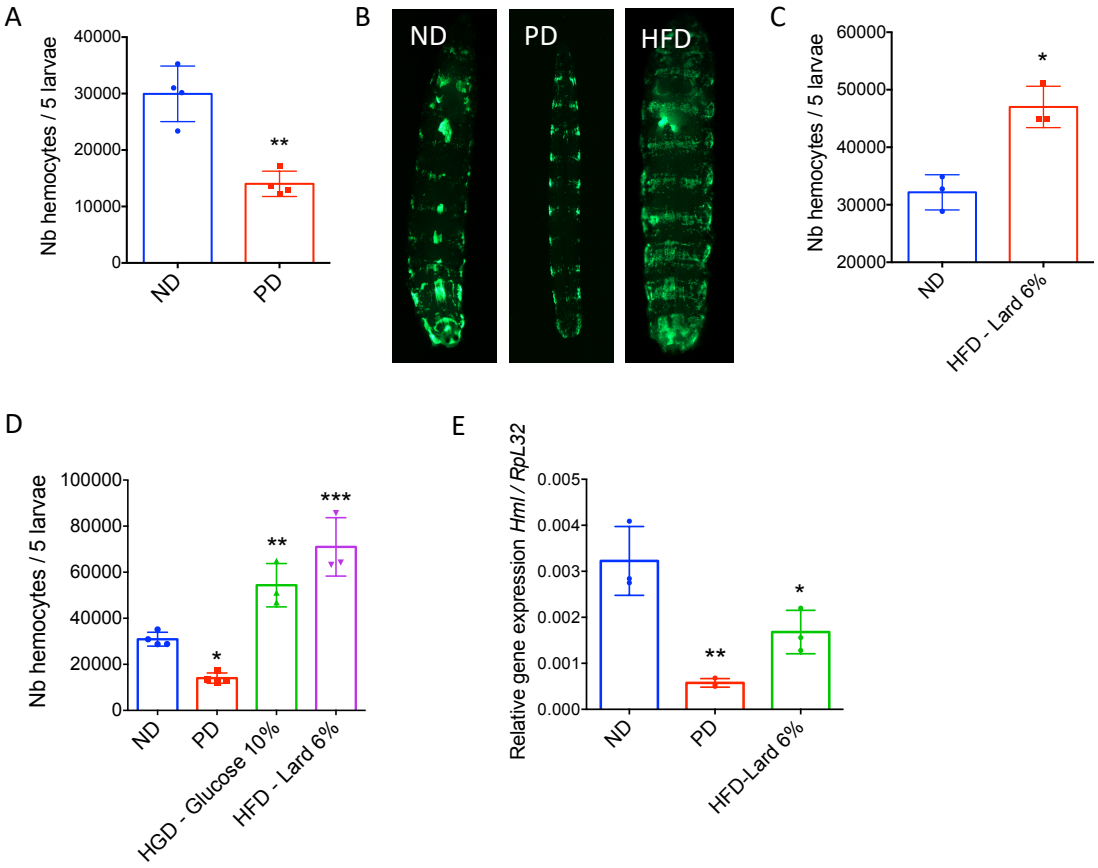

Figure 2.4 Nutrient availability influences peripheral hematopoiesis

(**A, C**) Total counts of peripheral hemocytes from *Hml$^{\Delta}$-Gal4,UAS-GFP* L3 wandering larvae fed on normal diet (ND), poor diet (PD) (**A**) or high fat diet with lard (HFD-lard 6%) (**C**) from hatching. (**B**) Representative images illustrating *Hml$^{\Delta}$-Gal4,UAS-GFP* L3 wandering larvae fed on normal diet (ND), poor diet (PD) or high fat diet (HFD). (**D**) Total counts of peripheral hemocytes from *Hml$^{\Delta}$-Gal4,UAS-GFP* L3 wandering larvae fed on normal diet (ND), poor diet (PD), normal diet supplemented with glucose 10% (High glucose diet, HGD) and normal diet supplemented with lard (HFD-lard 6%). n = 6 animals for each condition. (**E**) RT-qPCR quantification of *Hml* transcripts of mid-L3 larvae that were raised on ND, PD and HFD after hatching. Data are represented as mean ± SD from three (**C, D and E**) or four (A) independent experiments with 5 animals each. **P* < 0.05, ***P* < 0.01 by Student's *t*-test for (A and C). **P* < 0.05, ***P* < 0.01, ****P* < 0.001 by Anova test for (**D and E**).

2.3.3 *NimB5* is expressed in the fat body upon nutrient scarcity

The experiments described above indicate that hemocyte division and sessility are controlled by a factor that is sensitive to the metabolic state. In *Drosophila*, the fat body has been shown to sense and relay nutrient availability to coordinate the growth of the whole larvae [41]. We

then searched for genes expressed in the fat body that encode secreted factors susceptible to interact with hemocytes during the early stages. Our attention focused on *NimBs*, which encode secreted proteins of the Nimrod family; some of them being expressed in the fat body at the larval stage. The Nimrod family comprises six transmembrane proteins (NimA; NimC1, C2, and C4 (SIMU); Draper and Eater) and five secreted proteins (Nimrod B (NimB) family: B1, B2, B3, B4, and B5) with characteristic EGF-like repeats, also called "NIM repeats" [42]. Studies have revealed important links between transmembrane Nimrod proteins and hemocytes all along *Drosophila* life, by being implicated in bacterial phagocytosis (NimC1, Eater) and apoptotic corpses (SIMU, Draper), and in hemocyte sessility and adhesion (Eater) [32,37,43-46]. So far, none of the secreted NimBs have been functionally characterized. Interestingly, one *NimB*, *NimB5*, is induced in a mitochondrial mutant, that mimics a starvation state [47]. To better characterize *NimBs* expression profiles, we monitored their transcripts in larvae raised 4h, 8h, and 16h on a poor diet from the early L3 stage. *NimB5* was the only gene significantly upregulated with a four-fold induction level compared to wild-type at 8h (Figure 2.5A). We then checked simultaneously *NimB5* expression in fat body and hemocytes, on a normal diet and poor diet. As shown in Figure 2.5B, *NimB5* is expressed in both tissues, but to a much lesser extent in hemocytes; about 26 times less when normalized on *RpL32*. Interestingly, an increase in *NimB5* transcripts in larvae raised on poor diet was solely observed in fat body and not in hemocytes (Figure 2.5B). As the total contribution of the fat body to the larval body mass is much more important than hemocytes, we conclude that the contribution of hemocytes to the production of NimB5 is negligible compared to the fat body. To further confirm that *NimB5* gene is sensitive to the host metabolic state, we generated transgenic fly lines carrying a V5-sGFP-tagged *NimB5* fusion under its own regulatory sequences (derived from the Dresden pFlyfos collection) [48]. We confirmed that *NimB5* was expressed in fat body and that its expression increases when animals are raised on poor diet compared to animals raised on normal diet. In contrast, *NimB5* was hardly detected in hemocytes cytoplasm in both contexts (Figure 2.5C).

Consistent with our finding, published ModENCODE developmental and tissue array data showed that *NimB5* is almost exclusively expressed in the fat body of larvae [49], with the expression peaking at the wandering stage when larvae migrate away from food and prepare for pupariation. This developmentally induced starvation precedes the extended pupal feeding arrest. The RNA profiles matched proteomic profiles performed on whole animals that

confirmed the increased *NimB5* expression at the onset of pupariation and higher levels as animals reach the end of the pupal stage and emerge [50].

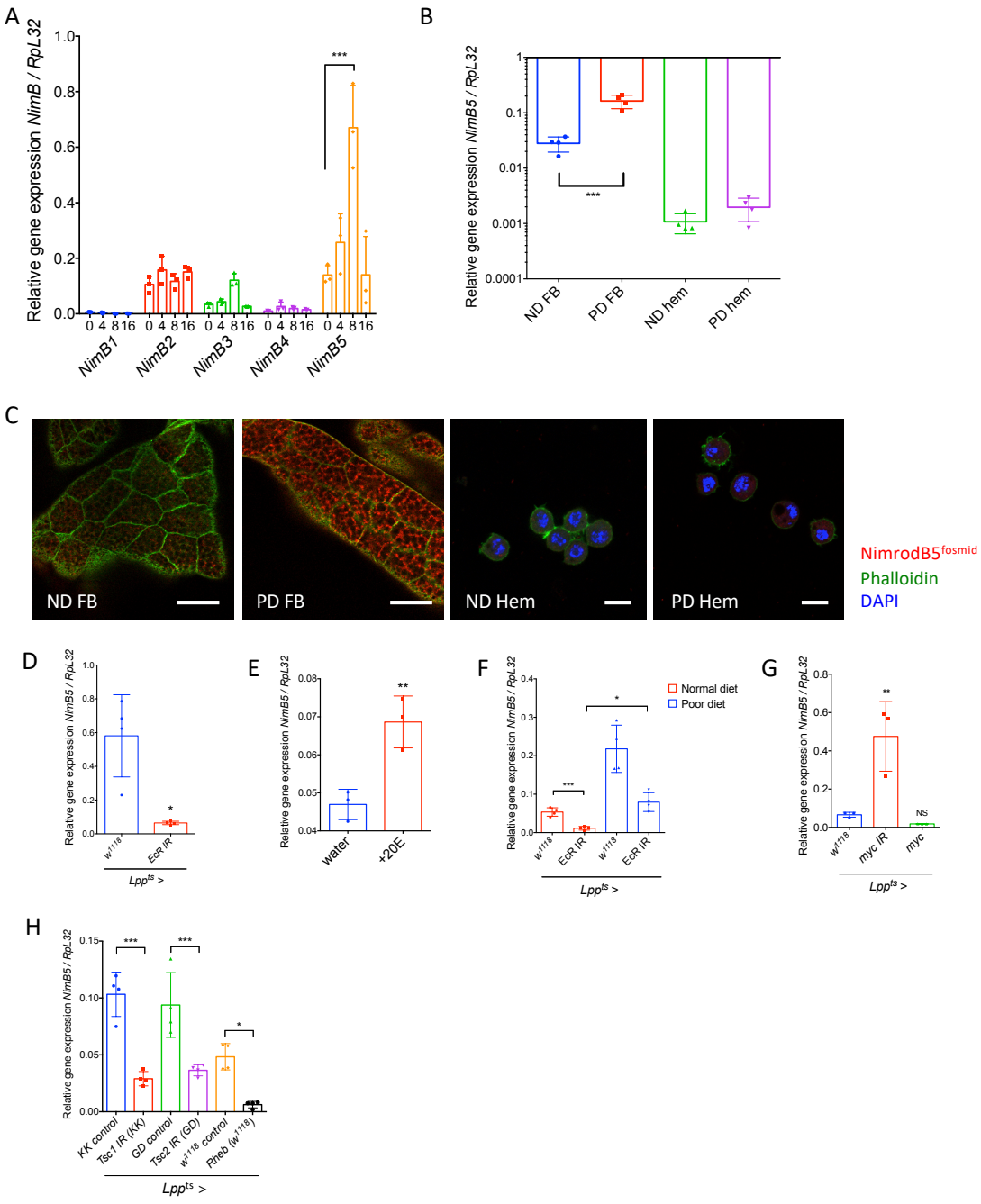

Figure 2.5 NimB5 expression is activated upon starvation and controlled by ecdysone and metabolic cues.

(**A**) RT-qPCR quantification of *NimB1, NimB2, NimB3, NimB4* and *NimB5* transcripts, normalized upon *RpL32* transcripts, from fat-bodies of mid-L3 larvae raised on poor diet dissected at indicated time points. (**B**) RT-qPCR quantification on *NimB5* gene in mid-L3 larvae raised on normal diet (ND) or poor diet (PD), in fat body (FB) or hemocytes (hem). (**C**) Representative apotome images of NimB5^{flyfos} in fat body (FB) and hemocytes (Hem) from mid-L3 animals raised on normal diet (ND) or poor diet (PD). FB

scale bars = 58 µm, Hem scale bars = 10 µm. n = 8 for each condition. (**D-H**) Relative expression of *NimB5* gene upon *RpL32* transcripts in fat bodies of $Lpp^{ts} > w^{1118}$ and $Lpp^{ts} > Ecd\ IR$ L3 wandering larvae (**D**), in fat bodies of mid-L3 larvae raised for 4h on crushed banana supplemented with water or 20-hydroxyecdysone (final concentration 0.5 mM) (**E**), in fat bodies of animals raised on normal or poor diet, after 8h of *EcR* silencing in fat bodies (**F**) in fat bodies of $Lpp^{ts} > w^{1118}$, $Lpp^{ts} > Myc\ IR$ and $Lpp^{ts} >$ *UAS-Myc* from L3 wandering larvae (**G**) and finally in fat bodies where TOR pathway was induced by silencing *Tsc1* and *Tsc2* and overexpressing *Rheb* specifically in the fat body. All results were compared to their corresponding control (**H**). Data are represented as mean ± SD from three (**A, E and G**) or four (**B, D, F and H**) independent experiments with 5 animals each. $*P < 0.05$, $**P < 0.01$, $***P < 0.001$ by Anova test for (**A, B, F, G and H**). $*P < 0.05$, $**P < 0.01$ by Student's *t*-test for (**D and E**).

2.3.4 *NimB5* is under the control of the growth metabolic regulators Myc, TOR and EcR

The rapid and high increase of *NimB5* expression during the late larval stage, as well as its sustained expression during the pupal stage, coincides with the peak of ecdysone titers at the larval-pupal transition and the high titers in pupae, respectively. Therefore, we checked whether the developmental expression of *NimB5* could be controlled by ecdysone. For this, we silenced the gene encoding the ecdysone receptor (EcR) specifically in the fat body ($Lpp^{ts} >$ *EcR-IR*) at the mid-L3 larval stage to limit the impact on animal growth [51]. We observed lower *NimB5* transcript levels in $Lpp^{ts} > EcR\text{-}IR$ wandering L3 larvae compared to wild-type (**Figure 2.5D**). Consistent with the role of ecdysone in the regulation of *NimB5*, feeding mid-L3 larvae for five hours with the steroid hormone 20-hydroxyecdysone significantly increased *NimB5* expression in the fat body (**Figure 2.5E**). However, the *NimB5* gene was still inducible to some extent by starvation in larvae with reduced fat body EcR signaling (**Figure 2.5F**). This result indicates the existence of other signaling inputs to regulate *NimB5* gene expression upon nutrient scarcity.

The transcription factor Myc is a well-established downstream target of EcR signaling in the fat body [51]. Myc is repressed upon EcR activation and is known to control organism growth. Thus, we hypothesized that *NimB5* could be negatively regulated by Myc, as *NimB5* is expressed in conditions of reduced growth. Accordingly, silencing *Myc* specifically in the fat body significantly increased *NimB5* expression, whereas overexpressing *Myc* in the fat body led to a slight downregulation of *NimB5* without reaching significance (**Figure 2.5G**). We conclude that *NimB5* regulation receives input from both Myc and EcR, two key metabolic

integrators of the fat body. Finally, we tested the effect of TOR metabolic pathway on *NimB5* transcription. For this, we monitored *NimB5* expression in larvae with higher TOR pathway activity in the fat body, a metabolic state that mimics nutrient uptake. To achieve this, we reduced the expression of *Tsc1* and *Tsc2* (tuberous sclerosis 1 and 2 proteins, two negative regulators of TOR) or overexpressed *Rheb* (a positive regulator of TOR signaling) in the fat body by using Lpp^{ts} driver [52]. Interestingly, genetic manipulations that increase the level of TOR signaling reduced *NimB5* expression (Figure 2.5H). We conclude that important metabolic regulators that sense the nutritional stage and EcR activation regulate *NimB5* expression.

2.3.5 NimB5 binds on hemocytes

NimB5 belongs to the Nimrod family that has been shown to regulate many essential biological functions of hemocytes [42]. This function raised the hypothesis that NimB5 produced by the fat body could bind to hemocytes. To test this notion, we generated transgenic fly lines carrying a *UAS-NimB5-RFP*. Figure 2.6A shows that Lpp^{ts} > *UAS-NimB5-RFP* larvae express NimB5-RFP in the fat body of larvae. Western blot analysis with hemolymph extract confirmed that NimB5-RFP protein is indeed secreted with the expected size (60-65kDa, Figure 2.6B). Strikingly, hemocytes collected from these larvae exhibit small RFP dots on their surface, showing that NimB5-RFP does indeed bind to circulating hemocytes (Figures 2.6C). Orthogonal views of hemocytes extracted from Lpp^{ts} > *UAS-NimB5-RFP* larvae show that NimB5-RFP proteins are both located on the surface of hemocytes (black arrows) and internalized (white arrows, Figures 2.6D). We hypothesize that the internalization of NimB5 could be linked to the protein recycling. We then compared the hemocyte binding ability of NimB5-RFP to that of the RFP protein fused with the signal peptide of the Viking protein [53]. Figure 2.6E shows that NimB5-RFP has a stronger ability to bind to hemocytes than secreted RFP, reinforcing the notion that NimB5 specifically interacts with hemocytes. Finally, immunostainings of the endogenously *V5*-tagged *NimB5* locus confirm that NimB5 localizes on the surface of hemocytes (Figures 2.6F, G). Histological cross-sections also revealed the presence of NimB5-RFP signals on the membrane of sessile hemocytes (Figures 2.6H, white arrows). We conclude that NimB5 is a protein secreted by the fat body that can interact with hemocytes.

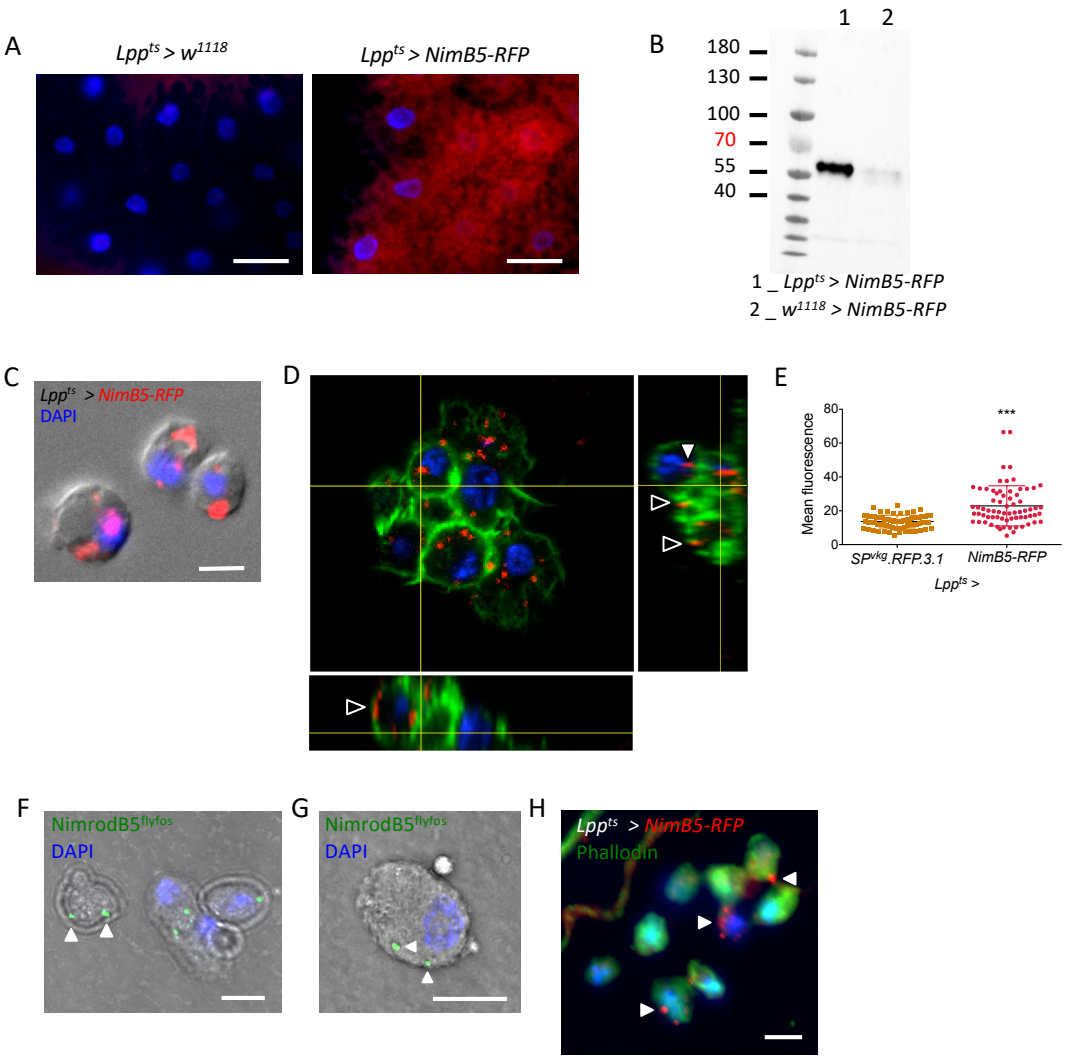

Figure 2.6 NimB5 is generated by the fat body and binds to blood cells

(A) Representative apotome images of NimB5-RFP generating by the fat body (*Lpp^{ts} > UAS-NimB5-RFP*) compared to non-secreting line (*Lpp^{ts} > w^{1118}*). n = 10 animals (B) Western blot analysis with hemolymph extract from L3 wandering larvae over-expressing *UAS-NimB5-RFP* with the driver *Lpp^{ts}* reveals the presence of the RFP fusion protein at the expected size of ≈60-65 kDa molecular weight (NimB5: 35.34 kDa and RFP: 27 kDa). Non-induced *UAS-NimB5-RFP* control line does not show protein signal from hemolymph. Experiment performed in triplicate. (C) Representative apotome image of hemocytes stained with DAPI (blue), illustrating the localization of NimB5-RFP (red) secreted from fat body (*Lpp^{ts} > UAS-NimB5-RFP*). Overlay of fluorescence and DIC. Scale bar = 10 µm. n = 8 animals. (D) Orthogonal views from 488 Phallodin stained hemocytes extracted from *Lpp^{ts} > UAS-NimB5-RFP* animals. Images help to determine membrane-bound (black arrows) and internalized particles (white arrow). Scale bar = 10 µm. n = 5 animals. (E) Mean fluorescence of RFP signal on hemocytes from *Lpp^{ts} > UAS-SP^{vkg}.RFP.3.1* and *Lpp^{ts} > UAS-NimB5-RFP*. (F-G) Apotome images of hemocytes stained with DAPI, illustrating the localization of endogenous NimrodB5 when fed on poor diet. Hemocytes are extracted from larvae carrying Flyfos-*NimB5* transgene and stained against V5 antigen. Overlay of fluorescence and phase contrast images. Scale bar = 10 µm. n = 8 animals. (H) Cross section of L3 wandering larvae, showing hemocytes patches with NimB5-RFP secreted from fat body (*Lpp^{ts} > UAS-NimB5-RFP*). Scale bar = 10 µm. n = 5 animals. Data in (E) are collected from 5 animals and analyzed by Mann-Whitney test. ***$P < 0.001$

2.3.6 NimB5 negatively regulates hemocyte numbers

The inducibility of *NimB5* upon nutrient scarcity and its ability to bind to hemocytes makes it an excellent candidate to contribute to fat-body hemocyte signaling. To further investigate the function of NimB5 in peripheral hematopoiesis, we generated a null mutation in the *NimB5* gene by Crispr-Cas9, referred to as $NimB5^{SK1}$ [54]. $NimB5^{SK1}$ has a 13bp deletion in the first exon, inducing a premature stop codon and leading to a truncated protein of 54 amino acids instead of 351 (Figures 2.7A-D). $NimB5^{SK1}$ mutants were viable on standard diet and did not show any morphological defect. We then investigated whether the *NimB5* mutation affects hemocyte numbers by counting both sessile and circulating hemocytes using a method developed by Petraki et al., [55] coupled with flow cytometry. First, FACS counting revealed that wild-type and $NimB5^{SK1}$ third instar wandering larvae have the same percentage of mature hemocytes with respectively 93.0% and 94.6% of Hml^{+} cells (Figures 2.8A). Importantly, $NimB5^{SK1}$ third instar larvae and white prepupae had, respectively, 1.7 and 2.2 times more hemocytes compared to wild-type larvae when raised on a normal diet (Figures 2.8B, C). These higher hemocyte numbers in $NimB5^{SK1}$ larvae were not due to higher numbers of embryonic hemocytes since $NimB5^{SK1}$ and wild type larvae contained comparable numbers at the L2 stage (Figures 2.8D). Since hemocyte numbers markedly vary from one genetic background to another, we performed additional experiments to confirm that the *NimB5* mutation is responsible for the higher number of hemocytes.

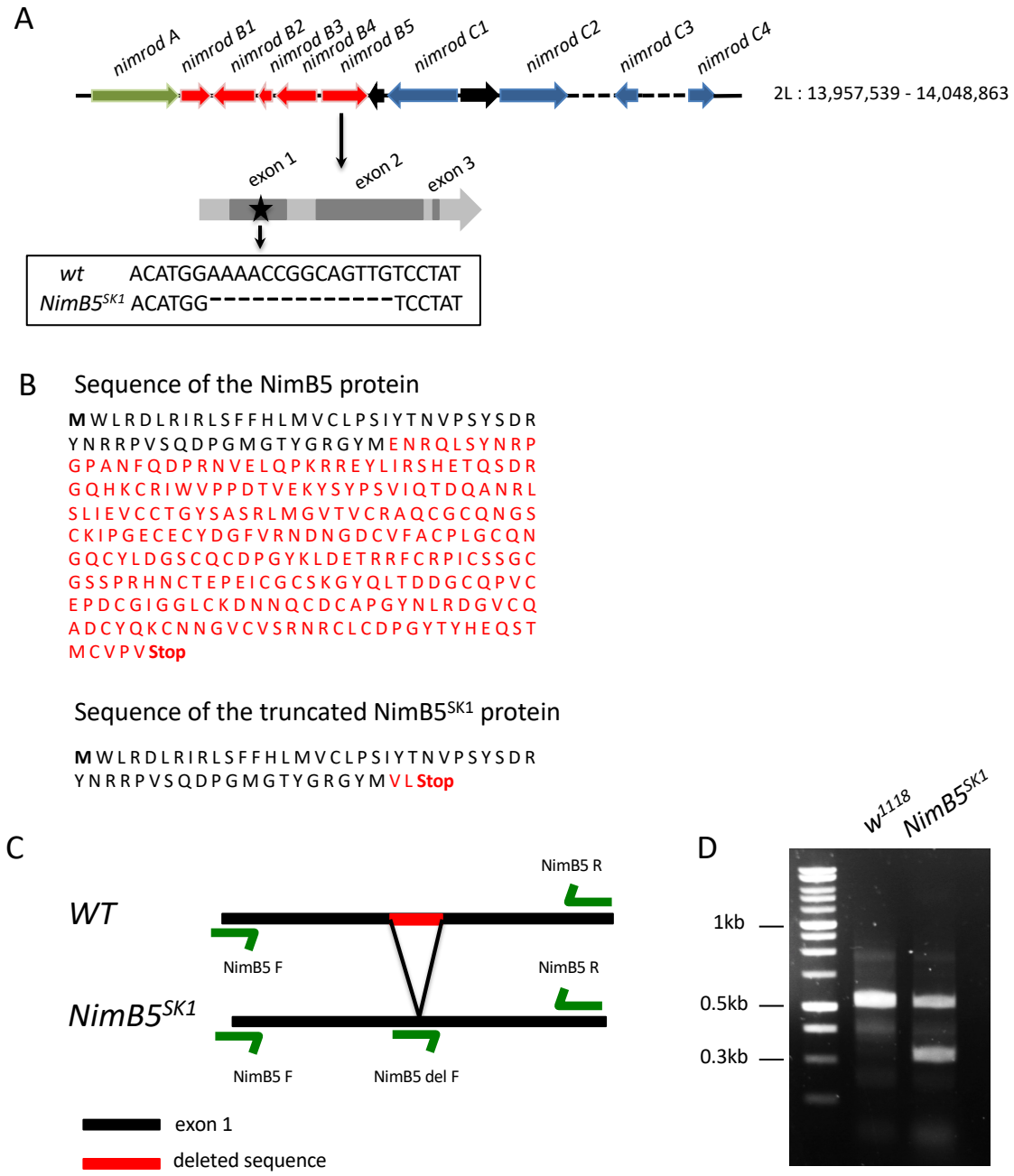

Figure 2.7 Generation of *NimB5* deficient flies by CRISPR-Cas9 system.
(A) Representation of the *Nimrod* gene locus on the 2nd chromosome (34E5). The *NimB5* gene is mutated in the first exon via a deletion of 13 bp. (B) The mutation of *NimB5* gene leads to a premature translation stop resulting in a truncated protein lacking 297 amino acids. (C) Experimental design of qPCR verification to validate *NimB5*^{SK1} mutants. (D) PCR result that confirms the presence of the deletion in *NimB5*^{SK1} mutant. n = 10 animals. The Flybase (www.flybase.org) accession number for *NimB5* is CG16873

First, we introgressed the *NimB5*^{SK1} mutation by successive backcrosses into the *w, Drosdel* background [56]. Figure 2.8E shows that isogenized *NimB5*^{SK1} larvae also have higher hemocyte numbers compared to their *w, Drosdel* counterparts. Second, higher hemocyte numbers were also observed in trans-heterozygous *NimB5*^{SK1}/*Df(2L)BSC252* larvae carrying the mutation over a deficiency that removes the *Nimrod* locus, but not in heterozygous *NimB5*^{SK1} animals (**Figure 2.8F**). We noticed that *NimB5*^{SK1}/*Df(2L)BSC252* larvae, however, had fewer hemocytes compared to homozygous *NimB5*^{SK1} larvae. This result is likely because the deficiency removes several other *Nimrod* genes, which may also influence peripheral hematopoiesis.

Furthermore, we tested the effect of *RNAi*-mediated knockdown of NimB5, in various tissues, on hemocytes proliferation. We selected two RNAi lines from public stock centers, the KK VDRC 105320 and the Trip BDSC 51162, and confirmed their ability to silence effectively *NimB5* expression when expressed in the fat body or in hemocytes using respectively the *Lpp*^{ts} and *Hml*$^{\Delta}$ drivers (**Figure 2.8G, H**). Over-expression of these RNAi constructs ubiquitously (*Act5C-Gal4*) or in the fat body (*Lpp*^{ts}) led to significant increases in the hemocyte population, mimicking the *NimB5*^{SK1} mutation (**Figure 2.8I, J**). In contrast, silencing *NimB5* in hemocytes (*Hml*$^{\Delta}$*-Gal4*) using these two RNAi constructs did not affect the hemocyte numbers (**Figure 2.8I, J**), confirming that NimB5 is required in the fat body to control peripheral hematopoiesis. We observed that overexpressing a wild-type copy of *NimB5* ubiquitously or specifically in the fat body or hemocytes in an otherwise wild-type background did not affect hemocyte proliferation. We hypothesize that the level of endogenously produced NimB5 is sufficient to control hemocyte proliferation (**Figure 2.8K**). Finally, overexpressing *NimB5* in the fat body of *NimB5*^{SK1} mutant larvae rescued the over-proliferation phenotype by reducing hemocyte numbers to normal levels (**Figure 2.8L**). All these experiments led us to conclude that the *NimB5*^{SK1} mutation impacts peripheral hemocyte number.

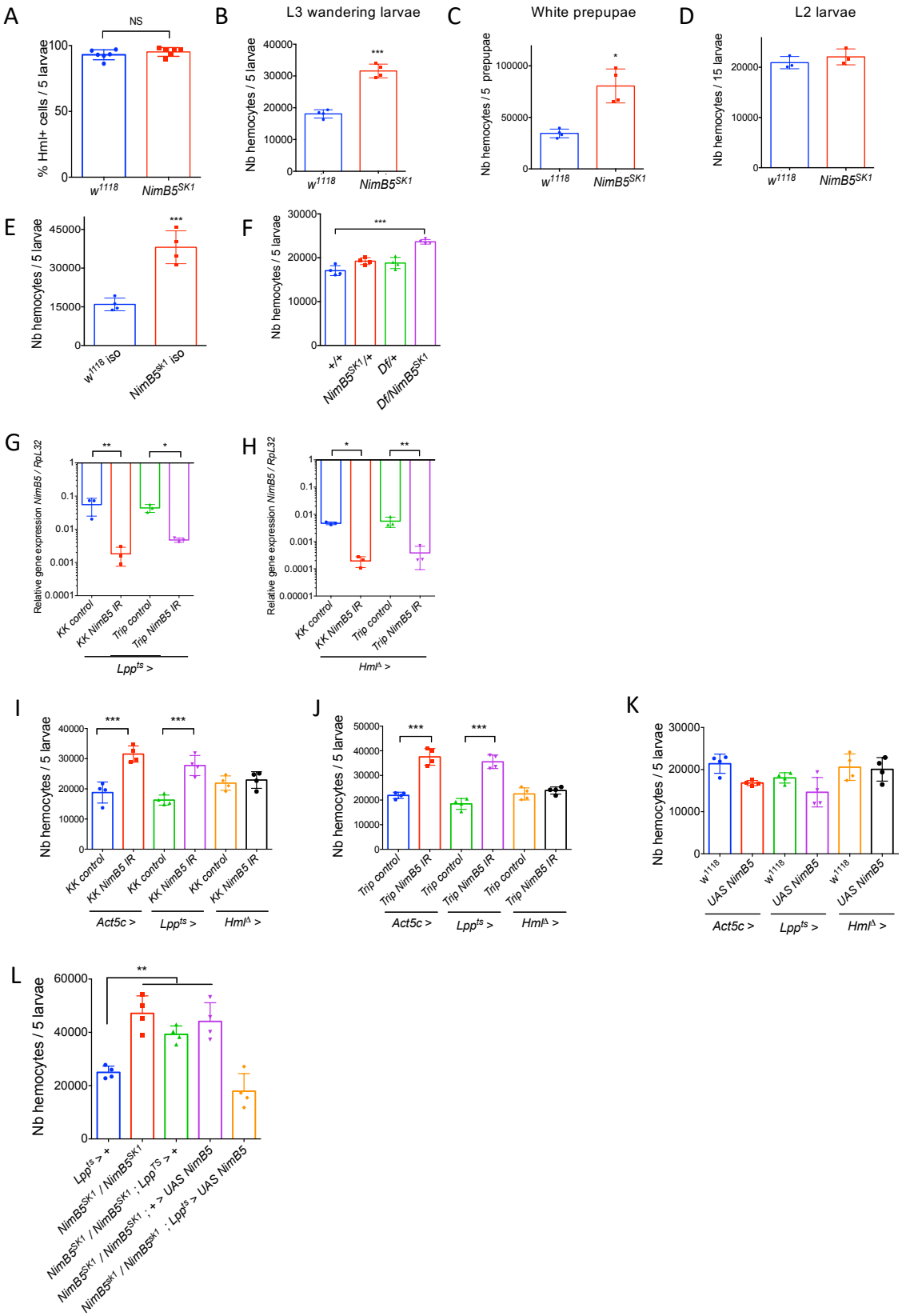
A
NS
% Hml+ cells / 5 larvae
w1118
NimB5SK1
B
L3 wandering larvae
Nb hemocytes / 5 larvae
C
White prepupae
Nb hemocytes / 5 prepupae
D
L2 larvae
Nb hemocytes / 15 larvae
E
Nb hemocytes / 5 larvae
w1118 iso
NimB5SK1 iso
F
Nb hemocytes / 5 larvae
+/+
NimB5SK1/+
Df/+
Df/NimB5SK1
G
Relative gene expression NimB5 / RpL32
KK control
KK NimB5 IR
Trip control
Trip NimB5 IR
Lppts >
H
Relative gene expression NimB5 / RpL32
Hml∆ >
I
Nb hemocytes / 5 larvae
Act5c >
Lppts >
Hml∆ >
J
Nb hemocytes / 5 larvae
K
Nb hemocytes / 5 larvae
UAS NimB5
L
Nb hemocytes / 5 larvae
Lppts > +
NimB5SK1 / NimB5SK1 ; Lppts > +
NimB5SK1 / NimB5SK1 ; + > UAS NimB5
NimB5SK1 / NimB5SK1 ; Lppts > UAS NimB5

Figure 2.8 NimB5 blocks hemocyte proliferation.

(A) Percentage of mature peripheral hemocytes (Hml+ cells) among hemolymph free floating cells extracted from w^{1118} vs $NimB5^{SK1}$ animals, measured by flow cytometry. (B-D) Peripheral (sessile and circulating) hemocyte counts of w^{1118} or $NimB5^{SK1}$ animals combined with $Hml^{\Delta}.dsred.nls$ from L3 wandering larvae (B), white prepupae (C) and L2 larvae (D). (E) Peripheral hemocyte counts of w^{1118} and $NimB5^{SK1}$ isogenized lines at L3 wandering stage. (F) Peripheral hemocyte counts from w^{1118}, heterozygous $NimB5^{SK1}$, heterozygous *Df(2L)ED793* and *Df(2L)ED793 /* $NimB5^{SK1}$ L3 wandering larvae with the $Hml^{\Delta}.dsred.nls$ marker. (G-H) RT-qPCR quantification of *NimB5* transcription in fat body (G) and hemocytes (H), where *NimB5* was silenced by using *KK-NimB5 IR* (VDRC) or *Trip-NimB5 IR* (BDSC) and their corresponding controls. (I-J) Peripheral hemocyte counts in larvae where *NimB5* was silenced ubiquitously (*Act5c>*), in fat body (Lpp^{ts}>) and in hemocytes (Hml>) by using *KK-NimB5 IR* (VDRC) (I) or *Trip-NimB5 IR* (BDSC) (J) and their corresponding controls. (K) Peripheral hemocyte counts in larvae where *NimB5* was overexpressed in all tissues, specifically in fat body or in hemocytes. (L) Peripheral hemocyte counts in Lpp^{ts}> w^{1118} *(+),* $NimB5^{SK1}$*,* homozygous $NimB5^{SK1}$ coupled either with Lpp^{ts} driver or *UAS-NimB5* transgene and $NimB5^{SK1}$*;* Lpp^{ts}*> UAS-NimB5.* Data are represented as mean ± SD from four independent experiments with 5 animals each. **P* < 0.05, ***P* < 0.01, ****P* < 0.001 by Student's *t*-test for (A-E) and Anova test for (F-L).

2.3.7 NimB5 does not impede hemocyte function

We then assessed the proliferation rate of peripheral hemocytes. Phosphohistone 3 (PH3) staining and EdU incorporation assays [21] showed that $NimB5^{SK1}$ larvae exhibited a higher frequency of mitotic hemocytes compared to wild-type (**Figures 2.9A, B**). Histological analysis and EdU incorporation experiments showed that the $NimB5^{SK1}$ mutation did not affect lymph gland hematopoiesis (**Figures 2.9C, D**).

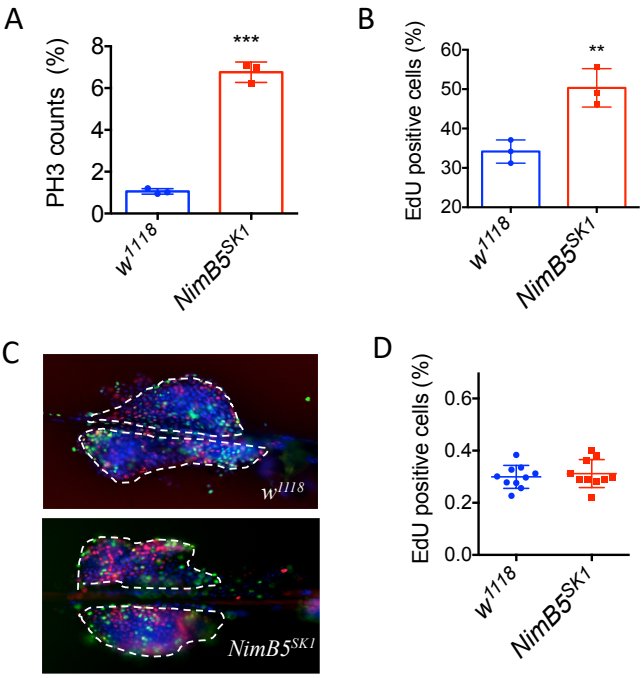

Figure 2.9 Lymph gland is not affected in *NimB5^{SK1}* mutant

Percentages of PH3 (A) or EdU (B) positive cells in peripheral cells positive for *Hml$^{\Delta}$.dsred.nls*, from *w^{1118}* and *NimB5^{SK1}* at L3 wandering stage. (C) Images of lymph glands from *w^{1118}* and *NimB5^{SK1}* animals combined to *Hml$^{\Delta}$.dsred.nls* marker (red) from L3 wandering larvae, stained with EdU proliferation marker (green). Scale bar = 96 µm. n=10. (D) Percentages of EdU positive cells from 10 lymph glands of *w^{1118}* or *NimB5^{SK1}* animals combined with *Hml$^{\Delta}$.dsred.nls* marker at L3 wandering larval stage. Data are represented as mean ± SD from three independent experiments with 5 animals each for (A and B) and 10 lymph glands for (D). $^{**}P < 0.01$, $^{***}P < 0.001$ by Student's *t*-test. For D, data were analyzed by Mann Whitney test and gave no significant difference (NS).

Importantly, hemocytes in the *NimB5^{SK1}* mutants appeared fully functional since they were perfectly able to phagocytose bacteria (Figure 2.10A). *NimB5^{SK1}* mutant larvae did not show any significant defect in melanization or encapsulation, indicating that *NimB5^{SK1}* larvae retain the ability to differentiate crystal cells and lamellocytes (Figures 2.10B-E). We then evaluate the number of crystal cells by analyzing *NimB5^{SK1}* mutant larvae carrying the *Lz-Gal4,UAS-GFP* crystal cell marker. The absolute number of crystal cells per larva was higher in *NimB5^{SK1}* larvae compared to the wild-type as expected for a mutant with higher hemocyte counts (Figure 2.10F). However, the ratio of crystal cells over plasmatocytes was lower (Figure 2.10G). As a significant fraction of crystal cells derived from plasmatocytes differentiation in sessile patches [33], we speculate that NimB5 might favoring plasmatocytes proliferation over crystal cells differentiation possibly as a consequence of decrease adherence ([33], see below). To test this, we estimated the number of sessile crystal cells using the cooking assay that induces the spontaneous activation of prophenoloxidases within crystal cells, allowing them to be visible through the cuticle as black spots [57]. Indeed, we observe less melanized crystal cells attached underneath the integument of *NimB5^{SK1}* larvae compared to wild-type larvae (Figure 2.10H, I), also strongly suggesting an adherence defect in *NimB5^{SK1}* animals. Collectively, our data reveal that a secreted factor emanating from the fat body upon nutrient scarcity, NimB5, negatively regulates the rate of peripheral hemocyte proliferation without impeding hemocyte function.

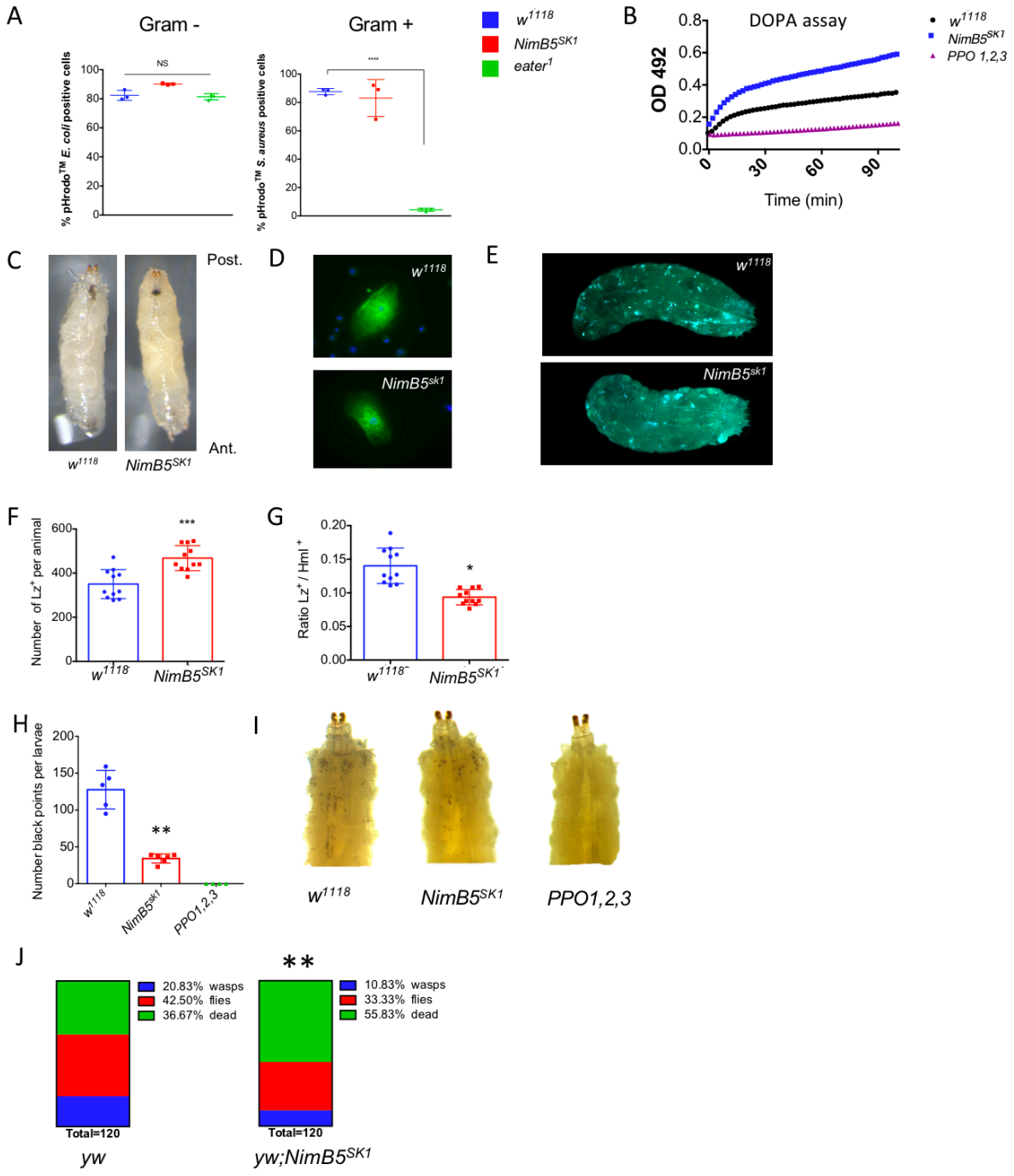

Figure 2.10 NimB5 is not essential for phagocytosis, melanization and encapsulation.

(A) Phagocytic assay using green pHrodo particles. Hemocytes dissected from *WT* or *NimB5*^{SK1} L3 wandering larvae show identical phagocytic capacity towards *E. coli* and *S. aureus* conjugated bioparticles. Data were acquired using flow cytometry with gating against red fluorescent cells, then green positive cells. (B) A DOPA enzymatic assay reveals that hemolymph from *NimB5*^{SK1} L3 wandering larvae has higher melanization activity compared to wild-type larvae. This higher level can be explained by the higher absolute number of hemocytes (and crystal cells) in *NimB5*^{SK1} larvae. n=10 (C) Pricking assay shows identical melanization reaction as monitored by the size of the black spot at the injury site in wild-type and *NimB5*^{SK1} larvae. Scale bar = 1 µm. n = 10 animals. (D, E) Representative images of lamellocytes spread on a slide (D) or circulating in whole animals (E). Scale bars respectively = 10 µm and 1 mm. n = 10 for both experiments. Larvae carry the *PPO3-Gal4,UAS-GFP* insertion, that is specifically

expressed in lamellocytes [76]. Hemocytes and larvae were collected two days after *L. boulardi* wasp infestation. Wild-type and *NimB5^{SK1}* larvae do not show any difference in their ability to differentiate lamellocytes upon wasp infestation. (**F**) Number of *lz-Gal4,UAS-GFP* positive cells in animals (**G**) Ratio of *lz-Gal4,UAS-GFP* positive cells (crystal cells) over *Hml$^{\Delta}$.dsred.nls* positive cells (plasmatocytes). (**G**) and (**F**) are performed in L3 wandering larvae. (**H**) Heating assay reveals a lower number of visible black punctae (crystal cells) below the carcass of *NimB5^{SK1}* larvae compared to wild-type larvae. (**I**) Representative images of data presented in (**H**). Scale bar = 0.5 mm. n = 15 animals. (**J**) *Leptopilina boulardi* infestation of *wild-type and NimB5* y,w larvae. Results are represented as a sum of 120 animals for each genotype in six different experiments. In this experiment, we monitored the three possible outcomes of infestation: 1) wasp-infested individuals die as larvae or as pupae (both wasp and fly die, green), 2) a wasp emerges from the pupa (wasp success, blue), or 3) a fly emerges from the infested pupa (fly success, red). This experiment shows that the endoparasitoid wasp *L. boulardi* is less successful to infect NimB5 deficient mutants compared to wild-type. This is likely due to increased hemocyte number of NimB5 larvae that either improves the cellular response (i.e. encapsulation) against the parasitoids or depletes lipid store. A depletion of lipid store would explain why we observe increased lethality at the pupal stage corresponding to case 1 *(both wasp and fly die). PPO1, PPO2, PPO3* deficient larvae lacking cellular and hemolymphatic phenoloxidase were used as a control for B and H [76].Data are represented as mean ± SD from three independent experiments with 5 animals each for (**A**), 11 animals for (**F, G**), five independent experiments including 3 animals each for (**H**) and at least 120 animals for (**J**). ***P* < 0.01, ****P* < 0.001 by Anova test for (**A and H**) and Student's *t*-test for (**F and G**). For J, **, *P* < 0.0071 by chi-square = 9,885; df = 2.

2.3.8 NimB5 affects hemocyte sessility and adhesion

Adherent cells, notably when establishing contacts with other cells, are less proliferative, a process called “contact inhibition of proliferation” [58]. This observation raised the question of whether the higher hemocyte proliferation *NimB5^{SK1}* larvae could be associated with decreased adhesion, or hemocytes establishing fewer contacts with neighboring cells. We thus explored whether NimB5 affects hemocyte adhesion and sessility. Consistent with the increased hemocyte counts, *NimB5^{SK1}* mutants showed larger sessile hemocyte patches beneath the cuticle, but also more circulating hemocytes (**Figure 2.11A**) that suggest an adherence defect from blood cells. To test this hypothesis, we seeded hemocytes from wild-type, *NimB5^{SK1}* and *NimB5 RNAi* larvae on glass, allowed them to adhere for 30 min, and performed a phalloidin staining. Images analysis revealed that hemocytes of *NimB5^{SK1}* mutants spread much less compared to wild-type (**Figure 2.11B, C**). RNAi silencing of *NimB5* in fat body but not in hemocytes recapitulates the adhesion defect (**Figure 2.11B, C**). Importantly, we could rescue the adhesion defect of *NimB5^{SK1}* mutants raised on a poor diet by overexpressing NimB5 specifically in the fat body (**Figure 2.11C**).

Notably, this spreading defect was not due to smaller hemocyte size, as revealed by a *Tali™* Image-Based Cytometer that shows similar circulating hemocytes diameter from both genotypes (Figure 2.11D).

To assess how NimB5 affected hemocyte sessility *in vivo*, we subsequently performed scanning electron microscopy analysis of sessile hemocytes, focusing on the inner side of the cuticle of L3 wandering larvae. We observed that hemocytes in the *NimB5*^{SK1} mutant spread less and lacked filopodia as compared to wild-type (Figure 2.11E, black arrows). Finally, we recombined the *Hml*$^{\Delta}$*-Gal4,UAS-GFP* hemocyte marker with the *NimB5*^{SK1} mutation to analyze the localization of peripheral hemocytes. Although *NimB5*^{SK1} mutant larvae still contained sessile hemocyte patches, the cells were only loosely attached to the inner wall of the larvae (Figure 2.11F). Collectively, our results show that NimB5 regulates both peripheral hemocyte proliferation rate and adhesive properties.

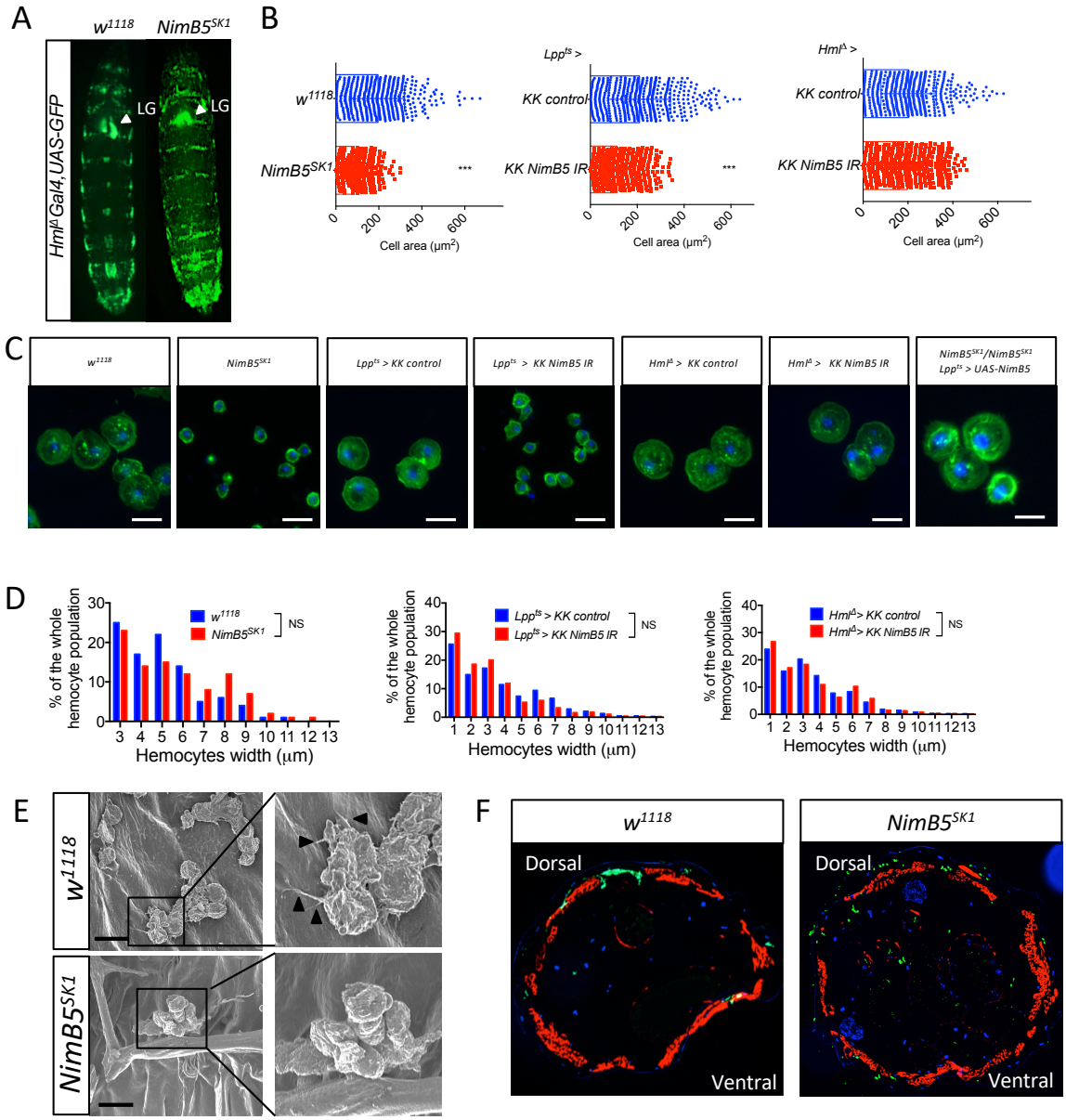

Figure 2.11 NimB5 promotes hemocyte adhesion *in vitro* and *in vivo*.

(A) Images of live *Hml$^{\Delta}$-Gal4,UAS-GFP* and *NimB5^{SK1},Hml$^{\Delta}$-Gal4,UAS-GFP* L3 wandering larvae. Scale bar = 0.5 mm. n = 10 (B) Bar diagram of hemocyte areas from *w^{1118}* vs *NimB5^{SK1}* larvae, larvae where *NimB5* was silenced in fat body (*Lpp^{ts} > KK control* vs *Lpp^{ts} > KK NimB5 IR*) and larvae where *NimB5* was silenced in hemocytes (*Hml$^{\Delta}$ > KK control* vs *Hml$^{\Delta}$ > KK NimB5 IR*) at L3 wandering stage. Hemocytes were allowed to spread on slides for 30 min and were stained with 488 Phalloidin. (C) Representative images of hemocytes collected from identical individuals than panel B and stained with phalloidin. We also show phenotype rescue when *NimB5* is expressed in fat body of *NimB5^{SK1}* animals (right image) Scale bar = 10 µm. n = 5 for each condition. (D) Width hemocytes measurement from wild-type and *NimB5^{SK1}* mutant L3 wandering larvae. Analysis are processed with Tali® Image-Based Cytometer. (E) Scanning electron microscopy of internal cuticle side of L3 wandering larvae. *w^{1118}* and *NimB5^{SK1}* animals were opened ventrally and all organs were removed to allow visualization. Scale bar = 10 µm. n = 5. (F) Cross-sections from w^{1118} and *NimB5^{SK1}* larvae coupled with *Hml$^{\Delta}$-Gal4,UAS-GFP* at L3 wandering stage. Rodhamine phalloidin and DAPI stainings. Scale bar = 0.2 mm. n = 5. Data in (B and D) are analyzed by Mann-Whitney test. ***P < 0.001, NS = Not Significant.

2.3.9 NimB5 contributes to the survival of larvae raised on a poor diet

All in all, our data show that NimB5 is a fat body derived factor, upregulated in response to nutrient scarcity, and required to maintain physiological hemocyte numbers. We hypothesized that if NimB5 regulates hemocyte numbers in response to nutrient availability, *NimB5* mutants should exhibit fitness defects when raised on a poor diet. Thus, we shifted *NimB5* and wild-type mid-instar larvae from a standard to a poor diet and analyzed adult eclosion rate. Despite no delay in development, *NimB5* ^{SK1} but not wild-type animals showed significant pupal lethality at the pharate stage on poor diet (**Figures 2.12A, B**). This lethality was likely to be caused by the high hemocyte numbers as *NimB5*^{SK1} mutants were unable to fully down-regulate hemocyte numbers under poor diet (**Figure 2.12C**). It is important to note that the hemocyte number of *NimB5*^{SK1} larvae still decrease when raised on a poor diet, although remaining higher compared to the wild-type (**Figure 2.12C**).

To confirm that the lethality of *NimB5*^{SK1} mutant on a poor diet was linked to its depletion in the fat body, we repeated the experiment using the KK and Trip- *NimB5* IR constructs under the regulation of *Lpp*^{ts} or *Hml*$^{\Delta}$ drivers. Before, we checked that feeding animals on poor diet did not affect the expression level of *Lipophorin* (*Lpp*) and *Hemolectin* (*Hml*) genes (**Figure 2.12D, E**). We observed that silencing *NimB5* in the fat body but not in hemocytes recapitulated the animals' survival defect observed with *NimB5* mutant raised on poor diet (**Figure 2.12F, G**). The hypothesis that *NimB5*^{SK1} animals lethality is due to the high numbers of hemocytes is also supported by the observation that the elimination of hemocytes by over-expressing the pro-apoptotic gene Bax [59,60] in blood cells suppresses the pupal lethality observed in poor diet conditions (**Figure 2.12H**). This indicates that other mechanisms beyond NimB5 can down-regulate hemocyte number upon food scarcity. Importantly, we could rescue the lethality of *NimB5*^{SK1} mutant raised on a poor diet by overexpressing NimB5 specifically in the fat body (**Figure 2.12I**).

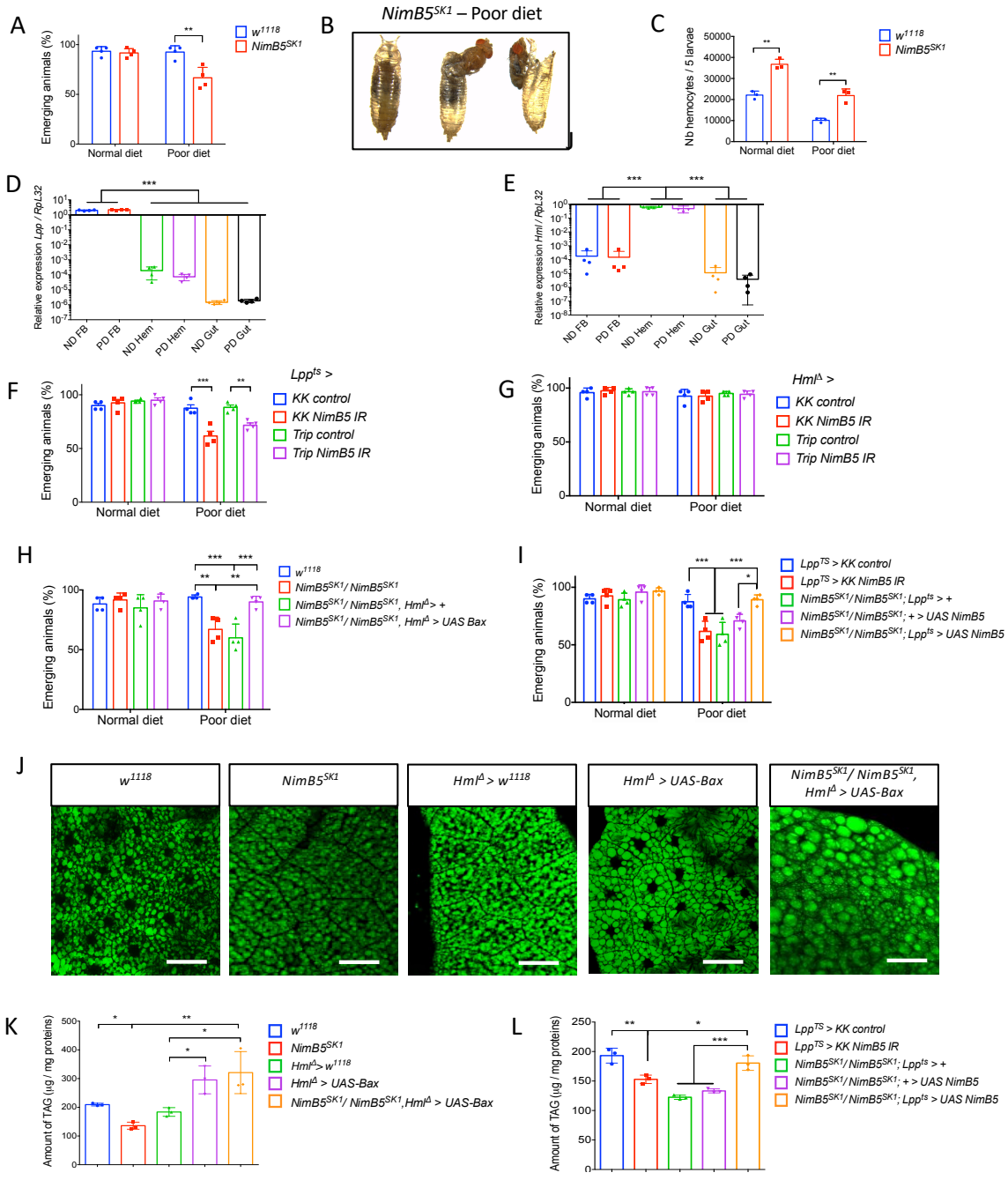

Figure 2.12 NimB5 promotes adaptation to poor diet.

(A) Percentages of emerging *w*^{1118} and *NimB5*^{SK1} animals raised on normal diet until mid-L3 stage and then transferred to fresh normal diet or poor diet. (B) Representative image of non-emerging *NimB5*^{SK1} animals. Development stops at pharate stage. Scale bar = 1 mm. (C) Peripheral hemocyte counts from *w*^{1118} or *NimB5*^{SK1} larvae combined to *Hml*$^{\Delta}$*.dsred.nls* marker at L3 wandering stage. (D, E) RT-qPCR on *Lipophorin* (*Lpp,* D) and *Hemolectin* (*Hml,* E) genes in larval mid-L3 fat body, hemocytes and gut compartments, when raised on normal diet and poor diet. Results are normalized to *RpL32* transcripts. (F, G) Percentages of emerging animals raised on normal diet or poor diet, with *NimB5* silencing in the fat body (F) or in hemocytes (G) using *KK-NimB5 IR* or *Trip-NimB5 IR* and their corresponding controls. (H) Percentages of emerging animals in *NimB5*^{SK1} animals expressing the pro-apoptotic gene *Bax* specifically in hemocytes (*Hml*$^{\Delta}$*-Gal4,UAS-GFP > UAS-Bax).* (I) Percentages of emerging animals when *NimB5*^{SK1} animals express *NimB5* specifically in the fat body. (J) Representative confocal images showing Bodipy stainings of fat bodies from *w*^{1118}*, NimB5*^{SK1}*, Hml*$^{\Delta}$ *> w*^{1118}*, Hml*$^{\Delta}$*-Gal4,UAS-GFP > UAS-Bax*

and *Hml$^{\Delta}$-Gal4,UAS-GFP* > *UAS-Bax* combined with *NimB5^{SK1}* mutation. Scale bars = 33 µm. n = 5 for each condition. (**K, L**) Triacylglycerol (TAG) quantification of dissected fat bodies from indicated crossings. Data are represented as mean ± SD from three (**K and L**) or four (**A, C, D, E, F, G, H, I**) independent experiments. **P* < 0.05, ***P* < 0.01 and ****P* < 0.001 by Anova test.

We hypothesize that the high hemocyte count observed in the *NimB5* mutant could deplete fat body stores as shown above larvae over-expressing *Pvf2*, *Ras85D^{V12}* or mutated for *eater*. We therefore explored the amount of lipid in the fat body of NimB5^{SK1} larvae. As expected for a higher hemocyte count mutant, NimB5^{SK1} larvae have smaller amount of TAG as well as smaller and less stained lipid droplets compared to the wild-type as shown by Bodipy staining (**Figure 2.12J, K**). In contrast, *NimB5 hemoless* larvae expressing the pro-apoptotic gene *Bax* in hemocytes have higher amount of TAG with bigger lipid droplets confirming that lipid store depletion is indeed linked to hemocytes (**Figure 2.12J, K**). Interestingly, we also show that expressing NimB5 specifically in NimB5^{SK1} larvae restore TAG content in the fat body (**Figure 2.12L**). Taken together, these results demonstrate that fat body-hemocyte regulatory loop which involves NimB5 is critical for survival on a poor medium.

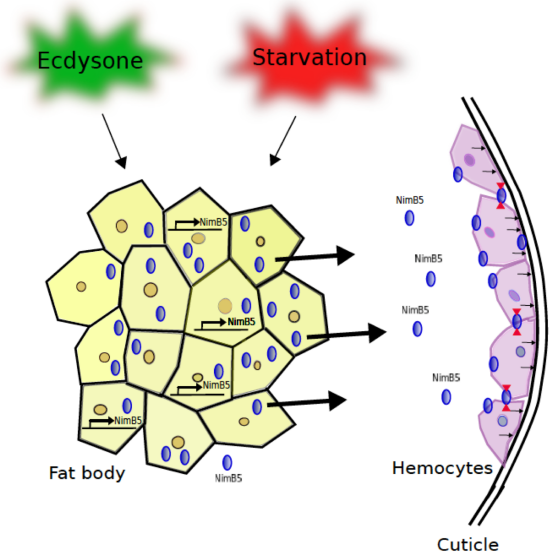

Figure 2.13 Model of NimB5 role in the control of hemocyte function.
NimB5 expression adjusts the growth of the peripheral hematopoietic compartment to the metabolic state of the host. NimB5 is produced by the fat body upon starvation or during metamorphosis, and subsequently secreted into the hemolymph. NimB5 binds to hemocytes to promote adhesion to the cuticle (black arrows), and possibly contact between cells (red arrowheads) and reduce hemocyte proliferation.

2.4 Discussion

Nutrition is an essential environmental parameter in the determination of body size. In Metazoans, the coordination of growth among different body parts according to environmental conditions relies on cross-talk between different organs via the production of long-range signaling molecules [61]. In this study, we uncover an adipokine, NimB5, which is produced by the fat body upon nutrient scarcity that reduces hemocyte adhesion and proliferation (See model on Figure 2.13). The disruption of this signaling loop results in conditional lethality when larvae are raised on a poor diet. Our study shows that larvae die from their inability to reduce hemocyte numbers, which is likely detrimental to energy storage and not from an over-activation of the immune response. In this article, we have privileged the notion that the depletion of the metabolic store due to the high energy demand of numerous hemocytes causes larval lethality on a poor diet. This is supported by the observation that lethality on poor diet correlates with hemocyte number. At first sight, it is surprising that a two-threefold increase in hemocyte number is so detrimental to animal fitness, taking into consideration the small size of the hemocyte compartment compared to other tissues. It is likely that *Drosophila* plasmatocytes are strong energy users, as mammalian macrophages, and energetically costly. Nevertheless, we cannot definitely exclude that the lethality we observed has another cause. For instance, this lethality could be due to a hemocyte factor that directly regulates fat body metabolism rather than metabolic competition between tissues. Further studies are required to better characterize the interactions between the fat body and hemocytes.

Adjustment of hemocyte numbers to the nutritional status

Our study demonstrates that the growth of the larval hemocyte compartment is not stereotypical but influenced by nutritional cues and that hemocyte proliferation has a metabolic cost. Larvae fed on a rich diet have higher hemocyte numbers, while larvae experiencing nutrient deprivation have reduced hemocyte counts. This reveals flexibility in the way an organism allocates energy to build the immune system. We further show that this adjustment is critical since hemocyte production has a significant metabolic cost and can compete with the fat body building up metabolic stores. Energy reallocation and systemic

energy switch is also important in the context of wasp infestation. Indeed, it was demonstrated that under immune stress, the host energy resources are reallocated to immune cells production, leading to fat body storage depletion [62]. Consequently, larvae with higher hemocyte numbers fail to develop correctly when raised on a poor diet. Even when grown on standard diet, these larvae store lower lipid amounts in their fat body. This indicates that a high hemocyte population has a critical metabolic cost, which cannot be fully compensated through increased nutrient uptake. The adjustment of hemocyte numbers to nutritional cues might explain the high variability in hemocyte numbers observed both within and between fly stocks among laboratories using different fly mediums and distinct crowding conditions. While the coordination of organ growth is the focus of intense studies in *Drosophila* research, the variation in the size of circulating blood cell compartments is rarely taken into consideration. As hemocytes are mainly dispensable in normal conditions [59,60], the reduction of their numbers offers a mechanism to survive adverse dietary conditions. Nevertheless, this adaptation comes at the expense of a robust immune system. The existence of regulatory mechanisms tailoring investment in the immune system to nutrient availability is likely to be a general principle of animal host defense, to reduce potential trade-offs between immunity and other physiological functions.

In 1997, a landmark paper demonstrated that *Drosophila* selected for improved resistance against a parasitoid wasp had reduced larval competitive ability, notably when raised on poor diet, pointing to the existence of a trade-off between a robust immune system and growth [8]. Later on, effective resistance to parasitoid wasps in selected lines was associated with a doubling of hemocyte numbers [63,64]. These studies are entirely consistent with our observation that increased size of the hemocyte compartment affects the ability of larvae to survive on a poor diet. Our present study sheds some light on the molecular mechanisms underlying this trade-off, showing that excessive hemocyte numbers hamper fat body energy storage. The existence of phenotypic plasticity in the growth of peripheral hematopoiesis is likely adaptive for fruit flies that live on rotting fruit, an ephemeral ecosystem, and frequently experience nutrient stress. As the maintenance of hemocytes tends to affect metabolic storage, we cannot exclude that the increased resistance to parasitoids of larvae with higher hemocyte counts does not result from more potent cellular immunity, but is instead due to the depletion of lipid storage which is a critical resource for parasitoids [64,65]. In this line, we performed survival analyses, which revealed that endoparasitoids have a lower success when

they infest *NimB5* mutants, compared to wild-type, due to increased pupal lethality in infested mutants (Figure 2.10J). This observation could likely be explained by the higher hemocyte number leading to a stronger encapsulation reaction or the depletion of lipids that prevents the development of both the *Drosophila* larvae and the wasps.

Regulation of *NimB5* by central metabolic cues

We observed that *NimB5* transcription is upregulated at the third instar wandering stage, when larvae stop feeding before entering pupariation. *NimB5* is also induced by nutrient shortage mainly at early time points, which suggests that it is involved in the early adaptation to poor food. During development, the expression profile of *NimB5* is very similar to that of *Dilp6,* which encodes an insulin-like peptide produced by the fat body to regulate growth at non-feeding stages [66]. *Dilp6* is also induced by starvation. Much like *Dilp6*, the Ecdysone Receptor positively regulates *NimB5* expression. In *Drosophila*, ecdysone is not only involved in the activation of molts and metamorphosis but also plays a growth-inhibitory function during larval development, notably by inhibiting Myc in the fat body [51,67]. Thus, *NimB5* is regulated in the fat body by key metabolic pathway integrators, which signal 'growth arrest'. Since *NimB5* is still induced in *EcR* deficient larvae upon starvation, this gene likely receives additional regulatory inputs.

Previous studies have shown that nutritional deprivation also impinges on the maintenance of blood progenitors in the lymph gland causing the expansion of mature blood cells. These studies reveal that both systemic and local signals (e.g. TOR and insulin pathways) regulate blood progenitor maintenance in the lymph gland [68-72]. Additionally, a very recent work highlights the existence of a protein called Lime, which is both expressed in the fat body and the hemocytes, [49], and that simultaneously regulates metabolism with blood cells survival in the lymph gland and in the peripheral compartment [73]. The observation that NimB5 does not regulate hematopoiesis in the lymph gland reveals that distinct mechanisms upon nutrient deprivation regulate central (lymph gland) and peripheral hematopoiesis. The existence of NimB5 likely provides more versatility in the control of animal growth by uncoupling hemocyte development from that of other organs, which is regulated by more generic growth signals (e.g. insulin-like peptides).

NimB5 promotes adhesion and inhibits proliferation

Our study reveals that NimB5 binds to peripheral hemocytes to regulate adhesion and proliferation. In this article, we have favored the notion that increased hemocyte proliferation in *NimB5* larvae is a secondary consequence of an adhesion defect, which prevents cells from interacting with each other. Future studies should address whether this proliferation defect is a consequence of impaired adhesion, or whether adhesion and proliferation are uncoupled. An important point is to clarify whether NimB5 function is a growth factor that activates a downstream signaling pathway in hemocytes and/or directly favors hemocyte-hemocyte contacts. Of note, NimB5 could inhibit hemocyte adhesion, preventing sessile hemocytes from being under the influence of the neuronal system, as shown by Makhijani et al. [21,74]. The phenotypes of *NimB5* and *eater* mutated animals share many similarities, suggesting that the secreted NimB5 protein and the transmembrane receptor Eater, could function in the same process. The observation that $NimB5^{sk1}$,$eater^{1}$ double mutants exhibit even higher hemocyte counts (data not shown) than single mutants suggests that NimB5 could also interact with another receptor. *eater* null mutants show a stronger hemocyte phenotype than *NimB5* mutants both in term of hemocyte increase and defect in sessility. This could also be explained by the implication of other NimB members. The involvement of other NimBs is also supported by the observation that *NimB5* deficient larvae have the ability, albeit reduced compared to the wild-type, to limit hemocyte population expansion when raised on a poor diet (Figure 2.12 C). The Nimrod gene family has experienced diversification in *Drosophila* species. We hypothesize that the expansion of the Nimrod family, with five secreted forms and six proteins bearing a transmembrane domain, could underlie the constitution of a complex platform to regulate peripheral hematopoiesis, notably hemocyte proliferation and sessility. Future studies should characterize the role of the other secreted Nimrod members, notably those expressed in the fat body.

2.5 Materials and methods

Drosophila stocks and rearing conditions

All fly stocks (and their corresponding references) used in this work are defined in the Supplementary Figure 2.1. All stocks were reared on standard fly medium comprising 6% cornmeal, 6% yeast, 0.62% agar, 0.1% fruit juice, supplemented with 10.6g/L moldex and 4.9ml/L propionic acid. Fly stocks and crosses were maintained at 25°C on a 12 h light/ 12 h dark cycle. For poor diet experiments, mid-L3 larvae were raised on medium that corresponds to 20% nutrients of regular medium, with 1.2% cornmeal, 1.2% yeast, 0.62% agar supplemented with 0.98ml/L propionic acid. L2 larvae were selected 48-52 hours after egg laying (AEL), early L3 larvae were selected 72-90 hours AEL (3 days), mid-L3 larvae were selected 96-110 hours AEL (4 days) and L3 wandering larvae were selected 110-120 hours AEL (5 days).

Mutated and transgenic lines generation

To generate *NimB5*^{SK1} line, we crossed *yw;;nos-Cas9(III-attP2)* flies (germline specific expression) with *y w; U6-gRNA/TM6B*. We used the following guideRNA: GTCGATTATAGGACAACTGC. For overexpression and complementation studies, the genomic region from the 5'UTR to the stop codon of the *NimB5* gene was amplified from BACR09N24 and cloned into the pDONR207 Gateway vector (Invitrogen) and subsequently sub-cloned in the pTW (Drosophila Genomics Resource Center plasmid) transgenesis vector and used to generate transgenic *UAS-NimB5* flies. For the *UAS-NimB5-RFP*, the *NimB5* cDNA sequence without STOP codon was cloned into the entry vector pENTR/D-Topo (Invitrogen) and subsequently shuttled into the RFP expression vectors pTWR (C-terminal RFP tag), obtained from the DGRC *Drosophila* Gateway vector collection. Plasmids were injected either at the *Fly facility* platform of Clermont-Ferrand (France) or by *BestGene* Inc. (Chino Hills, CA, USA). All plasmids required are listed in Supplementary Figure 2.2. Primers sequences are provided in Supplementary Figure 2.3

Hemocyte counts by flow cytometry

Hemocytes were bled into 120 µL of PBS containing 1 nM phenylthiourea (PTU, Sigma) to prevent melanization according to Petraki et al [55]. Hemocytes were counted based on their morphometric properties with a BD Accuri C6 flow cytometer, USA. Cells were selected based on their size with a FSC-A from $2.5.10^6$ to $3.5.10^6$ and based on their granularity with a SSC-A from $1.8.10^5$ to $2.5.10^5$. In a second part, cells were gated for singlets (FSC-H versus FSC-A). For fluorescent hemocytes, we used FL1 (GFP) or FL2 (dsred) detectors.

Animals' viability and transition assays

Twenty-four hours after the embryo collection, 1st instar larvae raised at 18°C were picked from the grape juice collection plates using a paintbrush and transferred to fresh plates with poor diet and switched to 29°C when required. The number of living/dead animals was counted and scored for larval stage (1st, 2nd, 3rd instar). Larval stages were determined by mouth hook or anterior and posterior spiracle morphology.

Triglyceride measurements

We quantified free glycerol and all CCA substrates with the free glycerol reagent (F6428, Sigma) and the triglyceride reagent (TR, T2449, Sigma). Fat bodies from 15-20 wandering L3 larvae were dissected in water, heated to 70°C for 10 min and centrifuged for 2 min at 13000 RPM. Protein concentration was measured by colorimetric method (Pierce™ BCA Protein Assay Kit, Thermo Fisher Scientific). Flat-bottom 96-wells plates containing 20 µL of sample supernatants (in 4 wells) with either 20 µL of PBS (2 wells) or 20 µL of TR (2 wells) were centrifuged for 3 min at maximum speed and incubated for 30 min at 37°C. After incubation, 100 µL of free glycerol kit reagent were added to each sample and incubated for 10 min. Results were normalized using a standard curve generated after serial dilutions of glycerol standard solution. Plates were measured on an Infinite 200 Pro microplate reader (Tecan) at 540nm. For data analysis, the value of the "PBS incubated sample" was first subtracted from the value of the "TR incubated sample" to remove the background. Then the amount of triglycerides was estimated using the glycerol standard curve and divided by the protein concentration for each sample.

Ecdysone feeding experiments

20 early L3 larvae (96–110hours AEL) were incubated in 400 µl of crushed banana supplemented with 20 µl of 20-hydroxyecdysone (H5142, Sigma, dissolved in water) at the final concentration of 0.5 mM for 5 hours. Experiments were repeated thrice.

RT-qPCR

20–25 dissected fat bodies from mid-L3 or wandering L3 larvae were collected in 300 µl of Trizol (Invitrogen). Total RNA was extracted according to the manufacturer's instructions. RNA quality and quantity were determined using a NanoDrop ND-1000 spectrophotometer. 500 ng of RNA was used to generate cDNA using SuperScript II (Invitrogen, Carlsbad, California, United States). qPCR was performed using dsDNA dye SYBR Green I (Roche Diagnostics, Basel, Switzerland). Expression values were normalized to *RpL32*. Primer sequences used are provided in Table S3.

Live imaging, staining and microscopy

For Nile red and Bodipy™ staining (to observe intracellular lipid droplets), fat bodies from wandering L3 larvae were dissected in PBS and fixed for 30 min. For Nile Red staining, fixed fat bodies were incubated in Nile Red solution (diluted 1:100 in 1X PBS from a 100 µg/ml stock solution in acetone, Sigma N3013) for 60 min and washed with 1X PBS before mounting. For Bodipy™ staining, fat bodies were incubated for 30 min in Bodipy™ 493/503 (diluted 1:100 in 1X PBS, Life technologies, D3922).

For PH3 staining of hemocytes, mid-L3 larvae were bled in 1X PBS on slides and allowed to adhere for 15 min. Cells were fixed for 20 minutes in PBS, 0.1% Tween 20 (PBT), and 4% paraformaldehyde; then stained with primary antibody [1/500 rabbit anti-PH3 (Upstate/Millipore)]. Secondary staining was performed with Alexa488 anti-rabbit antibodies (Invitrogen). Then cells were stained with a 1/15000 dilution of 4',6- diamidino-2-phenylindole (DAPI) (Sigma) and mounted in antifading agent Citifluor AF1 (Citifluor Ltd.). The mitotic index was determined by counting the number of PH3 positive cells (green) over all hemocytes (marked with live *Hml$^{\Delta}$DsRed.nls*). More than 500 cells were counted per genotype and per assay. The mean and S.E.M. of mitoses per hemocyte pool are shown for each genotype or treatment in the graphs. For EdU labeling, mid-L3 larvae were fed on fly food containing 1 mM 5-ethynyl-2 deoxyuridine (Click-iT EdU, Thermo Fisher Scientific) for 4 hours for hemocyte

staining and 3 hours for lymph gland staining at 25°C. Click-iT EdU staining was performed on released hemocytes or dissected lymph glands according to the manufacturer's instructions. Counts were performed by visual inspection. More than 500 cells were counted per genotype and per assay for peripheral hemocytes. For the visualization of NimB5-RFP on hemocytes, larvae were bled without vortexing. Hemocytes were allowed to adhere to slides for 45 min, then were fixed with PFA 4%/Triton0,1% and stained for DAPI (dilution 1/80000, Thermo Fisher Scientific D1306). Images were acquired with a Zeiss AxioImager Z.1, with a 63X objective. Images were taken on a Zeiss LSM 700 Upright confocal microscope at the "Bioimaging and optics platform" in EPFL. Images were processed using Image J. For the visualization of NimB5^{flyfos} in fat body and hemocytes, tissues were dissected and stained against V5 tag. Images were taken on a Zeiss LSM 700 Upright confocal microscope at the "BioImaging and Optics Platform" at EPFL. Images were processed using ImageJ.

Cell area measurement upon spreading

To measure hemocyte area upon spreading, we proceeded as for hemocyte counting. *Hml$^{\Delta}$DsRed.nls* hemocytes were let to spread on a glass slide for 45 minutes in Schneider medium supplemented with PTU. After 45 min, cells were fixed with PFA 4%/Triton 0,1% for 15 min, stained with Alexa Fluor^{TM} 488 phalloidin for 3h at a dilution of 1/100 (Thermo Fisher Scientific, A12379) and DAPI at a dilution of 1/80000 for 10min. Cells were imaged under a Zeiss AxioImager Z.1 with a 20X objective and images were analyzed with the Cell profiler software. We design software to select DAPI positive and *Hml$^{\Delta}$DsRed.nls* positive cells and to measure their respective GFP area staining. All settings were designed by visual inspection. About 1000 cells per genotype pooled from three independent experiments were analysed. To measure surface area in free floating hemocytes, third instar larvae were bled into PBS without calcium and magnesium, supplemented with EDTA 5mM at 37°C for 15 min and placed on ice until analysis. The Invitrogen™ Tali™ Image-based Cytometer was used to measure size of about 10 000 cells.

Ex vivo larval hemocyte phagocytosis assay

Ex vivo phagocytosis assay was performed with pHrodo™ Green succinimidyl ester (SE) labeled bacteria (Gram-negative, *Escherichia coli*, and Gram-positive, *Staphylococcus aureus*, Invitrogen) based on the following method [75]. pHrodo™ dye fluorescence increases strongly

when submitted to a low pH, so that it allows to follow the internalization process. Five wandering third instar larvae were bled into 120 µL Schneider medium (Gibco) containing 1 nM phenylthiourea (PTU, Sigma). Hemocytes were incubated in 1.5 mL LoBind tubes (Eppendorf) for 45 min at RT at a ratio of 10^5 pHrodo™ particules/hemocyte. To stop phagocytosis, tubes were kept on ice until FACS analysis. Phagocytosis of pHrodo™ particles was quantified using a flow cytometer (BD Accuri C6 flow cytometer, USA). 75 µL volume was read in ultra-low attachment 96-well flat bottom plates (Costar no. 3474, Corning) at medium speed (35 µL /min). In a first step, hemocytes were identified using the *Hml$^{\Delta}$DsRed.nls* live staining. The fluorescence intensity of single hemocytes was measured in the red channel with 488nm laser and 585/40 standard filter. The green pHrodo™ signal, indicative of hemocytes with effective phagocytosis, was monitored with 488nm laser and 533/30 standard filter. At least 2000 cells per genotype and per assay were analyzed. Results are an average of three independent experiments.

Crystal cell counts in whole hemocyte population

To determinate the ratio of crystal cells among the total population of hemocytes, we generated wild type and *NimB5^{SK1}* fly lines containing the *Lz-Gal4,UAS-GFP* reporter specific for crystal cells with *Hml$^{\Delta}$DsRed.nls* that marks both plasmatocytes and crystal cells. For each experiment, eight wandering third instar larvae were bled into 30 µL Schneider medium (Gibco) containing 1 nM PTU and 0.5% PFA to block crystal cell rupture. Larvae were bled individually into 12 wells slides coated with teflon/silane (Tekdon^{TM}). Cells were allowed to spread on slides for 30min, then blocked with 4% PFA and 0.1% triton and stained with DAPI. We counted by eye and calculated the ratio of all *Lz-Gal4,UAS-GFP* positive cells over *HmlΔDsRed.nls* positive cells. Results are expressed as an average of 12 wells and are representative of three independent experiments.

Melanization assays

Phenoloxidase assay: hemolymph was collected by dissecting larvae in 4 °C PBS. The protein concentration was adjusted after a BCA test. Sample volumes were adjusted in 20 µl of 5 mM $CaCl_2$ solution. After addition of 80 µl L-DOPA solution (20 mM, pH 6.6), the samples were incubated at 29 °C in the dark. The OD at 492 nm was then measured for 100 minutes using an Infinite 200 Pro microplate reader (Tecan). Reading was performed every 2 minutes after 2

seconds of shaking. A L-DOPA solution without hemolymph was used as a blank. Each experiment was repeated three times. Wild-type and *NimB5*^{sk1} third instar larvae were pricked between tracheae on the posterior side with a sterile needle (diameter ~5 µm). Larvae were transferred to 29°C for 30min. Pictures were captured with a Leica DFC300FX camera and Leica Application Suite. For publication purposes, brightness and contrast were increased on some images. For the visualization of sessile crystal cells, twenty third instar larvae were heated in 0.5 ml PBS in Eppendorf tubes for 15 min at 67 °C. Larvae were mounted on glass slides over a white background and imaged. For quantification, black punctae were counted circumferentially in the posterior-most segments A6, A7 and A8.

Wasp infestation and quantification of fly survival to wasp infestation

For wasp infestations, 25 synchronized second-instar wild-type or *NimB5* mutant larvae were placed on a pea-sized mound of fly food within a custom-built wasp trap in the presence of three female wasps for 2 h (*L. boulardi*). For survival experiments, parasitized larvae were kept at room temperature and scored daily for flies and wasps. The difference between enclosed flies and wasps to the initial number of larvae was set as dead larvae/pupae.

Statistical tests

Experiments were repeated at least three times on separate days. Unless otherwise indicated, error bars represent the standard error of replicate experiments. Data were analyzed in GraphPad Prism 6.0. For hemocyte counts, data successfully passed a Shapiro-Wilk normality test (alpha=0.05, n=10) so that we could assume that samples followed a Gaussian distribution. Significance tests were performed using the Student *t* test (with a confidence level of 95%). P values of < 0.05 = *, < 0.01 = ** and < 0.001 = ***. For experiments with more than 2 conditions, significance was tested using Anova test (with a confidence level of 95%). P values of < 0.05 = *, < 0.01 = ** and < 0.001 = ***

2.6 Supplementary materials

	Details	Source
w^{1118}		
y,w		
w;NimB5^{SK1}		This study

w^{iso};NimB5^{SK1}		This study
yw;NimB5^{SK1}		This study
UAS-NimB5-IR	KK line	VDRC (105320)
Control KK line		VDRC (60100)
UAS-NimB5-IR	GD line	VDRC (v15758)
UAS-NimB5-IR	Trip line	Bloomington (51162)
Control Trip line		Bloomington (36303)
w;UAS-NimB5 (II)	*NimB5* Genomic DNA	This study
w;;UAS-NimB5 (III)	*NimB5* Genomic DNA	This study
w;UAS-NimB5-RFP ; (II)	*NimB5* cDNA	This study
w;;NimB5-sGFP-V5	Injection of pFLYFOS 8882336809946705 in VK33 attP docking site	This study
;;eater^{1}		
w;; Hml$^{\Delta}$.DsRed.nls		[21]
w;NimB5^{SK1};HmlΔ.DsRed.nls		
w;Hml$^{\Delta}$-Gal4,UAS-GFP;		[77]
w;NimB5^{SK1}; Hml$^{\Delta}$ -Gal4,UAS-GFP;		
yw,lz-Gal4,UAS-GFP;; Hml$^{\Delta}$DsRed.nls		
yw,lz-Gal4,UAS-GFP; NimB5^{SK1}; Hml$^{\Delta}$DsRed.nls		
;Tub-gal80ts,UAS-GFP; Lpp-Gal4/TM3	*Referred to as Lpp^{ts}*	
;UAS-NimB5;Lpp-Gal4/TM3		
;Act5c/cyoGFP;		
;UAS-Bax/cyoGFP;		[78]
; NimB5^{SK1},UAS-Bax/cyoGFP;		
;UAS-Pvf2;		Gift from J.M. Reichhart
;UAS-Ras85D^{V12};		Bloomington (64196)
;UAS-Ras-IR;		Bloomington (31654)
;UAS-Ecd-IR		Bloomington (41676)
;UAS-dMyc.Z;		Bloomington (9674)
;UAS-dMyc-IR;		Bloomington (25783)
;;UAS-TSC2-IR;	GD line	VDRC (6313)
;UAS-TSC1-IR;	KK LINE	VDRC (110811)
;;UAS-rheb		Bloomington (9689)
;UAS-SP^{vkg}.RFP.3.1;	30 first amino acids of Viking protein followed by RFP	[53] Gift from Pastor-Pareja lab
Df(2L)ED793	*A deficiency encompassing the Nimrod locus*	Bloomington (9061)
wt iso		[56]
Iso ; iso ; TM2/TM6		[56]
FM7 ; iso ; iso		[56]

Iso ; Gla / cyo ; iso		[56]

Supplementary Figure 2.1. List of stocks generated and used in this manuscript

Plasmid name	Antibiotics selection	Origin
pENTR/D-TOPO	Kan^R	Invitrogen
pTW	Amp^R	DGRC
pTWR	Amp^R	DGRC
pOT2-CG16873 Full lenght cDNA clone	Cm^R	DGRC (IP09831)
pCaSpeR4	Amp^R	Our collection
BACR09N24 (RP98-9N24)	Cm^R	BACPAC Resources Center

Supplementary Figure 2.2. List of plasmids and BAC used in this manuscript

Primer name	Primer sequence	qRT primers efficiency
NimB5 F deletion screan	TAA GGA GTG CTC AAG ATG TG	
NimB5 R deletion screen	TTG CTT CCA ATT CTC AGT CT	
NimB5 deletion screen	GGG TAC ATG GTC CTA TAA TCG	
NimB1 qRT F	CGG CCA AAG TGT GAG AGA TT	1.945
NimB1 qRT R	TAT CGT CAC AGC TTC CGT TC	
NimB2 qRT F	GAG TGT CTG CCG AAG TGT GA	1.919
NimB2 qRT R	TCA CAT ATC CGG TCT TGC AG	
NimB3 qRT F	TCC CAA CTC CAG AAA TCG TC	1.988
NimB3 qRT R	AGC AGT CCT CCG AGC AAA T	
NimB4 qRT F	TTG TGC TCA ACT ACC GCA AC	1.950
NimB4 qRT R	CGT CCA GCT CGT ATC CCT TA	
NimB5 qRT F	CGT AAC GAC AAC GGT GAC TG	1.973
NimB5 qRT R	GTC TCG TCC AGC TTG TAG CC	
RpL32 qRT F	GAC GCT TCA AGG GAC AGT ATC TG	1.983
RpL32 qRT R	AAA CGC GGT TCT GCA TGA G	
Dipt qRT F	GCT GCG CAA TCG CTT CTA CT	2.027
Dipt qRT R	TGG TGG AGT GGG CTT CAT G	
Drs qRT F	CGT GAG AAC CTT TTC CAA TAT GAT G	1.963
Drs qRT R	TCC CAG GAC CAC CAG CAT	
Puc qRT F	CAA CCC CGC ACC TGA ATA GT	1.976
Puc qRT R	CTT CTC CTC CTC CTC TGG CT	
Act5c qRT F	GAGCGCGGTTACTCTTTCAC	1.983

Act5c qRT R	GCC ATC TCC TGC TCA AAG TC	
Lpp qRT F	GAA GTT CCT GGT GCA CAA CG	1.992
Lpp qRT R	CTT GCG CTT CTT GGA GGA GA	
Hml qRT F	GAG CAC TGC ATA CCC CTA CC	1.980
Hml qRT R	CCG TGC TGG TTA CAC TCC TT	
Socs36 qRT F	GCA CAG AAG GCA GAC C	1.989
Socs36 qRT R	ACG TAG GAG ACC CGT AT	
TotA qRT F	CTG CTC TTA TGT AAG TAG TAT CGA AT	1.965
TotA qRT R	CAA CGA TCC TCG CCT TTC GAC C	
TotM qRT F	TCG ACA GCC TGG TCA CTT TC	1.971
TotM qRT R	ACC AAG ACC ACA CGA GCA TT	
NimB5_attB1F	GGG GAC AAG TTT GTA CAA AAA AGC AGG CTG GAT GCA AAT AAA ATA TTT CAG TAA CCA AAA G	
NimB5_attB2R	GGG GAC CAC TTT GTA CAA GAA AGC TGG TAC TGG AAC GCA CAT GGT TG	
NimB5_gateway cloning F	CAC CAT GTG GTT GCG AGA CTT GCG	
NimB5_gateway cloning R	TAC TGG AAC GCA CAT GGT TGA	

Supplementary Figure 2.3. List of primers used in this manuscript

2.7 Miscellaneous

Authors contributions

Conceived and designed the experiments: ER BL. Performed the experiments: ER BP JPD JPB MP SK. Analyzed the data: ER BP JPD BL. Wrote the paper: ER BL.

Acknowledgments

We thank Marie Meister, Claudine Neyen and Mark Hanson for critical reading of the manuscript. We thank the BioEM platform (EPFL) for their important help with the electron microscopy experiments, the Flow Cytometry Core Facility (EPFL) for their constant assistance in the use of the Accuri DB machine, and the Bioimaging and optics platform (EPFL) for their help using confocal microscopes and designing the Cell profiler analyser. We thank the VDCR in Vienna and the Bloomington Stock Center (NIH P40OD018537) at Indiana University for the fly stocks.

Conflicts of interest

The authors declare no conflicts of interest.

2.8 References

1 Tennessen JM & Thummel CS (2011) Coordinating growth and maturation - insights from Drosophila. *Curr. Biol.* 21, R750–7.

2 Godfrey KM, Haugen G, Kiserud T, Inskip HM, Cooper C, Harvey NCW, Crozier SR, Robinson SM, Davies L, Group TSWSS & Hanson MA (2012) Fetal Liver Blood Flow Distribution: Role in Human Developmental Strategy to Prioritize Fat Deposition versus Brain Development. *PLoS ONE* 7, e41759.

3 Dolezal T, Krejcova G, Bajgar A, Nedbalova P & Strasser P (2019) Molecular regulations of metabolism during immune response in insects. *Insect Biochem. Mol. Biol.* 109, 31–42.

4 Rauw WM (2012) Immune response from a resource allocation perspective. *Front Genet* 3, 267.

5 Schmid-Hempel P (2013) *Evolutionary Parasitology*, Oxford Scholarship Oxford University Press.

6 Moret Y & Schmid-Hempel P (2000) Survival for immunity: the price of immune system activation for bumblebee workers. *Science* 290, 1166–1168.

7 van der Most PJ, de Jong B, Parmentier HK & Verhulst S (2010) Trade-off between growth and immune function: a meta-analysis of selection experiments. *Functional Ecology* 25, 74–80.

8 Kraaijeveld AR & Godfray HC (1997) Trade-off between parasitoid resistance and larval competitive ability in Drosophila melanogaster. *Nature* 389, 278–280.

9 Galati PC, Chiarello PG & Simões BP (2016) Variation of resting energy expenditure after the first chemotherapy cycle in acute leukemia patients. *Nutr Cancer* 68, 86–93.

10 Cheng LY, Bailey AP, Leevers SJ, Ragan TJ, Driscoll PC & Gould AP (2011) Anaplastic lymphoma kinase spares organ growth during nutrient restriction in Drosophila. *Cell* 146, 435–447.

11 McKean KA, Yourth CP, Lazzaro BP & Clark AG (2008) The evolutionary costs of immunological maintenance and deployment. *BMC Evol. Biol.* 8, 76–19.

12 Katona P & Katona-Apte J (2008) The interaction between nutrition and infection. *Clin. Infect. Dis.* 46, 1582–1588.

13 Rice AL, Sacco L, Hyder A & Black RE (2000) Malnutrition as an underlying cause of childhood deaths associated with infectious diseases in developing countries. *Bull. World Health Organ.* 78, 1207–1221.

14 Binggeli O, Neyen C, Poidevin M & Lemaitre B (2014) Prophenoloxidase activation is required for survival to microbial infections in Drosophila. *PLoS Pathog.* 10, e1004067.

15 Honti V, Csordás G, Kurucz É, Márkus R & Andó I (2014) The cell-mediated immunity of Drosophila melanogaster: hemocyte lineages, immune compartments, microanatomy and

regulation. *Dev. Comp. Immunol.* 42, 47–56.
16 Stofanko M, Kwon SY & Badenhorst P (2010) Lineage tracing of lamellocytes demonstrates Drosophila macrophage plasticity. *PLoS ONE* 5, e14051.
17 Anderl I, Vesala L, Ihalainen TO, Vanha-Aho L-M, Andó I, Rämet M & Hultmark D (2016) Transdifferentiation and Proliferation in Two Distinct Hemocyte Lineages in Drosophila melanogaster Larvae after Wasp Infection. *PLoS Pathog.* 12, e1005746.
18 Wood W & Jacinto A (2007) Drosophila melanogaster embryonic haemocytes: masters of multitasking. *Nat. Rev. Mol. Cell Biol.* 8, 542–551.
19 Lanot R, Zachary D, Holder F & Meister M (2001) Postembryonic hematopoiesis in Drosophila. *Dev. Biol.* 230, 243–257.
20 Jung S-H, Evans CJ, Uemura C & Banerjee U (2005) The Drosophila lymph gland as a developmental model of hematopoiesis. *Development* 132, 2521–2533.
21 Makhijani K, Alexander B, Tanaka T, Rulifson E & Brückner K (2011) The peripheral nervous system supports blood cell homing and survival in the Drosophila larva. *Development* 138, 5379–5391.
22 Evans CJ & Banerjee U (2003) Transcriptional regulation of hematopoiesis in Drosophila. *Blood Cells Mol. Dis.* 30, 223–228.
23 Honti V, Csordás G, Márkus R, Kurucz É, Jankovics F & Andó I (2010) Cell lineage tracing reveals the plasticity of the hemocyte lineages and of the hematopoietic compartments in Drosophila melanogaster. *Mol. Immunol.* 47, 1997–2004.
24 Crozatier M & Meister M (2007) Drosophila haematopoiesis. *Cell. Microbiol.* 9, 1117–1126.
25 Makhijani K & Brückner K (2012) Of blood cells and the nervous system: hematopoiesis in the Drosophila larva. *Fly (Austin)* 6, 254–260.
26 Makki R, Cinnamon E & Gould AP (2014) The development and functions of oenocytes. *Annu. Rev. Entomol.* 59, 405–425.
27 Babcock DT, Brock AR, Fish GS, Wang Y, Perrin L, Krasnow MA & Galko MJ (2008) Circulating blood cells function as a surveillance system for damaged tissue in Drosophila larvae. *Proc. Natl. Acad. Sci. U.S.A.* 105, 10017–10022.
28 Welman A, Serrels A, Brunton VG, Ditzel M & Frame MC (2010) Two-color photoactivatable probe for selective tracking of proteins and cells. *J. Biol. Chem.* 285, 11607–11616.
29 Holz A, Bossinger B, Strasser T, Janning W & Klapper R (2003) The two origins of hemocytes in Drosophila. *Development* 130, 4955–4962.
30 Munier A-I, Doucet D, Perrodou E, Zachary D, Meister M, Hoffmann JA, Janeway CA & Lagueux M (2002) PVF2, a PDGF/VEGF-like growth factor, induces hemocyte proliferation in Drosophila larvae. *EMBO Rep.* 3, 1195–1200.
31 Lee T, Feig L & Montell DJ (1996) Two distinct roles for Ras in a developmentally regulated cell migration. *Development* 122, 409–418.
32 Bretscher AJ, Honti V, Binggeli O, Burri O, Poidevin M, Kurucz É, Zsámboki J, Andó I & Lemaitre B (2015) The Nimrod transmembrane receptor Eater is required for hemocyte attachment to the sessile compartment in Drosophila melanogaster. *Biol Open* 4, 355–363.
33 Leitão AB & Sucena E (2015) Drosophila sessile hemocyte clusters are true hematopoietic

tissues that regulate larval blood cell differentiation. *Elife* 4, 239.
34 Paredes JC, Welchman DP, Poidevin M & Lemaitre B (2011) Negative regulation by amidase PGRPs shapes the Drosophila antibacterial response and protects the fly from innocuous infection. *Immunity* 35, 770–779.
35 Dionne MS, Pham LN, Shirasu-Hiza M & Schneider DS (2006) Akt and FOXO dysregulation contribute to infection-induced wasting in Drosophila. *Curr. Biol.* 16, 1977–1985.
36 Bretscher AJ, Honti V, Binggeli O, Burri O, Poidevin M, Kurucz É, Zsámboki J, Andó I & Lemaitre B (2015) The Nimrod transmembrane receptor Eater is required for hemocyte attachment to the sessile compartment in Drosophila melanogaster. *Biol Open* 4, 355–363.
37 Melcarne C, Ramond E, Dudzic J, Bretscher AJ, Kurucz É, Andó I & Lemaitre B (2019) Two Nimrod receptors, NimC1 and Eater, synergistically contribute to bacterial phagocytosis in Drosophila melanogaster. *FEBS J.* 1248, 1116008.
38 Figueroa-Clarevega A & Bilder D (2015) Malignant Drosophila tumors interrupt insulin signaling to induce cachexia-like wasting. *Dev. Cell* 33, 47–55.
39 Kwon Y, Song W, Droujinine IA, Hu Y, Asara JM & Perrimon N (2015) Systemic organ wasting induced by localized expression of the secreted insulin/IGF antagonist ImpL2. *Dev. Cell* 33, 36–46.
40 Woodcock KJ, Kierdorf K, Pouchelon CA, Vivancos V, Dionne MS & Geissmann F (2015) Macrophage-derived upd3 cytokine causes impaired glucose homeostasis and reduced lifespan in Drosophila fed a lipid-rich diet. *Immunity* 42, 133–144.
41 Colombani J, Raisin S, Pantalacci S, Radimerski T, Montagne J & Léopold P (2003) A nutrient sensor mechanism controls Drosophila growth. *Cell* 114, 739–749.
42 Somogyi K, Sipos B, Pénzes Z, Kurucz É, Zsámboki J, Hultmark D & Andó I (2008) Evolution of genes and repeats in the Nimrod superfamily. *Mol. Biol. Evol.* 25, 2337–2347.
43 Hashimoto Y, Tabuchi Y, Sakurai K, Kutsuna M, Kurokawa K, Awasaki T, Sekimizu K, Nakanishi Y & Shiratsuchi A (2009) Identification of lipoteichoic acid as a ligand for draper in the phagocytosis of Staphylococcus aureus by Drosophila hemocytes. *J. Immunol.* 183, 7451–7460.
44 Kurant E, Axelrod S, Leaman D & Gaul U (2008) Six-microns-under acts upstream of Draper in the glial phagocytosis of apoptotic neurons. *Cell* 133, 498–509.
45 Freeman MR, Delrow J, Kim J, Johnson E & Doe CQ (2003) Unwrapping glial biology: Gcm target genes regulating glial development, diversification, and function. *Neuron* 38, 567–580.
46 Kurucz É, Márkus R, Zsámboki J, Folkl-Medzihradszky K, Darula Z, Vilmos P, Udvardy A, Krausz I, Lukacsovich T, Gateff E, Zettervall C-J, Hultmark D & Andó I (2007) Nimrod, a putative phagocytosis receptor with EGF repeats in Drosophila plasmatocytes. *Curr. Biol.* 17, 649–654.
47 Fernández-Ayala DJM, Chen S, Kemppainen E, O'Dell KMC & Jacobs HT (2010) Gene expression in a Drosophila model of mitochondrial disease. *PLoS ONE* 5, e8549.
48 Sarov M, Barz C, Jambor H, Hein MY, Schmied C, Suchold D, Stender B, Janosch S, K J VV, Krishnan RT, Krishnamoorthy A, Ferreira IRS, Ejsmont RK, Finkl K, Hasse S, Kämpfer P,

Plewka N, Vinis E, Schloissnig S, Knust E, Hartenstein V, Mann M, Ramaswami M, VijayRaghavan K, Tomancak P & Schnorrer F (2016) A genome-wide resource for the analysis of protein localisation in Drosophila. *Elife* 5, e12068.

49 Graveley BR, Brooks AN, Carlson JW, Duff MO, Landolin JM, Yang L, Artieri CG, van Baren MJ, Boley N, Booth BW, Brown JB, Cherbas L, Davis CA, Dobin A, Li R, Lin W, Malone JH, Mattiuzzo NR, Miller D, Sturgill D, Tuch BB, Zaleski C, Zhang D, Blanchette M, Dudoit S, Eads B, Green RE, Hammonds A, Jiang L, Kapranov P, Langton L, Perrimon N, Sandler JE, Wan KH, Willingham A, Zhang Y, Zou Y, Andrews J, Bickel PJ, Brenner SE, Brent MR, Cherbas P, Gingeras TR, Hoskins RA, Kaufman TC, Oliver B & Celniker SE (2011) The developmental transcriptome of Drosophila melanogaster. *Nature* 471, 473–479.

50 Casas-Vila N, Bluhm A, Sayols S, Dinges N, Dejung M, Altenhein T, Kappei D, Altenhein B, Roignant J-Y & Butter F (2017) The developmental proteome ofDrosophila melanogaster. *Genome Res.* 27, 1273–1285.

51 Delanoue R, Slaidina M & Léopold P (2010) The steroid hormone ecdysone controls systemic growth by repressing dMyc function in Drosophila fat cells. *Dev. Cell* 18, 1012–1021.

52 Wullschleger S, Loewith R & Hall MN (2006) TOR signaling in growth and metabolism. *Cell* 124, 471–484.

53 Liu M, Feng Z, Ke H, Liu Y, Sun T, Dai J, Cui W & Pastor-Pareja JC (2017) Tango1 spatially organizes ER exit sites to control ER export. *J. Cell Biol.* 216, 1035–1049.

54 Kondo S & Ueda R (2013) Highly improved gene targeting by germline-specific Cas9 expression in Drosophila. *Genetics* 195, 715–721.

55 Petraki S, Alexander B & Brückner K (2015) Assaying Blood Cell Populations of the Drosophila melanogaster Larva. *J Vis Exp*.

56 Ferreira ÁG, Naylor H, Esteves SS, Pais IS, Martins NE & Teixeira L (2014) The Toll-dorsal pathway is required for resistance to viral oral infection in Drosophila. *PLoS Pathog.* 10, e1004507.

57 Rizki TM, Rizki RM & Grell EH (1980) A mutant affecting the crystal cells inDrosophila melanogaster. *Wilehm Roux Arch Dev Biol* 188, 91–99.

58 Fagotto F & Gumbiner BM (1996) Cell contact-dependent signaling. *Dev. Biol.* 180, 445–454.

59 Charroux B & Royet J (2009) Elimination of plasmatocytes by targeted apoptosis reveals their role in multiple aspects of the Drosophila immune response. *Proc. Natl. Acad. Sci. U.S.A.* 106, 9797–9802.

60 Defaye A, Evans I, Crozatier M, Wood W, Lemaitre B & Leulier F (2009) Genetic ablation of Drosophila phagocytes reveals their contribution to both development and resistance to bacterial infection. *J Innate Immun* 1, 322–334.

61 Boulan L, Milán M & Léopold P (2015) The Systemic Control of Growth. *Cold Spring Harb Perspect Biol* 7, a019117.

62 Bajgar A, Kucerova K, Jonatova L, Tomcala A, Schneedorferova I, Okrouhlik J & Dolezal T (2015) Extracellular adenosine mediates a systemic metabolic switch during immune response. *PLoS Biol.* 13, e1002135.

63 Kraaijeveld AR, Ferrari J & Godfray HCJ (2002) Costs of resistance in insect-parasite and insect-parasitoid interactions. *Parasitology* 125 Suppl, S71–82.

64 Visser B, Le Lann C, Blanken den FJ, Harvey JA, van Alphen JJM & Ellers J (2010) Loss of lipid synthesis as an evolutionary consequence of a parasitic lifestyle. *Proc. Natl. Acad. Sci. U.S.A.* 107, 8677–8682.

65 Paredes JC, Herren JK, Schüpfer F & Lemaitre B (2016) The Role of Lipid Competition for Endosymbiont-Mediated Protection against Parasitoid Wasps in Drosophila. *MBio* 7, e01006–16.

66 Slaidina M, Delanoue R, Gronke S, Partridge L & Léopold P (2009) A Drosophila insulin-like peptide promotes growth during nonfeeding states. *Dev. Cell* 17, 874–884.

67 Colombani J, Bianchini L, Layalle S, Pondeville E, Dauphin-Villemant C, Antoniewski C, Carré C, Noselli S & Léopold P (2005) Antagonistic actions of ecdysone and insulins determine final size in Drosophila. *Science* 310, 667–670.

68 Shim J, Mukherjee T & Banerjee U (2012) Direct sensing of systemic and nutritional signals by haematopoietic progenitors in Drosophila. *Nat. Cell Biol.* 14, 394–400.

69 Benmimoun B, Polesello C, Waltzer L & Haenlin M (2012) Dual role for Insulin/TOR signaling in the control of hematopoietic progenitor maintenance in Drosophila. *Development* 139, 1713–1717.

70 Dragojlovic-Munther M & Martinez-Agosto JA (2012) Multifaceted roles of PTEN and TSC orchestrate growth and differentiation of Drosophila blood progenitors. *Development* 139, 3752–3763.

71 Tokusumi T, Tokusumi Y, Hopkins DW & Schulz RA (2015) Bag of Marbles controls the size and organization of the Drosophila hematopoietic niche through interactions with the Insulin-like growth factor pathway and Retinoblastoma-family protein. *Development* 142, 2261–2267.

72 Banerjee U, Girard JR, Goins LM & Spratford CM (2019) Drosophila as a Genetic Model for Hematopoiesis. *Genetics* 211, 367–417.

73 Mihajlovic Z, Tanasic D, Bajgar A, Perez-Gomez R, Steffal P & Krejci A (2019) Lime is a new protein linking immunity and metabolism in Drosophila. *Dev. Biol.* 452, 83–94.

74 Makhijani K, Alexander B, Rao D, Petraki S, Herboso L, Kukar K, Batool I, Wachner S, Gold KS, Wong C, O'Connor MB & Brückner K (2017) Regulation of Drosophila hematopoietic sites by Activin-β from active sensory neurons. *Nat Commun* 8, 15990.

75 Miksa M, Komura H, Wu R, Shah KG & Wang P (2009) A novel method to determine the engulfment of apoptotic cells by macrophages using pHrodo succinimidyl ester. *J. Immunol. Methods* 342, 71–77.

76 Dudzic JP, Kondo S, Ueda R, Bergman CM & Lemaitre B (2015) Drosophila innate immunity: regional and functional specialization of prophenoloxidases. *BMC Biol.* 13, 81.

77 Sinenko SA & Mathey-Prevot B (2004) Increased expression of Drosophila tetraspanin, Tsp68C, suppresses the abnormal proliferation of ytr-deficient and Ras/Raf-activated hemocytes. *Oncogene* 23, 9120–9128.

78 Gaumer S, Guénal I, Brun S, Théodore L & Mignotte B (2000) Bcl-2 and Bax mammalian

regulators of apoptosis are functional in Drosophila. *Cell Death Differ.* 7, 804–814.

Chapter 3
A secreted factor NimrodB4 promotes the elimination of apoptotic corpses by phagocytes in *Drosophila*

Note: This chapter is based on the published article: "A secreted factor NimrodB4 promotes the elimination of apoptotic corpses by phagocytes in *Drosophila.* 2021, EMBO reports"

Authors: Bianca Petrignani, Samuel Rommelaere, Ketty Hakim-Mishnaevski, Florent Masson, Elodie Ramond, Reut Hilu-Dadia, Mickael Poidevin, Shu Kondo, Estee Kurant & Bruno Lemaitre

Contributions of Bianca Petrignani: Designed the study and wrote the manuscript, conducted FACS, qPCR, cell culture and related imaging assays, conducted histological assays.

3.1 Abstract

Programmed cell death plays a fundamental role in development and tissue homeostasis. Professional and non-professional phagocytes achieve the proper recognition, uptake, and degradation of apoptotic cells, a process called efferocytosis. Failure in efferocytosis leads to autoimmune and neurodegenerative diseases. In *Drosophila*, two transmembrane proteins of the Nimrod family, Draper and SIMU, mediate the recognition and internalization of apoptotic corpses. Beyond this early step, little is known about how apoptotic cell degradation is regulated. Here, we study the function of a secreted member of the Nimrod family, NimB4, and reveal its crucial role in the clearance of apoptotic cells. We show that NimB4 is expressed by macrophages and glial cells, the two main types of phagocytes in *Drosophila*. Similar to *draper* mutants, *NimB4* mutants accumulate apoptotic corpses during embryogenesis and in the larval brain. Our study points to the role of NimB4 in phagosome maturation, more specifically in the fusion between the phagosome and lysosomes. We propose that similar to bridging molecules, NimB4 binds to apoptotic corpses to engage a phagosome maturation program dedicated to efferocytosis.

3.2 Introduction

The clearance of apoptotic cells by phagocytes is an essential process during development and for the maintenance of tissue homeostasis (Arandjelovic & Ravichandran, 2015). Defective apoptotic cell clearance affects organ function and leads to the release of cytotoxic molecules and the development and progression of inflammatory and immune responses (Elliott & Ravichandran, 2010; Nagata *et al*, 2010; Poon *et al*, 2014). Recent studies also point to the importance of apoptotic cell clearance in the brain, as excessive or reduced phagocytosis can lead to neurodegeneration (Etchegaray *et al*, 2016; Purice *et al*, 2016; Hakim-Mishnaevski *et al*, 2019; Hilu-Dadia & Kurant, 2020). Efferocytosis, the phagocytosis of apoptotic cells, is a multi-step process often mediated by professional phagocytes such as macrophages and glia. It begins with the identification of the target cells by receptors that recognize specific “eat-me” signals that are exposed at the surface of apoptotic cells and distinguish them from living cells (Elliott & Ravichandran, 2016; Boada-Romero *et al*, 2020).

One of the best characterized "eat-me" signals is phosphatidylserine (PS), a membrane phospholipid species usually found in the inner leaflet of the plasma membrane, but exposed on the surface of cells undergoing apoptosis (Segawa & Nagata, 2015; Nagata *et al*, 2016). Upon ligand recognition, phagocytic receptors engage downstream signaling pathways that initiate the uptake of the particle through an active and dynamic remodeling of the plasma membrane, which is mainly guided by the actin cytoskeleton (Pearson *et al*, 2003; Stuart & Ezekowitz, 2005; Melcarne *et al*, 2019a). Newly formed phagosomes undergo a maturation process to acquire digestive activity. The phagosome matures through fusion with endosomes and lysosomes, a process involving small GTPases of the Rab family (Kinchen & Ravichandran, 2010). Rab5 regulates the initial fusion events, by tethering early endosomes to the newly formed phagosome (Alvarez-Dominguez *et al*, 1996; Duclos *et al*, 2000; Kinchen *et al*, 2008). As the phagosome matures, Rab5 is replaced by Rab7 in a process called Rab conversion (Kinchen & Ravichandran, 2010; Poteryaev *et al*, 2010; Yousefian *et al*, 2013). Once recruited, Rab7 is responsible for inducing fusion of the phagosome and the lysosome, initiating acidification and digestion of the corpse. A characteristic protein present on the phagolysosome membrane is lysosomal-associated membrane protein 1 (Lamp1), which is needed for lysosome fusion with the phagosome (Huynh *et al*, 2007). Less is known about the final stage of phagosome resolution and how the phagosome is resorbed to allow the phagocyte to return to homeostasis. However, studies have shown that bacteria-containing phagolysosomes in macrophages undergo fragmentation through vesicle budding and constriction (Levin *et al*, 2016; Botelho *et al*, 2020; preprint: Lancaster *et al*, 2020).

Recent studies in mammals have highlighted the importance of bridging molecules in the regulation of efferocytosis. Bridging molecules are secreted proteins that bind to the "eat-me" signal to provide a link between apoptotic cells and phagocytic receptors and enhancing recognition and phagocytosis of apoptotic cells (Savill & Fadok, 2000; Ravichandran, 2003, 2011). In mammals, several bridging molecules have been identified, including milk fat globule-epidermal growth factor 8 (MFG-E8) and growth arrest-specific 6 (Gas6) (Wu *et al*, 2006). Studies have shown that MFG-E8 binds in a Ca^{2+}-dependent manner to PS exposed at the surface of apoptotic cells, engaging their uptake by integrins αvβ3/5 (Hanayama *et al*, 2002; Borisenko *et al*, 2004; Kusunoki *et al*, 2012). Moreover, the absence of MFG-E8 in murine models causes a lupus-like autoimmune disease due to defective clearance of apoptotic cells (Huang *et al*, 2017). In *Caenorhabditis elegans* (*C. elegans*), the secreted

protein TTR-52 mediates recognition of dying cells by linking PS with the phagocyte receptor CED-1 (Wang *et al*, 2010). While these studies have highlighted the relevance of bridging molecules in efferocytosis, the precise function of these molecules remains poorly understood. Some studies point to a role during the early phase of phagocytosis, facilitating apoptotic cell uptake, while others suggest that bridging molecules orient the maturation of the phagosome (Peng & Elkon, 2011; Galvan *et al*, 2012). The mechanism underlying efferocytosis has been well characterized in *Drosophila* (Serizier & McCall, 2017; Davidson & Wood, 2020). In this insect, three phagocytic receptors, the α-PS3/βv integrin heterodimer, Draper, and SIMU, have been identified for their role in the uptake of apoptotic cells (Freeman *et al*, 2003; Manaka *et al*, 2004a; Kurant *et al*, 2008; Nagaosa *et al*, 2011; Nonaka *et al*, 2013; Roddie *et al*, 2019). Studies have shown that the phagocytic ability of embryonic glia to engulf and degrade apoptotic neurons is determined by both SIMU and Draper. SIMU is required for recognition and engulfment of apoptotic neurons by glia, whereas Draper is mostly needed for their degradation (Kurant *et al*, 2008; Shklyar *et al*, 2014). Flies deficient for the two main receptors for apoptotic cells, Draper and SIMU, are viable but their lifespan is reduced and their central nervous system accumulates apoptotic bodies (Draper *et al*, 2014; Etchegaray *et al*, 2016). Although several engulfment receptors in *Drosophila* have been identified, little is known about their mechanism of action. So far, no bridging molecules have been identified in *Drosophila*.

In this study, we find that NimB4, a secreted protein of the Nimrod family, binds to apoptotic corpses in a PS-dependent manner to promote phagocytosis of apoptotic cells by glia and macrophages (also called plasmatocytes). Macrophages from *NimB4* mutants show defective phagocytosis of apoptotic cells *ex vivo*. Similar to *draper* mutants, *NimB4* mutants accumulate apoptotic cells in both embryonic and larval phagocytes, and exhibit motor defect in larvae and reduced lifespan of adults. Further functional studies reveal the role of NimB4 in phagosome maturation, notably in the formation of the phagolysosome. Collectively, this study identifies the first secreted factor involved in the phagocytosis of apoptotic cells in *Drosophila* and suggests an evolutionarily conserved role of bridging molecules in efferocytosis.

3.3 Results

3.3.1 NimB4 is a secreted protein enriched in phagocytes

To identify potential bridging molecules, we searched for secreted proteins expressed in phagocytes that could promote the phagocytosis of apoptotic cells. We focused our attention on secreted members of the Nimrod superfamily with characteristic EGF-like repeats (Bork *et al*, 1996; Callebaut *et al*, 2003; Kurucz *et al*, 2007), transmembrane Nimrod proteins have already been implicated in phagocytosis of bacteria (NimC1, Eater) or apoptotic corpses (SIMU, Draper), and in macrophages sessility and adhesion (Eater). In addition to these receptors, there are five secreted proteins of the Nimrod family called NimB1, B2, B3, B4, and B5 (Ju *et al*, 2006; Kurucz *et al*, 2007; Somogyi *et al*, 2008). Of these, only NimB5 has been characterized and has been shown to regulate peripheral hematopoiesis (Ramond *et al*, 2020). As bridging molecules are usually secreted by phagocytes, we monitored the expression of these five NimBs in macrophages of third-instar larvae. Consistent with a recent transcriptome analysis (Ramond *et al*, 2020), RT–qPCR analysis showed that NimB4 was the most highly expressed NimB member in macrophages (Fig 3.1A). To track the expression of NimB4 at the subcellular level, we generated a transgenic fly line carrying a V5-sGFP-tagged *NimB4* fusion under its own regulatory sequences, derived from the Dresden pFlyFos collection (Sarov *et al*, 2016). We used this reporter gene to follow NimB4 during embryonic and larval stages with a focus on glia and macrophages. At the embryonic stage, NimB4-sGFP appeared to be strongly enriched exclusively in macrophages (Fig 3.1B), whereas at the larval stage NimB4-sGFP was expressed in both macrophages and glial cells (Fig 3.1C,D and Supplementary Figure 3.1). Live and fixed imaging of third-instar larval macrophages showed that NimB4-sGFP is present intracellularly. Live confocal imaging showed that NimB4-sGFP localizes in small dots throughout the cytoplasm, suggesting a localization in the endosomal compartment (Fig 3.1C).

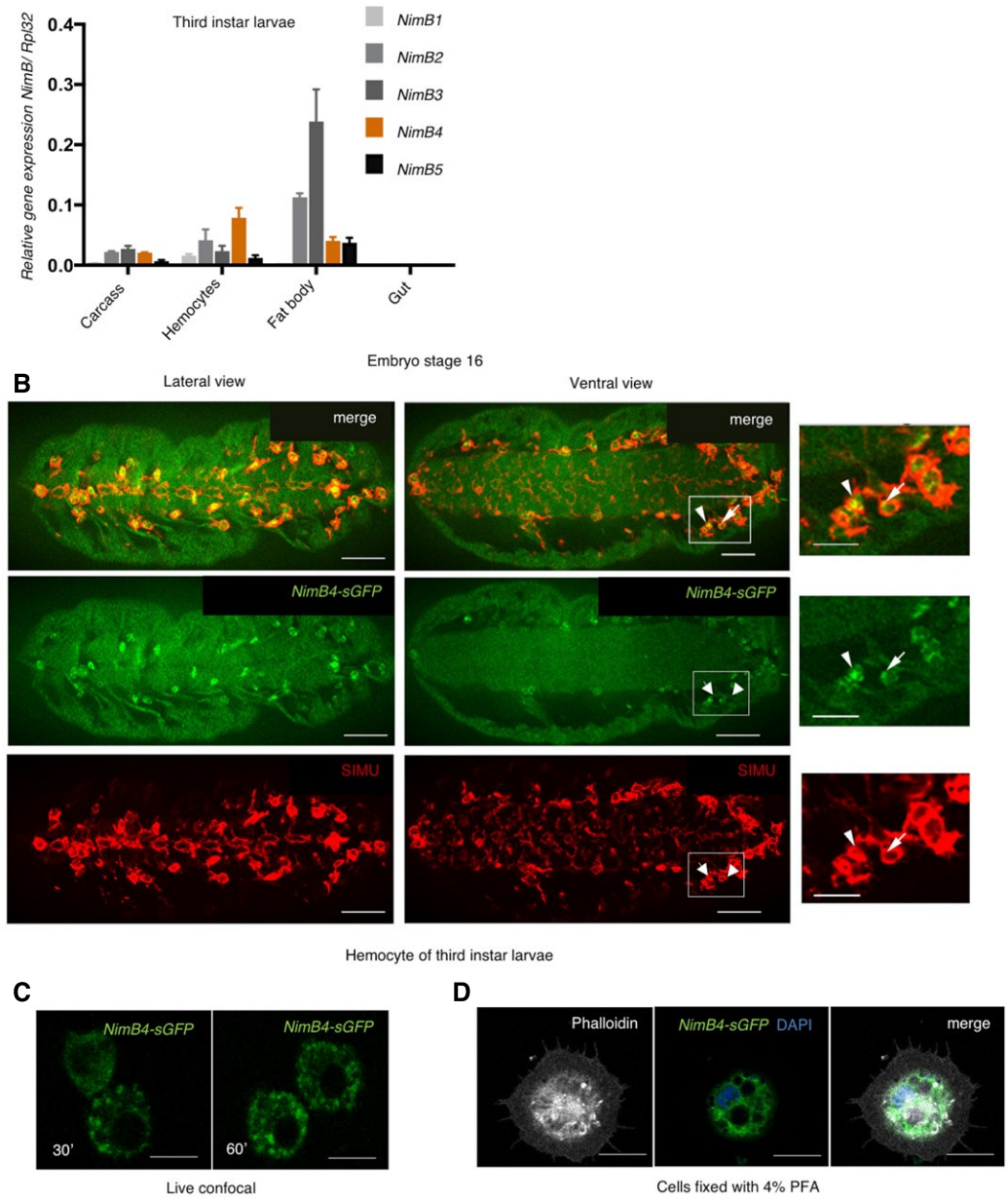

Figure 3.1 *NimB4* is enriched in phagocytes

(A) RT–qPCR analysis of *NimB1, NimB2, NimB3, NimB4,* and *NimB5* transcripts, normalized to *RpL32*, from carcass, macrophages, fat body, and gut of wild-type (w^{1118}) L3 wandering larvae. Data are represented as mean ± SD from three independent experiments. (B) Representative confocal imaging of *NimB4-sGFP* macrophages of embryo at stage 16; lateral (left) and ventral (right) views; tissues were stained with anti-GFP (green, corresponding to *NimB4-sGFP)* and anti-SIMU antibodies (red, corresponding to macrophages). The arrows show the presence of *NimB4-sGFP* inside the embryonic macrophages. Scale bars = 20 µm.(C) Representative live confocal imaging of *NimB4-sGFP* macrophages of L3 wandering larvae at 30 and 60 min after dissection. Scale bars = 10 µm.(D) Representative confocal imaging of *NimB4-sGFP* macrophages of L3 wandering larvae after fixation. Cells were stained with phalloidin (gray), DAPI (blue), and anti-GFP (green, corresponding to *NimB4-sGFP*). Scale bars = 10 µm.

To investigate whether expression of *NimB4* was modulated upon tissue damage, we collected larvae after clean injury with a thin needle in the anterior dorsal cuticle and monitored *NimB4* expression in the two major immune-responsive tissues, the fat body, and hemocytes. We observed that clean injury induces *NimB4* expression in hemocytes with an acute phase profile 1 h following challenge (**Supplementary Figure 3.1B**). In contrast, the transcription of *NimB4* in the fat body remained low and unchanged (**Supplementary Figure 3.1C**).

3.3.2 NimB4 binds to apoptotic cells

NimB4 is predicted to be a secreted protein due to the presence of a signal peptide (Somogyi *et al*, 2008). We generated a transgenic fly lines carrying a *UAS-NimB4-RFP* insertion and overexpressed *NimB4-RFP* in the fat body using the fat body-specific Gal4 driver *Lpp*. Western blot analysis of larval hemolymph extracts confirmed that NimB4-RFP protein was enriched in the hemolymph, as expected for a secreted protein (**Supplementary Figure 3.1D**). Furthermore, a strong NimB4-RFP signal was detected in the nephrocytes (a filtrating organ involved in the removal of hemolymph proteins) when NimB4-RFP was expressed either from the fat body or the hemocytes (**Supplementary Figure 3.1E,F**) (Ivy *et al*, 2015; Troha *et al*, 2019).

MFG-E8 binds PS exposed at the surface of apoptotic cells in a Ca^{2+}-dependent manner, engaging their uptake by the integrin $\alpha_v\beta_{3/5}$ phagocytic receptor (Borisenko *et al*, 2004). To explore if NimB4 could similarly bind to apoptotic cells, we incubated hemolymph containing NimB4-RFP with healthy S2 cells, or with S2 cells undergoing apoptosis. We observed that NimB4-RFP protein colocalized exclusively with the apoptotic cells, stained with carboxyfluorescein succinimidyl ester (CFSE; **Figure 3.2B,D**, **Supplementary Figure 3.2A**). The binding of NimB4 to apoptotic cells was specific as no binding was observed when labeled apoptotic corpses were incubated with a control secreted protein composed of the RFP protein fused to the signal peptide of the Viking protein (SP^{vkg}-RFP) (Liu *et al*, 2017) (**Figure 3.2A, D**).

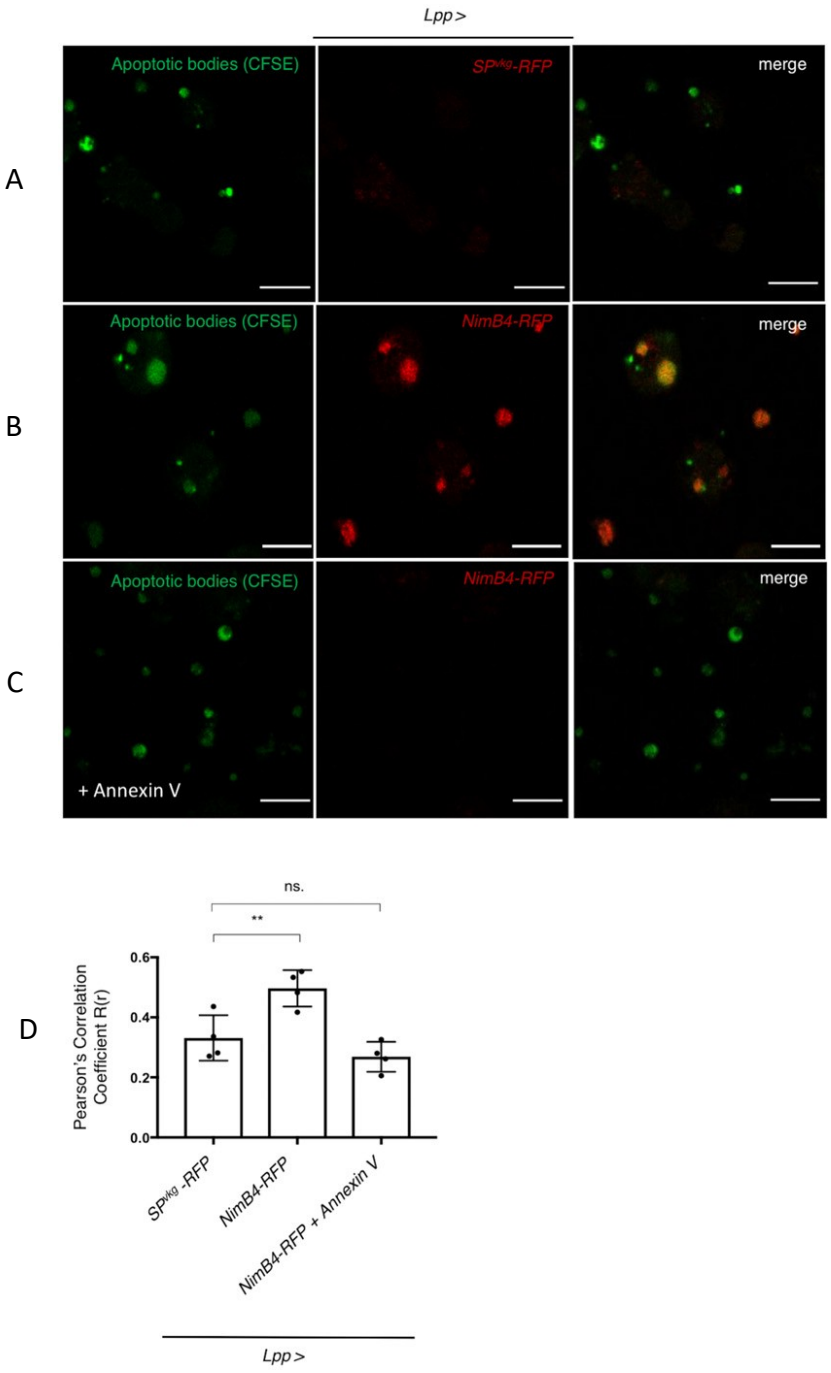

Figure 3.2 NimB4 binds to apoptotic cells *ex vivo*

(A–C) Representative confocal imaging of CFSE-stained apoptotic bodies (green) incubated with secreted NimB4-RFP (B, C) or SP^{vkg}-RFP (A). Apoptotic bodies were pre-incubated in absence (A, B) or presence (C) of Annexin V (25 µg/ml). Scale bar = 10 µm.D.Quantification of the colocalization of NimB4-RFP or SP^{vkg}-RFP with the apoptotic bodies in presence or absence of Annexin V, as measured by Pearson's correlation coefficient. Values from at least four independent experiments are represented as mean ± SD (**$P < 0.01$ by ANOVA test followed by *post hoc* Dunnett's multiple comparison tests. ns: not significant).

We then repeated the same experiment, but pre-treated apoptotic cells with Annexin V, a protein that coats apoptotic cells by binding to PS (Engeland *et al*, 1998; Janko *et al*, 2013). Pre-incubation of apoptotic corpses with Annexin V strongly reduced the binding of NimB4-RFP to the apoptotic cells, supporting the notion that NimB4 binds to apoptotic corpses in a PS-dependent manner (Figure 3.2C,D).

Next, we investigated if NimB4 can bind to apoptotic cells *in vivo*. For this, we induced apoptosis by expressing the apoptosis activator *reaper* in the imaginal wing disk using the driver *Apterous-Gal4*. After induction of apoptosis, we observed the binding of NimB4-sGFP to the region of the wing disk that expressed *Apterous-Gal4* (Supplementary Figure 3.2B) Additionally, we observed the binding of NimB4 to apoptotic cells released in the hemolymph after clean injury. No binding was observed between apoptotic corpses and the secreted protein SPvkg-RFP (Supplementary Figure 3.2C,D). Collectively, our studies revealed that NimB4 has key features of a bridging molecule in that it is secreted and binds to apoptotic corpses in a PS-dependent manner.

3.3.3 NimB4-deficient animals accumulate apoptotic corpses during development

To investigate the role of NimB4 *in vivo*, we generated a null mutation in the *NimB4* gene by CRISPR-Cas9, referred to as $NimB4^{sk2}$. The $NimB4^{sk2}$ mutant has a 14bp deletion in the second exon, inducing a stop codon at amino acid 113 (Supplementary Figure 3.3A-C).

We isogenized the $NimB4^{sk2}$ mutation by backcrossing into the w^{1118} *DrosDel* background. $NimB4^{sk2}$ homozygous flies were viable and did not show any striking morphological defect. We investigated the role of NimB4 in developmentally regulated apoptosis in the embryo and the larval brain (Kurant, 2011; Zheng *et al*, 2017). Stage 16 embryos were co-stained with an anti-SIMU antibody that marks macrophages, and anti-Dcp-1 that marks apoptotic cells by staining activated Death caspase-1 (Dcp-1). Macrophages of $NimB4^{sk2}$ mutants were normally localized throughout the embryo (Figure 3.3A). Interestingly, we noted an increased level of Dcp-1-positive apoptotic cells in $NimB4^{sk2}$ embryos. Embryonic macrophages of $NimB4^{sk2}$ but not wild-type embryos appeared highly vacuolated and full of apoptotic corpses, a phenotype reminiscent of the $draper^{\Delta 5}$ mutant (Kurant *et al*, 2008) (Figure 3.3A, B) .This finding suggests that $NimB4^{sk2}$ phagocytes can engulf apoptotic corpses but are deficient in their

degradation. *H99* embryos do not show any developmentally induced apoptosis as they carry a small deficiency that removes the three pro-apoptotic genes *head involution defective (hid), reaper,* and *grim* (Chen *et al*, 1996). We recombined the *H99* deficiency and *NimB4*^{sk2} to confirm that the vacuolization of *NimB4*^{sk2} embryonic macrophages is indeed caused by the accumulation of apoptotic corpses. Consistent with this notion, *NimB4*-deficient macrophages in the apoptosis-null *H99* mutant background did not show any vacuoles or Dcp-1 staining (Figure 3.3A). This demonstrates that the vacuolization of *NimB4*^{sk2} embryonic macrophages is linked to the accumulation of apoptotic corpses inside the cell.

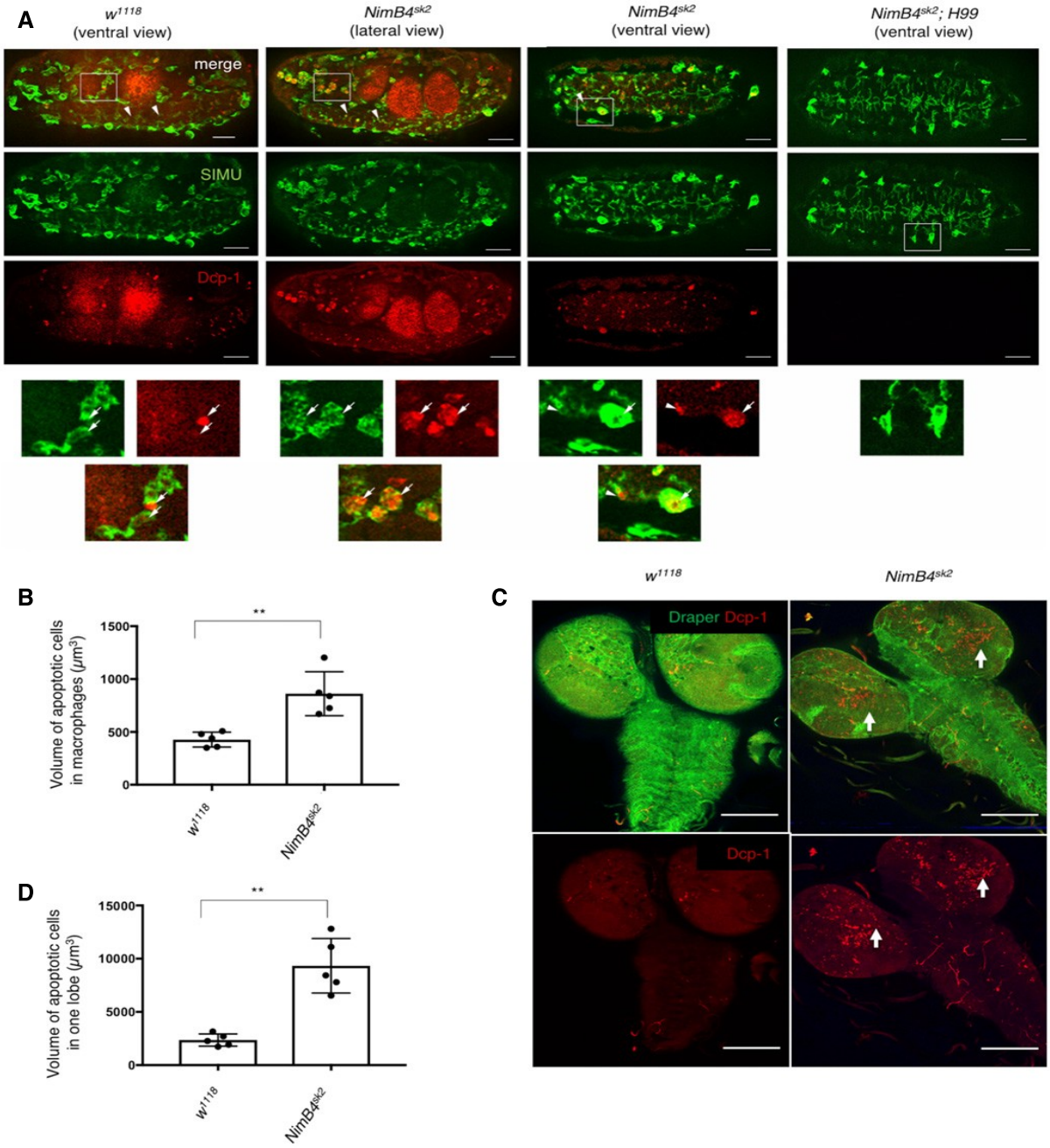

Figure 3.3 The *NimB4*^{sk2} mutant is defective in cell corpse clearance

(A) Representative confocal imaging of wild-type (*w*^{1118}), *NimB4*^{sk2}, and apoptosis-null *NimB4*^{sk2}*; Df(3L) H99* embryonic macrophages at stage 16 of development; ventral and lateral view; Tissues were co-stained with Dcp-1 (red, corresponding to apoptotic corpses) and anti-SIMU (green, corresponding to macrophages) antibodies. The arrows show the presence of apoptotic cells inside embryonic macrophages. Scale bars = 20 µm. **(B)** Quantification of caspase-positive particles (anti-Dcp-1, red) within macrophages (anti-SIMU, green). Values from at least five independent experiments are represented as mean ± SD total volume of caspase-positive particles (***P* < 0.01, by Mann–Whitney test). **(C)** Representative projections from confocal stacks of entire third-instar wild-type (*w*^{1118}) and *NimB4*^{sk2} larval brains stained with anti-Draper (green) and anti-Dcp-1 (red). The arrows show the presence of apoptotic cells in the central area of *NimB4*^{sk2} larval brain. Scale bars = 100 µm.**(D)** Quantification of caspase-positive particles in the central brain area of larval brain. Values from at least five independent experiments are represented as mean ± SD total volume of caspase-positive particles (***P* < 0.01, by Mann–Whitney test).

Moreover, we observed that the brain of *NimB4*^{sk2} larvae also displayed a greater amount of apoptotic cells than wild-type larvae (Figure 3.3C, D). These data demonstrate that NimB4 is required for proper clearance of apoptotic cells during embryonic and larval brain development.

Defective clearance of apoptotic cells may lead to lethality and organ dysfunction (Henson & Hume, 2006). Similarly to *draper*$^{\Delta 5}$ mutant, *NimB4*^{sk2} third-instar larvae displayed a crawling defect, with a drastic reduction of linear movement (Fuentes-Medel *et al*, 2009) (Supplementary Figure 3.3D). In contrast, no crawling defect was observed in *NimC1*^{1} deficient larvae lacking a phagocytic receptor involved in bacterial uptake (Melcarne *et al*, 2019b), indicating that this phenotype is specific to *draper*$^{\Delta 5}$ and *NimB4*^{sk2} mutants. At the adult stage, the *draper*$^{\Delta 5}$ flies have a shortened lifespan and an age-dependent locomotor defect (Draper *et al*, 2014).

A single-cell transcriptomic atlas of the aging *Drosophila* brain (Davie *et al*, 2018) revealed that *NimB4* is also expressed in the adult glial cells, suggesting its involvement in the phagocytosis. To evaluate the importance of *NimB4* during aging, we monitored two phenotypes usually associated with neurodegeneration in *NimB4*^{sk2} adult flies and found that similar to the *draper*$^{\Delta 5}$ mutant, *NimB4*^{sk2} flies displayed a climbing defect (suggesting declining motor activity), and reduced life span (Supplementary Figure 3.3E, F).

3.3.4 NimB4 enhances efferocytosis

Having shown that *NimB4* is required for the elimination of apoptotic cells, we then investigated at which step of the efferocytosis process NimB4 is required, using macrophages of third-instar larvae. Since NimB4 is secreted and binds to apoptotic corpses, we analyzed whether NimB4 contributes to the initial phase of uptake. To this end, we incubated macrophages and apoptotic cells on ice to inhibit the engulfment process, without altering binding to the phagocytic cell (Pearson *et al*, 2003). Macrophages of $NimB4^{sk2}$ larvae bound apoptotic corpses to the same extent as wild-type cells (**Figure 3.4A, B**). Conversely, the number of apoptotic corpses bound to the cell membrane of $draper^{\Delta 5}$ macrophages was reduced. Scanning electron microscopy experiments confirmed that apoptotic corpses bind to $NimB4^{sk2}$ but not $draper^{\Delta 5}$ macrophages (**Figure 3.4C**). This indicates that, unlike the Draper receptor, NimB4 is not involved in the initial phagocytic step of binding.

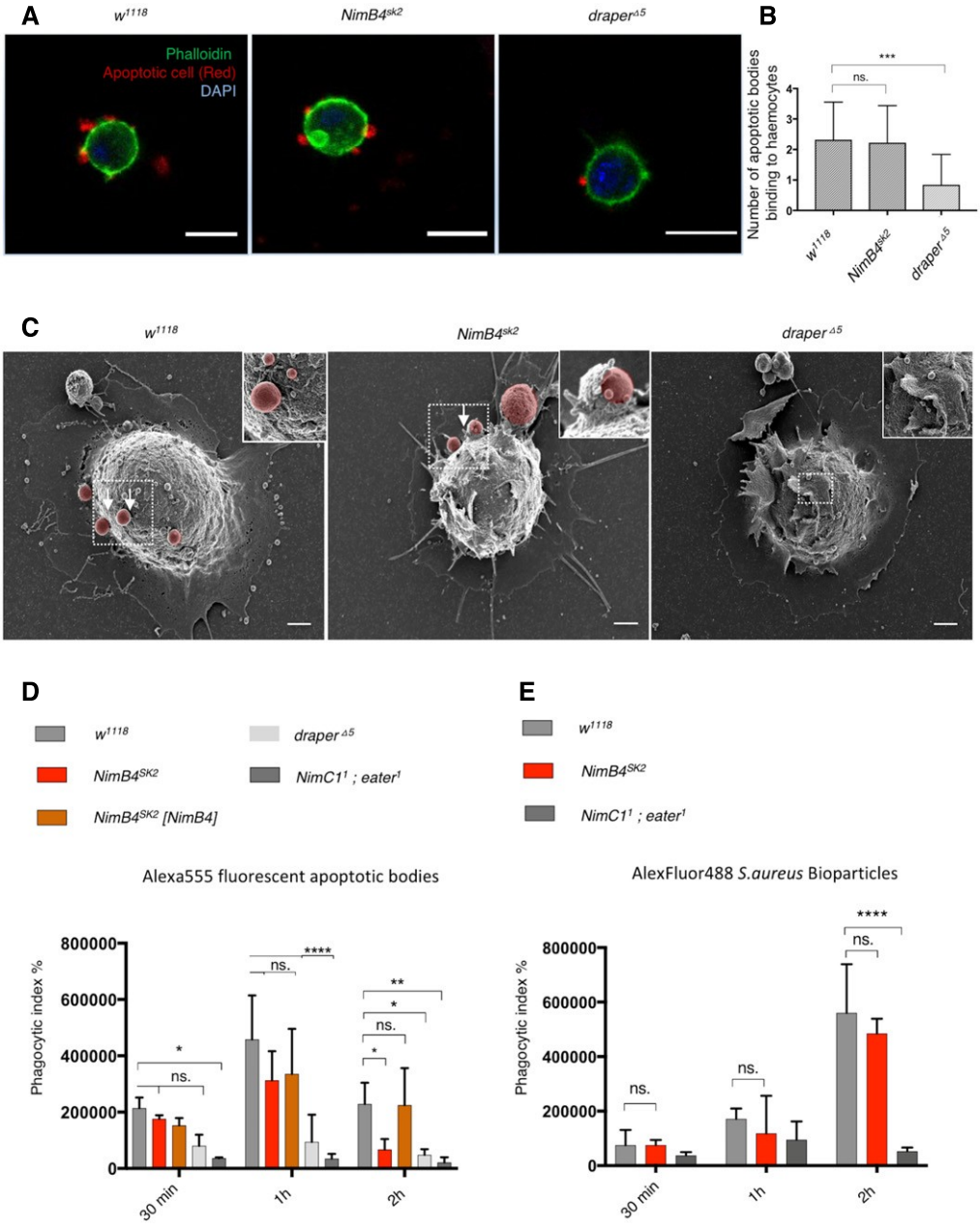

Figure 3.4 Phagocytosis of apoptotic cells is reduced in *NimB4*^{sk2} mutant

(A) Representative confocal imaging of wild-type (*w*^{1118}), *NimB4*^{sk2}, and *draper*$^{\Delta 5}$ macrophages incubated with fluorescently labeled apoptotic cells (red, CellTrace™ Red) on ice for 1 h and stained with Alexa Fluor™ 488 phalloidin (green). Scale bar: 10 µm.(B) Quantification of the number of apoptotic cells (red) binding to the macrophages (green). Values from three independent experiments are represented as mean ± SD (***$P < 0.001$ by ANOVA test followed by *post hoc* Dunnett's multiple comparison tests. ns: not significant). (C) Representative Scanning Electron Microscopy images of spread macrophages extracted from wild-type (*w*^{1118}), *NimB4*^{sk2}, and *draper*$^{\Delta 5}$ L3 wandering larvae and incubated 30 min with apoptotic cells (artificially colored in red) at room temperature. The arrows show the binding of apoptotic cells to the macrophages. Scale bar: 1 µm. (D) *Ex vivo* phagocytosis assay using Alexa555 fluorescent apoptotic bodies. Wild-type, *NimB4*^{sk2}, *NimB4* genomic rescue (*NimB4*^{sk2}, *[NimB4]*), *draper*$^{\Delta 5}$ and *NimC1*^{1}, *eater*^{1} macrophages from L3 wandering were incubated with Alexa555 fluorescent apoptotic bodies for 30, 60, or 120 min at room temperature. Phagocytosis was quantified by flow cytometry. Data are represented as mean ± SD from three independent experiments (*$P < 0.05$, **$P < 0.01$, ****$P < 0.0001$ by ANOVA test followed by *post hoc* Dunnett's multiple comparison tests ns: not

significant). (E) *Ex vivo* phagocytosis assay using AlexFluor488 *Staphylococcus aureus* Bioparticles. Wild-type, *NimB4*^{sk2}, and *NimC1*^{1}*, eater*^{1} macrophages from L3 wandering were incubated with bioparticles for 30, 60, or 120 min at room temperature. Phagocytosis was quantified by flow cytometry. Data are represented as mean ± SD from three independent experiments (****$P < 0.0001$ by ANOVA test followed by *post hoc* Dunnett's multiple comparison tests. ns: not significant).

We then investigated whether NimB4 is required for the subsequent step of phagocytosis, that is the engulfment of bound apoptotic corpses. For this, we tested the ability of *NimB4*^{sk2} larval macrophages to internalize fluorescently labeled apoptotic bodies using an *ex vivo* phagocytic assay. Macrophages from wild-type, *NimB4*^{sk2}, *draper*$^{\Delta 5}$, and the double mutant *NimC1*^{1}*, eater*^{1} were incubated for 30 min, 1 h, or 2 h with Alexa555 fluorescent apoptotic bodies, and flow cytometry was used to measure their phagocytic index. We found that, at 30 min, only the double mutant *NimC1*^{1}*, eater*^{1} exhibited a reduced phagocytosis. At 1 h, we observed reduced phagocytosis in both *NimC1*^{1}*, eater*^{1}, and *draper*$^{\Delta 5}$ mutants. Interestingly, the *NimB4*^{sk2} mutant exhibited reduced phagocytosis of apoptotic corpses at a later time point (2 h) compared to the wild type (**Figure 3.4D)** Use of a genomic fragment encompassing the *NimB4* gene rescued this decreased phagocytosis of the *NimB4*^{sk2} mutant at 2 h (**Figure 3.4D**). Of note, *NimC1*^{1}*; eater*^{1} mutants were unable to phagocytose apoptotic cells at all time points, indicating that the role of these two receptors is not restricted to bacterial phagocytosis. To test if the role of NimB4 is specific to efferocytosis, we performed the same experiment with fluorescent AlexFluor488 *Staphylococcus aureus* Bioparticles. Interestingly, *NimB4*^{sk2} macrophages retained the ability to phagocytose *S. aureus* bacteria at 2 h similar to the wild-type macrophages (**Figure 3.4E**). We included macrophages from *NimC1*^{1} *and eater*^{1} larvae that show impaired phagocytosis of bacteria as a positive control (Melcarne *et al*, 2019b). We conclude that NimB4 is not specifically required for the binding of apoptotic corpses but enhances phagocytosis of apoptotic cells.

3.3.5 Loss of *NimB4* inhibits phagosome maturation

The accumulation of apoptotic corpses in embryonic *NimB4*^{sk2} macrophages *in vivo* indicates impaired phagocytosis in these cells, while a reduction in phagocytosis only at late time points suggests a defect in phagosome maturation. We therefore explored if the loss of NimB4 alters the phagosome maturation process. In these experiments, we included as

controls *draper*$^{\Delta 5}$ *and croquemort*$^{\Delta}$ mutants previously shown to have defective phagosome maturation (Kurant *et al*, 2008; Han *et al*, 2014). The intracellular vesicles were analyzed using the fluorochrome LysoTracker Red, which fluoresces in acidic compartments. We observed that *NimB4*^{sk2}, *draper*$^{\Delta 5}$, and *croquemort*$^{\Delta}$ but not *eater*^{1} or *NimC1*^{1} macrophages contained numerous and enlarged acidic vesicles compared to wild-type macrophages (Figure 3.5A, B and Supplementary Figure 3.4A). To study possible NimB4 interactions with phagocytic receptors, we measured LysoTracker signal in macrophages double mutants for *NimB4*^{sk2} and *draper*$^{\Delta 5}$, *croquemort*$^{\Delta}$, *eater*^{1}, or *NimC1*^{1} (Supplementary Figure 3.4A). We observed an increased LysoTracker signal in the *NimB4*^{sk2}*; draper*$^{\Delta 5}$ mutant suggesting that Draper and NimB4 additively contribute to phagosome maturation. The *NimB4*^{sk}, *croquemort*$^{\Delta}$ double mutants did not show any increased LysoTracker signal compared to the single mutants. This result suggests that Croquemort and NimB4 might work together in the phagosome maturation process.

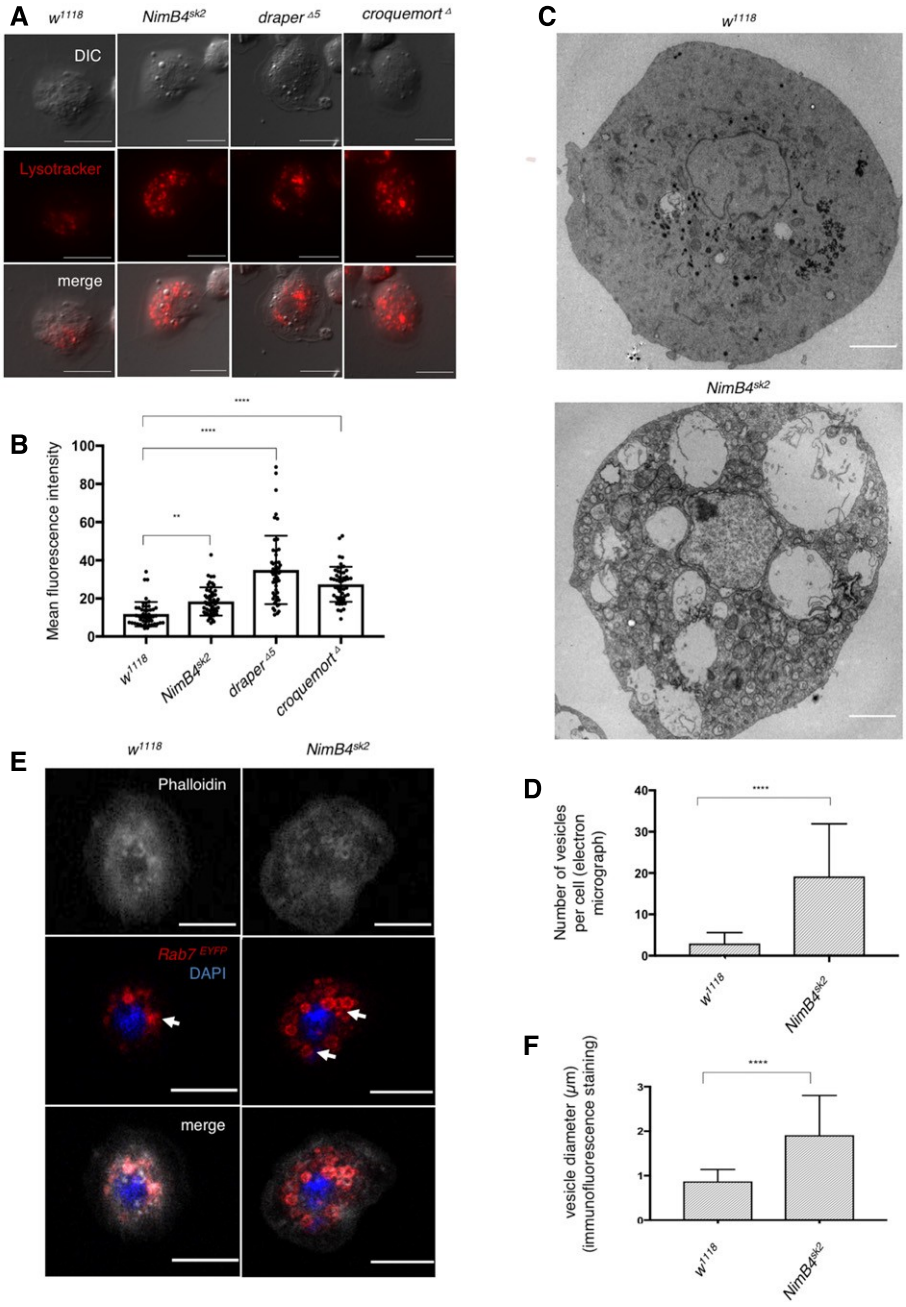

Figure 3.5 *NimB4*^{sk2} mutant macrophages have an increased number of vesicles

(**A**) Representative fluorescence microscopy images of wild-type (*w*^{1118}), *NimB4*^{sk2}, *draper* $^{\Delta 5}$, *eater*^{1}, and *croquemort* $^{\Delta}$ third-instar larvae macrophages stained with LysoTracker Red (live imaging). Overlay of fluorescence and differential interference contrast microscopy (DIC). Scale bar = 10 µm. (**B**) Mean fluorescence intensity after staining with LysoTracker Red (live confocal imaging). Values from at least three independent experiments are represented as mean ± SD (**$P < 0.01$, ****$P < 0.0001$ by ANOVA test followed by *post hoc* Dunnett's multiple comparison tests). (**C**) Representative transmission electron micrographs of macrophages from wild-type (top, *w*^{1118}) and *NimB4*^{sk2} (bottom) L3 wandering larvae. Scale bar: 2 µm. (**D**) Quantification of the number of vesicles per macrophages in the electron micrographs. Values from at least three independent experiments are represented as mean ± SD (****$P < 0.0001$ by Mann–Whitney test). (**E**) Representative confocal imaging of *Rab7*^{EYFP} immunostaining in *wild*-type (*w*^{1118}) and *NimB4*^{sk2} macrophages. Tissues were stained with anti-GFP (red, Rab7), counterstained with phalloidin (gray) and DAPI (blue). The arrows indicate the enlarged

vesicles are decorated with *Rab7^{EYFP} in the NimB4^{sk2}* macrophages. Scale bar = 10 µm. (**F**) Quantification of the diameter of the vesicles. Values from at least three independent experiments are represented as mean ± SD (****P < 0.0001 by Mann–Whitney test).

The accumulation of intracellular vesicles in *NimB4^{sk2}* macrophages was rescued by complementing the mutant with a transgene containing a wild-type copy of *NimB4* gene (**Supplementary Figure 3.4B, C**). In addition, silencing *NimB4* using RNAi with the *Hml-Gal4* macrophage driver reproduced this phenotype, confirming that the accumulation of intracellular vesicles was indeed caused by the inactivation of *NimB4* in macrophages (**Supplementary Figure 3.4D, E**). We next analyzed the subcellular morphology of *NimB4^{sk2}* intracellular vesicles by transmission electron microscopy. *NimB4^{sk2}* but not wild-type macrophages were filled with large intracellular vesicles that occupied most of the cell volume. These vesicles were surrounded by a single lipid bilayer and had a clear lumen (**Figure 3.5C, D).** A similar vesicle accumulation was also observed upon silencing of *NimB4* by RNAi (**Supplementary Figure 3.4F, G**). To confirm that this phenotype was not linked to a defect due to loss of *NimB4* during development, we used a temperature-inducible macrophages driver (*HmlΔ^{ts})* to express *NimB4*-RNAi after the second-instar larval (L2) stage. LysoTracker staining showed that hemocytes in which *NimB4* was inactivated after the L2 stage also showed accumulation of acidic vesicles (**Supplementary Figure 3.4H, I**). Therefore, we conclude that the accumulation of acidic vesicles in *NimB4* macrophages is not caused by a defect at the early stages of development.

3.3.6 NimB4 plays a crucial role in phagosome–lysosomes fusion

Phagosome maturation culminates in the fusion of the phagosome with lysosomes, leading to the formation of an acidic phagolysosome. The formation of phagolysosomes is a necessary step to ensure efficient digestion of apoptotic corpses (Zhou & Yu, 2008). During phagosome maturation, the transition from early phagosome to late phagosome is marked by the conversion of Rab5 to Rab7. In addition, the phagosome acquires Lamp1, which is required for phagolysosome fusion (Huynh *et al*, 2007). Our observation that accumulated vesicles in *NimB4^{sk2}* macrophages are LysoTracker-positive and have therefore initiated acidification

suggests that NimB4 is required at a later stage of phagosome maturation. To determine more precisely the step at which maturation of *NimB4*^{sk2} phagosomes is blocked, we tested whether Rab7, a marker of late phagosomes, was enriched on the vesicular membrane of *NimB4*^{sk2} macrophages. We observed that the enlarged vesicles of *NimB4*^{sk2} macrophages were positive for Rab7^{EYFP}, confirming that phagosomes are blocked at a late stage of maturation (Figure 3.5E, F). To determine whether fusion between the phagosome and lysosomes requires NimB4, we analyzed the fate of wild-type, *NimB4*^{sk2}, and *draper*$^{\Delta 5}$ macrophages stained with the phagosome marker LysoTracker and the lysosome marker Lamp1-mcherry. In wild-type macrophages, these markers colocalized, indicating correct formation of the phagolysosomes. In contrast, we found no colocalization of LysoTracker and Lamp1-mcherry in the *NimB4*^{sk2} and *draper*$^{\Delta 5}$ macrophages (Figure 3.6A, B). The Lamp1-mcherry lysosomal signals appeared as small punctate structures between the LysoTracker-positive vacuoles. This suggests that a loss of *NimB4* or *draper* impairs the fusion rather than the clustering of phagosomes with lysosomes (Figure 3.6A, B). An increased Lamp1-mcherry fluorescent signal in *NimB4*^{sk2} mutant macrophages indicated that the blockage of phagolysosome fusion was not due to a reduced number of lysosomes in the *NimB4*^{sk2} mutant. Interestingly, we observed a similar increase in the number of Lamp1-mcherry-positive structures when wild-type macrophages were pre-treated with chloroquine, a drug that inhibits endosomal acidification, which is used here to block phagosome maturation (Supplementary Figure 3.5A, B).

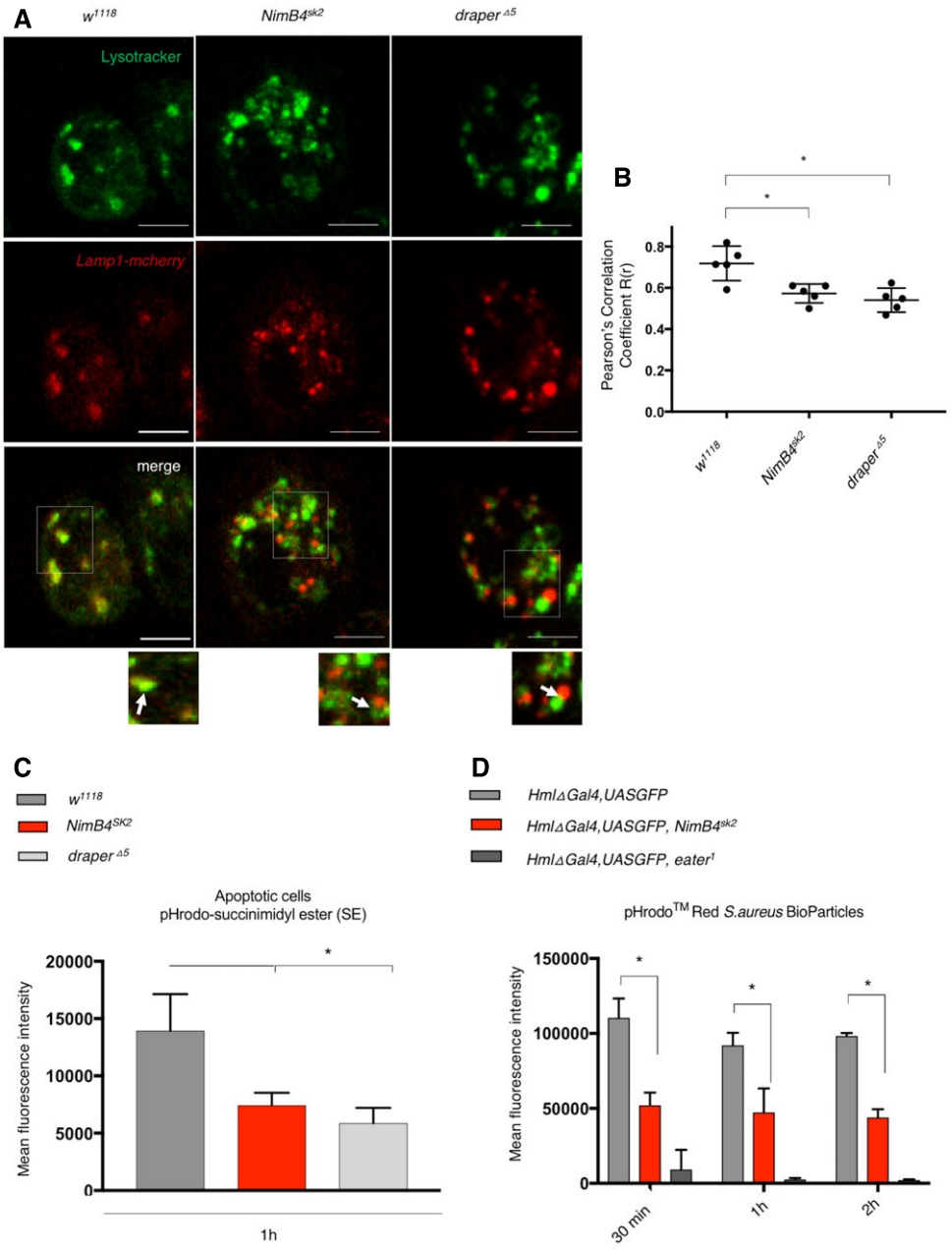

Figure 3.6 Loss of NimB4 blocks the phagosome maturation process by impairing the phagosome-lysosome fusion

(A) Representative confocal imaging of localization of Lamp1-mcherry and LysoTracker Green in wild-type (*w^{1118}*), *NimB4* ^{sk2}, *and draper* $^{\Delta 5}$ macrophages (live imaging). The arrows indicate the colocalization (*w^{1118}*) or the clustering (*$NimB4^{sk2}$ and draper* $^{\Delta 5}$) of Lamp1-mcherry and LysoTracker Green signals. Scale bar: 10 µm. (B) Quantification of the colocalization of Lamp1-mcherry with LysoTracker Green, as measured by Pearson's correlation coefficient between the two signals. Values from at least five independent experiments are represented as mean ± SD (*$P < 0.05$ by ANOVA test followed by *post hoc* Dunnett's multiple comparison tests). (C) *Ex vivo* phagocytosis assay using apoptotic cells labeled with pHrodo™ Red. Wild-type (*w^{1118}*), *$NimB4^{sk2,}$* and *draper* $^{\Delta 5}$ macrophages from L3 wandering larvae were incubated with pHrodo™ Red apoptotic cells for 60 min at room temperature. Phagocytosis was quantified by flow cytometry. Data are represented as mean ± SD from three independent experiments (*$P < 0.05$ by ANOVA test followed by *post hoc* Dunnett's multiple comparison tests. ns: not significant). (D) *Ex vivo* phagocytosis assay using pHrodo™ Red *Staphylococcus aureus* Bioparticles™ conjugates. Wild-type, *$NimB4^{sk2}$* and *$NimC1^{1}$, $eater^{1}$ HmlΔ-Gal4 > UAS-*

GFP macrophages from L3 wandering larvae were incubated with pHrodo™ Red *S. aureus* Bioparticles™ for 30, 60, or 120 min at room temperature. Phagocytosis was quantified by flow cytometry. Data are represented as mean ± SD from three independent experiments (*$P < 0.05$ by ANOVA test followed by *post hoc* Dunnett's multiple comparison tests. ns: not significant).

The fusion of the phagosome with the lysosome allows the acidification of the phagosome. We therefore assessed the acidification of phagosomes in both *NimB4^{sk2}, draper$^{\Delta 5}$,* and wild-type macrophages. For this, we used apoptotic cells labeled with pHrodo-succinimidyl ester (SE), a pH-sensitive fluorescent dye. We then assessed the acidification of the phagosome measuring the mean fluorescence intensity at 1 h after incubation as the *NimB4^{sk2}* mutant did not show phagocytosis defects at this time point. We observed by flow cytometry a reduced fluorescence intensity in the *NimB4^{sk2}* and the *draper$^{\Delta 5}$* mutant compared to wild type consistent with defective acidification of the phagosome (Figure 3.6C).

We repeated the same experiment with pHrodo bioparticles labeled with *S. aureus* as the *NimB4^{sk2}* mutant previously showed no defect in the phagocytosis of *S. aureus* Alexa Fluor 488 BioParticles (Figure 3.6D). We observed by flow cytometry a reduced fluorescence intensity of pHrodo-labeled *S. aureus* bioparticles in the *NimB4^{sk2}* mutant macrophages compared to wild type (Figure 3.6D) consistent with defective acidification of the phagosome.

It has been shown that overexpression of Rab7 efficiently promotes the phagosome-lysosome fusion (Harrison *et al*, 2003). We therefore investigated whether increased expression of Rab7 could rescue the phagosome-lysosome fusion defect of *NimB4^{sk2}* macrophages. Overexpression of Rab7, but not Rab5, strongly reduced the number of accumulated vacuoles in *NimB4^{sk2}* macrophages, showing that promoting the phagosome-lysosome fusion is sufficient to rescue the *NimB4^{sk2}* cells (Figure 3.7A-C). In this experiment, we found that the overexpression of *Rab5* in wild-type macrophage has a pronounced defect on its own as previously described (Bucci *et al*, 1992). We conclude that NimB4 is required for the late stage of phagosome maturation and more specifically, for the fusion of the phagosome and lysosome.

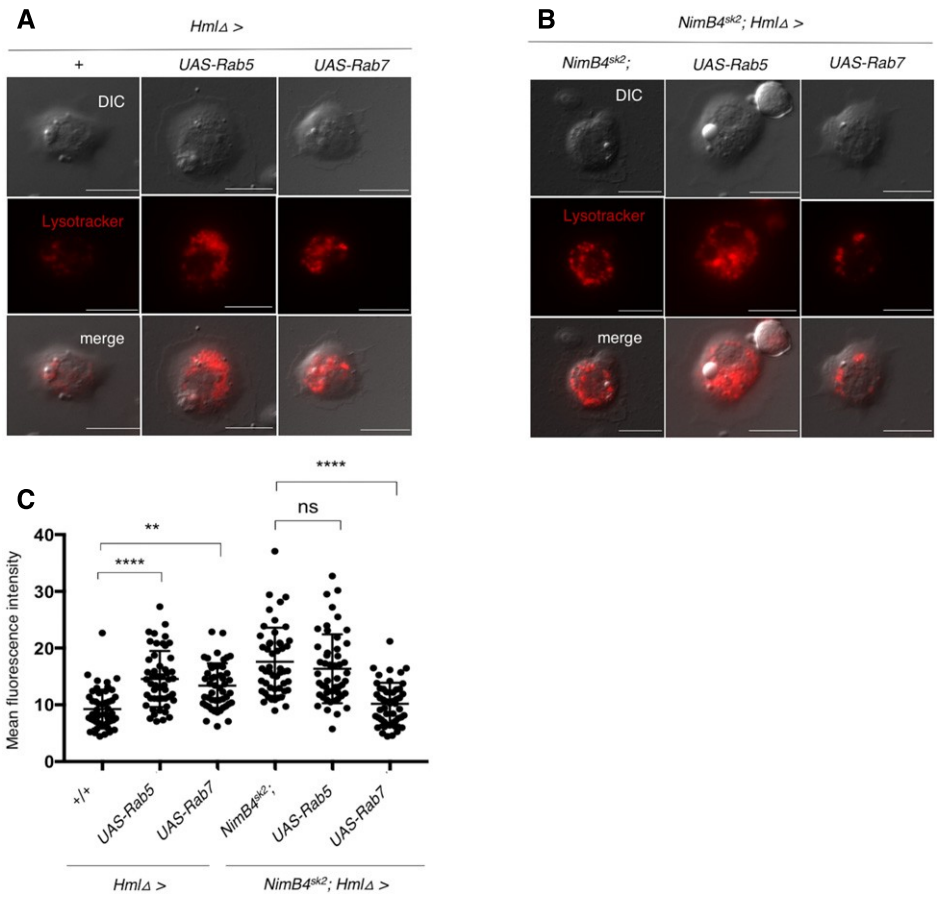

Figure 3.7 The increased expression of RAB7 rescues the phagosome accumulation in *NimB4*^{sk2} macrophages
(A–B) Representative fluorescence microscopy images of wild-type (A) or *NimB4*^{sk2} (B) macrophages expressing Rab5 (middle panel) or Rab7 (right panel) driven by *HmlΔ-Gal4 and* stained with the LysoTracker Red (live imaging). Overlay of fluorescence and DIC. Scale bar = 10 µm.(C) Quantification of the mean fluorescence intensity of LysoTracker in macrophages from larvae (confocal live imaging). Values from at least three independent experiments are represented as mean ± SD (**$P < 0.01$, ****$P < 0.0001$ by ANOVA test followed by *post hoc* Dunnett's multiple comparison tests. ns: not significant).

3.4 Discussion

The clearance of apoptotic cells by phagocytes is a critical event during the development of all multicellular organisms. Failure in this process can lead to autoimmune or neurodegenerative diseases. In this study we identified a secreted protein of the Nimrod family, NimB4, that binds to apoptotic corpses in a PS-dependent manner to promote efferocytosis. Similar to mutants of the phagocytic receptor Draper, the *NimB4*^{sk2} mutant accumulates apoptotic cells in both embryonic and larval macrophages. Further functional studies reveal its role in phagosome maturation, notably the formation of the phagolysosome. Our study identifies the first

secreted factor involved in the phagocytosis of apoptotic cells in *Drosophila,* resembling in many respects the bridging molecules found in mammals.

NimB4 is a secreted factor that promotes the phagocytosis of apoptotic cells

NimB4 was initially identified as a secreted member of the Nimrod family of unknown function. Our results show that *NimB4* is expressed in macrophages and glial cells, and that its expression is induced upon injury, a stimulus associated with increased apoptosis (Steller, 2008). In mammals, the expression of the gene encoding the bridging molecule MFG-E8 is regulated by a "find me factors" released by apoptotic cells (Miksa *et al*, 2007). Further study should identify the signaling pathway regulating *NimB4* upon injury and test whether *Drosophila* "find me factor" are involved in this process (Ravichandran, 2010, 2011). We also observed that NimB4 is secreted by macrophages and that it is likely associated with the endosomal compartments intracellularly. *NimB4* mutants display a shorter lifespan and a locomotor defect that can be causally linked to defective apoptotic cell clearance during development and aging. These phenotypes are very similar to those previously described for *draper* mutants, albeit slightly weaker (Kurant *et al*, 2008; Draper *et al*, 2014; Etchegaray *et al*, 2016).

Our data also indicate that NimB4 binds to apoptotic corpses in a PS-dependent manner. As a member of the Nimrod family, NimB4 shares homology with SIMU and Draper, two phagocytic receptors that also interact with PS (Shklyar *et al*, 2013a; Tung *et al*, 2013). This suggests that the common EGF/Nimrod domain found in Nimrod family members may contribute to binding PS. However, it is unclear whether NimB4 binds to apoptotic cells alone and interacts directly with receptors involved in efferocytosis, or whether other co-factors are required. It is worth noting that the *Drosophila* genome encodes several other secreted NimB proteins such as NimB1, NimB2, and NimB3 that are not yet characterized (Somogyi *et al*, 2008). It is tempting to speculate that some of these proteins could work synergistically with NimB4 in the process of efferocytosis. The similarities between the $NimB4^{sk2}$ and $draper^{\Delta 5}$ mutant phenotypes suggest that both proteins function in a similar efferocytosis pathway. In this study, we did not find any evidence that NimB4 interacts with Draper. Future studies should address whether NimB4 establishes a direct bridge between apoptotic corpses and phagocytic receptors.

NimB4 is specifically required for the phagocytosis of apoptotic cells

NimB4 is required for the phagocytosis of apoptotic cells but not bacteria. This indicates that it is not a core component of the phagocytic machinery. This result is in line with many studies that show that the phagocytic process is multi-faceted and is tailored to the nature of the ingested particle. For instance, studies have shown that phagosomes containing apoptotic cells mature faster than those containing opsonized viable cells (Erwig *et al*, 2006). These observations indicate that phagocytic targets can differentially affect the maturation rate, perhaps through the recruitment of different phagocytic receptors. In contrast to NimB4, Draper contributes to the phagocytosis of both bacteria (*S. aureus*) and apoptotic cells (Manaka *et al*, 2004b; Shiratsuchi *et al*, 2012), pointing to more versatile functions. In this study, we incidentally showed that NimC1 and Eater, two immune receptors implicated in the phagocytosis of microbes, are also required for the efferocytosis process. In contrast, the role of SIMU seems to be restricted to apoptotic cell clearance during embryonic and early adult phase development (Kurant *et al*, 2008). These authors speculated that the presence of SIMU reinforces uptake of apoptotic cells at critical developmental stages characterized by massive apoptosis. We hypothesize that, like SIMU, NimB4 may have a more specific function related to a particular efferocytosis program.

The secreted NimB4 participates in phagosome maturation

Importantly, our study shows that secreted NimB4 binds to apoptotic cells and is an essential component of the machinery that promotes efferocytosis. Thus, as observed in mammals and *C. elegans*, our study reveals that secreted factors contribute to the apoptotic cell clearance in *Drosophila*. However, NimB4 is not required for macrophages binding to apoptotic bodies. Instead, apoptotic corpse uptake is reduced only at late time points.

We hypothesize that this phenotype is a secondary consequence of a defect in phagosome maturation. The accumulation of immature phagosomes that are not properly eliminated would indirectly impair the uptake of new apoptotic corpses. Efferocytosis would then be impaired only at late time points when the accumulation of phagosomes reaches a threshold preventing further phagocytosis. Phagosome maturation is punctuated by two main events: the Rab5-Rab7 conversion and the fusion between the phagosome and the lysosome (Vieira *et al*, 2002; Kinchen & Ravichandran, 2008; Akbar *et al*, 2011; Pauwels *et al*, 2017;

Pradhan *et al*, 2019). Interestingly, overexpression of Rab7 rescues the phagosome maturation blockage of *NimB4* mutant. Our study suggests that NimB4 is required late in the process, at the step of phagosome-lysosome fusion. Interestingly, the receptors Draper and Croquemort, initially thought to be involved in the early phase of phagocytosis, were later shown to be critical for phagosome maturation (Kurant *et al*, 2008; Han *et al*, 2014). How those receptors and NimB4 contribute to the maturation of phagosome is currently unknown. We speculate that the binding of NimB4 to apoptotic cells could orient the maturation process; that is, apoptotic corpses may require specific "digest me" signals similar to the "eat-me" signals that are required for uptake. Several mechanisms could explain how a secreted factor can impact phagosome maturation. Binding of NimB4 to apoptotic cells could cluster phagocytic receptors or activate a specific phagocytic receptor that initiates a dedicated digestion program affecting the degradation speed of ingested apoptotic cells. Alternatively, NimB4 could promote phagocytosis and lysosome maturation independently by interacting with different partners in the phagocytic process.

Is NimB4 a bridging molecule?

Bridging molecules recognize "eat-me" signals on apoptotic cells facilitating their uptake by phagocytic receptors (Ravichandran, 2010). In mammals, several soluble bridging molecules such as MFG-E8, Gas6, and protein S mediate recognition of apoptotic cells by cross-linking the PS "eat-me" signal with specific phagocytic receptors. For instance, MFG-E8 binds to the integrin receptor of phagocytic cells (Hanayama *et al*, 2002; Akakura *et al*, 2004; Nandrot *et al*, 2007). In *C. elegans,* the protein TTR-52 bridges the surface-exposed PS on apoptotic cells and the CED-1 receptor on phagocytes, which mediates recognition and engulfment of apoptotic cells (Wang *et al*, 2010). While the initial concept viewed bridging molecules as opsonins dedicated to the uptake of apoptotic cells, recent studies suggest greater complexity. Similar to NimB4, subsequent studies showed that MFG-E8 is required in the maturation phase of phagocytosis as well as in the recognition step. While apoptotic cells ingested by wild-type dendritic cells rapidly fused with lysosomes, in dendritic cells deficient for MFG-E8 smaller fragments of apoptotic cells persisted in endosomes (Peng & Elkon, 2011). NimB4 shares key features of bridging molecules, in that it is secreted by phagocytic cells, binds

to apoptotic cells in the PS-dependent manner, and is specifically required for efficient efferocytosis.

Although this study has not conclusively demonstrated that NimB4 interacts with phagocytic receptors as mammalian bridging molecules do (Boada-Romero *et al*, 2020), our results reveal the importance of secreted factors that enhance efferocytosis and reinforce the notion that "bridging molecules" could play a broader role than initially thought, in orienting phagosome maturation. Future studies should characterize how secreted factors promote and direct the process of efferocytosis, and *Drosophila* offers a powerful system to address these questions.

3.5 Materials and Methods

Reagents and Tools table

Reagent/Resource	Reference or Source	Identifier or Catalog Number
Experimental models		
DrosDel w^{1118} isogenic (wild type)	Gift from Luis Teixeria (Pais, 2018)	N/A
w^{1118}; NimB4 ^{sk2}	This study	N/A
w^{iso}; NimB4^{sk2} (isogenized in the DrosDel background)	This study	N/A
w; UAS-NimB4 IR	VDRC	106392
w, UAS-NimB4	This study	N/A
w; UAS-NimB4-RFP	This study	N/A
w;; UAS-NimB4-HA	This study	N/A
w; NimB4 ^{sk2}, UAS-NimB4-RFP	This study	N/A
w; NimB4 ^{sk2}; UAS-NimB4-HA	This study	N/A
w; NimB4 ^{sk2}, [NimB4]	This study	N/A
w;; NimB4-sGFP-V5 (Injection in VK33 attP docking site)	This study	pFLYFOS 8882336809946705
w^{1118};; eater^{1}	Bretscher et al (2015)	N/A
w^{1118}; NimC1^{1}	Melcarne et al (2019b)	N/A
draper$^{\Delta 5}$	Gift from M. Freeman (Freeman, 2015)	N/A
; croquemort *	Gift from Yuh-Nung jang (Han et al, 2014)	N/A
w^{1118}; NimC1^{1}; eater^{1}	Melcarne et al (2019b)	N/A
w; HmlΔ-Gal4, UAS-GFP;	Sinenko and Mathey-Prevot (2004)	N/A
w;; HmlΔ-Gal4	Sinenko and Mathey-Prevot (2004)	N/A
; Tub-gal80^{ts}, UAS-GFP; HmlΔ-Gal4	This study	N/A
w; HmlΔ -Gal4, UAS-GFP, NimB4 ^{sk2}	This study	N/A
w^{1118}; NimC^{1}, HmlΔGal4,UAS-GFP;eater^{1}	Melcarne et al (2019b)	N/A
w; NimB4^{sk2}; HmlΔ-Gal4	This study	N/A
; Tub-gal80^{ts},UAS-GFP; Lpp-Gal4/TM3 (Referred to as Lpp^{ts})	Brankatschk et al (2018)	N/A
;; Lpp-Gal4/TM3	N/A	N/A
; NimB4^{sk2}; Lpp-Gal4/TM3	This study	N/A
; Act5c-gal4/cyoGFP	Bretscher et al (2015)	N/A
; UAS-SP^{vkg}-RFP.3.1; (30 first amino acids of Viking protein followed by RFP)	Gift from Pastor-Parja I (Liu et al,	N/A

Reagents and Tools table (continued)

Reagent/Resource	Reference or Source	Identifier or Catalog Number
FM7; iso; iso	Gift from Luis Teixeira	N/A
Iso; Gla/cyo; iso	Gift from Luis Teixeira	N/A
Recombinant DNA		
pENTR/D-TOPO	Invitrogen	K240020
pTW	DGRC	1129
pTWR	DGRC	1136
pOT2-CG16873 Full length cDNA clone	DGRC	IP09831
pCaSpeR4	Our collection	N/A
BACR09N24	BACPAC Resources Center	RP98-9N24
Antibodies		
Chicken anti-GFP	Abcam	Cat# ab13970
Rabbit monoclonal anti-SIMU antibody	Shklyar et al (2013b)	N/A
Mouse monoclonal anti-Draper antibody	Kurant et al (2008)	N/A
Rabbit anti Dcp-1 antibody	Cell Signaling	Cat # 9578
Mouse monoclonal anti mCherry antibody	Invitrogen	Cat #M11217
Goat anti-Mouse IgG (H+L) Secondary Antibody, HRP	Jackson ImmunoResearch labs	Cat# 31430
Goat anti-Chiken IgY (H+L) Secondary antibody, Alexa Fluor 488	Thermo Fisher Scientific	Cat# A11039
Goat anti-Mouse IgG (H+L) Highly Cross-adsorbed Secondary Antibody, Alexa Fluor 555	Thermo Fisher Scientific	Cat# A21424
Goat anti-Rabbit IgG (H+L) Highly Cross-adsorbed Secondary Antibody, AlexaFluor 555	Thermo Fisher Scientific	Cat# A32731
Oligonucleotides and sequence-based reagents		
NimB4 F deletion screen: CGA TCT CTG TGC CTC CAC TC	Microsynth	N/A
NimB4 R deletion screen CTT GCA ACA AAC CTC GAT CA	Microsynth	N/A
NimB4 deletion screen CCC AAC GGT TTG TCC GGA ACA TC	Microsynth	N/A
NimB1 qRT F CGG CCA AAG TGT GAG AGA TT	Microsynth	N/A
NimB1 qRT R TAT CGT CAC AGC TTC CGT TC	Microsynth	N/A
NimB2 qRT F GAG TGT CTG CCG AAG TGT GA	Microsynth	N/A
	2017)	
;; Df(3L)H99, $kni^{ri\text{-}1}$ p^{p}/TM3, Sb^{1}	DGGR	106395
; $NimB4^{sk2}$; Df(3L)H99, $kni^{ri\text{-}1}$ p^{p}/TM3, Sb^{1}	This study	N/A
; $tubGal80^{ts}$; repoGal4	Hakim-Mishnaevski et al (2019)	N/A
w^{1118};; TI{TI}Rab7[EYFP]	BDSC	62545
w^{1118}; $NimB4^{sk2}$; TI{TI}Rab7[EYFP]	This study	N/A
yw; UAS-Rab5-YFP	Bloomington	9771
yw; UAS-Rab5-YFP, $NimB4^{sk2}$	This study	N/A
; UAS-venus-rab7	Gift from Brian McCabe	N/A
; UAS-venus-rab7, NimB4 ^{sk2}	This study	N/A
;; Lamp1–mCherry	Gift from Gábor Juhász (Lőw et al, 2013)	N/A
; $NimB4^{sk2}$; Lamp1–mCherry	This study	N/A
Iso; iso; TM2/TM6	Gift from Luis Teixeira	N/A

Reagents and Tools table (continued)

Reagent/Resource	Reference or Source	Identifier or Catalog Number
FM7; iso; iso	Gift from Luis Teixeira	N/A
Iso; Gla/cyo; iso	Gift from Luis Teixeira	N/A
Recombinant DNA		
pENTR/D-TOPO	Invitrogen	K240020
pTW	DGRC	1129
pTWR	DGRC	1136
pOT2-CG16873 Full length cDNA clone	DGRC	IP09831
pCaSpeR4	Our collection	N/A
BACR09N24	BACPAC Resources Center	RP98-9N24
Antibodies		
Chicken anti-GFP	Abcam	Cat# ab13970
Rabbit monoclonal anti-SIMU antibody	Shklyar et al (2013b)	N/A
Mouse monoclonal anti-Draper antibody	Kurant et al (2008)	N/A
Rabbit anti Dcp-1 antibody	Cell Signaling	Cat # 9578
Mouse monoclonal anti mCherry antibody	Invitrogen	Cat #M11217
Goat anti-Mouse IgG (H+L) Secondary Antibody, HRP	Jackson ImmunoResearch labs	Cat# 31430
Goat anti-Chiken IgY (H+L) Secondary antibody, Alexa Fluor 488	Thermo Fisher Scientific	Cat# A11039
Goat anti-Mouse IgG (H+L) Highly Cross-adsorbed Secondary Antibody, Alexa Fluor 555	Thermo Fisher Scientific	Cat# A21424
Goat anti-Rabbit IgG (H+L) Highly Cross-adsorbed Secondary Antibody, AlexaFluor 555	Thermo Fisher Scientific	Cat# A32731
Oligonucleotides and sequence-based reagents		
NimB4 F deletion screen: CGA TCT CTG TGC CTC CAC TC	Microsynth	N/A
NimB4 R deletion screen CTT GCA ACA AAC CTC GAT CA	Microsynth	N/A
NimB4 deletion screen CCC AAC GGT TTG TCC GGA ACA TC	Microsynth	N/A
NimB1 qRT F CGG CCA AAG TGT GAG AGA TT	Microsynth	N/A
NimB1 qRT R TAT CGT CAC AGC TTC CGT TC	Microsynth	N/A
NimB2 qRT F GAG TGT CTG CCG AAG TGT GA	Microsynth	N/A
NimB2 qRT R TCA CAT ATC CGG TCT TGC AG	Microsynth	N/A
NimB3 qRT F TCC CAA CTC CAG AAA TCG TC	Microsynth	N/A
NimB3 qRT R AGC AGT CCT CCG AGC AAA T	Microsynth	N/A
NimB4 qRT F TTG TGC TCA ACT ACC GCA AC	Microsynth	N/A
NimB4 qRT R CGT CCA GCT CGT ATC CCT TA	Microsynth	N/A
NimB5 qRT F CGT AAC GAC AAC GGT GAC TG	Microsynth	N/A
NimB5 qRT R GTC TCG TCC AGC TTG TAG CC	Microsynth	N/A
RpL32 qRT F GAC GCT TCA AGG GAC AGT ATC TG	Microsynth	N/A

Reagents and Tools table (continued)

Reagent/Resource	Reference or Source	Identifier or Catalog Number
RpL32 qRT R AAA CGC GGT TCT GCA TGA G	Microsynth	N/A
NimB4_gateway cloning F CAC CAT GTC AAC AAT ACT GCG A	Microsynth	N/A
NimB4_gateway cloning R CAA CCA CCA CAT ATC GCT GAG	Microsynth	N/A
Chemicals, enzyme and other reagents		
PrimeScript RT	TAKARA	Cat# RR037B
CFSE (5(6)-CFDA/SE	Thermo Fisher Scientific	Cat# C34554
CellTracker™ Red CMTPX dye	Thermo Fisher Scientific	Cat# C34572
pHrodo™ Red, succinimidyl ester	Invitrogen	Cat# P3660
Triton-X-114 (10% solution)	Thermo Scientific	Cat# 28332
Complete protease inhibitor	Sigma	11697498001
4′,6-Diamidino-2-phenylindole dihydrochloride (DAPI)	Sigma	Cat# D9542
AlexaFluor 488 Phalloidin	Life Technologies	Cat# A22287
AlexaFluor 555 Phalloidin	Life Technologies	Cat# A34055
LysoTracker® Red DND-99	Thermo Fisher Scientific	Cat# L7528
LysoTracker® Green DND-26	Thermo Fisher Scientific	Cat# L7526
phenylmethylsulfonyl fluoride	Sigma	P7626
AlexFluor™ 488 S. aureus Bioparticles™	Thermo Fisher Scientific	Cat# s23371
pHrodo™ Red S. aureus Bioparticles™	Thermo Fisher Scientific	Cat# A10010
Software		
Prism 5	GraphPad Prism	N/A
Fiji 2.1.0/1.53c	Image J	N/A
Others		
Tecan Infinite M200	Tecan	N/A
Leica SP8 IN1	Leica	N/A
The Zeiss AxioImager Z1	Zeiss	N/A

Drosophila rearing conditions

All Drosophila stocks were maintained at 25°C on standard fly medium consisting of 6% cornmeal, 6% yeast, 0.6% agar, 0.1% fruit juice (consisting of 50% grape juice and 50% multifruit juice), supplemented with 10.6 g/l moldex and 4.9 ml/l propionic acid. Third-instar (L3) wandering larvae were selected at 110–120 h AEL.

Mutant and transgenic lines generation

NimB4^{sk2} flies were generated using the *CRISPR/Cas9* technique as previously described *(Kondo & Ueda, 2013).* Briefly, a transgenic fly line expressing Cas9 protein using the germline-specific nanos promoter was crossed to a line expressing a custom guide RNA (gRNA). The cross-produces offspring with an active Cas9–gRNA complex specifically in germ cells, which cleaves and mutates the genomic target site. The following gRNA sequence was used: *GGTTTGTCGCTGCCCCGGAG.* To avoid any background effects, we introgressed NimB4^{sk2} mutant into the *w^{1118} DrosDel* isogenic background for seven generations. For complementation studies, the genomic region of *NimB4* was amplified from genomic DNA including 2 kb upstream and 2 kb downstream of the *NimB4* coding sequence. Gibson assembly was used to clone the fragment into a pUAST-attB-GFP-V5-His backbone *(Rauskolb* et al*, 2011).* The *NimB5* and *NimB3* genes present in the upstream and downstream sequence of *NimB4,* respectively, were inactivated by directed mutagenesis. Mutagenic primers were designed to delete the G of the ATG start codon of NimB3 and to add GA in position 44 of *NimB5* to generate non-sense coding sequences. The plasmid was then microinjected in the VK33 attP embryos. For overexpression studies, the genomic region from the 5'UTR to the stop codon of the intron-less *NimB4* gene was amplified from BACR09N24 and cloned into the pDONR207 Gateway vector (Invitrogen, Carlsbad, CA, USA) and subcloned in the pTW (Drosophila Genomics Resource Center plasmid) transgenesis vector and used to generate transgenic *UAS-NimB4* flies. For the *UAS-NimB4-RFP,* the NimB4 cDNA sequence without STOP codon was cloned into the entry vector pENTR/D- Topo (Invitrogen) and subsequently shuttled into the RFP expression vectors pTWR (C-terminal RFP tag), obtained from the DGRC Drosophila Gateway vector collection. Plasmids were injected either at the Fly facility platform of Clermont-Ferrand (France) or by BestGene Inc. (Chino Hills, CA, USA).

RT–qPCR experiments

For quantification of mRNA, whole third-instar larvae (n = 8) or dissected tissues (n = 20–40) were isolated by TRIzol reagent and dissolved in RNase-free water. 500ng total RNA was then reverse-transcribed in 100 μl reaction volume using PrimeScript RT (TAKARA) and a mixture of oligo-dT and random hexamer primers. Quantitative PCR was performed on cDNA samples on a LightCycler 480 (Roche) in 96-well plates using the LightCycler 480 SYBR Green I master mix (Roche Diagnostics, Basel, Switzerland). Expression values were normalized to that of RpL32.

Western blot

Hemolymph samples were collected as follows: Forty L3 larvae were bled on a glass slide on ice; hemolymph was recovered by dissection, mixed with 10 μl of PBS supplemented with complete protease inhibitor solution (Roche) and 1mM phenylmethylsulfonyl fluoride (Sigma) and N-Phenylthiourea (Sigma), and then centrifuged for 10 min at 1,000 g, 4°C. This was followed by a second centrifugation 5 min 10,000 g. Protein concentration of the samples was determined by BCA assay, and 40 μg of protein extract was separated on a 4–12% acrylamide precast Novex NuPage gel (Invitrogen) under reducing conditions and transferred to membranes (Invitrogen iBlot 2). After blocking in 5% non-fat dry milk in PBS containing 0.1% for 1 h, membranes were incubated at 4°C overnight with a mouse anti-RFP antibody (Abcam) in a 1:1,000 dilution. Anti-mouse-HRP secondary antibody (Jackson ImmunoResearch) in a 1:15,000 dilution was incubated for 45 min at room temperature. Bound antibody was detected using ECL (GE Healthcare) according to the manufacturer's instructions. Membranes were imaged on a ChemiDoc XRS+ (Bio-Rad).

Apoptotic cells preparation

The S2 cells were cultured in Schneider's insect medium (Sigma-Aldrich) containing 10% FBS (Gibco™), penicillin (Sigma-Aldrich), and streptomycin (Sigma-Aldrich) at a concentration of 100 U/ml. To induce apoptosis, cycloheximide (CHX, Sigma-Aldrich) was added at a final concentration of 50 μg/ml. 24 h after the cycloheximide treatment, the cells were isolated and removed by pelleting with centrifugation at 400 g for 5 min at 4°C. In order to stain the apoptotic bodies, CFSE (5(6)-CFDA/SE, Molecular Probes™, or CellTracker™ Red CMTPX dye was added to the supernatant harvested from the cells at a final concentration of 5 μM and incubated 15 min at room temperature in the dark.

pHrodo staining of apoptotic cells

Apoptotic cells were labeled with the pH-sensitive stain pHrodo™ Red, succinimidyl ester (Invitrogen), which is nonfluorescent at neutral pH and emits a strong red fluorescence (532 nm) in an acidic environment (pH 4–6). After the induction of apoptosis by cycloheximide treatment, apoptotic cells were washed twice with PBS and resuspended in PBS at 10^6 cells/ml. 1 µl of 1 mg/ml pHrodo-SE (stock solution in DMSO) was added to 50 ml of cell suspension. After incubation for 30 min at RT, cells were washed twice with PBS and resuspended in PBS.

Immunohistochemistry

For immunofluorescence, L3 larvae were dissected into 150 µl PBS pH 7.4, and macrophages were allowed to adhere on a glass slide for 40 min and fixed for 10 min in PBS containing 4% paraformaldehyde. Larval tissues were dissected in PBS and fixed for at least 1 h at room temperature in 4% paraformaldehyde in PBS. For immunostaining, fixed tissues were subsequently rinsed in PBS + 0.1% Triton X-100 (PBT), permeabilized, and blocked in PBT + 2% bovine serum albumin (BSA) for 1 h and incubated with primary antibodies in PBT + 2% BSA overnight at 4°C. After 1 h washing, secondary antibodies and DAPI were applied at room temperature for 2 h. Primary antibodies used are as follows: chicken anti-GFP (Abcam, 1:1,000), rabbit anti-SIMU 1:100 (Shklyar et al, 2013b)), mouse anti-Draper (Developmental Studies Hybridoma Bank, 1:100), rabbit anti-Dcp-1(cell Signaling, 1:100), Mouse anti-mCherry (Invitrogen, 1:1,000). Alexa Fluor 488 and Alexa Fluor 555-conjugated secondary antibodies (Life technologies, 1:100) were used. For the chloroquine experiment, macrophages were dissected into 150 µl PBS pH 7.4. with 50 µg/ml of chloroquine and allowed to adhere on a glass slide in this solution for 40 min. Cells were then fixed with PFA 4% and immunostained as described above. Finally, cells were stained with 1/15,000 dilution of DAPI (Sigma-Aldrich) and mounted in Dako fluorescence media. Imaginal wing disks were dissected in PBS and then fixed for 15 min at room temperature in 4% PFA in PBS. Samples were rinsed twice with PBS, stained with 1/15,000 dilution of DAPI (Sigma-Aldrich), and mounted in Dako fluorescence media.

Macrophages LysoTracker red staining

Macrophages were allowed to adhere on slides for 45 min and then incubated with 1 µM LysoTracker® Red DND-99 (Invitrogen™, L7528) or LysoTracker® Green DND-26 (Invitrogen™, L7526) in PBS for 1 min at RT. The samples were washed twice in PBS and mounted for immediate observations under fluorescence or confocal microscope.

Scanning electron microscopy

Samples for SEM were prepared as follows. Six wandering third-instar larvae were bled into 50 µl of Schneider's insect medium (Sigma-Aldrich) containing 1 µM phenylthiourea (PTU; Sigma-Aldrich). The collected hemolymph was incubated on a glass coverslip for 30 min with apoptotic cells, before being fixed for 1 h with 1.25% glutaraldehyde in 0.1 M phosphate buffer, pH 7.4. Samples were then washed in cacodylate buffer (0.1 M, pH 7.4), fixed again in 0.2% osmium tetroxide in the same washing buffer, and then dehydrated in graded alcohol series. Samples underwent critical point drying and Au/Pd coating (4 nm). Scanning electron micrographs were taken with a field emission scanning electron microscope Merlin, (Zeiss, Oerzen, Embsen, Germany).

Transmission electron microscopy

Third-instar wandering larvae were bled in 50 µl of Schneider's insect medium (Sigma-Aldrich) containing 1 µM phenylthiourea (PTU; Sigma-Aldrich). The collected hemolymph was incubated on a glass coverslip for 1 h before being fixed for 2 h with 2% paraformaldehyde + 2.5% glutaraldehyde in 0.1 M phosphate buffer, pH 7.4. Samples were then washed in cacodylate buffer (0.1 M, pH 7.4), fixed again in 1% osmium tetroxide and potassium ferrocyanide 1.5% in cacodylate buffer. After several washes in distilled water, samples were stained in 1% uranyl acetate in water, washed again, and then dehydrated in graded alcohol series (50, 70, 90, 95, 100%). Embedding was performed first in 1: 1 Hard EPON and ethanol 100%, and afterward in pure EPON, before being embedded on coated glass slides and placed at 60°C overnight. Images were acquired with a FEI Tecnai Spirit 120 kV (FEI Company, Eagle, The Netherlands).

Binding assay with apoptotic cells

L3 wandering larvae were bled into Schneider's insect medium (Sigma-Aldrich) on a previously chilled glass slide. After larva bleeding, macrophages and apoptotic cells (CellTracker™ Red CMTPX Dye) were incubated directly on the prechilled slide, in cold Schneider's medium, on ice for 60 min. After fixation in 4% paraformaldehyde PBS, Alexa Fluor488-phalloidin staining (Molecular Probes™) was performed. Finally, cells were stained with 1/15,000 dilution of DAPI (Sigma-Aldrich) Fluorescent preparations were mounted in Dako fluorescence media.

Ex vivo larval macrophage phagocytosis assay

Ex vivo phagocytosis assays of red apoptotic cells, Alexa Fluor™ 488 S. aureus Bioparticles™ or pHrodo™ Red S. aureus Bioparticles™ conjugate for Phagocytosis (Invitrogen) were performed as follows. Five L3 wandering larvae carrying the HmlΔgal4,UAS-GFP macrophages marker were bled into 150 µl of Schneider's insect medium (Sigma-Aldrich) containing 1 µM phenylthiourea (PTU; Sigma-Aldrich). The macrophage suspension was then transferred to 1.5 ml low binding tubes (LoBind, Eppendorf, Hamburg, Germany). The samples were incubated, respectively, with 2×10^7 Bioparticles®-Texas Red® Conjugate from S. aureus Wood (Invitrogen), 1×10^6 Red-labeled apoptotic cells or 10^5 pHrodo™ Red S. aureus Bioparticles™ for 30, 60, or 120 min to enable phagocytosis, and then placed on ice in order to stop the reaction. Phagocytosis was quantified using a flow cytometer (BD Accuri C6 flow cytometer, Becton Dickinson biosciences, Franklin Lakes, NJ, USA) in order to measure the fraction of cells phagocytosing, and their fluorescent intensity. 75 µl volume was read in ultra-low attachment 96-well flat-bottom plates (Costar no. 3474, Corning, Midland, NY, USA) at medium speed (35 µl/min). In a first step, macrophages were identified using the *HmlΔgal4UASGFP* live staining. The fluorescence intensity of single macrophages was measured in the green channel with 488nm laser and 530/30 standard filter. The Red signal of apoptotic cells, Alexa Fluor™ 488 S. aureus Bioparticles™ (Invitrogen), or pHrodo™ Red S. aureus Bioparticles™, indicative of macrophages with effective phagocytosis, was monitored with 488 nm laser and 585/40 standard filter. At least 2,000 cells per genotype and per assay were analyzed. Results are an average of three independent experiments.

The phagocytic index was calculated as follows:

$$\textbf{Fraction of hemocytes phagocytosing (f)} = \frac{[number\ of\ hemocytes\ in\ fluorescence\ positive\ gate]}{[total\ number\ of\ hemocytes]}$$

$$\textbf{Phagocytic index (PI)} = [Mean\ fluorescence\ intensity\ of\ hemocytes\ in\ fluorescence\ positive\ gate]\ x\ f$$

Image analysis and quantification

All images used for quantification were captured with a Zeiss LSM700 microscope, and all analyses were performed using ImageJ. For quantification of the fluorescence signal intensity, the fluorescent images were first converted to 8-bit images, and the total intensity value with an identical threshold was captured and measured with ImageJ. The freehand selection tool in ImageJ was used to capture and measure the area of the macrophages. Colocalization analysis was done with the ImageJ plugin "Just another Colocalization Plugin" after channel splitting and background subtraction. Rr (Pearson's correlation coefficient), Ch1:Ch2 ratios, M1 and M2 (Manders' colocalization coefficient for channel 1 and 2) were tabulated for each image.

Crawling assay

For the crawling assay, wandering third-instar larvae were used. Each larvae was taken out of the wall of the vial using a paint brush and placed onto a 10 cm Petri dish plate containing 1.5% agar. A transparent, 1.5-cm-wide plastic ring was placed on the outer rim of the agar to prevent the animal from crawling to the edge of the plate. The animal was then left on the plate for at least 1 min to acclimate to the media. Total larval movement was followed for 1 min at 25°C.

Lifespan and behavioral assays

Lifespan experiments were repeated independently at least three times using two cohorts of 20 male flies per genotype/treatment each time. Freshly emerged flies were allowed to mate for 2 days at room temperature and sorted according to sex and genotype. Experiments were performed at 25°C, and flies were flipped to fresh vials every other day using standard medium. For climbing assays, flies were gently tapped to the bottom of a tube and filmed with a digital camera. The percentage of flies climbing above 7 cm within 10 s was calculated.

Statistical tests

Each experiment was repeated independently a minimum of three times (unless otherwise indicated), error bars represent the standard error of the mean of replicate experiments. Data were analyzed using appropriate statistical tests as indicated in figure legends using the GraphPad Prism software. Significance tests were performed using the Mann–Whitney test. For experiments with more than two conditions, significance was tested using ANOVA test followed by *post hoc* Dunnett's multiple comparison tests. *P* values of < 0.05 = *, < 0.01 = **, and < 0.001 = ***.

3.6 Supplementary data

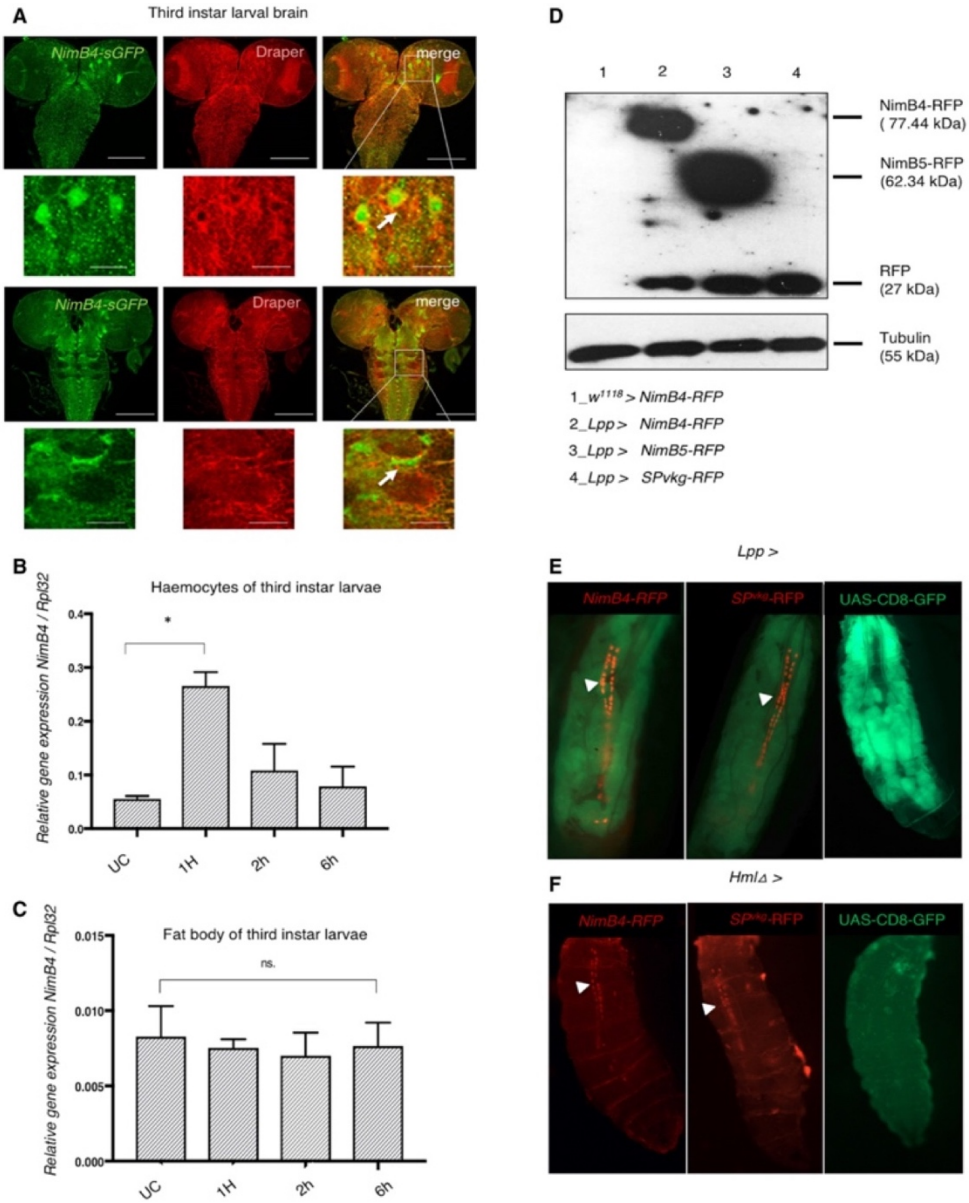

Supplementary Figure 3.1. *NimB4* is induced by clean injury

(A) Representative confocal images from confocal stacks of *NimB4-sGFP* third-instar larval brains. Tissues were stained with anti-GFP (green, corresponding to *NimB4-sGFP)* and anti-Draper (red, corresponding to glial cells). The arrows indicate the presence of NimB4-sGFP in the glial cells of third-instar larval brain. Scale bars = 100 µm. (B, C) Quantification of the *NimB4* transcripts, relative to *RpL32* expression from macrophages (B) and fat body (C) extracts of wild-type (w^{1118}) animals in unchallenged conditions (UC) and 1, 2, 6 h after clean injury. Statistics compare a challenged sample and its own unchallenged sample. Data are represented as mean ± SD from three independent experiments with five animals each (*$P < 0.05$ by ANOVA test followed by *post hoc* Dunnett's multiple comparison tests. ns: not significant). (D) Western blot analysis of hemolymph from L3 larvae expressing *NimB4-RFP, NimB5-RFP,* or SP^{vkg}*-RFP* from the fat body with the driver *Lpp-Gal4* driver. (NimB4: 77.4 kDa, NimB5: 62.3 kDa and RFP: 27 kDa, Tubulin: 55 kDa). (E) Representative images of L3 larvae overexpressing NimB4-RFP, SP^{vkg}-RFP (a secreted RFP), or CD8-GFP in the fat body (CD8-GFP is a membrane-addressed GFP used to confirm that the *Gal4* driver is not expressed in the nephrocytes) in the fat body. NimB4-RFP and SP^{vkg}-RFP accumulate in the pericardial nephrocytes indicating that both proteins are secreted into the hemolymph. CD8-GFP is absent from the pericardial nephrocyte indicating that the *Lpp* driver is not expressed in this tissue. The arrows show the presence of RFP in the pericardial nephrocytes of the larvae. The brightness of the image is modified to improve visualization of the signal. (F) Representative images of L3 larvae overexpressing *NimB4-RFP,* SP^{vkg}*-RFP,* or *CD8-GFP* in the hemocyte. NimB4-RFP and SP^{vkg}-RFP accumulate in the pericardial nephrocytes indicating that both proteins are secreted into the hemolymph. CD8-GFP is absent from the pericardial nephrocyte indicating that the *Hml* driver is not expressed in nephrocytes. The arrows show the presence of RFP in the pericardial nephrocytes of the larvae. The brightness of the image is modified to improve visualization of the signal.

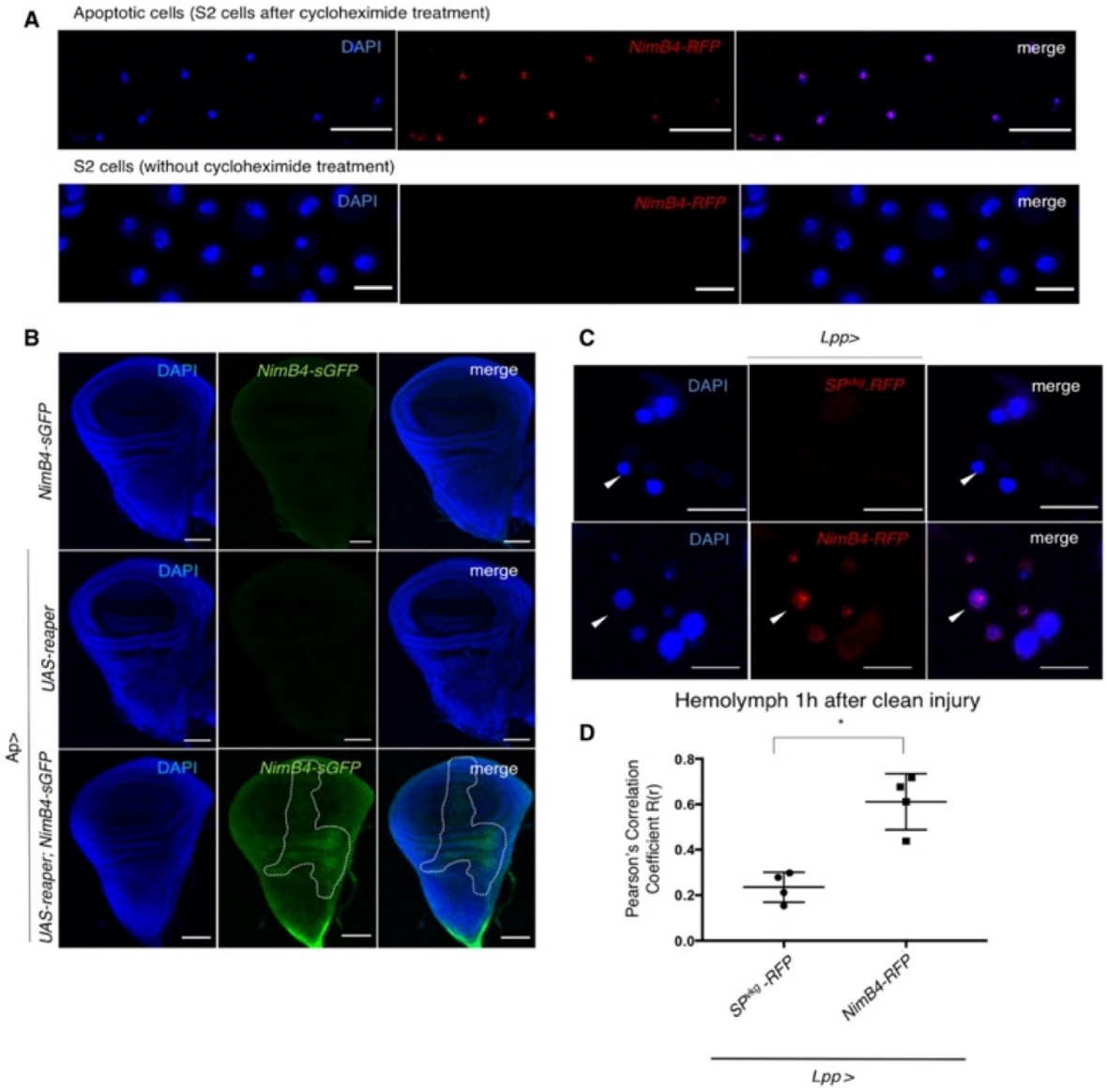

Supplementary Figure 3.2. NimB4 binds apoptotic cells *in vivo*

(A) Representative confocal imaging of apoptotic bodies (blue) and S2 cells (blue) incubated with secreted NimB4-RFP. The brightness of the image is modified to improve visualization of the signal. Scale bar = 10 µm.(B) Representative confocal imaging of imaginal wing disks from *NimB4-sGFP* third-instar larvae expressing or not the pro-apoptotic gene in the imaginal wing disk (*Ap > UAS-reaper NimB4-sGFP)*. Imaginal wing disks were stained with DAPI (blue). The binding of *NimB4-sGFP* is delimited inside the dashed line corresponding to *apterous-Gal4* expression. Scale bar = 10 µm. (C) Representative confocal imaging of apoptotic bodies (blue) derived from *Lpp > NimB4-RFP* or *Lpp >* SP^{vkg}-RFP third-instar larvae after clean injury. The brightness of the image is modified to improve visualization of the signal. Scale bar = 10 µm.(D) Quantification of the colocalization of NimB4-RFP or SP^{vkg}-RFP with the apoptotic bodies, as measured by Pearson's correlation coefficient. Values from at least four independent experiments are represented as mean ± SD (*$P < 0.05$, by Mann–Whitney test).

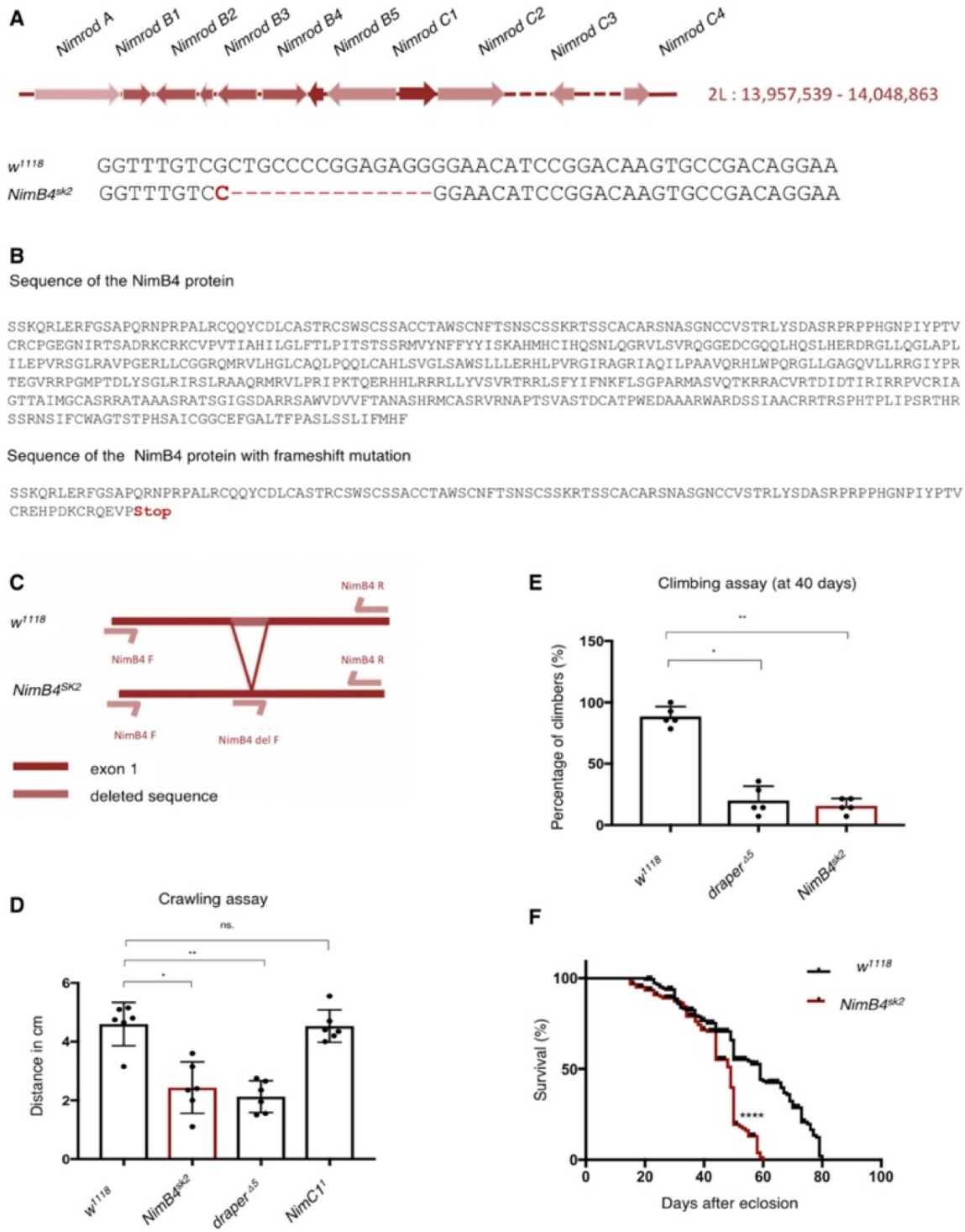

Supplementary Figure 3.3. Generation of *NimB4*-deficient flies by CRISPR-Cas9 system

(**A**) Representation of the *Nimrod* gene locus on the 2nd chromosome (cytology: 34E5). The $NimB4^{sk2}$ mutation is a 14 bp deletion in the first exon. Scheme adapted from Ramond *et al,* (2020).(**B**) The mutation of *NimB4* gene induces a frameshift leading to a premature stop codon.(**C**) Experimental design of qPCR assay to validate $NimB4^{sk2}$ mutants. Scheme adapted from Ramond *et al* (2020).(**D**) Quantification of the distance (in cm) traveled in 1 min by wild-type (w^{1118}), $NimB4^{sk2}$, $draper^{\Delta 5}$, and $NimC1^{1}$ larvae (n = 60 per genotype). The result shown is a mean of three independent experiments containing two cohorts each (*$P < 0.05$, **$P < 0.01$, ***$P < 0.001$ by ANOVA test followed by *post hoc* Dunnett's multiple comparison tests. ns: not significant).(**E**) Forty days old wild-type (w^{1118}), $draper^{\Delta 5}$, and $NimB4^{sk2}$ flies were tested using a standard climbing assay

(mean ± SD), (n = 100 flies for each genotype), (*P < 0.05, ** P < 0.01, by ANOVA test followed by *post hoc* Dunnett's multiple comparison tests. ns: not significant).(F) Lifespan of *NimB4*^{sk2} (red) and wild-type (*w*^{1118}, black) males kept on standard food at 25°C. The result shown is a mean of three independent experiments containing two cohorts of 20 male flies each (****P < 0.0001; log-rank test).

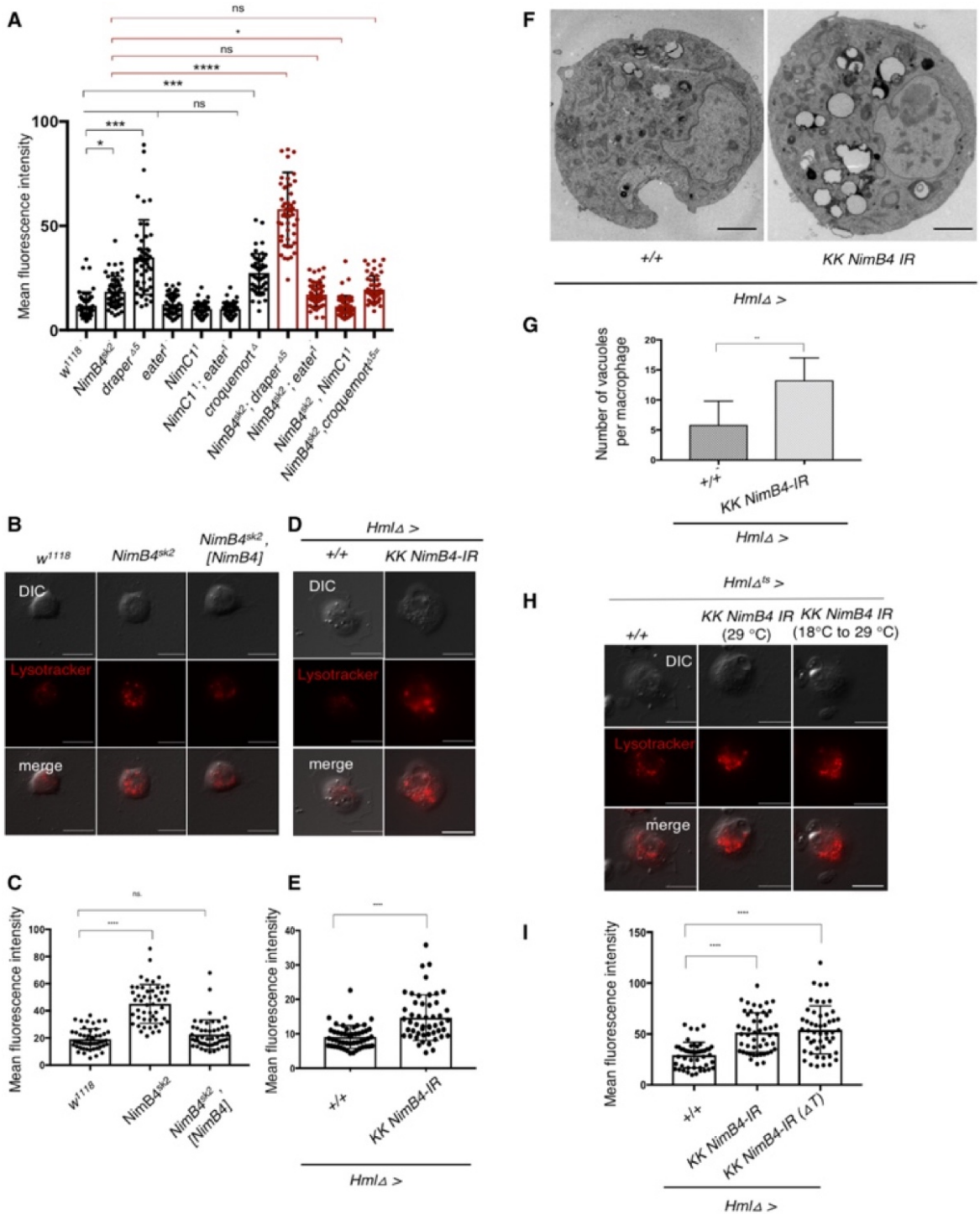

Supplementary Figure 3.4 Genomic rescue of the *NimB4*^{sk2} mutant

(A) Mean fluorescence intensity after staining with LysoTracker Red (confocal live imaging). Values from at least three independent experiments are represented as mean ± SD (*$P < 0.05$, ***$P < 0.001$ ****$P < 0.0001$ by ANOVA test followed by *post hoc* Dunnett's multiple comparison tests. ns: not significant). (B) Representative fluorescence microscopy images of wild-type (*w*^{1118}), *NimB4*^{sk2}, and *NimB4* genomic rescue (*NimB4*^{sk2}, *[NimB4]*) macrophages stained with LysoTracker Red probe (live imaging). Lower panels show an overlay of fluorescence and DIC. Scale bar = 10 µm. (C) Mean fluorescence intensity after staining with LysoTracker Red (confocal live imaging). Values from at least three independent experiments are represented as mean ± SD (****$P < 0.0001$ by ANOVA test followed by *post hoc* Dunnett's multiple comparison tests. ns: not significant). (D) Representative fluorescence microscopy images of wild-type macrophages (*HmlΔ*>+) and macrophages expressing *NimB4-RNAi (HmlΔ > NimB4-IR)* stained with LysoTracker Red probe (live imaging). Lower panels show an overlay of fluorescence and DIC. Scale bar = 10 µm. (E) Mean fluorescence intensity after staining with LysoTracker Red (confocal live imaging). Values from at least three independent experiments are represented as mean ± SD (****$P < 0.0001$ by Mann–Whitney test). (F) Representative transmission electron micrographs of macrophages from control macrophages (*HmlΔ*>+) and macrophages expressing *NimB4-RNAi* (*HmlΔ > NimB4-IR*) from L3 wandering larvae. Scale bar: 2 µm. (G) Quantification of the number of vacuoles per macrophages. Values from at least three independent experiments are represented as mean ± SD (**$P < 0.01$, by Mann–Whitney test). (H) Representative fluorescence microscopy images of macrophages from wild-type (*HmlΔ*^{ts}>+) or macrophages expressing *NimB4-IR (HmlΔ*^{ts} *> NimB4-IR)* using a temperature-inducible macrophage driver *HmlΔ*^{ts} to restrict the expression of *NimB4-IR* after the second-instar larval (L2) stage. *HmlΔ*^{ts} *> KK NimB4-IR* (29°C) larvae developed at 29°C whereas *HmlΔ*^{ts} *> KK NimB4-IR* (18–29°C) larvae were shifted from 18 to 29°C at the second-instar larval stage. Macrophages were stained with LysoTracker Red probe. Lower panels show an overlay of fluorescence and DIC. Scale bar = 10 µm. (I) Mean fluorescence intensity after staining with LysoTracker Red (confocal live imaging). Values from at least three independent experiments are represented as mean ± SD (****$P < 0.0001$ by ANOVA test followed by *post hoc* Dunnett's multiple comparison tests. ns: not significant).

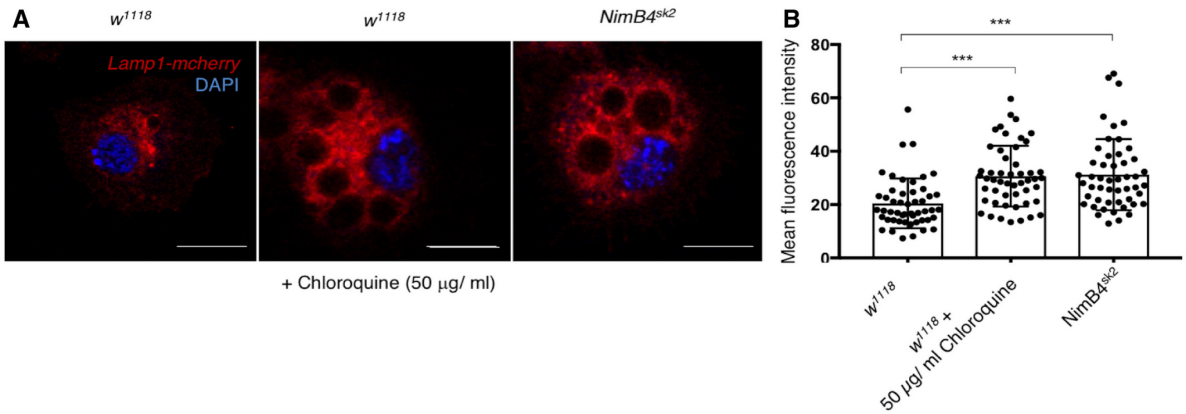

Supplementary Figure 3.5. Elevated Lamp1 levels in the *NimB4*^{SK2} macrophages

(A) Confocal imaging of wild-type and *NimB4* ^{sk2} larval macrophages expressing the reporter *Lamp1-mcherry*. Tissues were stained with an anti-mCherry antibody (red, corresponding to the Lamp1 signal) and DAPI (blue). Wild-type macrophages (*w*^{1118}) were incubated in the presence or in the absence of Chloroquine (50 µg/ml) for 40 min. Scale bar = 10 µm.. (B) Mean fluorescence intensity after staining with LysoTracker Red. Values from at least three independent experiments are represented as mean ± SD (***$P < 0.001$ by ANOVA test followed by *post hoc* Dunnett's multiple comparison tests. ns: not significant).

3.7 Miscellaneous

Authors contribution

BP, SR, and BL conceived and designed the experiments and wrote the paper. BP, SR, KH, FM, ER, RH, MP, SK performed the experiments. BP, SR, BL, EK analyzed the data.

Acknowledgments

We thank the VDRC in Vienna, the Bloomington Stock Center (NIH P40OD018537), Brian McCabe, and Gabor Juhas for the fly stocks. We thank the BIOP platform (EPFL) and the BioEM platform (EPFL) for help with electron microscopy experiments. This work was supported by the Sinergia grant CRSII5_186397. We thank Jean-Philippe Boquete for his precious technical support, we thank Hannah Westlake for critical reading of the manuscript, and Dominique Soldati (University of Geneva) and Brian McCabe (EPFL) for stimulating discussion

Conflicts of interest

The authors declare that they have no conflict of interest.

3.8 References

1. Arandjelovic, S. & Ravichandran, K. S. Phagocytosis of apoptotic cells in homeostasis. *Nat Immunol* 16, 907–917 (2015).
2. Elliott, M. R. & Ravichandran, K. S. Clearance of apoptotic cells: implications in health and disease. *J Cell Biol* 189, 1059–1070 (2010).
3. Nagata, S., Hanayama, R. & Kawane, K. Autoimmunity and the Clearance of Dead Cells. *Cell* 140, 619–630 (2010).
4. Poon, I. K. H., Lucas, C. D., Rossi, A. G. & Ravichandran, K. S. Apoptotic cell clearance: basic biology and therapeutic potential. *Nature Reviews Immunology* 14, 166–180 (2014).
5. Etchegaray, J. I. *et al.* Defective Phagocytic Corpse Processing Results in Neurodegeneration and Can Be Rescued by TORC1 Activation. *J. Neurosci.* 36, 3170–3183 (2016).
6. Hakim-Mishnaevski, K., Flint-Brodsly, N., Shklyar, B., Levy-Adam, F. & Kurant, E. Glial Phagocytic Receptors Promote Neuronal Loss in Adult Drosophila Brain. *Cell Reports* 29, 1438-1448.e3 (2019).

7. Hilu-Dadia, R. & Kurant, E. Glial phagocytosis in developing and mature Drosophila CNS: tight regulation for a healthy brain. *Current Opinion in Immunology* 62, 62–68 (2020).
8. Purice, M. D., Speese, S. D. & Logan, M. A. Delayed glial clearance of degenerating axons in aged Drosophila is due to reduced PI3K/Draper activity. *Nature Communications* 7, 12871 (2016).
9. Boada-Romero, E., Martinez, J., Heckmann, B. L. & Green, D. R. The clearance of dead cells by efferocytosis. *Nature Reviews Molecular Cell Biology* 21, 398–414 (2020).
10. Elliott, M. R. & Ravichandran, K. S. The Dynamics of Apoptotic Cell Clearance. *Developmental Cell* 38, 147–160 (2016).
11. Nagata, S., Suzuki, J., Segawa, K. & Fujii, T. Exposure of phosphatidylserine on the cell surface. *Cell Death Differ* 23, 952–961 (2016).
12. Segawa, K. & Nagata, S. An Apoptotic 'Eat Me' Signal: Phosphatidylserine Exposure. *Trends in Cell Biology* 25, 639–650 (2015).
13. Melcarne, C., Lemaitre, B. & Kurant, E. Phagocytosis in Drosophila: From molecules and cellular machinery to physiology. *Insect Biochemistry and Molecular Biology* 109, 1–12 (2019).
14. Pearson, A. M. *et al.* Identification of cytoskeletal regulatory proteins required for efficient phagocytosis in Drosophila. *Microbes and Infection* 5, 815–824 (2003).
15. Stuart, L. M. & Ezekowitz, R. A. B. Phagocytosis: Elegant Complexity. *Immunity* 22, 539–550 (2005).
16. Kinchen, J. M. & Ravichandran, K. S. Identification of two evolutionarily conserved genes regulating processing of engulfed apoptotic cells. *Nature* 464, 778–782 (2010).
17. Alvarez-Dominguez, C., Barbieri, A. M., Berón, W., Wandinger-Ness, A. & Stahl, P. D. Phagocytosed Live Listeria monocytogenes Influences Rab5-regulated in Vitro Phagosome-Endosome Fusion. *J. Biol. Chem.* 271, 13834–13843 (1996).
18. Duclos, S. *et al.* Rab5 regulates the kiss and run fusion between phagosomes and endosomes and the acquisition of phagosome leishmanicidal properties in RAW 264.7 macrophages. *J Cell Sci* 113 Pt 19, 3531–3541 (2000).
19. Kinchen, J. M. *et al.* A novel pathway for phagosome maturation during engulfment of apoptotic cells. *Nat Cell Biol* 10, 556–566 (2008).
20. Poteryaev, D., Datta, S., Ackema, K., Zerial, M. & Spang, A. Identification of the Switch in Early-to-Late Endosome Transition. *Cell* 141, 497–508 (2010).
21. Yousefian, J. *et al.* Dmon1 controls recruitment of Rab7 to maturing endosomes in Drosophila. *J Cell Sci* 126, 1583–1594 (2013).
22. Huynh, K. K. *et al.* LAMP proteins are required for fusion of lysosomes with phagosomes. *The EMBO Journal* 26, 313–324 (2007).
23. Botelho, R., Fountain, A., Lancaster, C. & Terebiznik, M. Clathrin-mediated phagosome resolution regenerates lysosomes and maintains degradative capacity of macrophages after phagocytosis. *The FASEB Journal* 34, 1–1 (2020).
24. Lancaster, C. *et al.* Phagosome resolution regenerates lysosomes and maintains the degradative capacity in phagocytes. *bioRxiv* 2020.05.14.094722 (2020) doi:10.1101/2020.05.14.094722.
25. Levin, R., Grinstein, S. & Canton, J. The life cycle of phagosomes: formation, maturation, and resolution. *Immunological Reviews* 273, 156–179 (2016).
26. Savill, J. & Fadok, V. Corpse clearance defines the meaning of cell death. *Nature* 407, 784–788 (2000).

27. Ravichandran, K. S. “Recruitment Signals” from Apoptotic Cells: Invitation to a Quiet Meal. *Cell* 113, 817–820 (2003).
28. Ravichandran, K. S. Beginnings of a Good Apoptotic Meal: The Find-Me and Eat-Me Signaling Pathways. *Immunity* 35, 445–455 (2011).
29. Wu, Y., Tibrewal, N. & Birge, R. B. Phosphatidylserine recognition by phagocytes: a view to a kill. *Trends in Cell Biology* 16, 189–197 (2006).
30. Borisenko, G. G., Iverson, S. L., Ahlberg, S., Kagan, V. E. & Fadeel, B. Milk fat globule epidermal growth factor 8 (MFG-E8) binds to oxidized phosphatidylserine: implications for macrophage clearance of apoptotic cells. *Cell Death & Differentiation* 11, 943–945 (2004).
31. Hanayama, R. *et al.* Identification of a factor that links apoptotic cells to phagocytes. *Nature* 417, 182–187 (2002).
32. Kusunoki, R. *et al.* Roles of Milk Fat Globule-Epidermal Growth Factor 8 in Intestinal Inflammation. *Digestion* 85, 103–107 (2012).
33. Huang, W. *et al.* Milk fat globule-EGF factor 8 suppresses the aberrant immune response of systemic lupus erythematosus-derived neutrophils and associated tissue damage. *Cell Death & Differentiation* 24, 263–275 (2017).
34. Wang, X. *et al.* Caenorhabditis elegans transthyretin-like protein TTR-52 mediates recognition of apoptotic cells by the CED-1 phagocyte receptor. *Nature Cell Biology* 12, 655–664 (2010).
35. Galvan, M. D., Greenlee-Wacker, M. C. & Bohlson, S. S. C1q and phagocytosis: the perfect complement to a good meal. *Journal of Leukocyte Biology* 92, 489–497 (2012).
36. Peng, Y. & Elkon, K. B. Autoimmunity in MFG-E8–deficient mice is associated with altered trafficking and enhanced cross-presentation of apoptotic cell antigens. *J Clin Invest* 121, 2221–2241 (2011).
37. Davidson, A. J. & Wood, W. Phagocyte Responses to Cell Death in Flies. *Cold Spring Harb Perspect Biol* 12, a036350 (2020).
38. Serizier, S. B. & McCall, K. Scrambled Eggs: Apoptotic Cell Clearance by Non-Professional Phagocytes in the Drosophila Ovary. *Front Immunol* 8, 1642 (2017).
39. Freeman, M. R., Delrow, J., Kim, J., Johnson, E. & Doe, C. Q. Unwrapping Glial Biology: Gcm Target Genes Regulating Glial Development, Diversification, and Function. *Neuron* 38, 567–580 (2003).
40. Kurant, E., Axelrod, S., Leaman, D. & Gaul, U. Six-Microns-Under Acts Upstream of Draper in the Glial Phagocytosis of Apoptotic Neurons. *Cell* 133, 498–509 (2008).
41. Manaka, J. *et al.* Draper-mediated and phosphatidylserine-independent phagocytosis of apoptotic cells by Drosophila hemocytes/macrophages. *J Biol Chem* 279, 48466–48476 (2004).
42. Nagaosa, K. *et al.* Integrin βv-mediated Phagocytosis of Apoptotic Cells in *Drosophila* Embryos. *J. Biol. Chem.* 286, 25770–25777 (2011).
43. Nonaka, S., Nagaosa, K., Mori, T., Shiratsuchi, A. & Nakanishi, Y. Integrin αPS3/βv-mediated Phagocytosis of Apoptotic Cells and Bacteria in *Drosophila*. *J. Biol. Chem.* 288, 10374–10380 (2013).
44. Roddie, H. G., Armitage, E. L., Coates, J. A., Johnston, S. A. & Evans, I. R. Simu-dependent clearance of dying cells regulates macrophage function and inflammation resolution. *PLOS Biology* 17, e2006741 (2019).

45. Shklyar, B. *et al.* Developmental regulation of glial cell phagocytic function during Drosophila embryogenesis. *Developmental Biology* 393, 255–269 (2014).
46. Draper, I. *et al.* Silencing of drpr Leads to Muscle and Brain Degeneration in Adult Drosophila. *The American Journal of Pathology* 184, 2653–2661 (2014).
47. Bork, P., Downing, A. K., Kieffer, B. & Campbell, I. D. Structure and distribution of modules in extracellular proteins. *Quarterly Reviews of Biophysics* 29, 119–167 (1996).
48. Callebaut, I., Mignotte, V., Souchet, M. & Mornon, J. P. EMI domains are widespread and reveal the probable orthologs of the Caenorhabditis elegans CED-1 protein. *Biochem Biophys Res Commun* 300, 619–623 (2003).
49. Kurucz, E. *et al.* Nimrod, a putative phagocytosis receptor with EGF repeats in Drosophila plasmatocytes. *Curr Biol* 17, 649–654 (2007).
50. Ju, J. S. *et al.* A Novel 40-kDa Protein Containing Six Repeats of an Epidermal Growth Factor-Like Domain Functions as a Pattern Recognition Protein for Lipopolysaccharide. *The Journal of Immunology* 177, 1838–1845 (2006).
51. Somogyi, K. *et al.* Evolution of Genes and Repeats in the Nimrod Superfamily. *Molecular Biology and Evolution* 25, 2337–2347 (2008).
52. Ramond, E. *et al.* The adipokine NimrodB5 regulates peripheral hematopoiesis in Drosophila. *The FEBS Journal* 287, 3399–3426 (2020).
53. Sarov, M. *et al.* A genome-wide resource for the analysis of protein localisation in Drosophila. *eLife* 5, e12068 (2016).
54. Ivy, J. R. *et al.* Klf15 Is Critical for the Development and Differentiation of Drosophila Nephrocytes. *PLOS ONE* 10, e0134620 (2015).
55. Troha, K. *et al.* Nephrocytes Remove Microbiota-Derived Peptidoglycan from Systemic Circulation to Maintain Immune Homeostasis. *Immunity* 51, 625-637.e3 (2019).
56. Liu, M. *et al.* Tango1 spatially organizes ER exit sites to control ER export. *J Cell Biol* 216, 1035–1049 (2017).
57. Engeland, M. van, Nieland, L. J. W., Ramaekers, F. C. S., Schutte, B. & Reutelingsperger, C. P. M. Annexin V-Affinity assay: A review on an apoptosis detection system based on phosphatidylserine exposure. *Cytometry* 31, 1–9 (1998).
58. Janko, C. *et al.* Cooperative binding of Annexin A5 to phosphatidylserine on apoptotic cell membranes. *Phys. Biol.* 10, 065006 (2013).
59. Kurant, E. Keeping the CNS clear: Glial phagocytic functions in Drosophila. *Glia* 59, 1304–1311 (2011).
60. Zheng, Q. *et al.* Apoptotic Cell Clearance in Drosophila melanogaster. *Front. Immunol.* 8, (2017).
61. Chen, P., Nordstrom, W., Gish, B. & Abrams, J. M. grim, a novel cell death gene in Drosophila. *Genes Dev* 10, 1773–1782 (1996).
62. Henson, P. M. & Hume, D. A. Apoptotic cell removal in development and tissue homeostasis. *Trends in Immunology* 27, 244–250 (2006).
63. Fuentes-Medel, Y. *et al.* Glia and Muscle Sculpt Neuromuscular Arbors by Engulfing Destabilized Synaptic Boutons and Shed Presynaptic Debris. *PLoS Biol* 7, e1000184 (2009).
64. Davie, K. *et al.* A Single-Cell Transcriptome Atlas of the Aging Drosophila Brain. *Cell* 174, 982-998.e20 (2018).
65. Han, C. *et al.* Epidermal Cells Are the Primary Phagocytes in the Fragmentation and Clearance of Degenerating Dendrites in Drosophila. *Neuron* 81, 544–560 (2014).

66. Zhou, Z. & Yu, X. Phagosome maturation during the removal of apoptotic cells: receptors lead the way. *Trends in Cell Biology* 18, 474–485 (2008).
67. Harrison, R. E., Bucci, C., Vieira, O. V., Schroer, T. A. & Grinstein, S. Phagosomes fuse with late endosomes and/or lysosomes by extension of membrane protrusions along microtubules: role of Rab7 and RILP. *Mol Cell Biol* 23, 6494–6506 (2003).
68. Steller, H. Regulation of apoptosis in Drosophila. *Cell Death Differ* 15, 1132–1138 (2008).
69. Shklyar, B., Levy-Adam, F., Mishnaevski, K. & Kurant, E. Caspase Activity Is Required for Engulfment of Apoptotic Cells. *Mol. Cell. Biol.* 33, 3191–3201 (2013).
70. Tung, T. T. *et al.* Phosphatidylserine recognition and induction of apoptotic cell clearance by Drosophila engulfment receptor Draper. *The Journal of Biochemistry* 153, 483–491 (2013).
71. Erwig, L.-P. *et al.* Differential regulation of phagosome maturation in macrophages and dendritic cells mediated by Rho GTPases and ezrin–radixin–moesin (ERM) proteins. *PNAS* 103, 12825–12830 (2006).
72. Manaka, J. *et al.* Draper-mediated and Phosphatidylserine-independent Phagocytosis of Apoptotic Cells by *Drosophila* Hemocytes/Macrophages. *J. Biol. Chem.* 279, 48466–48476 (2004).
73. Shiratsuchi, A. *et al.* Independent recognition of Staphylococcus aureus by two receptors for phagocytosis in Drosophila. *J Biol Chem* 287, 21663–21672 (2012).
74. Evans, I. R. & Wood, W. Drosophila blood cell chemotaxis. *Curr Opin Cell Biol* 30, 1–8 (2014).
75. Ravichandran, K. S. Find-me and eat-me signals in apoptotic cell clearance: progress and conundrums. *J Exp Med* 207, 1807–1817 (2010).
76. Akakura, S. *et al.* The opsonin MFG-E8 is a ligand for the αvβ5 integrin and triggers DOCK180-dependent Rac1 activation for the phagocytosis of apoptotic cells. *Experimental Cell Research* 292, 403–416 (2004).
77. Nandrot, E. F. *et al.* Essential role for MFG-E8 as ligand for alphavbeta5 integrin in diurnal retinal phagocytosis. *Proc Natl Acad Sci U S A* 104, 12005–12010 (2007).
78. Pais, I. S., Valente, R. S., Sporniak, M. & Teixeira, L. Drosophila melanogaster establishes a species-specific mutualistic interaction with stable gut-colonizing bacteria. *PLOS Biology* 16, e2005710 (2018).
79. Bretscher, A. J. *et al.* The Nimrod transmembrane receptor Eater is required for hemocyte attachment to the sessile compartment in Drosophila melanogaster. *Biology Open* 4, 355–363 (2015).
80. Freeman, M. R. *Drosophila* Central Nervous System Glia. *Cold Spring Harb Perspect Biol* 7, a020552 (2015).
81. Sinenko, S. A. & Mathey-Prevot, B. Increased expression of Drosophila tetraspanin, Tsp68C, suppresses the abnormal proliferation of ytr-deficient and Ras/Raf-activated hemocytes. *Oncogene* 23, 9120–9128 (2004).
82. Brankatschk, M. & Eaton, S. Lipoprotein Particles Cross the Blood–Brain Barrier in Drosophila. *J. Neurosci.* 30, 10441–10447 (2010).
83. Lőw, P. *et al.* Impaired proteasomal degradation enhances autophagy via hypoxia signaling in Drosophila. *BMC Cell Biology* 14, 29 (2013).
84. Rauskolb, C., Pan, G., Reddy, B. V. V. G., Oh, H. & Irvine, K. D. Zyxin Links Fat Signaling to the Hippo Pathway. *PLOS Biology* 9, e1000624 (2011).

85. Shklyar, B., Shklover, J. & Kurant, E. Live Imaging of Apoptotic Cell Clearance during Drosophila Embryogenesis. *JoVE (Journal of Visualized Experiments)* e50151 (2013) doi:10.3791/50151.

Chapter 4
Functional characterization of the secreted Nimrod *NimB1*

Note: This chapter is based on a study in preparation for publication

Authors: Bianca Petrignani, Asya Dolgikh, Samuel Rommelaere, Florent Masson, Bruno Lemaitre

Contribution of Bianca Petrignani: Designed the study, preformed the experiments and analysis,wrote the manuscript.

4.1 Introduction

The Nimrod gene superfamily encodes a family of proteins involved in phagocytosis and blood cell homeostasis in insects. Genes of the Nimrod family encode proteins with a varying number of NIM domain repeats, a particular type of epidermal growth factor (EGF) repeat, which often function in coagulation, adhesion, and receptor-target interaction (Bork *et al*, 1996; Somogyi *et al*, 2008). The *Drosophila* genome encodes 12 Nimrod members, ten of which are clustered on the second chromosome. The Nimrod proteins can be divided into two subgroups: Nimrod C-type and Nimrod B-type proteins. The products of *Nimrod C-type* genes (e.g., Nimrod C1-4 and Eater) are transmembrane proteins, whereas the products of *Nimrod B-type* genes (e.g., NimB1-5) are secreted proteins. Early studies implicated several Nimrod C-type proteins in phagocytosis of bacteria or apoptotic cells (Eater and NimC1, Draper and NimC4/SIMU), as well as macrophage adhesion and sessility (Eater and NimC1) (Kocks *et al*, 2005; Kurucz *et al*, 2007; Kurant *et al*, 2008; Bretscher *et al*, 2015).

Although the Nimrod transmembrane receptors have been well characterized in *Drosophila* immunity, little is known about the secreted Nimrod B-type proteins. So far, only the role of NimB5 and NimB4 proteins of the five NimBs have been characterized (Ramond *et al*, 2020b; Petrignani *et al*, 2021). NimB5 is part of a regulatory mechanism adjusting the number of macrophages to nutrient availability (Ramond *et al*, 2020b).The NimB5 protein is produced by the fat body upon starvation and regulates macrophage (plasmatocyte) adhesion and proliferation rate. Recently, it has been shown that NimB4 acts as a bridging molecule during phagocytosis of apoptotic cells. The NimB4 protein is secreted by phagocytes and binds to apoptotic corpses to engage a phagosome maturation program dedicated to efferocytosis (Petrignani *et al*, 2021).

In this study, we aim to characterize the function of another NimB protein in *Drosophila* immunity, NimB1. Our preliminary data showed that NimB1 may act as a bridging molecule. Like NimB4, NimB1 is secreted by macrophages and binds to apoptotic cells. Moreover, similar to the *NimB4* mutant, the *NimB1* mutant presents enlarged phagosomes, suggesting a defect in phagosome formation. However, we did not find defects in phagocytosis of apoptotic cells by third larval stage hemocytes. Interestingly, we showed that like NimB5,

NimB1 is also able to regulate macrophage number and adhesion properties. As such, NimB1 shares functions with both NimB4 and NimB5 proteins.

4.2 Results

4.2.1 NimB1 is a secreted protein enriched in macrophages and in neurons

In mammals, phagocytosis of apoptotic cells (efferocytosis) is a complex process that involves several interactions between the target and the effector cells (Arandjelovic & Ravichandran, 2015; Barth *et al*, 2017; Lemke, 2019). Many receptors and bridging molecules are involved in apoptotic cell recognition, forming a phagocytic synapse. Recently, the first bridging molecule in *Drosophila*, NimB4, was characterized (Petrignani *et al*, 2021). However, the function of other NimBs, NimB1, B2 and B3, which are candidate bridging molecules, have not been studied yet. Therefore, we decided to characterize NimB1 function in *Drosophila* to decipher whether this protein acts as a bridging molecule in the phagocytosis of apoptotic cells.

As bridging molecules are secreted from the phagocyte, we monitored the expression of *NimB1* in the macrophages of third-instar larvae. Consistent with a recent transcriptome analysis (Ramond *et al*, 2020a), we observed that *NimB1* and *NimB4* are most highly expressed in macrophages compared to the other tissues (**Figure 4.1A**). In contrast, NimB2, 3 and 5 are mainly expressed in the fat body.

Macrophages play an important role in removing apoptotic cells during embryogenesis. To see if *NimB1* is expressed at this stage, we monitored the expression of *NimB1* during the *Drosophila* life cycle. Interestingly, RT-qPCR analysis showed that *NimB1* and *NimB4* are more highly expressed during embryogenesis compared to other stages of *Drosophila* life cycle (**Figure 4.1B**). To further characterize the expression profile of the NimB1 protein, we monitored its expression at the subcellular level by generating a transgenic fly line carrying a *V5-sGFP-NimB1* fusion under the control of native *NimB1* regulatory sequences (NimB1-sGFP, derived from the Dresden pFlyFos collection, (Sarov *et al*, 2016). We used this reporter gene to follow *NimB1* expression during the larval stages, focusing on phagocytic cells such as macrophages and glial cells. Confocal imaging of third instar larval macrophages showed that NimB1-sGFP is present on the membrane of intracellular structures which may represent the

endosomal compartment of macrophages (Figure 4.2A). In contrast to NimB4, NimB1-sGFP is not expressed in glial cells but shows a clear pattern of expression in two distinct groups of neurons in the right and left central regions of the brain (Figure 4.2B).

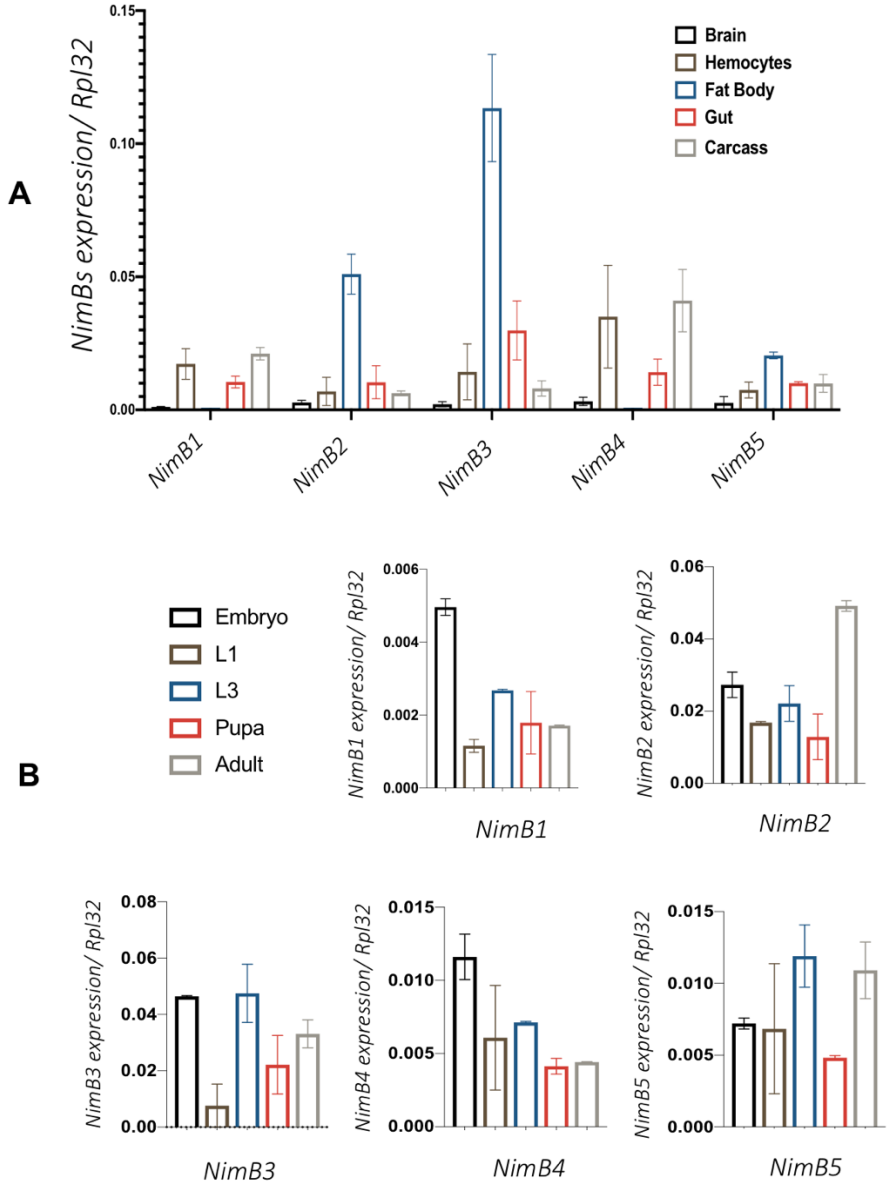

Figure 4.1 *NimB1* expression during the *Drosophila* life cycle

(A) RT-qPCR analysis of *NimB1, NimB2, NimB3, NimB4,* and *NimB5* transcripts, normalized to *Rpl32,* from brain, macrophages, fat body, gut and carcass of wild-type L3 wandering larvae. Data are represented as mean ± SD from three independent experiments. (B) RT-qPCR analysis of *NimB1, NimB2, NimB3, NimB4*, and *NimB5* transcripts, normalized to *Rpl32* from embryo, L1, L2, L3, pupa and adult wild-type *Drosophila*. Data are represented as mean ± SD from three independent experiments.

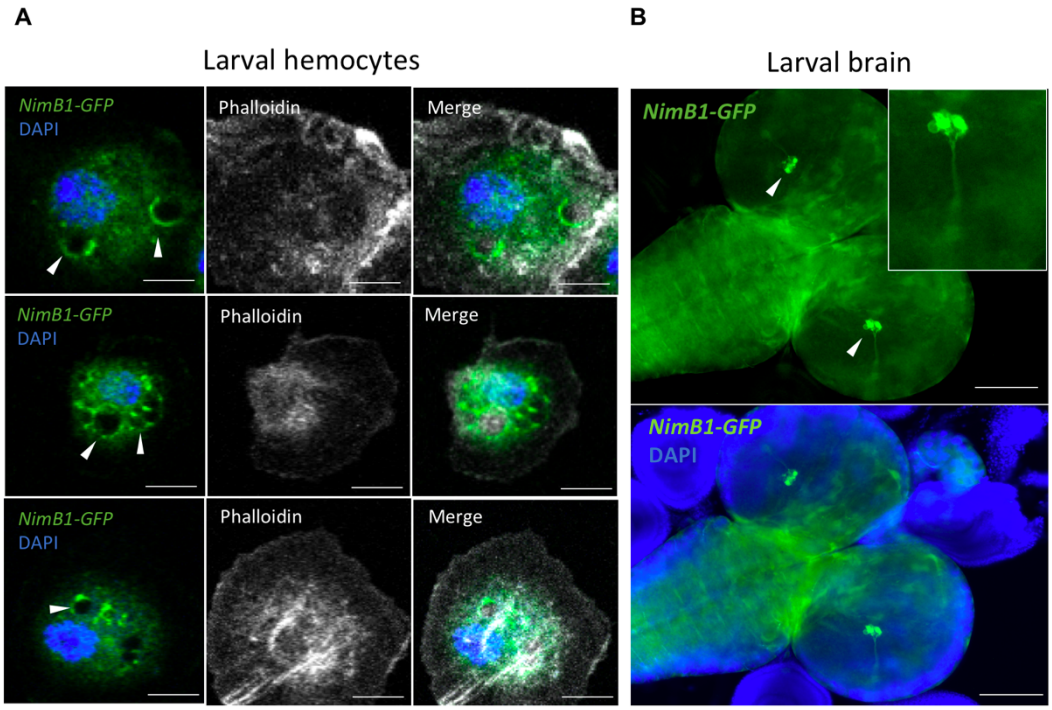

Figure 4.2 At the larval stage, NimB1 is present in macrophages and neurons.
(**A**) Three representative confocal images of NimB4-sGFP macrophages at the larval stage. The arrows show the presence of NimB4-sGFP inside the larval macrophages. Scale bars = 20 µm. (**B**) Representative confocal images of NimB4-sGFP brain at the larval stage. The arrows show the presence of NimB4-sGFP inside small groups of neurons. Scale bars = 100 µm

4.2.2 NimB1 is a secreted protein that binds to apoptotic cells

NimB1 is predicted to be a secreted protein due to the presence of a signal peptide (Somogyi et al.,2008). To confirm the secreted nature of NimB1, we generated a transgenic fly line carrying a *UAS-NimB1-RFP* insertion and overexpressed it in the fat body using the fat body-specific Gal4 driver *Lpp*. This resulted in a strong RFP signal in the larval nephrocytes, cells which form a filtrating organ involved in the removal of hemolymph proteins (**Figure 4.3A**). This observation confirms that NimB1 can be secreted.

It has been shown that NimB4 is up-regulated upon clean injury and binds to apoptotic cells (Petrignani *et al*, 2021). To explore if NimB1 shares these characteristics, we injured larvae with a thin clean needle in the anterior dorsal cuticle and monitored *NimB1* expression in the macrophages. We did not observe an up-regulation of *NimB1* in macrophages after clean injury (data not shown). This is consistent with a recent RNAseq analysis of gene expression in

third instar larval hemocytes upon injury (Ramond *et al*, 2020b). Next, we investigated the ability of NimB1 to bind to apoptotic cells. We performed a microscopic analysis of larvae expressing NimB1-GFP to see if NimB1-GFP binds to apoptotic cells released to the hemolymph after clean injury. We observed that after injury, NimB1-GFP colocalized with apoptotic cells stained with DAPI (**Figure 4.3B**). Collectively, our results indicate that NimB1 is a secreted protein produced by macrophages that binds to apoptotic cells.

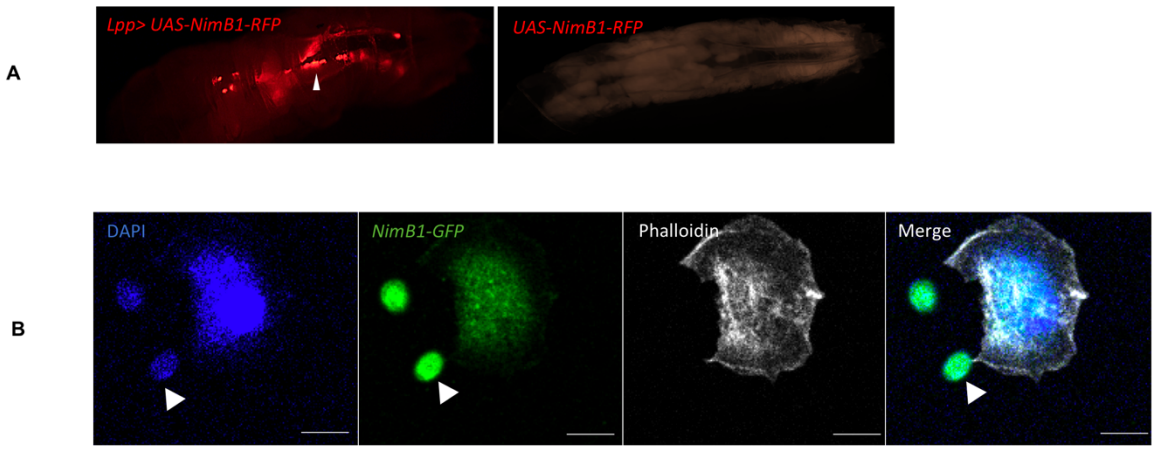

Figure 4.3 NimB1 is a secreted protein that binds to apoptotic cells
(**A**) Representative images of L3 larvae overexpressing NimB4-RFP in the fat body with an *Lpp*-Gal4 driver. The arrows show the accumulation of NimB4-RFP in the pericardial nephrocytes indicating that the protein NimB4-RFP is secreted into the hemolymph (left). Representative images of L3 larvae carrying *UAS-NimB4-RFP*, without the *Lpp* fat body driver (right). (**B**) Representative confocal imaging of apoptotic bodies (indicated with an arrow) generated by a clean injury in the NimB1-eGFP larval line. The brightness of the image is modified to improve visualization of the signal. Scale bar = 10 µm.

4.2.3 Apoptotic cell engulfment is not impaired in *NimB1*-deficient larval macrophages

The results above showed that NimB1-GFP binds to apoptotic cells after clean injury in third instar larvae. Therefore, we further investigated the role of NimB1 in the phagocytosis of apoptotic corpses in third instar larvae. For this, we generated a null mutation in the *NimB1* gene by CRISPR-Cas9, referred to as $NimB1^{229}$. The $NimB1^{229}$ mutant has an 11bp frameshift deletion which introduces a premature stop codon resulting in a truncated protein (**Figure 4.4A**). We isogenized the $NimB1^{229}$ mutation by backcrossing into the w^{1118} DrosDel

background. We observed that *NimB1*^{229} homozygous flies were viable and did not have a reduced lifespan compared to wild-types (Figure 4.4B).

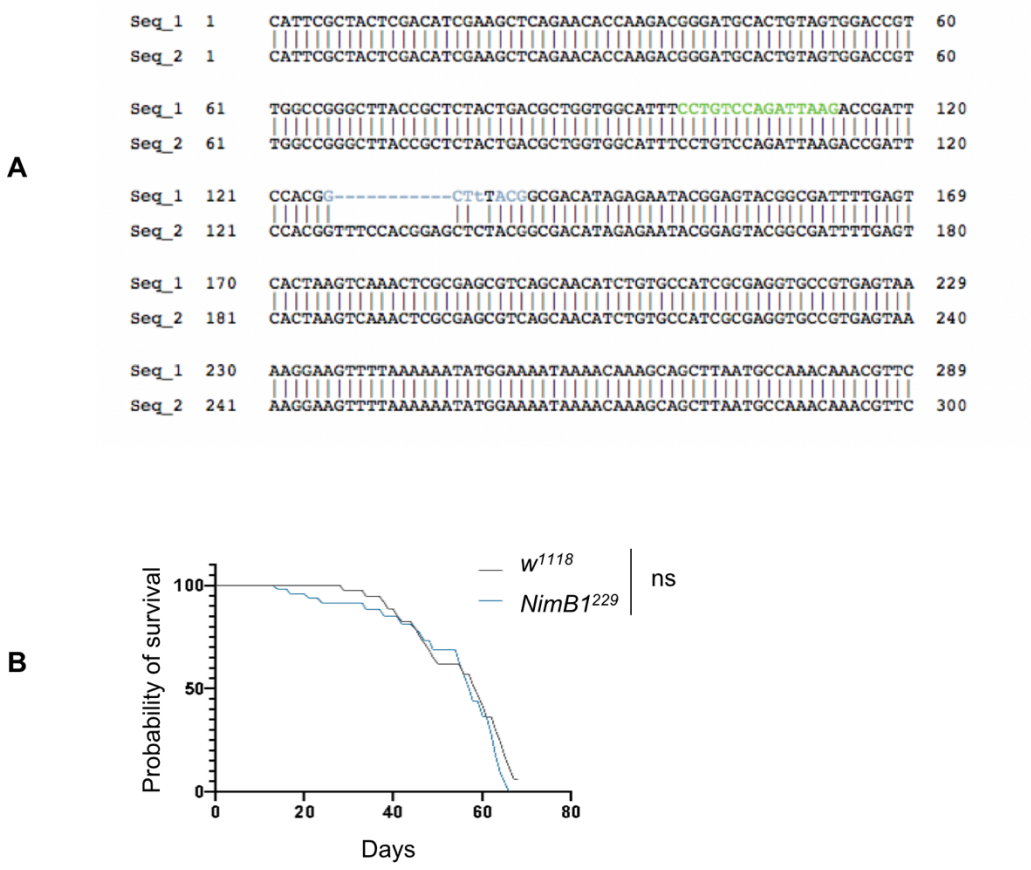

Figure 4.4 Generation of *NimB1*-deficient flies by CRISPR-Cas9 system
(A) The mutation of *NimB1*^{229} gene induces a frameshift leading to a premature stop codon. The binding sequence of the guide RNA is shown in green. In blue is the 11-bp deletion. (B) Lifespan of *NimB1*^{229} (blue) and wild-type (*w*^{1118}, black) males kept on standard food at 25°C. The result shown is a mean of three independent experiments containing two cohorts of 20 flies each (log-rank test).

We first tested the ability of *NimB1*^{229} larval macrophages to internalize fluorescently labeled apoptotic bodies using an *ex vivo* phagocytosis assay. Larval macrophages from *wild-type* (*w*^{1118}), *NimB4*^{sk2}, *Draper*$^{\Delta 5}$, and *NimB1*^{2229} mutants and the double mutant *NimC1*^{1}, *Eater*^{1} were incubated with Alexa^{555} fluorescent apoptotic bodies. Flow cytometry was used to measure the phagocytic index. As previously shown, we found that the *NimC1*^{1}, *Eater*^{1} double mutant and *Draper*$^{\Delta 5}$ mutant macrophages had a reduced phagocytic capacity at all the time points, while *NimB4*^{sk2} was affected only at the 2h time point. In contrast, *NimB1*^{229} phagocytes showed no defect in phagocytosis of apoptotic cells (Figure 4.5A). Thus, we

concluded that NimB1 does not play a role in the uptake of apoptotic cells at the larval stage. Therefore, we continued our investigation by looking at the role of NimB1 in phagosome formation, maturation, and fusion with lysosomes.

We first looked at the role of NimB1 in phagosome formation in macrophages of third instar larvae. For this, we analyzed the formation of intracellular vesicles in macrophages using the fluorochrome LysoTracker Red, which fluoresces in acidic compartments. Interestingly, we observed that the *NimB1*^{229} mutant hemocytes contained numerous and enlarged acidic vesicles compared to wild-type macrophages (Figure 4.5B). This phenotype is reminiscent of that of *NimB4* mutant macrophages, which also present enlarged intracellular vesicles (Petrignani *et al*, 2021).

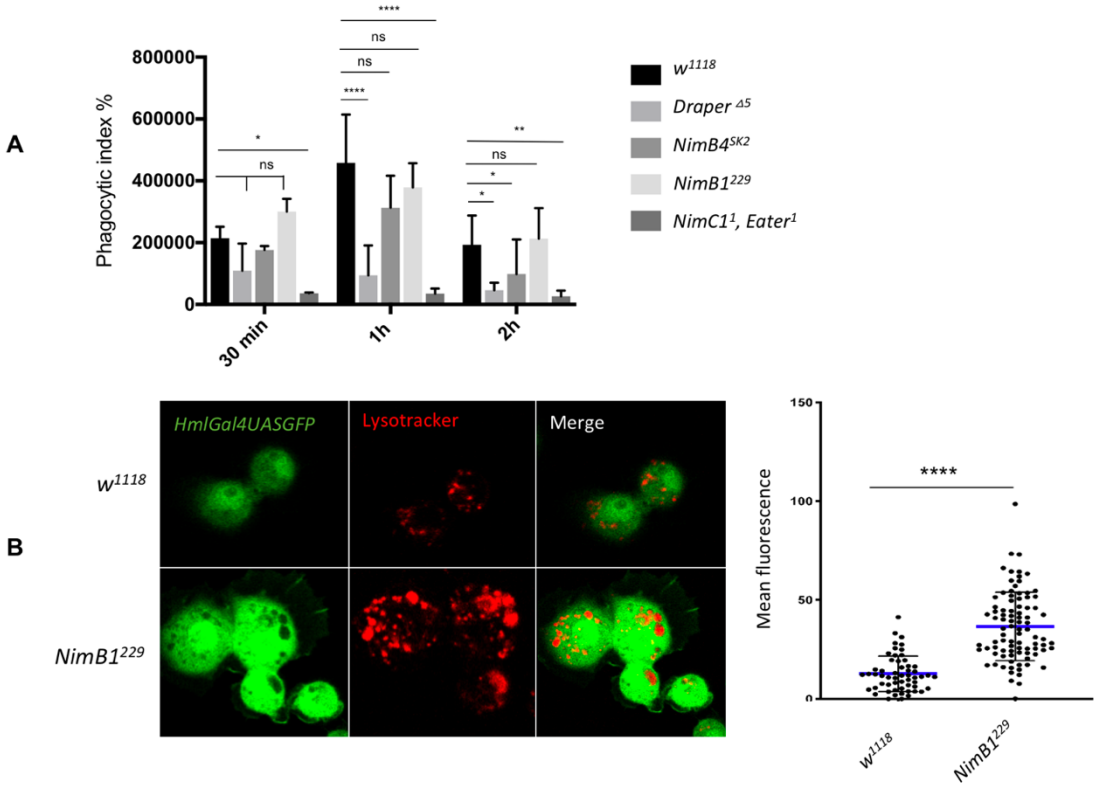

Figure 4.5 *NimB1*^{229} has a defect in phagosome formation

(A) *Ex vivo* phagocytosis assay using fluorescent apoptotic bodies. Wild-type (*w*^{1118}), *Draper*$^{\Delta 5}$, *NimB4*^{sk2}, *NimB1*^{229}and *NimC1*^{1}, *Eater*^{1} macrophages from L3 wandering larvae were incubated with Alexa555-labelled fluorescent apoptotic bodies for 30, 60, or 120 min at room temperature. Phagocytosis was quantified by flow cytometry. Data are represented as mean ± SD from three independent experiments (*P < 0.05, **P < 0.01, ****P < 0.0001 by ANOVA followed by a post hoc Dunnett's multiple comparison test. ns: not significant). (B) Representative fluorescence microscopy images of wild-type (*w*^{1118}) and *NimB1*^{229} third-instar larvae macrophages with the *HmlGAL4,UAS-GFP* marker and stained with LysoTracker Red (live imaging). Scale bar = 10 µm. (left). Mean fluorescence intensity after staining with LysoTracker Red (live confocal imaging). Values from at least three independent experiments are represented as mean ± SD (**P < 0.01, ****P < 0.0001 by ANOVA followed by post hoc Dunnett's multiple comparison test) (right).

During phagocytosis, the newly formed phagosome goes through a maturation process which ends with fusion of the phagosome with lysosomes, leading to the formation of an acidic phagolysosome. Phagolysosome formation is necessary to efficiently digest apoptotic corpses (Zhou & Yu, 2008). Next, we investigated if fusion between the phagosome and lysosome occurs correctly in *NimB1*^{229} mutant macrophages. For this, we collected *w*^{1118}, *NimB1*^{229}, *NimB4*^{sk2}, and *Draper*$^{\Delta 5}$ macrophages carrying the lysosome marker *Lamp1-mcherry* and stained the phagosomes with LysoTracker. Lamp1-mcherry and Lysotracker signals colocalized in the *w*^{1118} and *NimB1*^{229} macrophages, indicating correct formation of phagolysosomes (Figure 4.6A), whereas in the *NimB4*^{sk2} and *Draper*$^{\Delta 5}$ macrophages we observed an absence of colocalization, which confirms a blockage of the phagosome maturation process (Figure 4.6A).

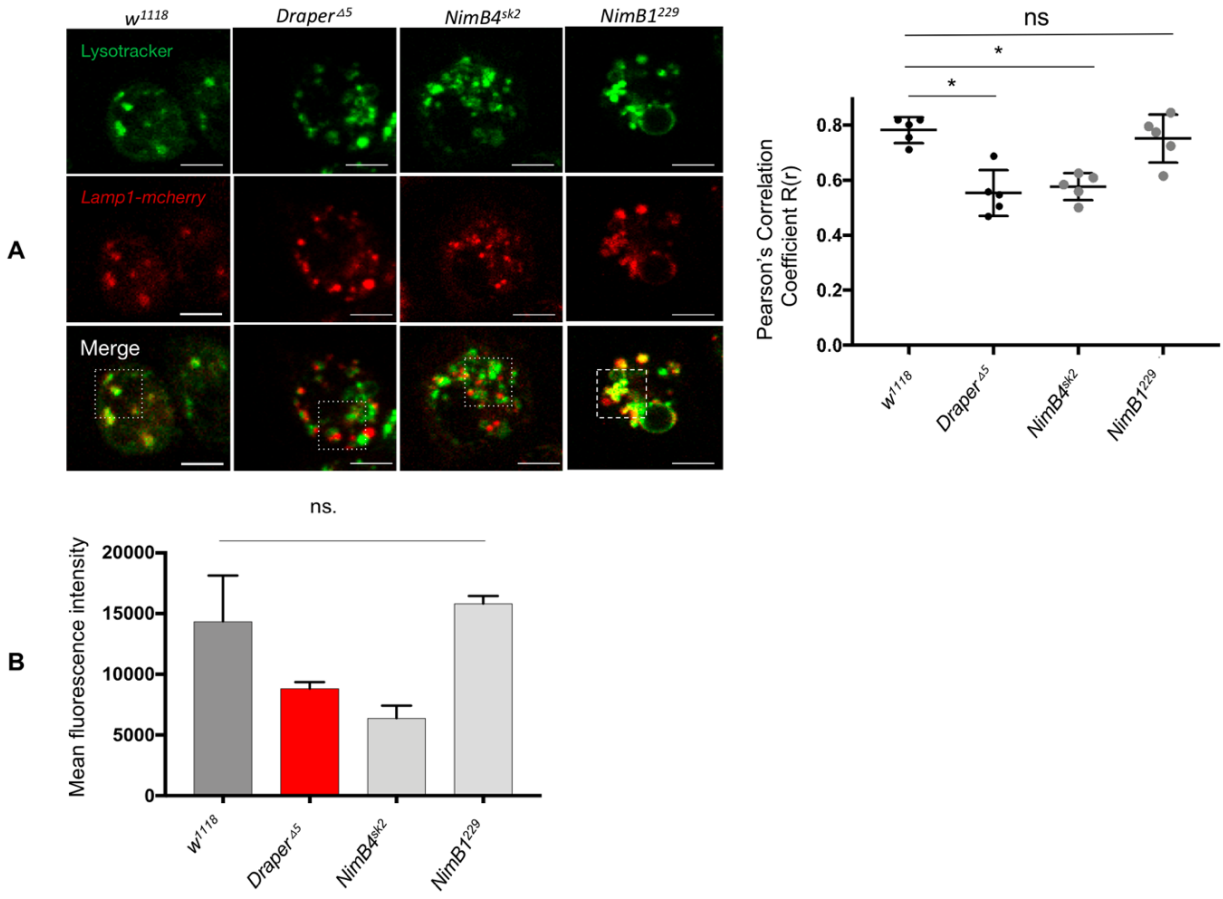

Figure 4.6 *NimB1* mutant macrophages have a normal phagosome maturation process

(A) Representative confocal imaging of localization of Lamp1-mcherry and LysoTracker Green in *wild-type* (*w*^{1118}), *Draper*$^{\Delta 5}$ *NimB4*^{SK2}, *NimB1*^{229} macrophages (live imaging). Scale bar: 10 µm (left). Quantification of the colocalization of Lamp1-mcherry with LysoTracker Green, as measured by Pearson's correlation coefficient between the two signals. Values from at least five independent experiments are represented as mean ± SD (*P <

0.05 by ANOVA followed by post hoc Dunnett's multiple comparison test) (right). (B) *Ex vivo* phagocytosis assay using apoptotic cells labeled with pHrodo™ Red. *Wild-type (w^{1118}), $Draper^{\Delta 5}$ $NimB4^{sk2}$*, and *$NimB1^{229}$* macrophages from L3 wandering larvae were incubated with pHrodo™ Red apoptotic cells for 60 min at room temperature. Phagocytosis was quantified by flow cytometry. Data are represented as mean ± SD from three independent experiments (*P < 0.05 by ANOVA followed by post hoc Dunnett's multiple comparison test. ns: not significant).

The increased vesicles fluorescence intensity in *$NimB1^{229}$* macrophages suggests a defect in phagosome formation. As such, we continued our investigation by comparing phagosome acidification in the *w^{1118}*, *$NimB1^{229}$*, *$NimB4^{sk2}$,* and *$Draper^{\Delta 5}$* macrophages. We used apoptotic cells labeled with pHrodo-succinimidyl ester (pHrodo™ Red), a pH-sensitive fluorescent dye. We then assessed the acidification of the phagosome by measuring the mean fluorescence intensity at 1h using flow cytometry. Wild-type and *$NimB1^{229}$* mutant macrophages had similar fluorescence intensity (Figure 4.6B), whereas the *$NimB4^{sk2}$* and *$Draper^{\Delta 5}$* control mutants both had decreased fluorescence intensity indicating incorrect fusion of phagosomes with lysosomes. In conclusion, *NimB1* has no apparent role in phagosome maturation at the larval stage; however, the presence of enlarged vesicles suggest that phagosomes do not correctly form.

4.2.4 NimB1 plays a critical role in regulating macrophage number

Immune cells use actin protrusions to migrate and explore the extracellular environment (Leithner *et al*, 2016). In macrophages, these actin protrusions lead to phagosome formation, allowing the internalization of extracellular material such as apoptotic cells (Condon *et al*, 2018). As such, phagocytosis and migration are closely linked. We observed that the *$NimB1^{229}$* mutant has enlarged phagosomes (Figure 4.5B). This phenotype prompted us to analyze other phenotypes linked to correct organization of the actin cytoskeleton, notably macrophage survival, adhesion, and the ability to form sessile patches of macrophages characteristic of the third instar larvae (Rougerie *et al*, 2013; Davidson *et al*, 2019; Davidson & Wood, 2016; Edwards-Jorquera *et al*, 2020; Evans *et al*, 2013; Brinkmann *et al*, 2016). First, we measured the number of macrophages (both sessile and circulating) by flow cytometry at different stages of the *Drosophila* life cycle. Interestingly, *$NimB1^{229}$* L2 and L3 larvae and adult flies have less than half of the number of macrophages found in wild-type controls (Figure 4.7A-C). Trans-heterozygous *$NimB1^{229}$/ Df(2L) BSC252* larvae carrying the mutation over a deficiency that

removes the *Nimrod* locus had similarly reduced macrophage numbers (Figure 4.7B). To further confirm this phenotype, we tested the effect of RNAi-mediated knockdown of *NimB1* in various tissues on macrophage number. We selected the RNAi KK VDRC 100043 line from public stock centers and overexpressed this RNAi construct ubiquitously (*Act5C-Gal4*), in the macrophages (*Hml-Gal4*), or in the fat body (*Lpp-Gal4*).

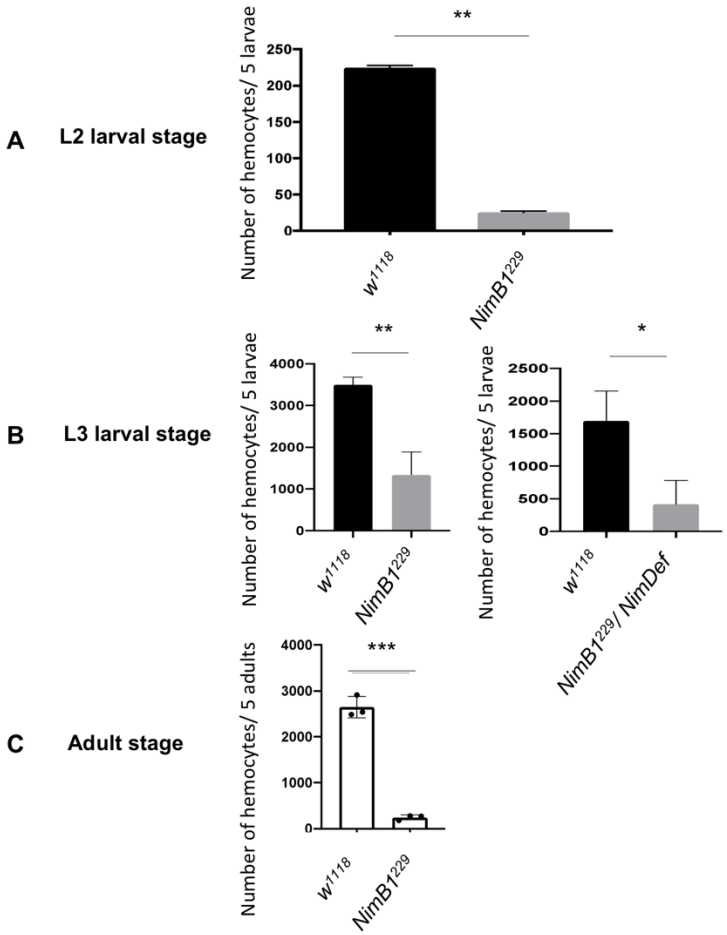

Figure 4.7 *NimB1* mutants have reduced numbers of macrophages

(A) Total counts of peripheral macrophages from *wild-type* (w^{1118}) and $NimB1^{229}$mutants at the L2 wandering larval stage. (B) Total counts of peripheral macrophages from w^{1118} and $NimB1^{229}$mutants at the L3 wandering larval stage (left). Total counts of peripheral macrophages from w^{1118} and trans-heterozygous $NimB1^{229}/Df(2L)BSC252$ larvae at the L3 wandering larval stage (right). (C) Total counts of peripheral macrophages from w^{1118} and $NimB1^{229}$ mutants at the adult stage. Data are represented as mean ± SD from four independent experiments with 5 animals each. *P < 0.05, **P < 0.01, ***P < 0.001 by Student's t-test for (A–C).

Silencing *NimB1* in macrophages or ubiquitously led to a significant decrease in the macrophage number at the larval and adult stages similar to the *NimB1* mutant (Figure 4.8A, 8B). In contrast, silencing *NimB1* in the fat body did not decrease macrophage number at any stage (Figure 4.8A, 8B). These observations led us to conclude that NimB1 expression specifically in the macrophages regulates macrophage number.

Interestingly, we observed that overexpression of a wild-type copy of *NimB1* in the fat body (*Lpp*) or in macrophages (*Hml*), increased macrophage numbers compared to the wild-type. We did not observe the same increase in macrophage number when *NimB1* was expressed in the muscle with the driver *Mef2-Gal4* (Figure 4.9A-C). This suggested that secretion of NimB1 from the macrophages or the fat body into the hemolymph can impact the macrophage number.

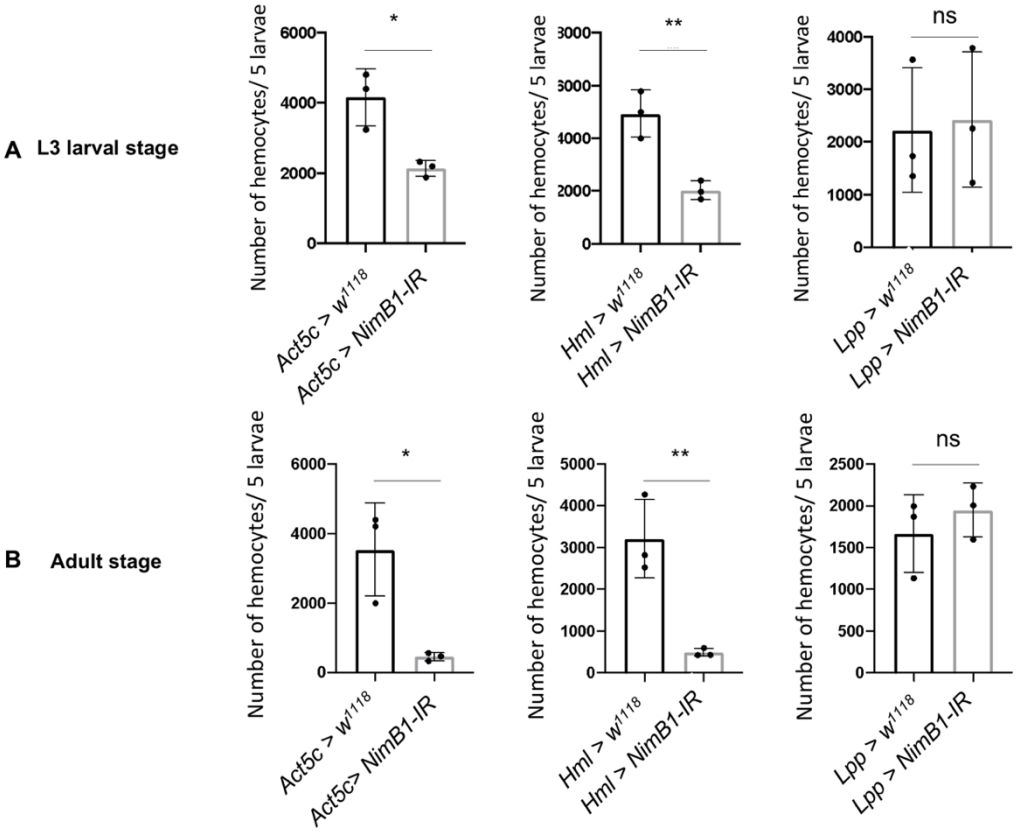

Figure 4.8 Silencing of *NimB1* in macrophages decreases macrophage numbers

Peripheral macrophage counts in (A) larvae and (B) adult flies where *NimB1* was silenced ubiquitously (*Act5c>*), in macrophages (*Hml>*) and in the fat body (*Lpp>*) using *KK-NimB1-IR* (VDRC). Data are represented as mean ± SD from four independent experiments with 5 animals each. *P < 0.05, **P < 0.01, ***P < 0.001 by Student's t-test for (A–B).

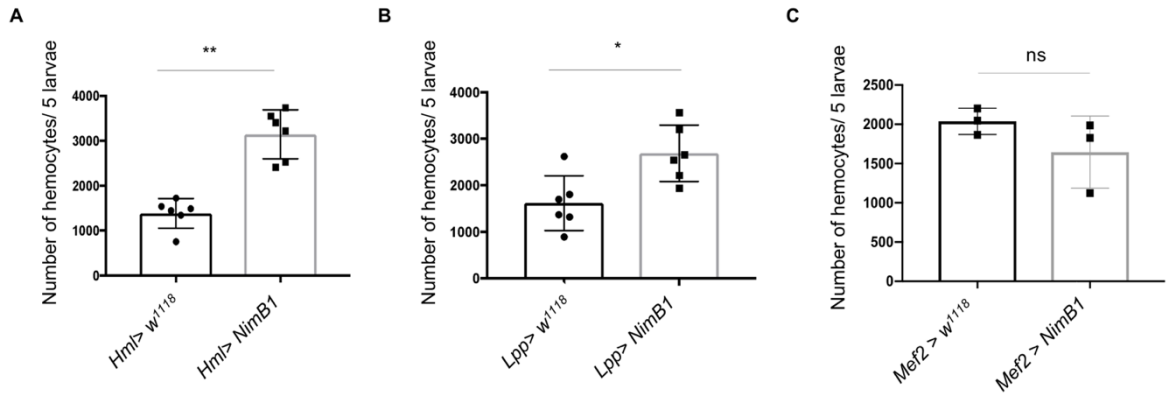

Figure 4.9 *NimB1* overexpression increases macrophage number

Peripheral macrophage counts in larvae where *NimB1* was overexpressed (**A**) in macrophages (*Hml>*), (**B**) in the fat body (*Lpp>*) or in (**C**) the muscles (*Mef2>*) compared to their respective controls. Data are represented as mean ± SD from four independent experiments with 5 animals each. *P < 0.05, **P < 0.01, ***P < 0.001 by Student's t-tests.

4.2.5 NimB1 impacts macrophage adhesion and sessility at the larval stage

We next explored whether NimB1 affects macrophage adhesion and sessility. To test if the *NimB1*^{229} mutant presents an adhesion defect, we allowed larval macrophages from wild-type and *NimB1*^{229} mutants to adhere to glass for 30 min and performed phalloidin staining. Image analysis revealed that the macrophages of *NimB1*^{229} mutants spread much more than the wild-type (**Figure 4.10A-B**). Notably, this spreading defect was not due to a change in macrophage size, as revealed by a Tali™ Image-Based cytometry showing that macrophages of both genotypes had similar diameters in suspension (**Figure 4.10C**). Finally, to observe the formation of sessile patches in third instar larvae, we recombined the *Hml-Gal4, UAS-GFP* macrophage marker with the *NimB1*^{229} mutation and analyzed the localization of peripheral macrophages. *NimB1*^{229} mutants had fewer sessile macrophages patches beneath the cuticle compared to wild-type larvae, which could either be a consequence of the reduced number of macrophages in these mutants or an additional defect in macrophage spatial organization (**Figure 4.10D**). Collectively, our results show that NimB1 impacts both macrophage number and adhesive properties.

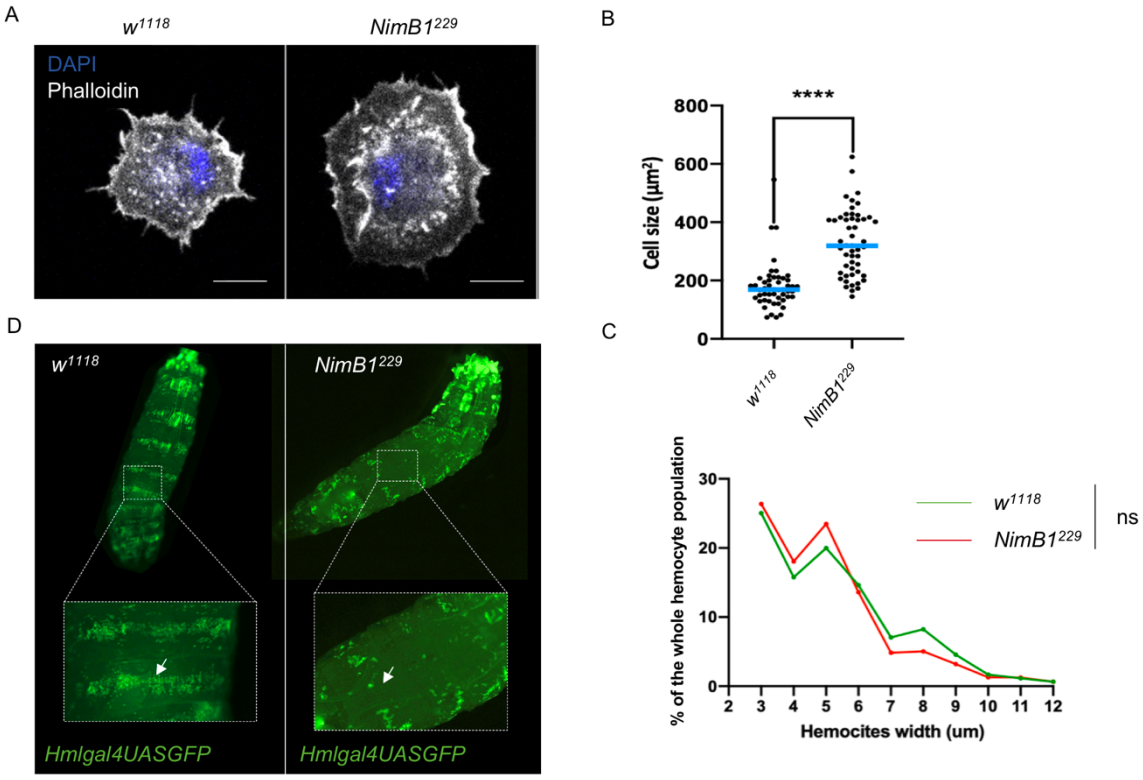

Figure 4.10 *NimB1*^{229} macrophages have spreading defects *in vitro*

(A) *Wild-type* (*w*^{1118}) and *NimB1*^{229} macrophages of the indicated genotypes were extracted by larval bleeding, allowed to spread for 30 min on a glass slide, and stained with Alexa488-labelled phalloidin (gray). Scale bar: 10 µm. (B) Mean cell area quantification of fixed macrophages spread for 30 min on slides and stained with Alexa488-labelled phalloidin. (C) Size distribution of free-floating macrophages from *w*^{1118} and *NimB1*^{229} L3 wandering larvae. Macrophage size was measured on more than 7000 cells per genotype with TALI imaged-based cytometer directly after larval bleeding. (D) Whole larva images of *w*^{1118} or *NimB1*^{229} third instar larvae specifically expressing UAS-GFP in macrophages driven by *Hml-Gal4*. The dorsal side of the animal is shown.

4.3 Discussion

Our preliminary data suggested that NimB1 might act as a bridging molecule. Indeed, NimB1 is secreted by macrophages and binds to apoptotic cells. However, the absence of *NimB1* in third instar larvae did not impact phagocytosis of apoptotic cells. Thus, future studies should clarify if NimB1 has a phagocytic role at another stage of the *Drosophila* life cycle, such as embryogenesis. Indeed, it has been shown that a member of the Nimrod family named SIMU has a restricted role in phagocytosis only during embryogenesis. SIMU is highly expressed on the membrane of embryonic macrophages, glia, and ectodermal cells and triggers the engulfment of apoptotic cells mainly during this stage (Kurant *et al*, 2008). In contrast to Draper, SIMU is not expressed in phagocytic cells at the larval stage. As such, it has been proposed that SIMU could be required exclusively when large numbers of apoptotic cells need

to be removed. Thus, like SIMU, NimB1 could have a punctuated role in the phagocytosis of apoptotic cells during *Drosophila* life cycle.

Additionally, we showed that NimB1 regulates macrophage number and adhesion in third instar larvae. The reduced macrophage number could result from various events, including a defect in proliferation or an increase in cell death. To answer this question, it is essential to determine the number of macrophages at the end of the embryonic stage. The low number of hemocytes could be due to a reduction in the number of embryonic hemocytes.

However, it is tempting to hypothesize that NimB1 could actively regulate macrophage number. One possibility is that NimB1 binds to hemocytes as NimB5 does, and activates a signal that induces their proliferation. Indeed, NimB1 could function as a growth factor and activate an intracellular signaling pathway which would lead to proliferation or regulate survival.

Decreased macrophage proliferation in *NimB1* mutants could also result from impaired adhesion at the larval stage, preventing peripheral hemocytes from retreating to hematopoietic niches that enhance proliferation. This is consistent with findings showing that hematopoietic peripheral niches regroup sensory neurons, providing a microenvironment that promotes embryonic hemocyte expansion and differentiation (Makhijani *et al*, 2011). More recently, it has been shown that sensory neurons of the peripheral nervous system produce Activin-B, which is an essential factor in regulating hemocyte proliferation and adhesion (Makhijani *et al*, 2017). To test these hypotheses, we plan also to monitor the level of proliferation and cell death in both larval sessile and circulating hemocytes.

It is interesting to note that that the *NimB1* mutant shares phenotypes with the *NimB5* mutant. Future studies should clarify if NimB1 interacts with NimB5 or binds a common phagocytic receptor, which would explain their joint role in regulation of hemocyte numbers. The Nimrod family could constitute a complex platform that regulates peripheral hematopoiesis, notably hemocyte proliferation and sessility. Future studies should characterize the role of the other secreted Nimrod members, notably those expressed in the fat body.

4.4 Materials and methods

Drosophila rearing conditions

All Drosophila stocks were maintained at 25°C on standard fly medium consisting of 6% cornmeal, 6% yeast, 0.6% agar, 0.1% fruit juice (consisting of 50% grape juice and 50% multifruit juice), supplemented with 10.6 g/l moldex and 4.9 ml/l propionic acid. Third-instar (L3) wandering larvae were selected at 110–120 h AEL.

Mutant and transgenic lines generation

NimB1^{229} flies were generated using the CRISPR/Cas9 technique as previously described (Kondo & Ueda, 2013). Briefly, a transgenic fly line expressing Cas9 protein using the germline-specific nanos promoter was crossed to a line expressing a custom guide RNA (gRNA). The cross-produces offspring with an active Cas9–gRNA complex specifically in germ cells, which cleaves and mutates the genomic target site. The following gRNA sequence was used *TATGTCGCCGTAGAGCTCCGTGG.* To avoid any background effects, we introgressed *NimB1*^{229} mutant into the *w*^{1118} DrosDel isogenic background for seven generations. For the UAS-NimB1-RFP, the NimB1 cDNA sequence without STOP codon was cloned into the entry vector pENTR/D- Topo (Invitrogen) and subsequently shuttled into the RFP expression vectors pTWR (C-terminal RFP tag), obtained from the DGRC Drosophila Gateway vector collection. Plasmids were injected either at the Fly facility platform of Clermont-Ferrand (France) or by BestGene Inc. (Chino Hills, CA, USA)

RT–qPCR experiments

For quantification of mRNA, whole third-instar larvae (n = 8) or dissected tissues (n = 20–40) were isolated by TRIzol reagent and dissolved in RNase-free water. 500ng total RNA was then reverse-transcribed in 10 ml reaction volume using PrimeScript RT (TAKARA) and a mixture of oligo-dT and random hexamer primers. Quantitative PCR was performed on cDNA samples on a LightCycler 480 (Roche) in 96-well plates using the LightCycler 480 SYBR Green I master mix (Roche Diagnostics, Basel, Switzerland). Expression values were normalized to that of RpL32.

Apoptotic cells preparation

The S2 cells were cultured in Schneider's insect medium (Sigma-Aldrich) containing 10% FBS (Gibco™), penicillin (Sigma-Aldrich), and streptomycin (Sigma-Aldrich) at a concentration of 100 U/ml. To induce apoptosis, cycloheximide (CHX, Sigma-Aldrich) was added at a final concentration of 50 μg/ml. 24 h after the cycloheximide treatment, the cells were isolated and removed by pelleting with centrifugation at 400 g for 5 min at 4°C.

Immunohistochemistry

For immunofluorescence, L3 larvae were dissected into 150 μl PBS pH 7.4, and macrophages were allowed to adhere on a glass slide for 40 min and fixed for 10 min in PBS containing 4% paraformaldehyde. Larval tissues were dissected in PBS and fixed for at least 1 h at room temperature in 4% paraformaldehyde in PBS. Finally, cells were stained with 1/15,000 dilution of DAPI (Sigma-Aldrich) and mounted in Dako fluorescence media.

Macrophages LysoTracker red staining

Macrophages were allowed to adhere on slides for 45 min and then incubated with 1 μM LysoTracker® Red DND-99 (Invitrogen™, L7528) or LysoTracker® Green DND-26 (Invitrogen™, L7526) in PBS for 1 min at RT. The samples were washed twice in PBS and mounted for immediate observations under fluorescence or confocal microscope.

Ex vivo larval macrophage phagocytosis assay

Ex vivo phagocytosis assays of red apoptotic cells, Alexa Fluor™ 488 S. aureus Bioparticles™ or pHrodo™ Red S. aureus Bioparticles™ conjugate for Phagocytosis (Invitrogen) were performed as follows. Five L3 wandering larvae carrying the HmlΔgal4,UAS-GFP macrophages marker were bled into 150 µl of Schneider's insect medium (Sigma-Aldrich) containing 1 µM phenylthiourea (PTU; Sigma-Aldrich). The macrophage suspension was then transferred to 1.5 ml low binding tubes (LoBind, Eppendorf, Hamburg, Germany). The samples were incubated, respectively, with 2×10^7 Bioparticles®-Texas Red® Conjugate from S. aureus Wood (Invitrogen), 1×10^6 Red-labeled apoptotic cells or 10^5 pHrodo™ Red S. aureus Bioparticles™ for 30, 60, or 120 min to enable phagocytosis, and then placed on ice in order to stop the reaction. Phagocytosis was quantified using a flow cytometer (BD Accuri C6 flow cytometer, Becton Dickinson biosciences, Franklin Lakes, NJ, USA) in order to measure the fraction of cells phagocytosing, and their fluorescent intensity. 75 µl volume was read in ultra-low attachment 96-well flat-bottom plates (Costar no. 3474, Corning, Midland, NY, USA) at medium speed (35 µl/min). In a first step, macrophages were identified using the HmlΔgal4UASGFP live staining. The fluorescence intensity of single macrophages was measured in the green channel with 488nm laser and 530/30 standard filter. The Red signal of apoptotic cells, Alexa Fluor™ 488 S. aureus Bioparticles™ (Invitrogen), or pHrodo™ Red S. aureus Bioparticles™, indicative of macrophages with effective phagocytosis, was monitored with 488 nm laser and 585/40 standard filter. At least 2,000 cells per genotype and per assay were analyzed. Results are an average of three independent experiments.

The phagocytic index was calculated as follows:

$$\textbf{Fraction of hemocytes phagocytosing (f)} = \frac{[number\ of\ hemocytes\ in\ fluorescence\ positive\ gate]}{[total\ number\ of\ hemocytes]}$$

$$\textbf{Phagocytic index (PI)} = [Mean\ fluorescence\ intensity\ of\ hemocytes\ in\ fluorescence\ positive\ gate]\ x\ f$$

Image analysis and quantification

All images used for quantification were captured with a Zeiss LSM700 microscope, and all analyses were performed using ImageJ. For quantification of the fluorescence signal intensity, the fluorescent images were first converted to 8-bit images, and the total intensity value with an identical threshold was captured and measured with ImageJ. The freehand selection tool in ImageJ was used to capture and measure the area of the macrophages. Colocalization analysis was done with the ImageJ plugin "Just another Colocalization Plugin" after channel splitting and background subtraction. Rr (Pearson's correlation coefficient), Ch1:Ch2 ratios, M1 and M2 (Manders' colocalization coefficient for channel 1 and 2) were tabulated for each image.

Lifespan

Lifespan experiments were repeated independently at least three times using two cohorts of 20 male flies per genotype/treatment each time. Freshly emerged flies were allowed to mate for 2 days at room temperature and sorted according to sex and genotype. Experiments were performed at 25°C, and flies were flipped to fresh vials every other day using standard medium.

Statistical tests

Each experiment was repeated independently a minimum of three times (unless otherwise indicated), error bars represent the standard error of the mean of replicate experiments. Data were analyzed using appropriate statistical tests as indicated in figure legends using the GraphPad Prism software. Significance tests were performed using the Mann–Whitney test. For experiments with more than two conditions, significance was tested using ANOVA test followed by post hoc Dunnett's multiple comparison tests. P values of < 0.05 = *, < 0.01 = **, and < 0.001 = ***.

4.5 References

Arandjelovic S & Ravichandran KS (2015) Phagocytosis of apoptotic cells in homeostasis. *Nat Immunol* 16: 907–917

Barth ND, Marwick JA, Vendrell M, Rossi AG & Dransfield I (2017) The "Phagocytic Synapse" and Clearance of Apoptotic Cells. *Frontiers in Immunology* 8: 1708

Bork P, Downing AK, Kieffer B & Campbell ID (1996) Structure and distribution of modules in extracellular proteins. *Q Rev Biophys* 29: 119–167

Bretscher AJ, Honti V, Binggeli O, Burri O, Poidevin M, Kurucz E, Zsamboki J, Ando I & Lemaitre B (2015) The Nimrod transmembrane receptor Eater is required for hemocyte attachment to the sessile compartment in Drosophila melanogaster. *Biology Open* 4: 355–363

Brinkmann K, Winterhoff M, Önel S-F, Schultz J, Faix J & Bogdan S (2016) WHAMY is a novel actin polymerase promoting myoblast fusion, macrophage cell motility and sensory organ development in Drosophila. *J Cell Sci* 129: 604–620

Condon ND, Heddleston JM, Chew T-L, Luo L, McPherson PS, Ioannou MS, Hodgson L, Stow JL & Wall AA (2018) Macropinosome formation by tent pole ruffling in macrophages. *Journal of Cell Biology* 217: 3873–3885

Davidson AJ, Millard TH, Evans IR & Wood W (2019) Ena orchestrates remodelling within the actin cytoskeleton to drive robust Drosophila macrophage chemotaxis. *Journal of Cell Science* 132

Davidson AJ & Wood W (2016) Unravelling the Actin Cytoskeleton: A New Competitive Edge? *Trends in Cell Biology* 26: 569–576

Edwards-Jorquera S, Bosveld F, Bellaïche Y, Lennon-Duménil A-M & Glavic A (2020) Trpml controls actomyosin contractility and couples migration to phagocytosis in fly macrophages. *The Journal of Cell Biology* 219

Evans IR, Ghai PA, Urbančič V, Tan K-L & Wood W (2013) SCAR/WAVE-mediated processing of engulfed apoptotic corpses is essential for effective macrophage migration in Drosophila. *Cell Death Differ* 20: 709–720

Kocks C, Cho JH, Nehme N, Ulvila J, Pearson AM, Meister M, Strom C, Conto SL, Hetru C, Stuart LM, *et al* (2005) Eater, a Transmembrane Protein Mediating Phagocytosis of Bacterial Pathogens in Drosophila. *Cell* 123: 335–346

Kurant E, Axelrod S, Leaman D & Gaul U (2008) Six-Microns-Under Acts Upstream of Draper in the Glial Phagocytosis of Apoptotic Neurons. *Cell* 133: 498–509

Kurucz É, Márkus R, Zsámboki J, Folkl-Medzihradszky K, Darula Z, Vilmos P, Udvardy A, Krausz I, Lukacsovich T, Gateff E, *et al* (2007) Nimrod, a Putative Phagocytosis Receptor with EGF Repeats in Drosophila Plasmatocytes. *Current Biology* 17: 649–654

Leithner A, Eichner A, Müller J, Reversat A, Brown M, Schwarz J, Merrin J, de Gorter DJJ, Schur F, Bayerl J, *et al* (2016) Diversified actin protrusions promote environmental exploration but are dispensable for locomotion of leukocytes. *Nat Cell Biol* 18: 1253–1259

Lemke G (2019) How macrophages deal with death. *Nat Rev Immunol* 19: 539–549

Makhijani K, Alexander B, Rao D, Petraki S, Herboso L, Kukar K, Batool I, Wachner S, Gold KS, Wong C, *et al* (2017) Regulation of Drosophila hematopoietic sites by Activin-β from active sensory neurons. *Nat Comms* 8: 15990

Makhijani K, Alexander B, Tanaka T, Rulifson E & Brückner K (2011) The peripheral nervous system supports blood cell homing and survival in the Drosophila larva. *Development* 138: 5379–5391

Petrignani B, Rommelaere S, Hakim-Mishnaevski K, Masson F, Ramond E, Hilu-Dadia R, Poidevin M, Kondo S, Kurant E & Lemaitre B (2021) A secreted factor NimrodB4 promotes the elimination of apoptotic corpses by phagocytes in Drosophila. *EMBO Rep* 22: e52262

Ramond E, Dudzic JP & Lemaitre B (2020a) Comparative RNA-Seq analyses of Drosophila plasmatocytes reveal gene specific signatures in response to clean injury and septic injury. *PLOS ONE* 15: e0235294

Ramond E, Petrignani B, Dudzic JP, Boquete J-P, Poidevin M, Kondo S & Lemaitre B (2020b) The adipokine NimrodB5 regulates peripheral hematopoiesis in Drosophila. *The FEBS Journal* 287: 3399–3426

Rougerie P, Miskolci V & Cox D (2013) Generation of membrane structures during phagocytosis and chemotaxis of macrophages: role and regulation of the actin cytoskeleton. *Immunol Rev* 256: 222–239

Sarov M, Barz C, Jambor H, Hein MY, Schmied C, Suchold D, Stender B, Janosch S, KJ VV, Krishnan R, *et al* (2016) A genome-wide resource for the analysis of protein localisation in Drosophila. *eLife* 5: e12068

Somogyi K, Sipos B, Penzes Z, Kurucz E, Zsamboki J, Hultmark D & Ando I (2008) Evolution of Genes and Repeats in the Nimrod Superfamily. *Molecular Biology and Evolution* 25: 2337–2347

Zhou Z & Yu X (2008) Phagosome maturation during the removal of apoptotic cells: receptors lead the way. *Trends in Cell Biology* 18: 474–485

Chapter 5
General discussion and perspectives

The purpose of this doctoral thesis was to provide a deeper characterization of the Nimrod B-type proteins in *Drosophila* immunity. Nimrod B-type proteins are part of the Nimrod superfamily implicated in phagocytosis and blood cell regulation (Somogyi *et al*, 2010; Cinege *et al*, 2017; Melcarne *et al*, 2019b). They are secreted proteins containing NIM repeats, a subtype of the epidermal growth factor repeats implicated in adhesion, coagulation, and receptor-target interactions (Bork *et al*, 1996). However, the specific involvement of the Nimrod B-type (NimB1-NimB5) proteins in *Drosophila* immunity has never been tested. To decipher their roles in immunity, we generated CRISPR/Cas9 mutants and transgenic fly lines expressing tagged versions of NimB proteins. These genetic tools allowed us to investigate the function of NimB5, NimB4, and NimB1 in *Drosophila* immunity.

Our work showed that the NimB5 protein is expressed in the fat body and regulates macrophage adhesion. Furthermore, NimB5 is induced upon starvation and adjusts macrophage number to the metabolic state of the host. Thus, Nimrod B5 is part of a regulatory mechanism tailoring investment in the immune system to nutrient availability. Additionally, we showed that NimB4 is expressed in hemocytes and plays an essential role in the phagocytosis of apoptotic cells. We provide evidence that NimB4 can act as a bridging molecule that has a significant role in regulating phagosome maturation, and specifically phagosome fusion with the lysosomes. Finally, our preliminary data show that NimB1 could also act as a bridging molecule. Indeed, NimB1 is secreted by macrophages and binds to apoptotic cells, and similar to the *NimB4* mutant, the *NimB1* mutant presents enlarged phagosomes consistent with incorrect phagosome formation. However, we did not find a defect in the phagocytosis of apoptotic cells in the third instar larval stage of *NimB1* mutants. Additionally, we showed that NimB1 affects macrophage number and adhesion properties. As such, NimB1 shares similar functions with both NimB4 and NimB5 proteins.

To better visualize the diverse roles of Nimrod B-type proteins, we present a summary table including a collection of phenotypes characterizing the Nimrod-B type mutants (Figure 5.1). This table covers a variety of read-outs of the cellular and humoral immune responses in *Drosophila*. In the following section, we will discuss the results of the two main projects of this thesis: the role of NimB4 in the phagocytosis of apoptotic cells and the role of NimB5 in peripheral hematopoiesis. The results obtained on NimB1 will be discussed in comparison to NimB4 and NimB5.

	NimB1	*NimB2*	*NimB3*	*NimB4*	*NimB5*
Viability	Yes	***No***	Yes	Yes	Yes
Higher expression during life cycle	Embryo	Adult	Embryo/ L3	Embryo	L3/ Adult
Tissue expression in L3 larvae	Hemocytes / Neurons	Fat body	Fat body	Hemocytes / Glial cells	Fat body/ Hemocytes
Inputs which induce gene expression up-regulation	_	Wasp infestation	Wasp infestation	Clean injury	Starvation/ Ecdyson/ Repression of myc
Biological function	_	_	_	Bridging molecule	Adipokine
Secreted protein	yes	_	_	yes	yes
Phosphatidylserine binding	_	_	_	yes	no
Hemocyte number in the embryo	_	_	_	WT	_
Hemocyte number in L2 larvae	↓	_	_	_	WT
Hemocyte number in L3 larvae	↓	_	_	WT	↑
Hemocyte number in adult	↓	_	_	WT	↑
Hemocyte spreading ex-vivo	↑	_	_	WT	↓
Hemocyte adhesion ex-vivo	_	_	_	_	↓
Hemocyte sessility in vivo	↓	_	_	↓	↓
Filopodia number	WT	_	_	↑	WT
Phagosome size	↑	_	_	↑	WT
Phagosome maturation	WT	_	_	↓	WT
Crystal cells number in L3 larvae	_	_	_	_	↑
Sessile crystal cells number (cooking assay)	↑	_	_	↓	WT
Lamellocyte number (After wasp infestation)	_	_	_	↑	WT
Survival after wasp infestation	_	_	_	_	↓
Melanization after pricking	WT	_	_	WT	WT
Phagocytosis apoptotic cells (2h)	WT	_	_	↓	WT
Phagocytosis *Gram -* (1h)	WT	_	_	WT	WT
Phagocytosis *Gram +* (1h)	WT			WT	WT
AMP genes expression	WT	_	_	WT	WT
Lipid droplet size in adult	↑	_	_	WT	↓
Lipid droplet size in L3 larvae	WT	_	_	WT	↓
Survival on poor medium	↓			WT	↓
Crawling assay	WT			↓	WT
Longevity	WT	_	_	↓	WT
References	Ramond et al.,2020b	_	_	Ramond et al., 2020 Ramond et al., 2020b Petrignani et al.,2021	Ramond et al., 2020 Ramond et al., 2020b

Figure 5.1 Phenotypic observations of the five *NimB* mutants.

List of read-outs in cellular and humoral immune responses in the five *Nimrod-B type* mutants. Measurement identical to wild type (WT), measurement increased compared to wild type (↑) measurement decreased compared to wild type (↓), missing data (-).

5.1 NimB4 is a new bridging molecule *in Drosophila*

Bridging molecules were initially defined as secreted molecules that recognize 'eat me' signals such as phosphatidylserine (PS) and function as bridges between apoptotic cells and cell surface receptors on phagocytes to enhance recognition of apoptotic cells (Savill & Fadok, 2000; Ravichandran, 2003, 2011). Several soluble proteins have been identified as bridging molecules in mammals, including milk fat globule EGF factor 8 (MFG-E8), growth arrest-specific 6 (Gas6), protein S, and C1q. Most studies point to roles of bridging molecules during the early phase of phagocytosis, specifically in apoptotic cell uptake. For instance, the bridging molecule MFG-E8 binds to apoptotic cells and interacts with αvβ3 integrin on phagocytes to promote apoptotic cell uptake (Hanayama *et al*, 2002; Fuller & Van Eldik, 2008; Akakura *et al*, 2004). More surprisingly, other studies suggest that bridging molecules also have roles in receptor activation or phagosome maturation (Peng & Elkon, 2011a; Galvan *et al*, 2012). For instance, the bridging molecule Gas6 is necessary to fully activate TAM phagocytic receptors (Geng *et al*, 2017). In addition, MFG-E8 binds to apoptotic cells and facilitates phagosome fusion with the lysosome (Peng & Elkon, 2011b). Interestingly, our study identifies the first bridging molecules in *Drosophila* and suggests that these also have roles in phagosome maturation. More specifically, we observed that both NimB4 and NimB1 are secreted proteins that bind to PS, and that NimB4 has a critical role in promoting the fusion of phagosomes with lysosomes. In sum, studies in mammals and *Drosophila* highlight characteristics of bridging molecules that go beyond the initial restricted definition. This thesis, and particularly results on NimB4, points to a much broader role for bridging molecules in processes including orientation of phagosome maturation.

It has been shown that during efferocytosis, bridging molecules bind to phagocytic receptors (Barth *et al*, 2017; Lemke, 2019). As such, future investigations should define which receptor(s) NimB4 and NimB1 bind during phagocytosis. In *Drosophila*, one of the best-characterized receptors involved in efferocytosis is Draper (Ziegenfuss *et al*, 2008). Intriguingly, we observed that the *NimB4* mutant shares many phenotypes with the *Draper* mutant, including increased phagosome size, a phagosome maturation defect, and crawling defects at the third instar larval stage. As such, it is tempting to speculate that NimB4 binds the phagocytic receptor Draper to promote efferocytosis. However, epistatic analysis showed that the *Draper, NimB4* double mutant has additive effects on phagosome size, suggesting that the receptor Draper and the

bridging molecule NimB4 may work in different phagocytic pathways. Surprisingly, the same epistatic analysis showed that a *NimB4, croquemort* double mutation had no additive effect on phagosome sizes, suggesting that Croquemort and NimB4 may work together in phagocytosis. Furthermore, recent studies have shown that Croquemort is not involved in the uptake of apoptotic cells as initially proposed but rather regulates phagosome maturation, as shown in epidermal cells (Han *et al*, 2014). Thus, both NimB4 and Croquemort seem to play a role in phagosome maturation. However, future studies should clarify the role of Croquemort in phagocytosis, as this receptor seems to have an additional role in the uptake of lipids, which could interfere with phagocytosis (Woodcock et al., 2015). Moreover, computational approaches predict the interaction of NimB1 with the calcium-binding protein (Ca^{2+}BP). Interestingly, it has been shown that Ca^{2+}BP binds to the Draper receptor during efferocytosis (Okada *et al*, 2012a). As such, this observation suggests that NimB1 may work in the same phagocytic pathway as Draper. However, these observations are too preliminary to conclude whether NimB4 and NimB1 bind to similar or distinct phagocytic receptors on the macrophage. Thus, future studies should characterize the mode of action of NimB1 and NimB4 and identify potential partners.

Studies have shown that SIMU promotes the phagocytosis of apoptotic cells in specific stages of the *Drosophila* life cycle, such as embryogenesis (Kurant et al.,2009). In contrast, Draper has a broader role in efferocytosis throughout the *Drosophila* life cycle (Kurant et al.,2009, Petrignani et al.,2021; MacDonald et al.,2006). It has been suggested that SIMU is expressed mainly during embryogenesis because it is required to facilitate uptake of the high number of apoptotic cells generated at this stage. As such, components involved in efferocytosis might differ from one context to another depending on the rate of apoptosis. In our study, the *NimB1* mutant does not present a blockage in efferocytosis at the larval stage. Therefore, we speculate that NimB1 like SIMU may play a role in phagocytosis solely in embryogenesis. Future studies should define the life cycle stage at which NimB1 plays a role in the phagocytosis of apoptotic cells.

Studies have shown that the phagocytic process is multi-faceted and is tailored to the nature of the ingested particle. Indeed, phagocytic targets can differentially affect the maturation rate. For instance, apoptotic cells initiate a specific maturation program, leading to the efficient elimination of corpses (Viegas *et al*, 2012; Kinchen & Ravichandran, 2008). Several Nimrod receptors including Draper, NimC1, and Eater have been implicated in phagocytosis of both

bacteria and apoptotic cells (Hashimoto *et al*, 2009; Kuraishi *et al*, 2009; Shiratsuchi *et al*, 2012; Tung *et al*, 2013). In contrast, the bridging molecule NimB4 is specifically required for the phagocytosis of apoptotic cells (Petrignani *et al*, 2021). This observation indicates that NimB4 is not a core component of the phagocytic machinery but plays a specific role in the phagocytosis of apoptotic cells. Therefore, we hypothesize that bridging molecules may signal the nature of the ingested particle to the phagocytic cell and determine the phagosome maturation program. Bridging molecules may play an important role in tailoring phagocytosis to the nature of the ingested particle in this way.

In sum, in this thesis we focused on the multi-faceted role of bridging molecules and clarified how this type of molecule can interact with phagocytosis. Further characterization of other bridging molecules in various organisms might help to define their function better. A prospect in the lab is to study the function of *NimB2,* as this gene seems to be essential during embryonic development and could play a significant role in efferocytosis.

5.2 Nimrod B1 and B5 regulate hemocyte number in *Drosophila*

We observed that NimB1 plays a role in hemocyte sessility and proliferation. This observation raises an interesting question about the effect of macrophage-apoptotic cell interaction on macrophage survival and multiplication. Studies in vertebrates have highlighted a clear link between the presence of apoptotic cells and the survival of phagocytic cells. Apoptotic cells can release soluble factors such as the bioactive lipid sphingosine-1-phosphate (S1P), which induces a Ca^{2+} dependent survival pathway in macrophages (Weigert *et al*, 2006). Moreover, apoptotic cells can induce the proliferation of phagocytic cells. Co-culture of apoptotic cells with macrophages induces macrophage proliferation through soluble factors (Knuth *et al*, 2021). A recent study in *Drosophila* showed that apoptotic cells induce proliferation of glial cells in the eye disc (Velarde *et al*, 2021). Phagocytosis of apoptotic cells can also prime *Drosophila* macrophages, determining their later ability to migrate to a wound and actively participate in the wound resolution (Weavers *et al*, 2016; Roddie *et al*, 2019). This acquisition of “immunological memory” involves an intracellular calcium burst and increased expression of Draper. Similarly, we suggest that the low number of hemocytes found in *NimB1* deficient larvae could be due to a defect in efferocytosis at the embryonic stage. A defect in embryonic efferocytosis may reduce hemocyte proliferation due to a lack of priming. Therefore, the

NimB1 mutant represents an interesting model to study the effect of embryonic efferocytosis on macrophage survival and proliferation. Future studies should clarify the correlation between the rate of efferocytosis during embryogenesis and the number of macrophages generated during development. We could address this question by modulating cell death levels during embryogenesis and monitoring hemocyte numbers in early larvae. These experiments would allow us to understand how efferocytosis could influence the survival of macrophages by providing energy or inducing the expression of phagocytic receptors.

During larval development, the peripheral hemocyte population undergoes significant proliferation, expanding by self-renewal (Lanot *et al*, 2001; Makhijani *et al*, 2011). Moreover, plasmatocytes are highly dynamic at the larval stage, continuously cycling between the sessile and circulating state. It has been shown that adherent cells, notably those establishing contacts with other cells, are less proliferative, a process called "contact inhibition" of proliferation (Fagotto & Gumbiner, 1997). We know that the Nimrod transmembrane receptor Eater is required cell-autonomously in plasmatocytes for sessility. Additionally, the *eater* mutant presents a higher hemocyte number (Bretscher *et al*, 2015). It is tempting to speculate that the higher proliferation rate observed in the *eater* mutant is a secondary consequence of the adhesion defect. This thesis shows that two Nimrod B-type proteins, NimB5 and NimB1, play a role in hemocyte adhesion in the third instar larva. Interestingly, *NimB5* mutants share many similarities with the e*ater* mutant, including a partial loss of sessility and an increased hemocyte number. This suggests that the secreted NimB5 protein and the transmembrane receptor Eater may function in a similar pathway. NimB5 could bind to Eater and regulate the adhesion and proliferation properties of hemocytes. Verification of this hypothesis is contingent on demonstration of a physical interaction between NimB5 and Eater in future studies. It is interesting to note that a recent study has shown that Eater on the hemocytes can physically interact with the Collagen XV/XVIII ortholog Multiplexin in the tissue-basement membranes, and this interaction is sufficient to induce immune cell-tissue association (Csordas et al.,2020). It is possible that some NimB proteins modulate Eater-Multiplexin interaction and thus affect sessility. Our preliminary study indicates that the *NimB1* mutant presents a loss of hemocyte sessility and decreased hemocyte numbers in the third instar larvae. As mentioned above, we hypothesize that reduced hemocyte numbers in the *NimB1* mutant may result from incorrect efferocytosis during embryogenesis. An alternate hypothesis is that proliferation of hemocytes during the third instar larval stage is not occurring correctly. Our observations

indicate that NimB1 (pro-proliferative) and NimB5 (anti-proliferative) have opposite functions in third instar larvae. Future studies should characterize how NimB1 proteins regulate hemocyte number. Two promising avenues are to investigate whether NimB1 is part of an intracellular signaling pathway regulating the self-renewal of hemocytes independent of sessility, or whether NimB1 regulates the number of hemocytes indirectly through a role in efferocytosis.

5.3 Nimrod B-type proteins at the intersection between metabolism and hemocyte number

Hemocyte production has a high metabolic cost and competes with the ability of the fat body to build up metabolic stores. Consequently, larvae with higher hemocyte numbers store lower lipid amounts in the fat body, while larvae with fewer hemocytes have larger lipid droplets in the fat body. For example, the *NimB5* mutant has a high number of hemocytes and few lipid droplets (Ramond et al.,2019). Consistent with this idea of metabolic competition between hemocytes and the fat body, we also observed that the *NimB1* mutant had fewer hemocytes and increased lipid droplets (data not shown in the thesis). It should be noted that another study challenges this notion of competition and instead suggest that hemocytes promote lipid storage by producing the PDGF factor Pvf-3, which activates the PVR pathway in the fat body (Cox *et al*, 2021). Future studies should clarify the cross-talk and metabolic tradeoff between hemocytes and fat body.

Finally, developmental studies in *Drosophila* should consider the metabolic demands of the hemocyte. *Drosophila* macrophages/plasmatocytes are likely very energy demanding, as has been shown for mammalian macrophages. Ramond et al. showed that *NimB5* regulation receives input from Myc, EcR, and TOR, three metabolic integrators of the fat body. Future studies should analyze how these pathways integrate to adjust the metabolism and proliferation of the blood cell compartment. Such a study would be relevant to the blossoming field of immune-metabolism.

5.4 Evolution of the Nimrod proteins

Phylogenetic analysis indicates that *NimB2* is the most ancient *NimB* gene. Furthermore, phylogenetic trees show that Nimrod B3 split off before Nimrod B5 during evolution and that

Nimrod B1 and B4 split most recently. As such, *NimB1* and *NimB4* are closely related paralogs genes (Cox *et al*, 2021). Considering the close evolution of *NimB1* and *NimB4*, it is tempting to speculate that these proteins have redundant roles as bridging molecules and might work in synergy. However, comparison of the *NimB1* and *NimB4* mutants showed subtle phenotypic differences. We observed that NimB1 has an additional role in hematopoiesis not seen for NimB4. Therefore, it would be interesting to clarify if the NimB1 protein interacts with NimB4 or NimB5 to complete its roles. Finally, characterization of *NimB1, NimB4*, and *NimB1, NimB5* double mutants might help to reveal a synergy between the NimB proteins. Preliminary data from our lab indicate that the *NimB1*, *NimB4* double mutant has no defect in the uptake of apoptotic cells at the larval stage. This result suggests that loss of *NimB1* compensates the phagocytic defects of the *NimB4* mutant. One hypothesis to explain this surprising result is that NimB1 and NimB4 work together in the phagocytosis of apoptotic cells. However, in unchallenged conditions, the *NimB1*, *NimB4* mutant has an increased number of lamellocytes, which suggests a defect in hematopoiesis. Thus, we should explore how NimB proteins function individually and collectively as it is likely that they have some overlapping functions.

In conclusion, we are still very far from understanding the function of Nimrod-B type proteins and Nimrod receptors in *Drosophila*. The availability of loss-of-function mutants will be helpful to delineate their roles further. Furthermore, study of these proteins could help to better understanding the process of efferocytosis and hematopoiesis in *Drosophila* and other insects where Nimrod proteins are found. Considering the importance of these mechanisms in both developmental and homeostatic conditions, this will provide general insights that could be of broad relevance beyond *Drosophila.*

5.5 Bibliography

Abrams JM, White K, Fessler LI & Steller H Programmed cell death during Drosophila embryogenesis. 15

Akakura S, Singh S, Spataro M, Akakura R, Kim J-I, Albert ML & Birge RB (2004) The opsonin MFG-E8 is a ligand for the αvβ5 integrin and triggers DOCK180-dependent Rac1 activation for the phagocytosis of apoptotic cells. *Experimental Cell Research* 292: 403–416

Apoptosis: A Review of Programmed Cell Death - Susan Elmore, 2007

Awasaki T, Tatsumi R, Takahashi K, Arai K, Nakanishi Y, Ueda R & Ito K (2006) Essential Role of the Apoptotic Cell Engulfment Genes draper and ced-6 in Programmed Axon Pruning during Drosophila Metamorphosis. *Neuron* 50: 855–867

Baños-Mateos S, Rojas AL & Hierro A (2019) VPS29, a tweak tool of endosomal recycling. *Current Opinion in Cell Biology* 59: 81–87

Barger SR, Gauthier NC & Krendel M (2020) Squeezing in a Meal: Myosin Functions in Phagocytosis. *Trends in Cell Biology* 30: 157–167

Barth ND, Marwick JA, Vendrell M, Rossi AG & Dransfield I (2017) The "Phagocytic Synapse" and Clearance of Apoptotic Cells. *Frontiers in Immunology* 8: 1708

Birge R & Ucker D (2008) Innate apoptotic immunity: the calming touch of death. *Cell Death and Differentiation*

Blander JM & Medzhitov R (2006) Toll-dependent selection of microbial antigens for presentation by dendritic cells. *Nature* 440: 808–812

Boada-Romero E, Martinez J, Heckmann BL & Green DR (2020) The clearance of dead cells by efferocytosis. *Nat Rev Mol Cell Biol* 21: 398–414

Bohdanowicz M & Grinstein S (2010) Vesicular Traffic: A Rab SANDwich. *Current Biology* 20: R311–R314

Bork P, Downing AK, Kieffer B & Campbell ID (1996) Structure and distribution of modules in extracellular proteins. *Quarterly Reviews of Biophysics* 29: 119–167

Botelho RJ & Grinstein S (2011) Phagocytosis. *Curr Biol* 21: R533-538

Botelho RJ, Teruel M, Dierckman R, Anderson R, Wells A, York JD, Meyer T & Grinstein S (2000) Localized biphasic changes in phosphatidylinositol-4,5-bisphosphate at sites of phagocytosis. *J Cell Biol* 151: 1353–1368

Bretscher AJ, Honti V, Binggeli O, Burri O, Poidevin M, Kurucz E, Zsamboki J, Ando I & Lemaitre B (2015) The Nimrod transmembrane receptor Eater is required for hemocyte attachment to the sessile compartment in Drosophila melanogaster. *Biology Open* 4: 355–363

Brown GC & Neher JJ (2012) Eaten alive! Cell death by primary phagocytosis: 'phagoptosis'. *Trends in Biochemical Sciences* 37: 325–332

Brown NH (2000) Cell-cell adhesion via the ECM: integrin genetics in fly and worm. *Matrix Biol* 19: 191–201

Buchmeier NA & Heffron F (1991) Inhibition of macrophage phagosome-lysosome fusion by Salmonella typhimurium. *Infect Immun* 59: 2232–2238

Callahan MK, Williamson P & Schlegel RA (2000) Surface expression of phosphatidylserine on macrophages is required for phagocytosis of apoptotic thymocytes. *Cell Death Differ* 7: 645–653

Campbell ID & Humphries MJ (2011) Integrin structure, activation, and interactions. *Cold Spring Harb Perspect Biol* 3: a004994

cattenoz 2020 phagocytosis - Cerca con Google

Christoforidis S, McBride HM, Burgoyne RD & Zerial M (1999) The Rab5 effector EEA1 is a core component of endosome docking. *Nature* 397: 621–625

Cinege G, Zsámboki J, Vidal-Quadras M, Uv A, Csordás G, Honti V, Gábor E, Hegedűs Z, Varga GIB, Kovács AL, *et al* (2017) Genes encoding cuticular proteins are components of the Nimrod gene cluster in Drosophila. *Insect Biochem Mol Biol* 87: 45–54

Cockram TOJ, Dundee JM, Popescu AS & Brown GC (2021) The Phagocytic Code Regulating Phagocytosis of Mammalian Cells. *Frontiers in Immunology* 12: 2144

Colacurcio DJ & Nixon RA (2016) Disorders of lysosomal acidification-The emerging role of v-ATPase in aging and neurodegenerative disease. *Ageing Res Rev* 32: 75–88

Collins RF, Schreiber AD, Grinstein S & Trimble WS (2002) Syntaxins 13 and 7 function at distinct steps during phagocytosis. *J Immunol* 169: 3250–3256

Cox D, Berg JS, Cammer M, Chinegwundoh JO, Dale BM, Cheney RE & Greenberg S (2002) Myosin X is a downstream effector of PI(3)K during phagocytosis. *Nat Cell Biol* 4: 469–477

Cox D, Lee DJ, Dale BM, Calafat J & Greenberg S (2000) A Rab11-containing rapidly recycling compartment in macrophages that promotes phagocytosis. *PNAS* 97: 680–685

Cox N, Crozet L, Holtman IR, Loyher P-L, Lazarov T, White JB, Mass E, Stanley ER, Elemento O, Glass CK, *et al* (2021) Diet-regulated production of PDGFcc by macrophages controls energy storage. *Science* 373: eabe9383

Damiani MT, Pavarotti M, Leiva N, Lindsay AJ, McCaffrey MW & Colombo MI (2004) Rab Coupling Protein Associates with Phagosomes and Regulates Recycling from the Phagosomal Compartment. *Traffic* 5: 785–797

DeCoursey TE (2010) Voltage-gated proton channels find their dream job managing the respiratory burst in phagocytes. *Physiology (Bethesda)* 25: 27–40

Denton D, Aung-Htut MT & Kumar S (2013) Developmentally programmed cell death in Drosophila. *Biochim Biophys Acta* 1833: 3499–3506

Desjardins M (1995) Biogenesis of phagolysosomes: the 'kiss and run' hypothesis. *Trends Cell Biol* 5: 183–186

Dingjan I, Linders PTA, Verboogen DRJ, Revelo NH, ter Beest M & van den Bogaart G (2018) Endosomal and Phagosomal SNAREs. *Physiological Reviews* 98: 1465–1492

Doherty J, Sheehan AE, Bradshaw R, Fox AN, Lu T-Y & Freeman MR (2014) PI3K Signaling and Stat92E Converge to Modulate Glial Responsiveness to Axonal Injury. *PLOS Biology* 12: e1001985

Duclos S, Diez R, Garin J, Papadopoulou B, Descoteaux A, Stenmark H & Desjardins M (2000) Rab5 regulates the kiss and run fusion between phagosomes and endosomes and the acquisition of phagosome leishmanicidal properties in RAW 264.7 macrophages. *J Cell Sci* 113 Pt 19: 3531–3541

Elliott MR & Ravichandran KS (2016) The Dynamics of Apoptotic Cell Clearance. *Developmental Cell* 38: 147–160

Etchegaray JI, Timmons AK, Klein AP, Pritchett TL, Welch E, Meehan TL, Li C & McCall K (2012) Draper acts through the JNK pathway to control synchronous engulfment of dying germline cells by follicular epithelial cells. *Development* 139: 4029–4039

Fadok VA, Bratton DL, Konowal A, Freed PW, Westcott JY & Henson PM (1998) Macrophages that have ingested apoptotic cells in vitro inhibit proinflammatory cytokine production through autocrine/paracrine mechanisms involving TGF-beta, PGE2, and PAF. *J Clin Invest* 101: 890–898

Fagotto F & Gumbiner B (1997) Cell Contact-Dependent Signaling. *Developmental biology* 180: 445–54

Feinstein-Rotkopf Y & Arama E (2009) Can't live without them, can live with them: roles of caspases during vital cellular processes. *Apoptosis* 14: 980–995

Flannagan RS, Jaumouillé V & Grinstein S (2012) The Cell Biology of Phagocytosis. *Annual Review of Pathology: Mechanisms of Disease* 7: 61–98

Freeman MR (2015) *Drosophila* Central Nervous System Glia. *Cold Spring Harb Perspect Biol* 7: a020552

Freeman MR, Delrow J, Kim J, Johnson E & Doe CQ (2003) Unwrapping Glial Biology: Gcm Target Genes Regulating Glial Development, Diversification, and Function. *Neuron* 38: 567–580

Fu YL & Harrison RE (2021) Microbial Phagocytic Receptors and Their Potential Involvement in Cytokine Induction in Macrophages. *Front Immunol* 12: 662063

Fuchs Y & Steller H (2011) Programmed Cell Death in Animal Development and Disease. *Cell* 147: 742–758

Fullard JF, Kale A & Baker NE (2009) Clearance of apoptotic corpses. *Apoptosis* 14: 1029–1037

Fuller AD & Van Eldik LJ (2008) MFG-E8 Regulates Microglial Phagocytosis of Apoptotic Neurons. *J Neuroimmune Pharmacol* 3: 246–256

Galluzzi L, Vitale I, Abrams JM, Alnemri ES, Baehrecke EH, Blagosklonny MV, Dawson TM, Dawson VL, El-Deiry WS, Fulda S, *et al* (2012) Molecular definitions of cell death subroutines: recommendations of the Nomenclature Committee on Cell Death 2012. *Cell Death Differ* 19: 107–120

Galvan MD, Greenlee-Wacker MC & Bohlson SS (2012) C1q and phagocytosis: the perfect complement to a good meal. *Journal of Leukocyte Biology* 92: 489–497

Geisow MJ, D'Arcy Hart P & Young MR (1981) Temporal changes of lysosome and phagosome pH during phagolysosome formation in macrophages: studies by fluorescence spectroscopy. *J Cell Biol* 89: 645–652

Geng K, Kumar S, Kimani SG, Kholodovych V, Kasikara C, Mizuno K, Sandiford O, Rameshwar P, Kotenko SV & Birge RB (2017) Requirement of Gamma-Carboxyglutamic Acid Modification and Phosphatidylserine Binding for the Activation of Tyro3, Axl, and Mertk Receptors by Growth Arrest-Specific 6. *Front Immunol* 8: 1521

Grant BD & Donaldson JG (2009) Pathways and mechanisms of endocytic recycling. *Nat Rev Mol Cell Biol* 10: 597–608

Guillou A, Troha K, Wang H, Franc NC & Buchon N (2016) The Drosophila CD36 Homologue croquemort Is Required to Maintain Immune and Gut Homeostasis during Development and Aging. *PLoS Pathog* 12: e1005961

Gutierrez MG (2013) Functional role(s) of phagosomal Rab GTPases. *Small GTPases* 4: 148–158

Hakim Y, Yaniv SP & Schuldiner O (2014) Astrocytes Play a Key Role in Drosophila Mushroom Body Axon Pruning. *PLoS ONE* 9: e86178

Hall A (1998) Rho GTPases and the actin cytoskeleton. *Science* 279: 509–514

Hamon Y, Trompier D, Ma Z, Venegas V, Pophillat M, Mignotte V, Zhou Z & Chimini G (2006) Cooperation between engulfment receptors: the case of ABCA1 and MEGF10. *PLoS One* 1: e120

Han C, Song Y, Xiao H, Wang D, Franc NC, Jan LY & Jan Y-N (2014) Epidermal cells are the primary phagocytes in the fragmentation and clearance of degenerating dendrites in Drosophila. *Neuron* 81: 544–560

Hanayama R, Tanaka M, Miwa K, Shinohara A, Iwamatsu A & Nagata S (2002) Identification of a factor that links apoptotic cells to phagocytes. *Nature* 417: 182–187

Harrison RE, Bucci C, Vieira OV, Schroer TA & Grinstein S (2003) Phagosomes fuse with late endosomes and/or lysosomes by extension of membrane protrusions along microtubules: role of Rab7 and RILP. *Mol Cell Biol* 23: 6494–6506

Hashimoto Y, Tabuchi Y, Sakurai K, Kutsuna M, Kurokawa K, Awasaki T, Sekimizu K, Nakanishi Y & Shiratsuchi A (2009) Identification of lipoteichoic acid as a ligand for draper in the phagocytosis of Staphylococcus aureus by Drosophila hemocytes. *J Immunol* 183: 7451–7460

Higgs HN & Pollard TD (2000) Activation by Cdc42 and PIP(2) of Wiskott-Aldrich syndrome protein (WASp) stimulates actin nucleation by Arp2/3 complex. *J Cell Biol* 150: 1311–1320

Hilu-Dadia R, Hakim-Mishnaevski K, Levy-Adam F & Kurant E (2018) Draper-mediated JNK signaling is required for glial phagocytosis of apoptotic neurons during Drosophila metamorphosis. *Glia* 66: 1520–1532

Holz A, Bossinger B, Strasser T, Janning W & Klapper R (2003) The two origins of hemocytes in Drosophila. *Development* 130: 4955–4962

Hoppe AD & Swanson JA (2004a) Cdc42, Rac1, and Rac2 display distinct patterns of activation during phagocytosis. *Mol Biol Cell* 15: 3509–3519

Hoppe AD & Swanson JA (2004b) Cdc42, Rac1, and Rac2 display distinct patterns of activation during phagocytosis. *Mol Biol Cell* 15: 3509–3519

Huh JR, Foe I, Muro I, Chen CH, Seol JH, Yoo SJ, Guo M, Park JM & Hay BA (2007) The Drosophila inhibitor of apoptosis (IAP) DIAP2 is dispensable for cell survival, required for the innate immune response to gram-negative bacterial infection, and can be negatively regulated by the reaper/hid/grim family of IAP-binding apoptosis inducers. *J Biol Chem* 282: 2056–2068

Huynh KK, Eskelinen E-L, Scott CC, Malevanets A, Saftig P & Grinstein S (2007) LAMP proteins are required for fusion of lysosomes with phagosomes. *EMBO J* 26: 313–324

Ikeda Y, Kawai K, Ikawa A, Kawamoto K, Egami Y & Araki N (2017) Rac1 switching at the right time and location is essential for Fcγ receptor-mediated phagosome formation. *J Cell Sci* 130: 2530–2540

Irving P, Ubeda J-M, Doucet D, Troxler L, Lagueux M, Zachary D, Hoffmann JA, Hetru C & Meister M (2005) New insights into Drosophila larval haemocyte functions through genome-wide analysis. *Cell Microbiol* 7: 335–350

Johansson M, Rocha N, Zwart W, Jordens I, Janssen L, Kuijl C, Olkkonen VM & Neefjes J (2007) Activation of endosomal dynein motors by stepwise assembly of Rab7-RILP-p150Glued, ORP1L, and the receptor betalll spectrin. *J Cell Biol* 176: 459–471

Kato K, Awasaki T & Ito K (2009) Neuronal programmed cell death induces glial cell division in the adult Drosophila brain. *Development* 136: 51–59

Kerr JFR, Wyllie AH & Currie AR (1972) Apoptosis: A Basic Biological Phenomenon with Wide-ranging Implications in Tissue Kinetics. *Br J Cancer* 26: 239–257

Kinchen JM & Ravichandran KS (2008) Phagosome maturation: going through the acid test. *Nat Rev Mol Cell Biol* 9: 781–795

Kinchen JM & Ravichandran KS (2010) Identification of two evolutionarily conserved genes regulating processing of engulfed apoptotic cells. *Nature* 464: 778–782

Kissing S, Hermsen C, Repnik U, Nesset CK, von Bargen K, Griffiths G, Ichihara A, Lee BS, Schwake M, De Brabander J, *et al* (2015) Vacuolar ATPase in phagosome-lysosome fusion. *J Biol Chem* 290: 14166–14180

Knuth A-K, Huard A, Naeem Z, Rappl P, Bauer R, Mota AC, Schmid T, Fleming I, Brüne B, Fulda S, *et al* (2021) Apoptotic Cells induce Proliferation of Peritoneal Macrophages. *Int J Mol Sci* 22: 2230

Koester SE & O'Leary DDM (1994) Development of projection neurons of the mammalian cerebral cortex. In *Progress in Brain Research*, Van Pelt J Corner MA Uylings HBM & Lopes Da Silva FH (eds) pp 207–215. Elsevier

Koh ALY, Sun CX, Zhu F & Glogauer M (2005) The role of Rac1 and Rac2 in bacterial killing. *Cell Immunol* 235: 92–97

Kroemer G, Galluzzi L, Vandenabeele P, Abrams J, Alnemri ES, Baehrecke EH, Blagosklonny MV, El-Deiry WS, Golstein P, Green DR, *et al* (2009) Classification of cell death: recommendations of the Nomenclature Committee on Cell Death 2009. *Cell Death Differ* 16: 3–11

Kuraishi T, Manaka J, Kono M, Ishii H, Yamamoto N, Koizumi K, Shiratsuchi A, Lee BL, Higashida H & Nakanishi Y (2007) Identification of calreticulin as a marker for phagocytosis of apoptotic cells in Drosophila. *Experimental Cell Research* 313: 500–510

Kuraishi T, Nakagawa Y, Nagaosa K, Hashimoto Y, Ishimoto T, Moki T, Fujita Y, Nakayama H, Dohmae N, Shiratsuchi A, *et al* (2009) Pretaporter, a Drosophila protein serving as a ligand for Draper in the phagocytosis of apoptotic cells. *EMBO J* 28: 3868–3878

Kurant E (2011) Keeping the CNS clear: Glial phagocytic functions in Drosophila. *Glia* 59: 1304–1311

Kurant E, Axelrod S, Leaman D & Gaul U (2008a) Six-Microns-Under Acts Upstream of Draper in the Glial Phagocytosis of Apoptotic Neurons. *Cell* 133: 498–509

Kurant E, Axelrod S, Leaman D & Gaul U (2008b) Six-microns-under acts upstream of Draper in the glial phagocytosis of apoptotic neurons. *Cell* 133: 498–509

Lan W, Liu S, Zhao L & Su Y (2020) Regulation of Drosophila Hematopoiesis in Lymph Gland: From a Developmental Signaling Point of View. *Int J Mol Sci* 21: 5246

Langemeyer L, Borchers A-C, Herrmann E, Füllbrunn N, Han Y, Perz A, Auffarth K, Kümmel D & Ungermann C (2020) A conserved and regulated mechanism drives endosomal Rab transition. *eLife* 9: e56090

Lanot R, Zachary D, Holder F & Meister M (2001) Postembryonic hematopoiesis in Drosophila. *Dev Biol* 230: 243–257

Lauber K, Blumenthal SG, Waibel M & Wesselborg S (2004) Clearance of apoptotic cells: getting rid of the corpses. *Mol Cell* 14: 277–287

Lebo DPV & McCall K (2021) Murder on the Ovarian Express: A Tale of Non-Autonomous Cell Death in the Drosophila Ovary. *Cells* 10: 1454

Lee WL, Kim M-K, Schreiber AD & Grinstein S (2005) Role of Ubiquitin and Proteasomes in Phagosome Maturation. *Mol Biol Cell* 16: 2077–2090

Leiserson WM, Harkins EW & Keshishian H (2000) Fray, a Drosophila serine/threonine kinase homologous to mammalian PASK, is required for axonal ensheathment. *Neuron* 28: 793–806

Leitão AB & Sucena É (2015) Drosophila sessile hemocyte clusters are true hematopoietic tissues that regulate larval blood cell differentiation. *eLife* 4: e06166

Leiva N, Pavarotti M, Colombo MI & Damiani MT (2006) Reconstitution of recycling from the phagosomal compartment in streptolysin O-permeabilized macrophages: role of Rab11. *Exp Cell Res* 312: 1843–1855

Lemke G (2019) How macrophages deal with death. *Nat Rev Immunol* 19: 539–549

Lin S, Huang Y & Lee T (2009) Nuclear receptor unfulfilled regulates axonal guidance and cell identity of Drosophila mushroom body neurons. *PLoS One* 4: e8392

Lindsay AJ, Hendrick AG, Cantalupo G, Senic-Matuglia F, Goud B, Bucci C & McCaffrey MW (2002) Rab coupling protein (RCP), a novel Rab4 and Rab11 effector protein. *J Biol Chem* 277: 12190–12199

Logan MA, Hackett R, Doherty J, Sheehan A, Speese SD & Freeman MR (2012) Negative regulation of glial engulfment activity by Draper terminates glial responses to axon injury. *Nat Neurosci* 15: 722–730

Lukacs GL, Rotstein OD & Grinstein S (1991) Determinants of the phagosomal pH in macrophages. In situ assessment of vacuolar H(+)-ATPase activity, counterion conductance, and H+ 'leak'. *J Biol Chem* 266: 24540–24548

Ma X, Liu K, Li J, Li H, Li J, Liu Y, Yang C & Liang H (2018) A non-canonical GTPase interaction enables ORP1L-Rab7-RILP complex formation and late endosome positioning. *J Biol Chem* 293: 14155–14164

MacDonald JM, Beach MG, Porpiglia E, Sheehan AE, Watts RJ & Freeman MR (2006) The Drosophila Cell Corpse Engulfment Receptor Draper Mediates Glial Clearance of Severed Axons. *Neuron* 50: 869–881

Makhijani K, Alexander B, Rao D, Petraki S, Herboso L, Kukar K, Batool I, Wachner S, Gold KS, Wong C, *et al* (2017) Regulation of Drosophila hematopoietic sites by Activin-β from active sensory neurons. *Nat Comms* 8: 15990

Makhijani K, Alexander B, Tanaka T, Rulifson E & Brückner K (2011) The peripheral nervous system supports blood cell homing and survival in the Drosophila larva. *Development* 138: 5379–5391

Manaka J, Kuraishi T, Shiratsuchi A, Nakai Y, Higashida H, Henson P & Nakanishi Y (2004) Draper-mediated and phosphatidylserine-independent phagocytosis of apoptotic cells by Drosophila hemocytes/macrophages. *J Biol Chem* 279: 48466–48476

Mangahas PM & Zhou Z (2005) Clearance of apoptotic cells in Caenorhabditis elegans. *Seminars in Cell & Developmental Biology* 16: 295–306

Marat AL & Haucke V (2016) Phosphatidylinositol 3-phosphates-at the interface between cell signalling and membrane traffic. *EMBO J* 35: 561–579

Marie-Anaïs F, Mazzolini J, Herit F & Niedergang F (2016) Dynamin-Actin Cross Talk Contributes to Phagosome Formation and Closure. *Traffic* 17: 487–499

Markus R, Laurinyecz B, Kurucz E, Honti V, Bajusz I, Sipos B, Somogyi K, Kronhamn J, Hultmark D & Ando I (2009) Sessile hemocytes as a hematopoietic compartment in Drosophila melanogaster. *Proceedings of the National Academy of Sciences* 106: 4805–4809

Marshansky V & Futai M (2008) The V-type H+-ATPase in vesicular trafficking: targeting, regulation and function. *Curr Opin Cell Biol* 20: 415–426

Maxson ME & Grinstein S (2020) The Role of Membrane Surface Charge in Phagocytosis. *Adv Exp Med Biol* 1246: 43–54

May RC, Caron E, Hall A & Machesky LM (2000) Involvement of the Arp2/3 complex in phagocytosis mediated by FcgammaR or CR3. *Nat Cell Biol* 2: 246–248

McBride HM, Rybin V, Murphy C, Giner A, Teasdale R & Zerial M (1999) Oligomeric complexes link Rab5 effectors with NSF and drive membrane fusion via interactions between EEA1 and syntaxin 13. *Cell* 98: 377–386

McGuinness WA, Kobayashi SD & DeLeo FR (2016) Evasion of Neutrophil Killing by Staphylococcus aureus. *Pathogens* 5: E32

Meehan TL, Joudi TF, Timmons AK, Taylor JD, Habib CS, Peterson JS, Emmanuel S, Franc NC & McCall K (2016) Components of the Engulfment Machinery Have Distinct Roles in Corpse Processing. *PLOS ONE* 11: e0158217

Meier P, Silke J, Leevers SJ & Evan GI (2000) The Drosophila caspase DRONC is regulated by DIAP1. *EMBO J* 19: 598–611

Melcarne C, Lemaitre B & Kurant E (2019a) Phagocytosis in Drosophila: From molecules and cellular machinery to physiology. *Insect Biochemistry and Molecular Biology* 109: 1–12

Melcarne C, Ramond E, Dudzic J, Bretscher AJ, Kurucz É, Andó I & Lemaitre B (2019b) Two Nimrod receptors, NimC1 and Eater, synergistically contribute to bacterial phagocytosis in Drosophila melanogaster. *The FEBS Journal* 286: 2670–2691

Mills DB (2020) The origin of phagocytosis in Earth history. *Interface Focus* 10: 20200019

Minakami R, Maehara Y, Kamakura S, Kumano O, Miyano K & Sumimoto H (2010) Membrane phospholipid metabolism during phagocytosis in human neutrophils. *Genes Cells* 15: 409–424

Miura M (2012) Apoptotic and nonapoptotic caspase functions in animal development. *Cold Spring Harb Perspect Biol* 4: a008664

Miyanishi M, Tada K, Koike M, Uchiyama Y, Kitamura T & Nagata S (2007) Identification of Tim4 as a phosphatidylserine receptor. *Nature* 450: 435–439

Moreira CGA, Jacinto A & Prag S (2013) Drosophila integrin adhesion complexes are essential for hemocyte migration in vivo. *Biology Open* 2: 795–801

Mosser DM & Zhang X (2011) Measuring opsonic phagocytosis via Fcγ receptors and complement receptors on macrophages. *Curr Protoc Immunol* Chapter 14: Unit 14.27

Mularski A, Wimmer R, Arbaretaz F, Goff GL & Niedergang F (2021) Dynamin-2 controls complement receptor 3- mediated phagocytosis completion and closure

Nagaosa K, Okada R, Nonaka S, Takeuchi K, Fujita Y, Miyasaka T, Manaka J, Ando I & Nakanishi Y (2011) Integrin βv-mediated Phagocytosis of Apoptotic Cells in *Drosophila* Embryos. *J Biol Chem* 286: 25770–25777

Nguyen JA & Yates RM (2021) Better Together: Current Insights Into Phagosome-Lysosome Fusion. *Frontiers in Immunology* 12: 209

Nicolson S, Denton D & Kumar S (2015) Ecdysone-mediated programmed cell death in Drosophila. *Int J Dev Biol* 59: 23–32

Nonaka S, Nagaosa K, Mori T, Shiratsuchi A & Nakanishi Y (2013) Integrin αPS3/βv-mediated phagocytosis of apoptotic cells and bacteria in Drosophila. *J Biol Chem* 288: 10374–10380

Okada R, Nagaosa K, Kuraishi T, Nakayama H, Yamamoto N, Nakagawa Y, Dohmae N, Shiratsuchi A & Nakanishi Y (2012a) Apoptosis-dependent Externalization and Involvement in Apoptotic Cell Clearance of DmCaBP1, an Endoplasmic Reticulum Protein of *Drosophila*. *J Biol Chem* 287: 3138–3146

Okada R, Nagaosa K, Kuraishi T, Nakayama H, Yamamoto N, Nakagawa Y, Dohmae N, Shiratsuchi A & Nakanishi Y (2012b) Apoptosis-dependent externalization and involvement in apoptotic cell clearance of DmCaBP1, an endoplasmic reticulum protein of Drosophila. *J Biol Chem* 287: 3138–3146

Park H & Cox D (2009) Cdc42 regulates Fc gamma receptor-mediated phagocytosis through the activation and phosphorylation of Wiskott-Aldrich syndrome protein (WASP) and neural-WASP. *Mol Biol Cell* 20: 4500–4508

Peiser L, Gough PJ, Kodama T & Gordon S (2000) Macrophage class A scavenger receptor-mediated phagocytosis of Escherichia coli: role of cell heterogeneity, microbial strain, and culture conditions in vitro. *Infect Immun* 68: 1953–1963

Peng Y & Elkon KB (2011a) Autoimmunity in MFG-E8–deficient mice is associated with altered trafficking and enhanced cross-presentation of apoptotic cell antigens. *J Clin Invest* 121: 2221–2241

Peng Y & Elkon KB (2011b) Autoimmunity in MFG-E8–deficient mice is associated with altered trafficking and enhanced cross-presentation of apoptotic cell antigens. *J Clin Invest* 121: 2221–2241

Petraki S, Alexander B & Brückner K (2015) Assaying Blood Cell Populations of the Drosophila melanogaster Larva. *J Vis Exp*: 52733

Petrignani B, Rommelaere S, Hakim-Mishnaevski K, Masson F, Ramond E, Hilu-Dadia R, Poidevin M, Kondo S, Kurant E & Lemaitre B (2021) A secreted factor NimrodB4 promotes the elimination of apoptotic corpses by phagocytes in Drosophila. *EMBO Rep* 22: e52262

Pinto-Teixeira F, Konstantinides N & Desplan C (2016) Programmed cell death acts at different stages of Drosophila neurodevelopment to shape the central nervous system. *FEBS Lett* 590: 2435–2453

Pols MS, ten Brink C, Gosavi P, Oorschot V & Klumperman J (2013) The HOPS Proteins hVps41 and hVps39 Are Required for Homotypic and Heterotypic Late Endosome Fusion. *Traffic* 14: 219–232

Poteryaev D, Datta S, Ackema K, Zerial M & Spang A (2010) Identification of the Switch in Early-to-Late Endosome Transition. *Cell* 141: 497–508

Pryor PR, Mullock BM, Bright NA, Lindsay MR, Gray SR, Richardson SCW, Stewart A, James DE, Piper RC & Luzio JP (2004) Combinatorial SNARE complexes with VAMP7 or VAMP8 define different late endocytic fusion events. *EMBO Rep* 5: 590–595

Raiborg C & Stenmark H (2009) The ESCRT machinery in endosomal sorting of ubiquitylated membrane proteins. *Nature* 458: 445–452

Ramond E, Petrignani B, Dudzic JP, Boquete J-P, Poidevin M, Kondo S & Lemaitre B (2020) The adipokine NimrodB5 regulates peripheral hematopoiesis in Drosophila. *The FEBS Journal* 287: 3399–3426

Ravichandran KS (2003) "Recruitment Signals" from Apoptotic Cells: Invitation to a Quiet Meal. *Cell* 113: 817–820

Ravichandran KS (2011) Beginnings of a Good Apoptotic Meal: The Find-Me and Eat-Me Signaling Pathways. *Immunity* 35: 445–455

Ribeiro SA, D'Ambrosio MV & Vale RD (2014) Induction of focal adhesions and motility in Drosophila S2 cells. *Mol Biol Cell* 25: 3861–3869

Rink J, Ghigo E, Kalaidzidis Y & Zerial M (2005) Rab conversion as a mechanism of progression from early to late endosomes. *Cell* 122: 735–749

Roddie HG, Armitage EL, Coates JA, Johnston SA & Evans IR (2019) Simu-dependent clearance of dying cells regulates macrophage function and inflammation resolution. *PLOS Biology* 17: e2006741

Rogulja-Ortmann A, Luer K, Seibert J, Rickert C & Technau GM (2007) Programmed cell death in the embryonic central nervous system of Drosophila melanogaster. *Development* 134: 105–116

Rohatgi R, Ho HY & Kirschner MW (2000) Mechanism of N-WASP activation by CDC42 and phosphatidylinositol 4, 5-bisphosphate. *J Cell Biol* 150: 1299–1310

Ross GD, Reed W, Dalzell JG, Becker SE & Hogg N (1992) Macrophage cytoskeleton association with CR3 and CR4 regulates receptor mobility and phagocytosis of iC3b-opsonized erythrocytes. *J Leukoc Biol* 51: 109–117

Rougerie P, Miskolci V & Cox D (2013) Generation of membrane structures during phagocytosis and chemotaxis of macrophages: role and regulation of the actin cytoskeleton. *Immunol Rev* 256: 222–239

Rugendorff A, Younossi-Hartenstein A & Hartenstein V (1994) Embryonic origin and differentiation of the Drosophila heart. *Rouxs Arch Dev Biol* 203: 266–280

Savill J & Fadok V (2000) Corpse clearance defines the meaning of cell death. *Nature* 407: 784–788

Savill J, Hogg N, Ren Y & Haslett C (1992) Thrombospondin cooperates with CD36 and the vitronectin receptor in macrophage recognition of neutrophils undergoing apoptosis. *J Clin Invest* 90: 1513–1522

Savina A & Amigorena S (2007) Phagocytosis and antigen presentation in dendritic cells. *Immunol Rev* 219: 143–156

Schrijvers DM, De Meyer GRY, Kockx MM, Herman AG & Martinet W (2005) Phagocytosis of apoptotic cells by macrophages is impaired in atherosclerosis. *Arterioscler Thromb Vasc Biol* 25: 1256–1261

Schwabe T, Bainton RJ, Fetter RD, Heberlein U & Gaul U (2005) GPCR signaling is required for blood-brain barrier formation in drosophila. *Cell* 123: 133–144

Scott CC, Dobson W, Botelho RJ, Coady-Osberg N, Chavrier P, Knecht DA, Heath C, Stahl P & Grinstein S (2005) Phosphatidylinositol-4,5-bisphosphate hydrolysis directs actin remodeling during phagocytosis. *J Cell Biol* 169: 139–149

Seaman MNJ (2012) The retromer complex – endosomal protein recycling and beyond. *J Cell Sci* 125: 4693–4702

Segawa K, Kurata S, Yanagihashi Y, Brummelkamp TR, Matsuda F & Nagata S (2014) Caspase-mediated cleavage of phospholipid flippase for apoptotic phosphatidylserine exposure. *Science* 344: 1164–1168

Segawa K & Nagata S (2015) An Apoptotic 'Eat Me' Signal: Phosphatidylserine Exposure. *Trends Cell Biol* 25: 639–650

Serizier SB & McCall K (2017) Scrambled Eggs: Apoptotic Cell Clearance by Non-Professional Phagocytes in the Drosophila Ovary. *Front Immunol* 8: 1642

Shao W-H & Cohen PL (2011) Disturbances of apoptotic cell clearance in systemic lupus erythematosus. *Arthritis Res Ther* 13: 202

Shin M, Cha N, Koranteng F, Cho B & Shim J (2020) Subpopulation of Macrophage-Like Plasmatocytes Attenuates Systemic Growth via JAK/STAT in the Drosophila Fat Body. *Front Immunol* 11: 63

Shiratsuchi A, Mori T, Sakurai K, Nagaosa K, Sekimizu K, Lee BL & Nakanishi Y (2012) Independent Recognition of *Staphylococcus aureus* by Two Receptors for Phagocytosis in *Drosophila*. *J Biol Chem* 287: 21663–21672

Shklover J, Levy-Adam F & Kurant E (2015) Apoptotic Cell Clearance in Development. In *Current Topics in Developmental Biology* pp 297–334. Elsevier

Shklyar B, Sellman Y, Shklover J, Mishnaevski K, Levy-Adam F & Kurant E (2014) Developmental regulation of glial cell phagocytic function during Drosophila embryogenesis. *Dev Biol* 393: 255–269

Somogyi K, Sipos B, Pénzes Z & Andó I (2010) A conserved gene cluster as a putative functional unit in insect innate immunity. *FEBS Letters* 584: 4375–4378

Somogyi K, Sipos B, Penzes Z, Kurucz E, Zsamboki J, Hultmark D & Ando I (2008) Evolution of Genes and Repeats in the Nimrod Superfamily. *Molecular Biology and Evolution* 25: 2337–2347

Stenmark H (2009) Rab GTPases as coordinators of vesicle traffic. *Nat Rev Mol Cell Biol* 10: 513–525

Swanson JA, Johnson MT, Beningo K, Post P, Mooseker M & Araki N (1999) A contractile activity that closes phagosomes in macrophages. *J Cell Sci* 112 (Pt 3): 307–316

Tasdemir-Yilmaz OE & Freeman MR (2014) Astrocytes engage unique molecular programs to engulf pruned neuronal debris from distinct subsets of neurons. *Genes & Development* 28: 20–33

Timmons AK, Mondragon AA, Schenkel CE, Yalonetskaya A, Taylor JD, Moynihan KE, Etchegaray JI, Meehan TL & McCall K (2016) Phagocytosis genes nonautonomously promote developmental cell death in the Drosophila ovary. *Proc Natl Acad Sci U S A* 113: E1246-1255

Tissot M & Stocker RF (2000) Metamorphosis in drosophila and other insects: the fate of neurons throughout the stages. *Prog Neurobiol* 62: 89–111

Tremblay M-E, Cookson MR & Civiero L (2019) Glial phagocytic clearance in Parkinson's disease. *Molecular Neurodegeneration* 14: 16

Tung TT, Nagaosa K, Fujita Y, Kita A, Mori H, Okada R, Nonaka S & Nakanishi Y (2013) Phosphatidylserine recognition and induction of apoptotic cell clearance by Drosophila engulfment receptor Draper. *The Journal of Biochemistry* 153: 483–491

Turk V, Stoka V, Vasiljeva O, Renko M, Sun T, Turk B & Turk D (2012) Cysteine cathepsins: From structure, function and regulation to new frontiers. *Biochimica et Biophysica Acta (BBA) - Proteins and Proteomics* 1824: 68–88

Underhill DM & Goodridge HS (2007) The many faces of ITAMs. *Trends Immunol* 28: 66–73

Velarde SB, Quevedo A, Estella C & Baonza A (2021) Dpp and Hedgehog promote the glial response to neuronal apoptosis in the developing Drosophila visual system. *PLOS Biology* 19: e3001367

Viegas MS, Estronca LMBB & Vieira OV (2012) Comparison of the kinetics of maturation of phagosomes containing apoptotic cells and IgG-opsonized particles. *PLoS One* 7: e48391

Vieira OV, Bucci C, Harrison RE, Trimble WS, Lanzetti L, Gruenberg J, Schreiber AD, Stahl PD & Grinstein S (2003) Modulation of Rab5 and Rab7 recruitment to phagosomes by phosphatidylinositol 3-kinase. *Mol Cell Biol* 23: 2501–2514

Walbaum S, Ambrosy B, Schütz P, Bachg AC, Horsthemke M, Leusen JHW, Mócsai A & Hanley PJ (2021) Complement receptor 3 mediates both sinking phagocytosis and phagocytic cup formation via distinct mechanisms. *J Biol Chem* 296: 100256

Wang H, Liang F-X & Kong X-P (2008) Characteristics of the phagocytic cup induced by uropathogenic Escherichia coli. *J Histochem Cytochem* 56: 597–604

Wang L, Wu D, Robinson CV, Wu H & Fu T-M (2020) Structures of a Complete Human V-ATPase Reveal Mechanisms of Its Assembly. *Mol Cell* 80: 501-511.e3

Weavers H, Evans IR, Martin P & Wood W (2016) Corpse Engulfment Generates a Molecular Memory that Primes the Macrophage Inflammatory Response. *Cell* 165: 1658–1671

Weigert A, Johann AM, von Knethen A, Schmidt H, Geisslinger G & Brüne B (2006) Apoptotic cells promote macrophage survival by releasing the antiapoptotic mediator sphingosine-1-phosphate. *Blood* 108: 1635–1642

Winterbourn CC (2008) Reconciling the chemistry and biology of reactive oxygen species. *Nat Chem Biol* 4: 278–286

Woodcock KJ, Kierdorf K, Pouchelon CA, Vivancos V, Dionne MS & Geissmann F (2015) Macrophage-derived upd3 cytokine causes impaired glucose homeostasis and reduced lifespan in Drosophila fed a lipid-rich diet. *Immunity* 42: 133–144

Yamaguchi H, Fujimoto T, Nakamura S, Ohmura K, Mimori T, Matsuda F & Nagata S (2010) Aberrant splicing of the milk fat globule-EGF factor 8 (MFG-E8) gene in human systemic lupus erythematosus. *Eur J Immunol* 40: 1778–1785

Yanagihashi Y, Segawa K, Maeda R, Nabeshima Y & Nagata S (2017) Mouse macrophages show different requirements for phosphatidylserine receptor Tim4 in efferocytosis. *PNAS* 114: 8800–8805

Yeo JC, Wall AA, Luo L & Stow JL (2016) Sequential recruitment of Rab GTPases during early stages of phagocytosis. *Cell Logist* 6: e1140615

Yeung T, Ozdamar B, Paroutis P & Grinstein S (2006) Lipid metabolism and dynamics during phagocytosis. *Current Opinion in Cell Biology* 18: 429–437

Yu S, Luo F & Jin LH (2018) The Drosophila lymph gland is an ideal model for studying hematopoiesis. *Dev Comp Immunol* 83: 60–69

Yuan W & Song C (2020) The Emerging Role of Rab5 in Membrane Receptor Trafficking and Signaling Pathways. *Biochem Res Int* 2020: 4186308

Zalevsky J, Lempert L, Kranitz H & Mullins RD (2001) Different WASP family proteins stimulate different Arp2/3 complex-dependent actin-nucleating activities. *Current Biology* 11: 1903–1913

Zheng Q, Ma A, Yuan L, Gao N, Feng Q, Franc NC & Xiao H (2017) Apoptotic Cell Clearance in Drosophila melanogaster. *Front Immunol* 8

Ziegenfuss JS, Biswas R, Avery MA, Hong K, Sheehan AE, Yeung Y-G, Stanley ER & Freeman MR (2008) Draper-dependent glial phagocytic activity is mediated by Src and Syk family kinase signalling. *Nature* 453: 935–939

Ziegenfuss JS, Doherty J & Freeman MR (2012) Distinct molecular pathways mediate glial activation and engulfment of axonal debris after axotomy. *Nat Neurosci* 15: 979–987

Zizzo G, Hilliard BA, Monestier M & Cohen PL (2012) Efficient Clearance of Early Apoptotic Cells by Human Macrophages Requires M2c Polarization and MerTK Induction. *The Journal of Immunology* 189: 3508–3520

Curriculum Vitae

Bianca Petrignani
PhD student
Lemaitre Lab, Global Health Institute.
École Polytechnique Fédérale de Lausanne, Switzerland

Avenue Montagibert 4
1005 Lausanne, Switzerland
+ 41 (0)79 393 94 57
bianca_petrignani@me.ch

- Education

2018-present PhD in Molecular Life Sciences, École Polytechnique Féderale de Lausanne, Switzerland

2016-2017 Maîtrise universitaire d'études avancées en Microbiologie (MAS)
Université de Genève, Switzerland
Final mark: 5.5/6

2014-2016 Msc in Molecular Biology, University of Milano, Italy
Final mark: 110/110 cum laude

2011-2013 Bsc in Biology, University of Milano, Italy

- Research experiences

2018- present **PhD student**
Global Health Institute EPFL, Lausanne, Switzerland
Project: "Role of the Nimrod proteins in *Drosophila melanogaster* immunity"
Supervisor: Prof. Bruno Lemaitre

2016-2017 **MAS student**
Faculty of Medecine, Departement of Mircobiologie, Geneva, Switzerland
Project: "The Study of cshA suppressor in *Staphylococcus Aureus*"
Supervisors: Prof. Patrick Linder
Project: **"**The role of flbT and flaF in *Caulobacter crescentus* flagellation"
Supervisors: Prof. Patrick Viollier

2014- 2016 **Master thesis project**

Global Health Institute EPFL, Lausanne, Switzerland
Project: "The role of autophagy in *Drosophila melanogaster* midgut"
Supervisors: Prof. Bruno Lemaitre

2011-2013 Bachelor thesis project
Department of Biology, University of Milano, Italy
Project: Expression profile of specific melanoma genes in human primary epithelial cells
Supervisors: Prof. Caterina La Porta

- Teaching experience

Physiology lab II, to EPFL Bachelor students
Physiologie par systèmes I, to EPFL Bachelor students

- Supervision experience

July-October 2018 Supervision of a Medical Student from Kyoto University
June-August 2019 Supervision of a Bachelor Student from EPFL
June 2020-2021 Supervision of a Master Student from Faculté de biologie et de médecine, Université de Lausanne

- Conference oral presentation and poster

2020 Swiss Drosophila Meeting, Lausanne, Switzerland, oral presentation
2019 European Drosophila Research conference, Switzerland, oral presentation

- Publications

« A secreted factor NimrodB4 promotes the elimination of apoptotic corpses by phagocytes in *Drosophila* » (Research article)
B. Petrignani, S. Rommelaere, K. Hakim-Mishnaevski, F. Masson, E. Ramond, R. Hilu-Dadia, M. Poidevin, S. Kondo, E. Kurant, B. Lemaitre
2021, *EMBO reports*

« *Immunologie : Exercices : QCM, Questions De Cours Et problèmes résolus* » (Textbook)
B. Petrignani, G. Clavarino, B. Lemaitre
2020, *Presses Polytechniques Et Universitaires Romandes*
« The Adipokine NimrodB5 Regulates Peripheral Hematopoiesis in Drosophila » (Research article)
E. Ramond, B. Petrignani, J.Dudzic, JP. Boquete, M. Poidevin, S. Kondo, B. Lemaitre

2020, *The FEBS Journal*

« Secretion Relieves Translational Co-Repression by a Specialized Flagellin Paralog » *(*Research article)
S. Ardissone, S. Kint, B. Petrignani, G. Panis, P. Viollier
2020, *Developmental Cell*

« The DEAD-Box RNA Helicase CshA Is Required for Fatty Acid Homeostasis in *Staphylococcus Aureus*» *(*Research article)
V. Khemici, J. Prados, B.Petrignani, B.Nolfi, E.Bergé, C. Manzano, C.Giraud, P.Linder
2020, *PLOS Genetics*

- Qualification courses

- Scientific writing for biomedical articles, EPFL, Switzerland

- Videomaking for science communication, EPFL, Switzerland

- Image Processing for life Science, EPFL, Switzerland